

**Finite Element Analysis and Genetic Algorithm Optimization Design  
for the Actuator Placement on a Large Adaptive Structure**

By

Lizeng Sheng

A DISSERTATION SUBMITTED TO THE FACULTY OF  
VIRGINIA POLYTECHNIC INSTITUTE AND STATE UNIVERSITY  
IN PARTIAL FULFILLMENT OF THE REQUIREMENTS FOR THE DEGREE OF  
DOCTOR OF PHILOSOPHY  
IN  
AEROSPACE ENGINEERING

Rakesh K. Kapania, Chair

Romesh C. Batra

Raymond H. Plaut

Alan Brown

Eric Johnson

December 9, 2004

Blacksburg, Virginia

**Keywords:** Smart Structures, Finite Element Analysis, Genetic Algorithms,  
Multidisciplinary Design & Optimization, Shape Control, Piezoelectric Actuator Locations,  
Parallel Computing.

Copyright 2004, Lizeng Sheng

# **Finite Element Analysis and Genetic Algorithm Optimization Design for the Actuator Placement on a Large Adaptive Structure**

By  
Lizeng Sheng  
Committee Chair: Rakesh K. Kapania  
Aerospace Engineering

## **(Abstract)**

The dissertation focuses on one of the major research needs in the area of adaptive /intelligent/smart structures, the development and application of finite element analysis and genetic algorithms for optimal design of large-scale adaptive structures. We first review some basic concepts in finite element method and genetic algorithms, along with the research on smart structures. Then we propose a solution methodology for solving a critical problem in the design of a next generation of large-scale adaptive structures -- optimal placements of a large number of actuators to control thermal deformations. After briefly reviewing the three most frequently used general approaches to derive a finite element formulation, the dissertation presents techniques associated with general shell finite element analysis using flat triangular laminated composite elements. The element used here has three nodes and eighteen degrees of freedom and is obtained by combining a triangular membrane element and a triangular plate bending element. The element includes the coupling effect between membrane deformation and bending deformation. The membrane element is derived from the linear strain triangular element using Cook's transformation. The discrete Kirchhoff triangular (DKT) element is used as the plate bending element. For completeness, a complete derivation of the DKT is presented. Geometrically nonlinear finite element formulation is derived for the analysis of adaptive structures under the combined thermal and electrical loads. Next, we solve the optimization problems of placing a large number of piezoelectric

actuators to control thermal distortions in a large mirror in the presence of four different thermal loads. We then extend this to a multi-objective optimization problem of determining only one set of piezoelectric actuator locations that can be used to control the deformation in the same mirror under the action of any one of the four thermal loads. A series of genetic algorithms, GA Version 1, 2 and 3, were developed to find the optimal locations of piezoelectric actuators from the order of  $10^{21} \sim 10^{56}$  candidate placements. Introducing a variable population approach, we improve the flexibility of selection operation in genetic algorithms. Incorporating mutation and hill climbing into micro-genetic algorithms, we are able to develop a more efficient genetic algorithm. Through extensive numerical experiments, we find that the design search space for the optimal placements of a large number of actuators is highly multi-modal and that the most distinct nature of genetic algorithms is their robustness. They give results that are random but with only a slight variability. The genetic algorithms can be used to get adequate solution using a limited number of evaluations. To get the highest quality solution, multiple runs including different random seed generators are necessary. The investigation time can be significantly reduced using a very coarse grain parallel computing. Overall, the methodology of using finite element analysis and genetic algorithm optimization provides a robust solution approach for the challenging problem of optimal placements of a large number of actuators in the design of next generation of adaptive structures.

## **Acknowledgments**

I would like to acknowledge the technical guidance of Professor Rakesh K. Kapania. I am grateful to my former department head Professor Bernard Grossman, current department head Professor Robert W. Walters, and my advisor Professor Rakesh K. Kapania for their encouragement and support. I would also like to thank Professor Romesh C. Batra, Professor Raymond H. Plaut, Professor Alan Brown, and Professor Eric Johnson for serving on my advisory committee and their patience. The helpful comments from Professor Raphael T. Haftka at the University of Florida and other AIAA Journal reviewers are appreciated. The support through the National Science Foundation (NSF Award Number: 9714128, Principal Investigator: Professor Shiv P. Joshi at the University of Texas at Arlington) and the Carilion Biomedical Institute is greatly appreciated.

# Contents

|  |            |
|--|------------|
| <b>List of Figures.....</b>  | <b>ix</b>  |
| <b>List of Tables .....</b>  | <b>xiv</b> |
| <b>Chapter 1. Introduction.....</b>  | <b>1</b>   |
| 1.1 Finite Element Method .....  | 1          |
| 1.1.1 Some basic Concepts of Finite Element Method. ....   | 2          |
| 1.1.2 Advances of Plate and Shell Finite Elements.....   | 8          |
| 1.2 Genetic Algorithms.....  | 12         |
| 1.3 Adaptive/Intelligent/Smart Structures .....  | 14         |
| 1.3.1 Piezoelectric Actuators and Sensors.....   | 15         |
| 1.3.2 Advances in Smart Structures .....   | 19         |
| 1.4 Objective and Scope of Present Research .....  | 23         |
| <b>Chapter 2. Finite Element Formulation.....</b>  | <b>26</b>  |
| 2.1 Galerkin weighted residual method, principle of virtual work and general<br>variational principles ..... | 28         |
| 2.2 Coordinate Transformation.....   | 33         |
| 2.3 Area/Natural Coordinates and Shape Functions for Triangular Elements ..                                  | 39         |
| 2.4 Numerical Integration .....  | 48         |
| 2.5 Membrane Element.....  | 52         |
| 2.6 Bending Element .....  | 60         |
| 2.7 Shell Element.....   | 75         |
| <b>Chapter 3. Genetic Algorithms for the Optimization of Piezoelectric Actuator<br/>    Locations.....</b>   | <b>98</b>  |

|                                   |     |
|-----------------------------------|-----|
| 3.1 Abstract.....                 | 98  |
| 3.2 Introduction.....             | 99  |
| 3.3 Genetic Algorithms.....       | 101 |
| 3.4 Problem Definition .....      | 104 |
| 3.5 Finite Element Modeling ..... | 106 |
| 3.6 Control Algorithms.....       | 106 |
| 3.7 Results and Discussion .....  | 108 |
| 3.8 Conclusions.....              | 112 |
| Acknowledgments .....             | 113 |
| References.....                   | 114 |

**Chapter 4. Toward More Effective Genetic Algorithms for the Optimization of**

|  |            |
|--|------------|
| <b>Piezoelectric Actuator Locations.....</b> | <b>123</b> |
| 4.1 Abstract.....                            | 123        |
| 4.2 Introduction.....                        | 124        |
| 4.3 Genetic Algorithms.....                  | 126        |
| 4.4 Problem Definition .....                 | 128        |
| 4.5 Finite Element Modeling .....            | 129        |
| 4.6 Control Algorithms.....                  | 130        |
| 4.7 Results and Discussion .....             | 131        |
| 4.8 Conclusions.....                         | 135        |
| Acknowledgments .....                        | 137        |
| References.....                              | 137        |

|   |            |
|---|------------|
| <b>Chapter 5. Extensive Experiments on Genetic Algorithms for the Optimization of Piezoelectric Actuator Locations through Parallel Computation .....</b> | <b>156</b> |
| 5.1 Abstract.....   | 156        |
| 5.2 Introduction.....   | 157        |
| 5.3 Genetic Algorithms.....   | 158        |
| 5.4 Problem Definition .....  | 161        |
| 5.5 Finite Element Modeling.....  | 166        |
| 5.6 Control Algorithms.....   | 166        |
| 5.7 Results and Discussions.....  | 167        |
| 5.8 Conclusions .....   | 208        |
| References.....   | 210        |
| <b>Chapter 6. Summary and Conclusions .....</b>   | <b>214</b> |
| 6.1 Major contributions .....   | 214        |
| 6.2 Perspective and Future directions.....  | 216        |
| <b>Appendix A. Optimization of Piezoelectric Actuator Locations by Finite Element Method and Genetic Algorithms .....</b>                                 | <b>218</b> |
| A.1 Abstract.....   | 218        |
| A.2 DeLorenzo’s algorithm .....   | 219        |
| A.3 Genetic Algorithms.....   | 219        |
| A.4 Case Studies .....  | 220        |
| A.5 Major Conclusions .....   | 225        |
| <b>Appendix B. Integration by Parts.....</b>  | <b>227</b> |

|   |            |
|---|------------|
| <b>Appendix C. Vector Cross Product, Area of the Triangle, Differential Area and<br/>Volume Element .....</b>                                 | <b>228</b> |
| <b>Appendix D. Geometrical Verification of the Relations between the Cartesian<br/>Coordinates and Area Coordinates of the Triangle .....</b> | <b>230</b> |
| <b>Appendix E. Exact Integration of a Polynomial Term in terms of Area Coordinates<br/>over the Triangular Region.....</b>                    | <b>231</b> |
| <b>Appendix F. Shape Functions and Their Derivatives of Linear Strain Triangular<br/>Element (Quadratic Triangular Element).....</b>          | <b>232</b> |
| <b>Appendix G. Derivation of the True Rotation in the Theory of Elasticity in the Allman<br/>Triangular Element .....</b>                     | <b>234</b> |
| <b>Appendix H. Slope at the Mid-Span of Cubic Beam Element .....</b>  | <b>238</b> |
| <b>Appendix I. Shape Functions and Their Derivatives of Discrete Kirchhoff Triangular<br/>(DKT) Element.....</b>                              | <b>239</b> |
| <b>References.....</b>  | <b>244</b> |
| <b>Vita .....</b>   | <b>276</b> |



## List of Figures

|  |     |
|--|-----|
| Figure 2.1 Cartesian coordinate systems $xyz$ and $x'y'z'$ .....   | 34  |
| Figure 2.2 Positive rotation of principal material axes from $xy$ axes .....   | 36  |
| Figure 2.3 Cartesian coordinate systems $xyz$ and $x'y'z'$ .....   | 38  |
| Figure 2.4 a) Area coordinates b) Natural coordinates .....  | 40  |
| Figure 2.5 Area coordinates along the side of the triangle .....   | 42  |
| Figure 2.6 The Pascal triangle .....   | 43  |
| Figure 2.7 A general triangular element .....  | 44  |
| Figure 2.8 a) Quadratic triangular element b) Cubic triangular element .....   | 44  |
| Figure 2.9 Relation between the area coordinates and natural coordinates .....   | 46  |
| Figure 2.10 a) Nodal d.o.f. of the Allman triangle b) Parabolic edge displacement created<br>by d.o.f. $\omega_2$ and $\omega_3$ c) D.o.f. of the linear strain triangle (LST) ..... | 53  |
| Figure 2.11 Definitions of variables in the formulation of the DKT element .....   | 61  |
| Figure 2.12 Relation between $\beta_x, \beta_y$ and $\beta_n, \beta_s$ .....   | 62  |
| Figure 2.13 Relation between $w_n, w_s$ and $\theta_x, \theta_y$ .....   | 63  |
| Figure 2.14 Geometry of the triangular element .....   | 64  |
| Figure 2.15 Local and global coordinate systems for a triangular element .....   | 76  |
| Figure 3.1 a) Piezoelectric actuator candidate locations b) Finite element mesh .....  | 115 |
| Figure 3.2 Performance of the GAs versus the number of evaluations on a) thermal load T1<br>b) thermal load T2; c) thermal load T3; and d) thermal load T4 .....                     | 116 |
| Figure 3.3 Optimal location for the thermal load T1 obtained by a) DeLorenzo algorithm<br>b) GA Version 1; c) GA Version 2, run1; and d) GA Version 2, run2 .....                    | 117 |
| Figure 3.4 Optimal location for the thermal load T2 obtained by a) DeLorenzo algorithm   |     |

|   |     |
|---|-----|
| b) GA Version 1; c) GA Version 2, run1; and d) GA Version 2, run2 .....                   | 118 |
| Figure 3.5 Optimal location for the thermal load T3 obtained by a) DeLorenzo algorithm    |     |
| b) GA Version 1; c) GA Version 2, run1; and d) GA Version 2, run2 .....                   | 119 |
| Figure 3.6 Optimal location for the thermal load T4 obtained by a) DeLorenzo algorithm    |     |
| b) GA Version 1; c) GA Version 2, run1; and d) GA Version 2, run2 .....                   | 120 |
| Figure 3.7 Performance of the GAs versus the number of evaluations a) and Optimal         |     |
| location for the thermal loads T1, T2, T3, and T4 obtained by b) GA Version 1             |     |
| c) GA Version 2, run1; and d) GA Version 2, run2 .....                                    | 121 |
| Figure 3.8 Optimal location for the thermal load T1 obtained using Version 2 with 30000   |     |
| evaluations. Note that for the thermal load T1, the RMS error has reduced by              |     |
| 11.3% .....   | 122 |
| Figure 3.9 Optimal location for the thermal loads T1, T2, T3, and T4 obtained using       |     |
| Version 2 with 20000 evaluations .....  | 122 |
| Figure 4.1 a) Piezoelectric actuator candidate locations b) Finite element mesh .....     | 139 |
| Figure 4.2 Performance of the GAs: The RMS error vs the number of evaluations for the     |     |
| first optimization problem for the case of, a) thermal load T1, b) thermal load T2        |     |
| c) thermal load T3, and d) thermal load T4 ( 30 actuators ) .....                         | 140 |
| Figure 4.3 Performance of the GAs: Maximum of the four minimum RMS errors vs. the         |     |
| number of evaluations for the second optimization problem ( 30 actuators ) ...            | 141 |
| Figure 4.4 Optimal location, obtained by a) GA Version 3, run1; b) GA Version 3, run2     |     |
| ( 30 actuators), for the first optimization problem for each of the four thermal          |     |
| loads .....   | 142 |
| Figure 4.5 Optimal location for the second optimization problem obtained by a) GA Version |     |

|   |     |
|---|-----|
| 3, run1; b) GA Version 3, run2 ( 30 actuators ) .....   | 143 |
| Figure 4.6 Performance of the GAs: The RMS error vs the number of evaluations for the first optimization problem for the case of, a) thermal load T1, b) thermal load T2 c) thermal load T3, and d) thermal load T4 ( 121 actuators ) ..... | 144 |
| Figure 4.7 Performance of the GAs: Maximum of the four minimum RMS errors vs the number of evaluations for the second optimization problem ( 121 actuators ) ..   | 145 |
| Figure 4.8 Optimal location, obtained by the DeLorenzo's algorithm (121 actuators), for the first optimization problem for each of the four thermal loads .....   | 146 |
| Figure 4.9 Optimal location, obtained by a) GA Version 3, run1; b) GA Version 3, run2 ( 121 actuators ), for the first optimization problems for each of four thermal loads .....   | 147 |
| Figure 4.10 Optimal location for the second optimization problem obtained by a) GA Version 3, run1; b) GA Version 3, run2 ( 121 actuators ) .....   | 148 |
| Figure 5.1 The flow chart for the micro-GAs .....   | 160 |
| Figure 5.2 a) Piezoelectric actuator candidate locations b) Finite element mesh .....   | 162 |
| Figure 5.3 a) The thermal loads T1 and T2 .....   | 164 |
| Figure 5.3 b) The thermal loads T3 and T4 .....   | 165 |
| Figure 5.4 a) Performance of the GAs: Maximum of the four minimum RMS errors vs. the number of evaluations ( 30 actuators, seed#1 ) .....   | 169 |
| Figure 5.4 b) Performance of the GAs: Maximum of the four minimum RMS errors vs. the number of evaluations ( 30 actuators, seed#2 ) .....   | 170 |
| Figure 5.5 RMS error and Optimal location of piezoelectric actuators obtained by GA Version 3 ( 30 actuators ) .....  | 172 |

|  |     |
|--|-----|
| Figure 5.6 a) Performance of the GAs: Maximum of the four minimum RMS errors vs. the number of evaluations ( 121 actuators, seed#1 ) ..... | 176 |
| Figure 5.6 b) Performance of the GAs: Maximum of the four minimum RMS errors vs. the number of evaluations ( 121 actuators, seed#2 ) ..... | 177 |
| Figure 5.7 RMS error and Optimal location of piezoelectric actuators obtained by GA<br>Version 3 ( 121 actuators ) .....                   | 179 |
| Figure 5.8 a) Performance of the GAs: Maximum of the four minimum RMS errors vs. the number of evaluations ( 15 actuators, seed#1 ) .....  | 185 |
| Figure 5.8 b) Performance of the GAs: Maximum of the four minimum RMS errors vs. the number of evaluations ( 15 actuators, seed#2 ) .....  | 186 |
| Figure 5.9 RMS error and Optimal location of piezoelectric actuators obtained by GA<br>Version 3 ( 15 actuators ) .....                    | 188 |
| Figure 5.10 a) Performance of the GAs: Maximum of the four minimum RMS errors vs. the number of evaluations ( 60 actuators, seed#1 ) ..... | 191 |
| Figure 5.10 b) Performance of the GAs: Maximum of the four minimum RMS errors vs. the number of evaluations ( 60 actuators, seed#2 ) ..... | 192 |
| Figure 5.11 RMS error and Optimal location of piezoelectric actuators obtained by GA<br>Version 3 ( 60 actuators ) .....                   | 194 |
| Figure 5.12 a) Performance of the GAs: Maximum of the four minimum RMS errors vs. the number of evaluations ( 90 actuators, seed#1 ) ..... | 200 |
| Figure 5.12 b) Performance of the GAs: Maximum of the four minimum RMS errors vs. the number of evaluations ( 90 actuators, seed#2 ) ..... | 201 |
| Figure 5.13 RMS error and Optimal location of piezoelectric actuators obtained by GA   |     |

|   |     |
|---|-----|
| Version 3 ( 90 actuators ) .....  | 203 |
| Figure A.1 Performance of the GAs versus the number of evaluations on thermal load T1,<br>T2, T3, and T4, respectively .....                        | 220 |
| Figure A.2 a) Optimal locations for the thermal load T1 and T2 obtained by DeLorenzo<br>algorithm and Genetic Algorithms ( 30 actuators ) .....     | 221 |
| Figure A.2 b) Optimal locations for the thermal load T3 and T4 obtained by DeLorenzo<br>algorithm and Genetic Algorithms ( 30 actuators ) .....     | 222 |
| Figure A.3 a) Optimal locations for the thermal load T1 and T2 obtained by DeLorenzo<br>algorithm and Genetic Algorithms ( 121 actuators ) .....    | 223 |
| Figure A.3 b) Optimal locations for the thermal load T3 and T4 obtained by DeLorenzo<br>algorithm and Genetic Algorithms ( 121 actuators ) .....    | 224 |
| Figure A.4 Optimal locations for the thermal load T3 and T4 obtained by Genetic<br>Algorithms ( 60 actuators and 90 actuators ) .....               | 225 |
| Figure C.1 Vector $\vec{A}$ and $\vec{B}$ in the plane of the triangle .....  | 228 |
| Figure D.1 Cartesian Coordinates and Area Coordinates of the triangle .....   | 230 |
| Figure F.1 Linear strain triangular element (Quadratic triangular element) in (a) area<br>coordinate system and (b) natural coordinate system ..... | 232 |
| Figure G.1 $\gamma$ definition along the sides of the triangle .....  | 234 |
| Figure H.1 Cubic beam element .....   | 238 |
| Figure I.1 Node locations of quadratic triangular element .....   | 239 |
| Figure I.2 Positive directions of $\beta_x$ and $\beta_y$ in 2D view .....  | 239 |

## List of Tables

|           |  |     |
|-----------|--|-----|
| Table 2.1 | Direction cosines between the two sets of axes .....   | 34  |
| Table 2.2 | Sampling points and weights in Gauss integration .....   | 49  |
| Table 2.3 | Gauss Integration for the triangular region .....  | 51  |
| Table 2.4 | Direction cosines between the two sets of axes .....   | 62  |
| Table 2.5 | Direction cosines between the two sets of axes .....   | 63  |
| Table 3.1 | Properties and geometry of the mirror and piezoelectric actuators .....                                  | 106 |
| Table 3.2 | Temperature distributions at the lower surface of the mirror .....                                       | 106 |
| Table 3.3 | Optimal voltages corresponding to optimal location (see Figure 3.9) for thermal<br>load type T1 .....    | 111 |
| Table 3.4 | Optimal voltages corresponding to optimal location (see Figure 3.9) for thermal<br>load type T2 .....    | 111 |
| Table 3.5 | Optimal voltages corresponding to optimal location (see Figure 3.9) for thermal<br>load type T3 .....    | 112 |
| Table 3.6 | Optimal voltages corresponding to optimal location (see Figure 3.9) for thermal<br>load type T4 .....    | 112 |
| Table 4.1 | Properties and geometry of the mirror and piezoelectric actuators .....                                  | 149 |
| Table 4.2 | Temperature distributions at the lower surface of the mirror .....                                       | 149 |
| Table 4.3 | Optimal voltages corresponding to optimal location (see Figure 4.5 b)) for thermal<br>load type T1 ..... | 150 |
| Table 4.4 | Optimal voltages corresponding to optimal location (see Figure 4.5 b)) for thermal<br>load type T2 ..... | 150 |
| Table 4.5 | Optimal voltages corresponding to optimal location (see Figure 4.5 b)) for thermal                       |     |

|   |     |
|---|-----|
| load type T3 .....  | 151 |
| Table 4.6 Optimal voltages corresponding to optimal location (see Figure 4.5 b)) for thermal load type T4 .....                         | 151 |
| Table 4.7 Optimal voltages corresponding to optimal location (see Figure 4.10 a)) for thermal load type T1 .....                        | 152 |
| Table 4.8 Optimal voltages corresponding to optimal location (see Figure 4.10 a)) for thermal load type T2 .....                        | 153 |
| Table 4.9 Optimal voltages corresponding to optimal location (see Figure 4.10 a)) for thermal load type T3 .....                        | 154 |
| Table 4.10 Optimal voltages corresponding to optimal location (see Figure 4.10 a)) for thermal load type T4 .....                       | 155 |
| Table 5.1 The main differences among the regular GAs, micro-GAs version 1, micro-GAs version 2 and micro-GAs version 3 .....            | 161 |
| Table 5.2 Properties and geometry of the mirror and piezoelectric actuators .....   | 163 |
| Table 5.3 Temperature distributions at the lower surface of the mirror .....  | 163 |
| Table 5.4 RMS errors corresponding to optimal placement (30 actuators) .....  | 168 |
| Table 5.5 Optimal voltages corresponding to optimal location (see Figure 5.5 upper left) for thermal load type T1. (30 actuators) ..... | 173 |
| Table 5.6 Optimal voltages corresponding to optimal location (see Figure 5.5 upper left) for thermal load type T2. (30 actuators) ..... | 173 |
| Table 5.7 Optimal voltages corresponding to optimal location (see Figure 5.5 upper left) for thermal load type T3. (30 actuators) ..... | 174 |
| Table 5.8 Optimal voltages corresponding to optimal location (see Figure 5.5 upper left) for thermal load type T4. (30 actuators) ..... | 174 |

|            |  |     |
|------------|--|-----|
| Table 5.9  | RMS errors corresponding to optimal placement (121 actuators) .....  | 175 |
| Table 5.10 | Optimal voltages corresponding to optimal location (see Figure 5.7 upper left)<br>for thermal load type T1 (121 actuators) ..... | 180 |
| Table 5.11 | Optimal voltages corresponding to optimal location (see Figure 5.7 upper left)<br>for thermal load type T2 (121 actuators) ..... | 181 |
| Table 5.12 | Optimal voltages corresponding to optimal location (see Figure 5.7 upper left)<br>for thermal load type T3 (121 actuators) ..... | 182 |
| Table 5.13 | Optimal voltages corresponding to optimal location (see Figure 5.7 upper left)<br>for thermal load type T4 (121 actuators) ..... | 183 |
| Table 5.14 | RMS errors corresponding to optimal placement (15 actuators) .....   | 184 |
| Table 5.15 | Optimal voltages corresponding to optimal location (see Figure 5.9 upper left)<br>for thermal load type T1 (15 actuators) .....  | 189 |
| Table 5.16 | Optimal voltages corresponding to optimal location (see Figure 5.9 upper left)<br>for thermal load type T2 (15 actuators) .....  | 189 |
| Table 5.17 | Optimal voltages corresponding to optimal location (see Figure 5.9 upper left)<br>for thermal load type T3 (15 actuators) .....  | 189 |
| Table 5.18 | Optimal voltages corresponding to optimal location (see Figure 5.9 upper left)<br>for thermal load type T4 (15 actuators) .....  | 189 |
| Table 5.19 | RMS errors corresponding to optimal placement (60 actuators) .....   | 190 |
| Table 5.20 | Optimal voltages corresponding to optimal location (see Figure 5.11 upper left)<br>for thermal load type T1 (60 actuators) ..... | 195 |
| Table 5.21 | Optimal voltages corresponding to optimal location (see Figure 5.11 upper left)<br>for thermal load type T2 (60 actuators) ..... | 196 |



|            |  |     |
|------------|--|-----|
| Table 5.22 | Optimal voltages corresponding to optimal location (see Figure 5.11 upper left)<br>for thermal load type T3 (60 actuators) ..... | 197 |
| Table 5.23 | Optimal voltages corresponding to optimal location (see Figure 5.11 upper left)<br>for thermal load type T4 (60 actuators) ..... | 198 |
| Table 5.24 | RMS errors corresponding to optimal placement (90 actuators) .....   | 199 |
| Table 5.25 | Optimal voltages corresponding to optimal location (see Figure 5.13 upper left)<br>for thermal load type T1 (90 actuators) ..... | 204 |
| Table 5.26 | Optimal voltages corresponding to optimal location (see Figure 5.13 upper left)<br>for thermal load type T2 (90 actuators) ..... | 205 |
| Table 5.27 | Optimal voltages corresponding to optimal location (see Figure 5.13 upper left)<br>for thermal load type T3 (90 actuators) ..... | 206 |
| Table 5.28 | Optimal voltages corresponding to optimal location (see Figure 5.13 upper left)<br>for thermal load type T4 (90 actuators) ..... | 207 |
| Table 5.29 | RMS error from all cases of actuators (best results only) .....  | 208 |

## **Chapter 1. Introduction**

Over the last two decades, the area of multidisciplinary adaptive/intelligent/smart structures and systems has been studied extensively under numerous programs sponsored by US Army, Air Force, Navy, Defense Agency, NASA, NSF, etc. Much of the work has been focused on shape control, vibration control, buckling control, acoustic reduction, aeroelastic control, aerodynamic and hydrodynamic flow control, optimization of lifting surfaces, structural health monitoring, active damping, new smart materials, sensors, actuators development, smart systems modeling, robust control techniques, and multidisciplinary optimization techniques. The systems range from next generation telescopes to antenna, fixed wing aircraft, rotary-wing helicopters, spacecraft, missiles, submarines, automobiles, civil structures, and medical systems.

The structure for our study is a thin hexagonal spherical primary mirror of the next generation astronomical telescope. The mirror has adaptability to its changing thermal environments through the control of distributed piezoelectric actuators. It is well-known that the effectiveness of the control system strongly depends on the actuator locations. However, the problem of the optimal placement of actuators is hard to solve, especially for a large number of actuators.

This dissertation is focused on solving this challenging problem. We propose a solution methodology, which combines the finite element analysis and genetic algorithms. In this chapter, we first review some basic concepts in finite element method and genetic algorithms, along with the research on smart structures. Then we present the objective and scope of present research.

### **1.1 Finite Element Method**

The finite element method has become one of the universally adopted methods for the analysis of general structural and continuum problems. The finite element analysis in many applications has become both routine and essential in engineering design. This is an approximate method in which the structure or the continuum is divided into small pieces of various shapes, sizes and types which are then assembled together using compatibility of displacements and equilibrium of forces to form an approximate mathematical model. The finite element method is used extensively in Aerospace, Automobile, Civil, Naval, and other applications.

An approach similar to the finite element method, involving the use of piecewise continuous trial functions defined over triangular regions, was first suggested by Courant in 1943. The original formulation of the finite element method was presented by Turner, et al. in 1956. The name finite element was coined by Clough in 1960. The more information about the history of finite element method can be found in the references [ Zienkiewicz and Taylor, 2000, Cook, et al., 2002, Yang, 1986, etc.].

### **1.1.1 Some basic Concepts of Finite Element Method.**

#### **Convergence**

Requirements for the convergence are described in the following.

*Continuity/compatibility requirement:* If the  $n$ th-order derivative of a function occurs in the integral form then the function has to be such that its  $n - 1$ st derivative is continuous ( $C_{n-1}$  continuity) within the elements and across the element boundaries. Physically, this requirement ensures that no gaps or overlaps occur between elements when the assemblage is performed. From a variational viewpoint, this requirement means that there is no strain energy gained or lost at the interface.

*Completeness requirement:* If the  $n$ th-order derivative of a function occurs in the integral form then the function has to be such that a constant value of the  $n$ th-order derivative is attainable in the element domain when the size of the element tends to zero. If the function is approximated by a polynomial this requirement means that the function has to be complete up to the  $n$ th order. In the displacement-based finite element method this requirement means that the displacement functions of the element must be able to represent the rigid body displacements and the constant strain states, including the condition of zero strain under rigid-body motion.

If each element in a model satisfies strain completeness (that is, assumed displacement functions contain zero strain under rigid body translations and rotations, and constant strain modes), and the model is a compatible one (internal compatibility, nodal compatibility, and inter-element boundary compatibility are all satisfied), the results will converge monotonically and will be a lower bound. On the other hand, if each element in a model satisfies stress completeness (that is, assumed stress functions contain zero stress and constant stress modes), and the model is in equilibrium (internal equilibrium, nodal equilibrium, and inter-element boundary equilibrium all satisfied), the results will converge monotonically and will be an upper bound. If the elements are complete but the model is a non-compatible or non-equilibrated one, the results may still converge but, in general, they will converge non-monotonically.

The completeness requirement for an individual element (element completeness test) is said to be satisfied if the constant strain/stress states and the rigid body modes are represented.

In the context of Kirchhoff/thin plate bending, the presence of the second derivatives of

the transverse deflection  $w$  in the internal work indicates that  $w$  should be  $C_1$  continuous at element interface. This means that along element interfaces we must have continuity of  $w$  as well as that of  $\frac{\partial w}{\partial n}$ , the derivative of  $w$  normal to the interface. However, it is difficult to implement the  $C_1$  compatibility. In fact, it is impossible to specify simple polynomial expressions for shape functions ensuring full  $C_1$  compatibility when only  $w$  and its first derivatives are prescribed at corner nodes. In the context of Kirchhoff/thin plate bending, the completeness means that  $w$  has to be complete up to 2<sup>nd</sup> order polynomial. Therefore, the terms 1,  $x$ ,  $y$ ,  $x^2$ ,  $xy$ , and  $y^2$  must be included in the expression for  $w$ , which is capable of representing rigid body, constant slope, and constant curvature states of deformation. If the element satisfies the compatibility and completeness requirements we can be sure that successive solutions obtained from element mesh refinement will converge monotonically to the correct displacements and stresses. Note that  $C_1$  continuity is not always a necessary condition for convergence. If such non-conforming elements satisfy the patch test then convergence will still occur. Experience indicates that convergence is more dependent on the completeness than on the compatibility of the element [Huebner, et al. 2001].

Similarly, it is easy to show that only  $C_0$  continuity is required for the Reissner-Mindlin/thick plate. Though it is easy to implement  $C_0$  continuity, there exists the so-called locking problem that is hard to solve for lower-order  $C_0$  elements.

### **Patch test and benchmark/test problems**

For the results for non-compatible or non-equilibrated models to converge, it is necessary that an assemblage of elements can also represent the constant strain or stress states. It must be realized that although an individual element may contain the constant strain or stress states an assemblage of the same elements may not do so for non-compatible or non-

equilibrium models. To check whether or not an assemblage of elements can represent the constant states the patch test was proposed by Irons [Zienkiewicz and Taylor, 2000]. The test consists of the following:

1. Assemble a group (patch) of elements with, at least, one internal node
2. Apply a system of forces or displacements and constraints to the external boundary nodes only which are consistent with a state of constant stress or strain
3. If the same constant state of stress or strain occurs in each element of the patch then it is assumed that any patch of the same elements will behave well in a general structure in a constant stress/strain field

The patch test is a completeness condition for an assemblage of elements as against an individual element. It has been found that the patch test may be passed by one kind of geometries or meshes but failed by the others. Therefore, it is important for the patch test to be performed on the different geometries or meshes before the element is claimed to have passed the patch test.

Since its first introduction by Irons [Bazeley, et al., 1966], the patch test has been analyzed, discussed, and reinterpreted at length [Zienkiewicz and Taylor, 1997]. The basic idea was that in the limit of decreasing mesh size the nonconforming finite element solution to the given problem posed on an arbitrary patch of elements should be able to represent the appropriate constant strain states (constant curvature for plate bending). A patch includes one or more finite elements which share some common interfaces. Note that in this definition even a single element constitutes a patch. Patch test is used to determine if a given nonconforming element (inter-element continuity was violated) is permissible. The nonconforming element may be successful, but only for one particular mesh pattern. It would

be wrong to leave the impression that the only interesting elements are those that pass the test. Patch test contains a single element patch and multi-element patch test in which at least one node is an internal node. Patch test tests both the consistency and stability of finite element equations [Zienkiewicz and Taylor, 2000].

The simple patch account immediately indicates which elements fail and which have a chance of success. The count condition [ $n_\theta + n_w \geq n_s$  and  $n_s \geq n_w$ , where  $n_w$ ,  $n_\theta$ , and  $n_s$  are the number of deflection, rotation and shear force variables, respectively. Zienkiewicz and Taylor, 2000] is necessary but not sufficient to define successful elements and numerical testing is always needed. The failure of the patch account test means that under some circumstances the element will fail. However, in many problems a reasonable performance can still be obtained and a non-singularity will be observed in the performance, provided consistency is also satisfied.

The accuracy of the finite elements is of primary concern. A standard set of problems to test finite element accuracy of shell elements was proposed [MacNeal and Harder, 1985].

### **Spurious modes/rank deficiencies and Locking problems**

The problems occur for the low order pure displacement finite elements if additional constraints need to be satisfied. In the extreme case these constraints may restrict the solution to such a degree that only a trivial solution will be obtained. In the other case locking effects may be present, which means that the finite element solution will ultimately converge, but the rate of convergence is drastically reduced so that the computational costs become unacceptable. Locking results from the relative inability of the finite element space to approximate the exact solution which is constrained in the analysis of beams, plates and shells or incompressible media where the poisson's ratio approaches 0.5.

Mindlin elements can exhibit spurious transverse shear stiffness (or locking) as the plate become thin. The spurious transverse shear stiffness arises from an interpolation inconsistency that the Kirchhoff condition from being satisfied as the plate becomes thin. The spurious shear stiffness can be alleviated by using a reduced/selective integration to compute certain terms in the element stiffness matrix, or by using higher-order elements. Although the reduced integration solution is the most economical alternative, such inexact integration can result in an element stiffness matrix rank deficiencies that have an excess number of zero eigenvalues and the corresponding spurious displacement modes (i.e. deformation modes that result in zero strain at the Gauss integration points) [Hughes, 1977]. These spurious deformation modes can be superimposed on the true displacement solution and make the solution meaningless. Thus, the elements with spurious modes must be used with care.

Locking can also result from the element distortions. Both membrane locking and shear locking can occur in the shell finite element analysis. The locking phenomenon can be alleviated by using higher-order elements(Lagrangian, not serendipity), extremely fine mesh, reduced and selective integration—whether the rank of the element stiffness matrix is less than (number of nodal degrees of freedom) minus (feasible rigid-body motions), which tests whether a single element can have spurious zero energy modes, assumed strain method, enhanced assumed strain methods, mixed interpolation, linked interpolation, patch account test, drilling degrees of freedom (vertex rotations), robust element, hybrid/mixed finite element formulation and higher order shear deformation theories.

### **Singularities**

A singularity may occur with the mesh refinement at some points such as the obtuse corners of the Morley skew plate [Huebner, et al., 2001]. The finite element solution



converges to the solution of corresponding mathematical model. Theoretically, what is not allowed [Hartmann and Katz, 2004]:

Kirchhoff plate: single moments;

Reissner-Mindlin plate: point loads, single moments;

Plates (2-D elasticity): point loads;

Elastic solids (3-D elasticity): point loads, line loads.

At these points the finite element solution for displacements and stresses will increase without limit with the mesh refinement. Of course, a concentrated force is a convenient mathematical tool. All real forces are distributed over an area greater than zero. The easiest way to apply a concentrated force at a prescribed location is to arrange the FE mesh so that a node appears at this location. A concentrated moment load cannot be applied at a node unless the node includes the appropriate rotational d.o.f. If nodes have only translational d.o.f., a moment must be applied as couple-forces on a pair of nodes [Cook, 2002].

### **1.1.2 Advances of Plate and Shell Finite Elements**

Plates and Shells are a particular form of a three dimensional solid. The thickness of such structures is very small when compared with other dimensions, and complete three-dimensional treatment is not only costly but often leads to serious numerical ill-conditioning problems. Although the finite element analysis for plate and shell structures now spans over forty years, the establishment of reliable and efficient finite element models continues to be the subject of research effort at the present. An enormous amount of effort has been devoted to the development of finite elements for the plate and shell analysis. The literature is extensive and we will not make an attempt to review it here. Review of the many contributions on the subject is given in a number of survey papers and books [Yang, et al.,

1990, 2000, MacNeal, 1998, Zienkiewicz and Taylor, 2000, etc.].

In 1965, Irons and Draper noted that an expression for deflection  $w$  which assures uniqueness of the bending curvatures over the surface can not assure slope  $w_{,x}$  and  $w_{,y}$  continuity along the common edges of adjacent elements when only  $w$ ,  $w_{,x}$  and  $w_{,y}$  are prescribed at nodes. Therefore, it is impossible to specify simple polynomial expressions for shape functions ensuring full  $C^1$  continuity when only deflection and its slopes are prescribed at corner nodes [Zienkiewicz and Taylor, 2000]. However, a full conforming rectangular element with  $w$ ,  $w_{,x}$ ,  $w_{,y}$  and  $w_{,xy}$  prescribed at the corner nodes has been successfully developed by Bogner, et al. in 1966.

The hybrid and mixed finite elements were first studied by T. H. H. Pian in 1964. Although the motivation for the early developments in hybrid and mixed finite elements was to avoid the difficulty in  $C^1$  continuity problem, such elements are found to be effective in plate and shell bending problems, incompressible or nearly incompressible materials, crack, elastic-plastic and creep problems.

The Kirchhoff thin plate and shell theory is very widely used in practice and proves adequate for a large number of structural problems. The theory is based on the following assumptions:

- (i) Cross-sections normal to the middle plane remain plane during the deformation;
- (ii) The direct strain in the normal direction is zero;
- (iii) Plates and Shells are assumed to be in plane stress state;
- (iv) The normal to the middle plane remain normal to it during deformation.

It is obvious that the assumptions (ii) and (iii) are contradictory from the perspective of theory of elasticity. However, this inconsistency in approximation is acceptable for most

engineering applications.

By removing the fourth assumption, we get the Reissner-Mindlin thick plates and shells.

By replacing the assumptions (i) and (ii) with the assumption that the in-plane displacements be expanded as polynomial of  $z$  in the normal direction, we get the higher order shear deformation plate and shell theories.

By removing all of the assumptions and assuming that the in-plane and lateral displacements be expanded as polynomial of  $z$  in the normal direction, we get the so-called higher order shear deformation plate and shell theories that consider transverse shear deformation and transverse normal strain. These are actually three dimensional models.

The membrane elements with drilling d.o.f. have been considerably improved since Allman published his original work in 1984 [Allman, 1988, Fellipa, 2003].

The concept of discrete Kirchhoff constraints was first introduced by Wempner et al., Stricklin et al., and Dhatt in 1968-69. An interesting study of three-node plate bending finite elements with nine degrees of freedom was presented by Batoz et al. in 1980 where it was concluded that the discrete Kirchhoff triangular element (DKT) was the most reliable and efficient. The displacements of this element are cubic polynomials defined only along the sides and the independent rotations are quadratic over the triangle. The Kirchhoff condition of zero transverse shear strain is employed to link the displacements and rotations at certain points of the element only. A new explanation of the DKT element was presented by Zienkiewicz, et al. in the context of mixed formulations of Reissner-Mindlin thick plate elements using collocation constraints [Zienkiewicz and Taylor, 2000].

The potential of the conventional six-node shell finite element for practical application is limited, however, because the element does not match with other important elements such as

standard edge beams; modeling stiffened shell structures like airframes therefore presents serious problems. The practical requirement for general thin shells is a three-node triangular finite element with the complete six degrees of freedom at each vertex node, namely: three displacement components and three rotational components. This matches with other standard elements.

The equivalence of certain mixed finite element methods with displacement methods employing the reduced and selective integration was presented by Malkus and Hughes in 1978.

Various elements, presented by Bogner, et al., 1966, Stricklin, et. al, 1969, Dhatt, 1969, Specht, 1988, etc., for comparison of performance for the thin plate analysis can be found in Table 4.3 in the reference [Zienkiewicz and Taylor, 2000].

An effective shell finite element must be applicable to membrane- and bending-dominated shell problems. Ideally, the element shows optimal convergence characteristics in both problem areas. Elements formulated using pure displacement interpolations are effective in membrane-dominated situations but lock when bending is encountered. To arrive at a general shell finite element discretization, a mixed formulation is usually used. For the analysis of general shell problems, the MITC (mixed interpolation of tensorial components) shell elements are shown to be effective [Bathe, 1996].

The derivation of finite elements has evolved from direct stiffness method to variational methods (Ritz method, Lagrange multiplier, general variational principles) to weak forms of equilibrium equations (Galerkin weighted residual methods -- generalized finite element method). However, the fact that a finite element can be derived from a variational method or Galerkin weighted residual methods does not necessarily mean that the element is reliable.

The element shape functions should be capable of reproducing basic conditions of rigid body movement and constant strain states, as dictated by the patch test.

To get reliable FEA results, it is important to choose an appropriate mathematical model, appropriate elements, and appropriate meshes. It is helpful to note that no single element is likely to be best for all applications.

## **1.2 Genetic Algorithms**

Genetic algorithms belong to evolutionary computation. The evolutionary computation includes evolution strategies (Rechenburg, I., 1965), genetic algorithms (Holland, J., 1992, and Goldberg, D., 1989), evolutionary programming (Fogel, L., et al., 1966) and genetic programming (Koza, J., et al., 1999). Other adaptive search algorithms include simulated annealing (Kirkpatrick, S., et al., 1983), tabu search (Glover, F., 1997). Genetic algorithms (GAs) are defined as search procedures based on the mechanics of natural selection and genetics. Genetic algorithms as an optimization method have been applied to a number of fields. The general procedure of genetic algorithms is as follows.

### **GA procedure**

The first step we must perform to apply a genetic algorithm to a specific problem is to encode it as an artificial chromosome or chromosomes. These artificial chromosomes can be strings of 1s and 0s, parameter lists, permutation codes, real number, etc.

The second step that we must perform in solving a problem is to have some means or a procedure for discriminating good solutions from a bad solution. This is usually done by choosing a proper fitness function in the GA context, which is called an objective function in the optimization context. The function will be used by the genetic algorithm to guide the evolution of future generations.

After encoding the problem and choosing fitness function, we create an initial population of encoded solutions. The population can be created randomly or by using prior knowledge of possibly good solutions, but either way a key idea is that the GA will search from a population, not a single point.

After creating an initial population, we apply genetic operators to process the population iteratively to create a sequence of populations that hopefully will contain more and more good solutions as time goes on. There is a wide variety of the types of operators that are used in GAs, but quite often selection, crossover, and mutation are used.

Selection is based on the survival of the fittest principle of natural evolution. It can be accomplished in various ways, including weighted roulette wheels, local tournaments, various ranking schemes, etc. The key idea is to prefer better solutions to worse ones.

Crossover is a genetic operator that exchange bits and pieces of parental solutions to form new, possibly better offspring. Again, there are many ways of accomplishing this, including one point, two points, multiple points, uniform crossover, etc. The key idea is that the offspring will not be identical to any particular parent and will instead combine parental traits in a novel manner.

Mutation acts by simply modifying a single individual. There are many variations of mutation, but the key idea is that the offspring be identical to the parental individual except that one or more changes are made to an individual's trait.

Selection is a stochastic process where better solutions have a greater probability of survival and duplication. However, there generally remains a probability that some low quality of solutions may also pass through to the next generation. The reason is that such solutions may also contain information that could be of benefit at a later stage. A random

mutation is also introduced to perform small numbers of change to individuals. This supports diversity and exploration whilst preventing premature convergence of the system.

### **1.3 Adaptive/Intelligent/Smart Structures**

Although the classification of adaptive structures was suggested in a paper 1990 [Wada, et al., 1990] the following use of these concepts in the literature doesn't seem to strictly adhere to it. Instead, the three concepts of adaptive/intelligent/smart structures are often used interchangeably. Similarly do the terms of adaptive/intelligent/smart materials. In the dissertation we accepted the conventional use. The smart material generally designates a material that changes one or more of its properties in response to an external stimulus. The most popular smart materials are piezoelectric materials, electrostrictive materials, magnetostrictive materials, shape memory alloys, electrorheological fluids, and optical fibers. An adaptive/intelligent/smart structures can be viewed as a structure or system that is capable of a corresponding desired response to the changing external or internal environment such as external loads change or internal damage, etc. Thus, an adaptive structure is an integration of structure, sensors, actuators, and control systems. It is an emerging multidisciplinary area. The development of such structures depends on the advances of structures and materials, sensors and actuators, power electronics, digital signal processors, microprocessors, communication, and high performance computing technologies.

Numerous applications of smart-structures technology exist obviously such as shape control, vibration control, noise control, aeroelastic control, and health monitoring.

Applications range from space systems to fixed-wing and rotary wing aircraft, automotive, civil structures, machine tools, and medical systems. Much of the early development of smart-structures methodology was driven by space application such as vibration and shape

control of large flexible space structures, but now wider applications are envisaged for aeronautical and other systems. Embedded or surface-bonded smart actuators on an airplane wing or a helicopter blade, for example, can induce airfoil twist/camber change that in turn can cause a variation of lift distribution and can help to control static and dynamic aeroelastic problems.

### **1.3.1 Piezoelectric Actuators and Sensors**

Piezoelectric materials are the most popular smart materials. The typical piezoelectric materials include certain crystals such as quartz crystal and Rochelle salt, piezoelectric ceramics such as lead zirconate titanate (PZT), and piezoelectric polymer such as polyvinylidene fluoride (PVDF). Piezoelectricity, literally pressure electricity, is a property of these materials that develop a voltage when pressure is applied, and vice versa, produce deformation when a voltage is applied. The former is called the direct piezoelectric effect; the later is called the converse piezoelectric effect. The brothers Pierre and Jacques Curie discovered the direct piezoelectric effect in 1880 while studying crystals compressed in particular directions. The converse piezoelectric effect was predicted by the Gabriel Lippmann in 1881 and confirmed by the Curies that same year [Cady, 1964]. The direct and converse piezoelectric effects form a basis for the use of a piezoelectric material as a sensor and actuator, respectively. The common uses of piezoelectricity include in the devices such as electromechanical transducers, accelerometers, phonograph pickups, loudspeakers, sonar transmitters and receivers, and quartz crystal oscillators in clocks, watches, microprocessors, etc.

Piezoelectricity occurs naturally in some crystalline materials, such as quartz crystal and Rochelle salt. Piezoceramics are polycrystalline in nature and do not have piezoelectric



characteristics in their original state. Piezoelectric effects are induced in these materials through simple poling (application of high dc electric field at elevated temperatures results in polarization). The most commonly used piezoceramics is lead zirconate titanate (PZT). These are solid solutions of lead zirconate and lead titanate, often doped with other elements to obtain specific properties. These ceramics are manufactured by mixing together proportional amounts of lead, zirconium, and titanium oxide powders and heating the mixture to around 800–1000°C. They then react to form PZT perovskite aggregates, which are then milled into the PZT perovskite powder. This powder is mixed with a binder and sintered into the desired shape. During the cooling process, the material undergoes a paraelectric to ferroelectric phase transition at the Curie temperature and the cubic unit cell becomes tetragonal. As a result, the unit cell becomes elongated in one direction and yields an electric dipole. Due to randomly oriented ferroelectric domains, the unpoled ceramic has no net polarization [Chopra, 2002, Jordan and Ounaies, 2002].

Application of high electric field at elevated temperatures aligns most of the tetragonal domains in such a way that the polar axes of unit cells are oriented mostly parallel to the applied field. This process is called poling, and it imparts a permanent net polarization and mechanical deformation to the ceramic. Poling is performed in a silicon oil bath at an elevated temperature under a DC electric field of 1 to 3kV/mm.

Piezoceramic materials are linear at low electric fields and low mechanical stress levels; they show considerable nonlinearity at high values of electric field and mechanical stress. The piezoceramic material itself is mechanically isotropic, and by virtue of the poling process, is assumed transversely isotropic in the plane normal to the poling direction.

The most commonly used piezoelectric polymer is polyvinylidene fluoride (PVDF). The

PVDF consists of long chains of the repeating monomer ( $-CH_2 - CF_2 -$ ). The hydrogen atoms are positively charged and the fluorine atoms are negatively charged with respect to the carbon atoms and this leaves each monomer unit with an inherent dipole. PVDF film is manufactured by solidification of the film from a molten phase, which is then stretched in a particular direction and finally poled through the application of a strong electric field. In the liquid form the polymer has no net polarization because of randomly oriented polymer chains. After solidification, and stretching the film in one direction, the polymer chains are mostly aligned along the direction of stretching. This, combined with poling, imparts a net polarization to the film [Harrison and Ounaies, 2002].

The process of stretching the film, which orients the polymer chains in a specific direction, renders the material piezoelectrically orthotropic. The stretching direction is taken as the 1-direction.

The actuation strain can be modeled like an equivalent thermal strain. The constitutive relations are based on the assumption that the total strain in the actuator is the sum of the mechanical strain induced by the stress, the thermal strain caused by temperature, and the controllable actuation strain caused by the electric voltage. Assume that the axis 3 is in the direction of the initial polarization. For linear analysis, the piezoelectric actuator equations (the converse effect) are as follows,

$$\begin{Bmatrix} \varepsilon_1 \\ \varepsilon_2 \\ \varepsilon_3 \\ \gamma_{23} \\ \gamma_{31} \\ \gamma_{12} \end{Bmatrix} = \begin{bmatrix} S_{11} & S_{12} & S_{13} & 0 & 0 & 0 \\ S_{12} & S_{11} & S_{13} & 0 & 0 & 0 \\ S_{13} & S_{13} & S_{33} & 0 & 0 & 0 \\ 0 & 0 & 0 & S_{44} & 0 & 0 \\ 0 & 0 & 0 & 0 & S_{55} & 0 \\ 0 & 0 & 0 & 0 & 0 & S_{66} \end{bmatrix} \begin{Bmatrix} \sigma_1 \\ \sigma_2 \\ \sigma_3 \\ \tau_{23} \\ \tau_{31} \\ \tau_{12} \end{Bmatrix} + \begin{bmatrix} 0 & 0 & d_{31} \\ 0 & 0 & d_{32} \\ 0 & 0 & d_{33} \\ 0 & d_{24} & 0 \\ d_{15} & 0 & 0 \\ 0 & 0 & 0 \end{bmatrix} \begin{Bmatrix} E_1 \\ E_2 \\ E_3 \end{Bmatrix} + \begin{Bmatrix} \alpha_1 \\ \alpha_2 \\ \alpha_3 \\ 0 \\ 0 \\ 0 \end{Bmatrix} \Delta T$$

or

$$\begin{Bmatrix} \sigma_1 \\ \sigma_2 \\ \sigma_3 \\ \tau_{23} \\ \tau_{31} \\ \tau_{12} \end{Bmatrix} = \begin{bmatrix} C_{11} & C_{12} & C_{13} & 0 & 0 & 0 \\ C_{12} & C_{22} & C_{23} & 0 & 0 & 0 \\ C_{13} & C_{23} & C_{33} & 0 & 0 & 0 \\ 0 & 0 & 0 & C_{44} & 0 & 0 \\ 0 & 0 & 0 & 0 & C_{55} & 0 \\ 0 & 0 & 0 & 0 & 0 & C_{66} \end{bmatrix} \begin{Bmatrix} \varepsilon_1 \\ \varepsilon_2 \\ \varepsilon_3 \\ \gamma_{23} \\ \gamma_{31} \\ \gamma_{12} \end{Bmatrix} - \begin{bmatrix} 0 & 0 & e_{31} \\ 0 & 0 & e_{32} \\ 0 & 0 & e_{33} \\ 0 & e_{24} & 0 \\ e_{15} & 0 & 0 \\ 0 & 0 & 0 \end{bmatrix} \begin{Bmatrix} E_1 \\ E_2 \\ E_3 \end{Bmatrix} - \begin{Bmatrix} \lambda_1 \\ \lambda_2 \\ \lambda_3 \\ 0 \\ 0 \\ 0 \end{Bmatrix} \Delta T$$

The piezoelectric sensor equations (the direct effect) are as follows,

$$\begin{Bmatrix} D_1 \\ D_2 \\ D_3 \end{Bmatrix} = \begin{bmatrix} 0 & 0 & 0 & 0 & d_{15} & 0 \\ 0 & 0 & 0 & d_{24} & 0 & 0 \\ d_{31} & d_{32} & d_{33} & 0 & 0 & 0 \end{bmatrix} \begin{Bmatrix} \sigma_1 \\ \sigma_2 \\ \sigma_3 \\ \tau_{23} \\ \tau_{31} \\ \tau_{12} \end{Bmatrix} + \begin{bmatrix} e_{11}^\sigma & 0 & 0 \\ 0 & e_{22}^\sigma & 0 \\ 0 & 0 & e_{33}^\sigma \end{bmatrix} \begin{Bmatrix} E_1 \\ E_2 \\ E_3 \end{Bmatrix} + \begin{Bmatrix} a_1 \\ a_2 \\ a_3 \end{Bmatrix} \Delta T$$

where  $D_i$  is the electric displacement (charge per unit area) in coulombs/square meter,  $d_{ij}$  is the piezoelectric coefficients in meters/volt or coulombs/Newton, ( $e_{ij}$  is also the piezoelectric coefficients),  $e_{ij}^\sigma$  is the dielectric permittivity in newtons/square volt or farads/meter,  $S_{ij}$  is the elastic compliance matrix,  $C_{ij}$  is the stiffness matrix,  $\alpha_i$  is the thermal coefficient in 1/degrees Kelvin, ( $\lambda_i$  is also the thermal coefficients),  $a_i$  is the pyroelectric constants in newtons/volt-meter-degrees Kelvin,  $E_i$  is the applied electric field ( $V/t$ ) in volts/meter,  $\Delta T$  is the temperature change. For piezoelectric ceramics such as PZT,  $d_{31} = d_{32}$  and  $d_{15} = d_{24}$ ; for piezoelectric polymer such as PVDF,  $d_{31} \neq d_{32}$  and  $d_{15} \neq d_{24}$ . Normally, the converse effect is used to determine piezoelectric coefficients.

The maximum actuation strain of the PZT and PVDF is about 1000 microstrain and 700 microstrain, respectively. Most recently, strain levels more than 1.2% have been reported for the lead zirconate niobate and lead titanate (PZN-PT).

PVDF is flexible as opposed to PZT which is usually brittle. Most commonly used

sensors are piezofilm (PVDF) because of PVDF's low stiffness. Sometimes, piezoceramic (PZT) sensors are used for specific applications. It has been found that the performance of piezoelectric sensors surpasses that of conventional foil strain gages, with much less signal conditioning required, especially in applications involving low strain levels, and high noise levels.

It is not advisable to use piezoelectric sensors to measure strain above 150 microstrains because nonlinearities and change in material properties, especially  $d_{31}$ , with stress will affect the accuracy of the calibration. PVDF sensors are relatively sensitive to temperature compared with PZT sensor, and suitable temperature compensation must be included in measurements.

### **1.3.2 Advances in Smart Structures**

The area of adaptive/intelligent/smart structures has received significant attention since the late in 1980s. Numerous conferences and journals are dedicated to this high potential area for many technological revolutions. The literature in this multidisciplinary area has experienced tremendous growth. The comprehensive review of this field can be find in several excellent papers [Crawley, 1994, Sater, et. al., 2000, Chopra, 2002, etc.].

Crawley and de Luis in 1987 compared a variety of piezoelectric materials for possible use as actuators. A number of factors were used in the comparison, including embedability in composites, ratio of strain to applied voltage, and a performance criteria derived by maximizing the actuator effectiveness. The superiority of piezoelectric ceramics over other piezoelectric materials such as polymer film was conclusively demonstrated by this comparison.

A coupled thermal-piezoelectric-mechanical model was developed by Chattopadhyay, et

al. in 1999. A higher-order (third-order) shear deformation was used to capture the transverse shear effects in the moderately thick composite laminates. Numerical results show that the coupling could have significant effects on the static and dynamic response of some piezoelectric composite plates.

A completely coupled thermal-piezoelectric-mechanical theory, based on the improved layer wise displacement field and higher order electrical and temperature fields, was developed to study dynamic responses and control effects of smart composite shells [Chattopadhyay, et al., 2002]. The theory was implemented using a finite element technique that ensures the application to practical geometry and boundary conditions. Numerical analysis was conducted for simply-supported cylindrical shells with distributed self-sensing piezoelectric actuators. Comparisons were made with three dimensional NASTRAN solutions to verify the accuracy of the developed theory. Control authority was investigated using Linear Quadratic Gaussian (LQG) controller. Parametric studies were conducted to investigate the effects of the two-way coupling, actuator location and bending-torsion coupling and flexibility of the host structure.

Inflatable structures have special properties such as lightweight, low deflated volume, and high strength to-mass ratio. These remarkable properties make them suitable for cost-effective large space applications such as large solar antennas and optical mirrors. Finding optimal actuators and sensors is particularly important for these types of structures, as their vibration control and sensing require a large number of actuators and sensors, and their mode shapes are relatively complicated. Based on actuator and sensor performance indices, optimal locations and sizes of 5 actuators and 5 sensors for the vibration control of an inflated torus were determined by genetic algorithms so that the actuators and sensors provide good control

and sensing authorities in the considered modes. The simulation study indicated that actuators and sensors made of PVDF material can be used in the vibration control of an inflated torus [Jha and Inman, 2003].

Numerous analytical and computational models for linear static and dynamic response of smart structures using various theories was reviewed by Saravanos and Heyliger in 1999. Nonlinear finite element formulation of piezoelectric laminated plates undergoing large displacements and rotations was presented by Varelis and Saravanos in 2004. The coupled model uses both displacements and electric potential as field variables. The nonlinear static response of piezoelectric laminate under mechanical and electric loads was investigated by an eight-node element. The significance of the nonlinear effects in piezoelectric adaptive structures caused by large deformation was illustrated by the computational results.

The Defense Advanced Research Projects Agency (DARPA) has supported several programs with a focus on smart materials and structures such as Smart Rotor Program, Smart Wing program, and Smart Aircraft and Marine Propulsion System demonstration (SAMPSON) program. The primary focus of these programs has been to apply existing smart materials in an appropriate device form to reduce noise and vibration and to achieve aerodynamic and hydrodynamic flow control in a variety of structures. Achievement of the program objectives will potentially create paradigm shifts for the design of undersea vehicles, helicopter rotor blades, aircraft wings, and engine inlets [Sanders, et al., 2004].

The Smart Rotor Program, managed by the Boeing Company in Philadelphia, Pennsylvania, aimed to achieve active, real-time blade tracking adjustments through individual blade control by using smart materials and structures technology. The DARPA/AFRL/NASA Smart Wing program, performed by Northrop Grumman Corporation,

investigated techniques for wing twisting and camber control using smart structures. The overall objective of the smart wing program was to develop and demonstrate smart materials based control surface to improve the aerodynamic and aero-elastic performance of military aircraft. The demonstration of high actuation rate, large deformation, hinge-less, smoothly contoured control surfaces with chord-wise and span-wise shape variability represent an important milestone in the development and application of smart materials and structures technologies.

The SAMPSON program, conducted by the Boeing Company, Lockheed Martin Astronautics, General Dynamics, etc., is focused on both aircraft and undersea vehicle applications, with a specific interest in inlet shape control by applying smart materials based solutions.

More recently, the DARPA initiated another program -- Morphing air structures program. The program aims to create and advance enabling technologies and incorporate them into the design, build, and demonstration of a seamless, aero-efficient, radically shape changing vehicle during operation. A morphing wing is designed to drastically change wing geometric parameters such as aspect ratio, area, and twist to achieve truly multi-mission.

The National Aeronautics and Space Agency (NASA) Morphing project, led by the Langley Research Center, aims to develop and assess advanced technologies and integrated component concepts to enable efficient, multi-point adaptability in air and space vehicles. The three focus areas of the project are: adaptive structural morphing, micro-aero adaptive control, and biologically-inspired flight systems. These areas are supported by the core enabling areas of smart, nano and biologically-inspired materials, multi-disciplinary optimization, controls and electronics. An overview of NASA's Morphing Project as well as

highlights of recent results can be found in the reference [McGowan, et al., 2002].

#### **1.4 Objective and Scope of Present Research**

The dissertation is focused on one of the major research needs in the area of adaptive /intelligent/smart structures, that is, the development of finite element analysis and genetic algorithms optimization design for optimal placement of a large number of piezoelectric actuators on a thin hexagonal spherical primary mirror of the next generation astronomical telescope. First, we systematically derive and document the general flat triangular composite shell element under thermal and electric loads. Then we develop the genetic algorithms and combine the finite element analysis and the genetic algorithms for the optimization of piezoelectric actuator locations. Finally, we perform extensive experiments on genetic algorithms for the optimization of piezoelectric actuator locations through coarse-grain parallel computation to best understand genetic algorithms and to obtain the best design of smart structures. The following is the scope of remaining chapters.

In Chapter 2, after briefly reviewing the three most frequently used general approaches to derive the finite element formulation, we systematically present the key techniques associated with general shell finite element analysis using the flat shell elements by a combination of membrane element and plate bending element. The membrane element is obtained using the Cook's transformation from linear strain triangular element. It is clearly demonstrated that such an element is indeed the same as the Allman triangular element. The discrete Kirchhoff triangular element is chosen as plate bending element. Because of the high efficiency and accuracy of DKT element for thin plate bending analysis but lack of document for its derivation we present the detail derivation for DKT element. We present the geometrically nonlinear finite element formulation for general shell structures under the



combination of thermal and electrical loads.

In Chapter 3, we solve the two kinds of optimization problems of piezoelectric actuator locations in case of selecting 30 actuators from 193 candidate locations using our proposed methodology – combination of finite element analysis as an analyzer and genetic algorithms as an optimizer. We first find the optimal locations and optimal voltages for correcting thermal distortions caused by only one type of thermal loads. Then, we extend the optimization problems to the multi-objective optimization problems, that is, to determine just one set of actuator location for correcting thermal distortions caused by four different types of thermal loads. The advantages and disadvantage of genetic algorithms are presented. The genetic algorithms used in this chapter is GA version 2, which is developed from GA version 1 (see Appendix A) by mainly changing the mechanism of preserving the best solution and introducing the variable population in the genetic algorithms.

In Chapter 4, the more effective genetic algorithms, GA version 3, is developed from GA version 2 by mainly incorporating mutation and hill-climbing into micro-genetic algorithms. Using GA version 3, we resolve the two kinds of optimization problems studied in Chapter 3 and even larger problems of selecting 121 piezoelectric actuators from 193 candidate locations.

In Chapter 5, extensive numerical experiments are conducted on the multi-objective problems of the optimization of piezoelectric actuator locations using course grain parallel computing. The genetic algorithms used in this chapter is basically the same as the GA version 3 in Chapter 4 except we get results faster by reducing file operations. The time of investigation are significantly reduced by running multiple jobs at the same time on a Sun machine with 17 processors.

The major contributions, perspective and future directions are briefly summarized in Chapter 6. The feasibility investigation of using finite element analysis and genetic algorithms GA version 1 to optimize the piezoelectric actuator location is presented in Appendix A.

## Chapter 2. Finite Element Formulation

Basically, there are three most frequently used general approaches to derive the finite element formulation. The first approach is called the Galerkin weighted residual method, in which the original shape functions of the finite element are used as weights in the integral form or weak form of the differential equations (Not necessarily. The test functions may or may not be same as trial functions). The weak form is obtained by performing the integration by part of the integral form of the differential equations, obtained by multiplying the differential equations by so-called test functions, and integrating the resulting equations over the domain of the problem. The test functions generally satisfy the homogeneous part of the essential boundary condition. The integral form or the weak form forms the basis of finite element discretization.

The second approach is using the principle of virtual work i.e. the principle of virtual displacements, or alternatively the variational principle of total potential energy, either of which can be regarded as the basis of most frequently used displacement-based finite element method. Using the Galerkin procedure, it is easy to show that the principle of virtual work is precisely the weak form of the equilibrium equations. Because the variation of displacements can be regarded as virtual displacements, it is also easy to show that for conservative systems using the variational principle of minimum total potential energy is equivalent to using the principle of virtual work. It is important to note that the principle of virtual work is not same as the principle of total potential energy and that the principle of virtual work is more universal than the principle of total potential energy.

The last approach of the derivation of the finite element formulation is using general variational principles such as the Hu-Washizu variational principle, which can be derived

from the variational principle of total potential energy using Lagrange multiplier method.

The Hu-Washizu variational principle can be regarded as a generalization of the principle of virtual displacements, in which variations are performed on all unknown displacements, strains, stresses, and unknown surface tractions. The Hu-Washizu variational principle and its derivatives such as Hellinger-Reissner variational principles form the basis of mixed finite element methods, in which the strains and stresses can also be used as the unknown variables as displacements.

The mixed finite element formulations derived using either Galerkin weighted residual method from reducible differential equations or general variational principles are found to be effective in the analysis of plates and shells and incompressible media. The first approach - Galerkin weighted residual method has found wide applications in heat transfer, fluid mechanics, various field problems and also in the analysis of plates and shells and incompressible media. The last two approaches have been extensively used in solid mechanics. Using the natural variational principle will always produce a symmetric stiffness matrix for linear problems and in these cases Galerkin and variational procedures will produce the same results. It is well known that the natural variational principles do not exist for all the physical problems in which well-defined differential equations may be formulated. In this sense it seems that the Galerkin process has a greater range of applicability. However, there is another category of variational principles which can always be constructed for any set of differential equations by the Lagrange multiplier method. Therefore, we can derive the finite element formulation using either Galerkin procedure or variational procedure, and which procedure to choose depends on which one is more convenient for the specific problem or user's preference.

In this chapter, we will use the second approach, that is, the principle of virtual work, to derive the finite element formulation. It is important to note that for all of the approaches the key step is the assumption of the solution in the form of trial functions.

## 2.1 Galerkin weighted residual method, principle of virtual work and general variational principles

### Galerkin weighted residual method

Given a set of differential equations of a problem  $A(u) = 0$  in  $V$ , the integral form of the differential equations is

$$\int_V v^T A(u) dV = 0 \quad (2.1a)$$

where  $v$  is a set of arbitrary functions (called test functions) satisfying the homogeneous essential boundary conditions and  $u$  is chosen to satisfy the essential boundary conditions.

Integrating the left side of the equations by parts (see Appendix B) and applying the boundary conditions we can get the weak form of the differential equations

$$\int_V C(v)^T D(u) dV + \int_{S_p} E(v)^T F(u) dS = 0 \quad (2.1b)$$

where  $S_p$  is that part of the boundary on which natural or force boundary conditions are specified. In eqn. (2.1b), a lower order of continuity is required in the choice of the function used to express  $u$ . This is achieved at a price of requiring higher continuity for the  $v$  function (the test function).

The finite element approximation  $u$  is expressed as

$$u = \sum_{i=1}^n N_i a_i = Na \quad (2.2)$$

where  $N_i$  are shape functions that assume value 1 at the node corresponding to the degree  $i$

and 0 at the other nodes, and  $a_i$  are the nodal parameters. In Galerkin weighted residual method, we substitute  $v$  in the form of  $v = \sum_{j=1}^n N_j \delta a_j$  into the integral form or weak form and because  $\delta a_j$  are arbitrary ( except  $\delta a_j = 0$  on the essential boundary  $S_u$  ), we have

$$\int_V N_j^T A(Na) dV = 0 \quad j = 1 \text{ to } n \quad (2.3a)$$

or

$$\int_V C(N_j)^T D(Na) dV + \int_{S_p} E(N_j)^T F(Na) dS = 0 \quad j = 1 \text{ to } n \quad (2.3b)$$

### Principle of Virtual Work (Principle of Virtual displacement)

In the following presentation, the symbol  $\partial$  represents the partial differential operator on displacements  $u$  to obtain the strains  $\varepsilon$  as,

$$\partial = \begin{bmatrix} \frac{\partial}{\partial x} & 0 & 0 \\ 0 & \frac{\partial}{\partial y} & 0 \\ 0 & 0 & \frac{\partial}{\partial z} \\ 0 & \frac{\partial}{\partial z} & \frac{\partial}{\partial y} \\ \frac{\partial}{\partial z} & 0 & \frac{\partial}{\partial x} \\ \frac{\partial}{\partial y} & \frac{\partial}{\partial x} & 0 \end{bmatrix}$$

For any kinematically compatible deformation, that is,  $\delta u = 0$  on  $S_u$  and  $\delta \varepsilon = \partial \delta u$  in  $V$ , where  $\delta u$  is a variation of displacement  $u$  and may represent a virtual displacement field from a given equilibrium configuration, the necessary and sufficient condition for equilibrium is

$$\delta W_i = \delta W_e \quad (2.4)$$

where  $\delta W_i$  and  $\delta W_e$  are internal virtual work and external virtual work, respectively,

$$\delta W_i = \int_V \delta \varepsilon^T \sigma dV$$

$$\delta W_e = \int_V \delta u^T f dV + \int_{S_p} \delta u^T p dS$$

where  $f$  is body force in  $V$  and  $p$  is surface force on the natural boundary  $S_p$ . Most significant is the fact that the principle of virtual work is independent of the material constitutive relation and applies to any materials, linear or nonlinear. Similarly, it is applicable to structures with follower forces.

### General Variational Principles

The Hu-Washizu variational principle is one of the most general unconstrained variational principles in which independent variations are performed on all unknown quantities namely displacements, strains, stresses, and the surface traction. The significance of Lagrange multiplier method is that it converts a constrained variational principle to an unconstrained variational principle. The principle of virtual work is a constrained variational principle because the virtual displacements and virtual strains must be compatible, that is,  $\delta u = 0$  on  $S_u$ , the boundary where essential boundary conditions  $u = \bar{u}$  are specified, and  $\delta \varepsilon = \partial \delta u$  in  $V$ . Using Lagrange multiplier method to introduce the constraints in the principle of virtual work, the Hu-Washizu variational principle can be derived as follows,

$$\delta \Pi^* = \delta W_i - \delta W_e - \delta \int_V \lambda_1^T (\varepsilon - \partial u) dV - \delta \int_{S_u} \lambda_2^T (u - \bar{u}) dS = 0$$

where  $\delta W_i$  and  $\delta W_e$  are internal virtual work and external virtual work, respectively,

$$\delta W_i = \int_V \delta \varepsilon^T \sigma dV$$

$$\delta W_e = \int_V \delta u^T f dV + \int_{S_p} \delta u^T p dS$$

where  $f$  is body force in  $V$  and  $p$  is surface force on the natural boundary  $S_p$ . From the equation above, by integrating the term  $\int_V \lambda_1^T \delta \hat{\alpha} u dV$  by parts, the Lagrange multipliers  $\lambda_1$  and  $\lambda_2$  are identified, respectively, as the stresses  $\sigma$  in  $V$  and reactions  $p_u$  on  $S_u$ .

Therefore, we get the following Hu-Washizu variational principle,

$$\delta \Pi_{HW} = \delta W_i - \delta W_e - \delta \int_V \sigma^T (\varepsilon - \hat{\alpha} u) dV - \delta \int_{S_u} p_u^T (u - \bar{u}) dS = 0 \quad (2.5a)$$

in which there are no constraints on the unknown displacements  $u$ , strains  $\varepsilon$ , stresses  $\sigma$ , and reactions  $p_u$  on  $S_u$  and they can be assumed independently. However, it doesn't mean that these quantities can be assumed to be completely arbitrary in seeking a finite element solution. In general, to get a good solution, the assumption should reflect the true response as much as possible. For example, the assumption of these quantities needs to satisfy the completeness and keep an appropriate "balance" among these quantities. For the completeness, the assumption should be such that the rigid-body displacements including rigid-body translations and rotations, constant strains, constant stresses, and constant tractions can be represented in the limit as the element size approaches zero. Therefore, if these quantities are assumed to be a polynomial, the minimum requirements are that the displacements be linear, strains, stresses, and tractions be constant. It should be noted that the above derivation hasn't used the constitutive equation. Therefore, the formulation applies to any materials, linear or nonlinear. For example, substituting linear constitutive equation  $\sigma = C\varepsilon$  in the first item  $\delta W_i$ , we get the following unconstrained Hu-Washizu variational principle in linear elasticity,

$$\delta \Pi_{HW} = \int_V \delta \varepsilon^T (C\varepsilon - \sigma) dV - \int_V \delta \sigma^T (\varepsilon - \hat{\alpha} u) dV + \int_V \delta \hat{\alpha} u^T \sigma dV - \int_V \delta u^T f dV - \int_{S_p} \delta u^T p dS - \int_{S_u} \delta p_u^T (u - \bar{u}) dS - \int_{S_u} \delta u^T p_u = 0 \quad (2.5b)$$



in which there are no constraints on unknown displacements  $u$ , strains  $\varepsilon$ , stresses  $\sigma$ , and tractions  $p$  on  $S_u$  and they can be assumed independently. In most finite element applications, the displacement boundary condition  $u = \bar{u}$  on  $S_u$  is enforced. In these cases, the Hu-Washizu variational principle becomes,

$$\delta\Pi_{HW} = \int_V \delta\varepsilon^T (C\varepsilon - \sigma)dV - \int_V \delta\sigma^T (\varepsilon - \hat{\alpha}u)dV + \int_V \delta\hat{\alpha}^T \sigma dV - \int_V \delta u^T f dV - \int_{S_p} \delta u^T p dS = 0 \quad (2.5c)$$

where unknown displacements  $u$ , strains  $\varepsilon$  and stresses  $\sigma$  are the independent variables and they can be assumed independently. By enforcing the constitutive equation  $\sigma = C\varepsilon$ , we get the following two forms of Hellinger-Reissner variational principles,

$$\delta\Pi_{HR}(u, \sigma) = - \int_V \delta\sigma^T (S\sigma - \hat{\alpha}u)dV + \int_V \delta\hat{\alpha}^T \sigma dV - \int_V \delta u^T f dV - \int_{S_p} \delta u^T p dS = 0 \quad (2.6d)$$

$$\delta\Pi_{HR}(u, \varepsilon) = - \int_V \delta\varepsilon^T C(\varepsilon - \hat{\alpha}u)dV + \int_V \delta\hat{\alpha}^T C\varepsilon dV - \int_V \delta u^T f dV - \int_{S_p} \delta u^T p dS = 0 \quad (2.6b)$$

where  $S$  is the compliance matrix. In the first equation unknown displacements  $u$  and stresses  $\sigma$  can be assumed independently, whereas in the second equation unknown displacements  $u$  and strains  $\varepsilon$  are the independent variables and they can be assumed independently.

It is obvious that with various displacement, stress, and strain assumptions many different mixed finite element can be designed. However, by the limitation principle [B. Fraeijs de Veubeke, 1965], if the mixed formulation is capable of producing the same approximation as that produced by direct displacement form then it will in fact reproduce that form exactly and give identical and not any improved results. Any one considering for instance the addition of many higher order polynomials representing stress distribution in a linear triangle will soon find out that although the formulation is correct nothing is gained by its use as all the higher-order terms disappear [Zienkiewicz and Taylor, 2000].

## 2.2 Coordinate Transformation

Transformation of coordinates is vital in many contexts and must be fully understood. A general argument on the coordinate transformation is as follows.

We wish to replace a set of parameters  $\{a\}$  in which the system equations have been written by another one related to it by a transformation matrix  $[T]$  as

$$\{a\} = [T]\{b\} \quad (2.7)$$

In the linear case the system equations are of the form

$$[K]\{a\} = \{r\} \quad (2.8)$$

and on the substitution we have

$$[K][T]\{b\} = \{r\}$$

The new system can be pre-multiplied simply by  $[T]^T$ , yielding

$$[T]^T [K][T]\{b\} = [T]^T \{r\} \quad (2.9)$$

which will preserve the symmetry of equations if the matrix  $[K]$  is symmetric. It is important to note that the argument does not demand that  $[T]$  be either orthogonal or square.

Transformation matrices exist that have neither of these properties.

### **Transformation of stress, strain, stiffness and compliance matrix**

Let the two sets of coordinate systems denoted by  $xyz$  and  $x'y'z'$ , respectively, refer to Figure 2.1.

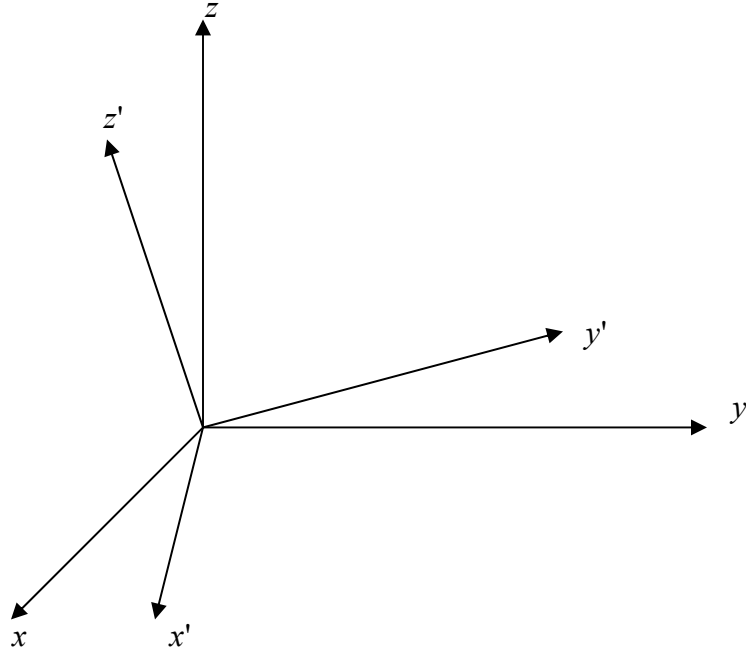


Figure 2.1 Cartesian coordinate systems  $xyz$  and  $x'y'z'$

Table 2.1 Direction cosines between the two sets of axes

|      | $x$          | $y$          | $z$          |
|------|--------------|--------------|--------------|
| $x'$ | $\cos(x',x)$ | $\cos(x',y)$ | $\cos(x',z)$ |
| $y'$ | $\cos(y',x)$ | $\cos(y',y)$ | $\cos(y',z)$ |
| $z'$ | $\cos(z',x)$ | $\cos(z',y)$ | $\cos(z',z)$ |

where  $\cos(x',x)$  is the cosine of the angle between the  $x'$  axis and the  $x$  axis, and so on.

Transformation of stress in tensor form is

$$\sigma'_{ij} = \lambda_{im} \lambda_{jn} \sigma_{mn} \quad (2.10a)$$

From which we can easily get the matrix form as

$$[\sigma'] = [\lambda][\sigma][\lambda]^T \quad (2.10b)$$

or

$$\{\sigma'\} = [T_\sigma]\{\sigma\} \quad (2.10c)$$

where  $[\lambda]$  is a  $3 \times 3$  matrix of direction cosines between the two sets of axes, that is,

$$[\lambda] = \begin{bmatrix} \cos(x',x) & \cos(x',y) & \cos(x',z) \\ \cos(y',x) & \cos(y',y) & \cos(y',z) \\ \cos(z',x) & \cos(z',y) & \cos(z',z) \end{bmatrix} \quad (2.10d)$$

$$[T_\sigma] = \begin{bmatrix} \lambda_{11}^2 & \lambda_{12}^2 & \lambda_{13}^2 & 2\lambda_{12}\lambda_{13} & 2\lambda_{13}\lambda_{11} & 2\lambda_{11}\lambda_{12} \\ \lambda_{21}^2 & \lambda_{22}^2 & \lambda_{23}^2 & 2\lambda_{22}\lambda_{23} & 2\lambda_{23}\lambda_{21} & 2\lambda_{21}\lambda_{22} \\ \lambda_{31}^2 & \lambda_{32}^2 & \lambda_{33}^2 & 2\lambda_{32}\lambda_{33} & 2\lambda_{33}\lambda_{31} & 2\lambda_{31}\lambda_{32} \\ \lambda_{21}\lambda_{31} & \lambda_{22}\lambda_{32} & \lambda_{23}\lambda_{33} & \lambda_{22}\lambda_{33} + \lambda_{23}\lambda_{32} & \lambda_{23}\lambda_{31} + \lambda_{21}\lambda_{33} & \lambda_{21}\lambda_{32} + \lambda_{22}\lambda_{31} \\ \lambda_{31}\lambda_{11} & \lambda_{32}\lambda_{12} & \lambda_{33}\lambda_{13} & \lambda_{32}\lambda_{13} + \lambda_{33}\lambda_{12} & \lambda_{33}\lambda_{11} + \lambda_{31}\lambda_{13} & \lambda_{31}\lambda_{12} + \lambda_{32}\lambda_{11} \\ \lambda_{11}\lambda_{21} & \lambda_{12}\lambda_{22} & \lambda_{13}\lambda_{23} & \lambda_{12}\lambda_{23} + \lambda_{13}\lambda_{22} & \lambda_{13}\lambda_{21} + \lambda_{11}\lambda_{23} & \lambda_{11}\lambda_{22} + \lambda_{12}\lambda_{21} \end{bmatrix} \quad (2.10e)$$

Similarly, and noting that the shear components of strain tensor are half of the corresponding engineering shear strains, we can get the transformation of strain in matrix form as

$$\{\varepsilon'\} = [T_\varepsilon]\{\varepsilon\} \quad (2.11a)$$

where

$$[T_\varepsilon] = \begin{bmatrix} \lambda_{11}^2 & \lambda_{12}^2 & \lambda_{13}^2 & \lambda_{12}\lambda_{13} & \lambda_{13}\lambda_{11} & \lambda_{11}\lambda_{12} \\ \lambda_{21}^2 & \lambda_{22}^2 & \lambda_{23}^2 & \lambda_{22}\lambda_{23} & \lambda_{23}\lambda_{21} & \lambda_{21}\lambda_{22} \\ \lambda_{31}^2 & \lambda_{32}^2 & \lambda_{33}^2 & \lambda_{32}\lambda_{33} & \lambda_{33}\lambda_{31} & \lambda_{31}\lambda_{32} \\ 2\lambda_{21}\lambda_{31} & 2\lambda_{22}\lambda_{32} & 2\lambda_{23}\lambda_{33} & \lambda_{22}\lambda_{33} + \lambda_{23}\lambda_{32} & \lambda_{23}\lambda_{31} + \lambda_{21}\lambda_{33} & \lambda_{21}\lambda_{32} + \lambda_{22}\lambda_{31} \\ 2\lambda_{31}\lambda_{11} & 2\lambda_{32}\lambda_{12} & 2\lambda_{33}\lambda_{13} & \lambda_{32}\lambda_{13} + \lambda_{33}\lambda_{12} & \lambda_{33}\lambda_{11} + \lambda_{31}\lambda_{13} & \lambda_{31}\lambda_{12} + \lambda_{32}\lambda_{11} \\ 2\lambda_{11}\lambda_{21} & 2\lambda_{12}\lambda_{22} & 2\lambda_{13}\lambda_{23} & \lambda_{12}\lambda_{23} + \lambda_{13}\lambda_{22} & \lambda_{13}\lambda_{21} + \lambda_{11}\lambda_{23} & \lambda_{11}\lambda_{22} + \lambda_{12}\lambda_{21} \end{bmatrix} \quad (2.11b)$$

Using the properties of direction cosines, we can easily verify

$$[T_\sigma]^{-1} = [T_\varepsilon]^T, \quad [T_\varepsilon]^{-1} = [T_\sigma]^T \quad (2.12)$$

We can also get the relation from  $\{\varepsilon'\}^T \{\sigma'\} = \{\varepsilon\}^T [T_\varepsilon]^T [T_\sigma] \{\sigma\} = \{\varepsilon\}^T \{\sigma\}$

From  $\{\varepsilon'\} = [T_\varepsilon]\{\varepsilon\}$  and the relation (2.12), we get the transformation of stiffness matrix as

$$[C] = [T_\varepsilon]^T [C'] [T_\varepsilon], \quad [C'] = [T_\sigma] [C] [T_\sigma]^T \quad (2.13)$$

From  $\{\sigma'\} = [T_\sigma]\{\sigma\}$  and the relation (2.12), we get the transformation of compliance matrix

as

$$[S] = [T_\sigma]^T [S'] [T_\sigma], \quad [S'] = [T_\varepsilon][S][T_\varepsilon]^T \quad (2.14)$$

### Coordinate Transformation for Composite Laminates

In the analysis of composite laminated plates and shells, we frequently assume the lamina of orthotropic material under plane stress. Refer to Figure 2.2, in which the 1–2 coordinate system is the principal material coordinate system and  $\theta$  is the angle from the  $x$  axis to the 1 axis.

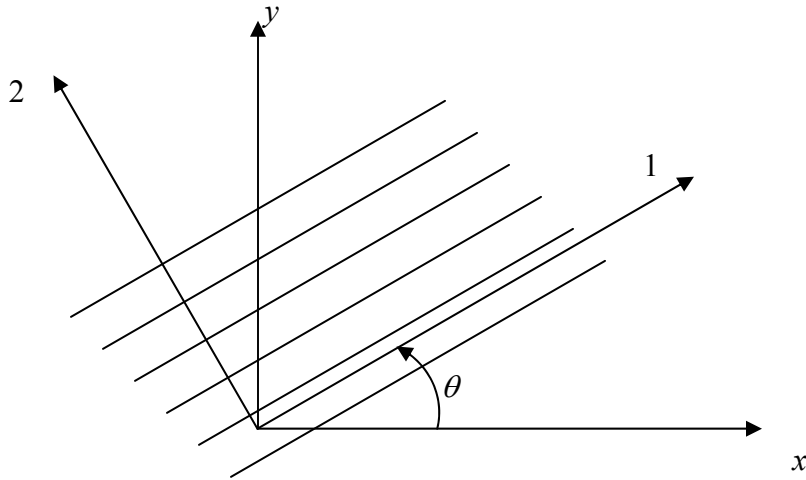


Figure 2.2 Positive rotation of principal material axes from  $xy$  axes.

We need to find the transformations from the principal material coordinate system to  $xy$  coordinate system. The matrix of direction cosines is,

$$[\lambda] = \begin{bmatrix} \cos(x,1) & \cos(x,2) & \cos(x,3) \\ \cos(y,1) & \cos(y,2) & \cos(y,3) \\ \cos(z,1) & \cos(z,2) & \cos(z,3) \end{bmatrix} = \begin{bmatrix} \cos\theta & -\sin\theta & 0 \\ \sin\theta & \cos\theta & 0 \\ 0 & 0 & 1 \end{bmatrix} \quad (2.15a)$$

In these problems we are concerned with  $\{\varepsilon\} = \{\varepsilon_x, \varepsilon_y, \gamma_{xy}\}^T$  and with  $\{\sigma\} = \{\sigma_x, \sigma_y, \sigma_{xy}\}^T$ .

Accordingly, discarding rows and columns 3, 4 and 5 from Eqs. (2.10e) and (2.11b) and using the matrix of direction cosines, we have

$$[T_\sigma] = \begin{bmatrix} c^2 & s^2 & -2cs \\ s^2 & c^2 & 2cs \\ cs & -cs & c^2 - s^2 \end{bmatrix}, \quad [T_\varepsilon] = \begin{bmatrix} c^2 & s^2 & -cs \\ s^2 & c^2 & cs \\ 2cs & -2cs & c^2 - s^2 \end{bmatrix} \quad (2.15b)$$

Therefore, the stiffness transformation is,

$$\begin{bmatrix} \bar{Q}_{11} & \bar{Q}_{12} & \bar{Q}_{16} \\ \bar{Q}_{12} & \bar{Q}_{22} & \bar{Q}_{26} \\ \bar{Q}_{16} & \bar{Q}_{26} & \bar{Q}_{66} \end{bmatrix} = \begin{bmatrix} c^2 & s^2 & -2cs \\ s^2 & c^2 & 2cs \\ cs & -cs & c^2 - s^2 \end{bmatrix} \begin{bmatrix} Q_{11} & Q_{12} & 0 \\ Q_{12} & Q_{22} & 0 \\ 0 & 0 & Q_{66} \end{bmatrix} \begin{bmatrix} c^2 & s^2 & -2cs \\ s^2 & c^2 & 2cs \\ cs & -cs & c^2 - s^2 \end{bmatrix}^T \quad (2.16)$$

$$\begin{aligned} \bar{Q}_{11} &= Q_{11}c^4 + 2(Q_{12} + 2Q_{66})s^2c^2 + Q_{22}s^4 \\ \bar{Q}_{12} &= (Q_{11} + Q_{22} - 4Q_{66})s^2c^2 + Q_{12}(s^4 + c^4) \\ \bar{Q}_{22} &= Q_{11}s^4 + 2(Q_{12} + 2Q_{66})s^2c^2 + Q_{22}c^4 \\ \bar{Q}_{16} &= (Q_{11} - Q_{12} - 2Q_{66})sc^3 + (Q_{12} - Q_{22} + 2Q_{66})s^3c \\ \bar{Q}_{26} &= (Q_{11} - Q_{12} - 2Q_{66})s^3c + (Q_{12} - Q_{22} + 2Q_{66})sc^3 \\ \bar{Q}_{66} &= (Q_{11} + Q_{22} - 2Q_{12} - 2Q_{66})s^2c^2 + Q_{66}(s^4 + c^4) \end{aligned}$$

where  $c = \cos \theta$ , and  $s = \sin \theta$ . The  $\bar{Q}_{ij}$  is the transformed reduced stiffness coefficients in the  $xy$  coordinate system and the  $Q_{ij}$  is the reduced stiffness coefficients in the principal material coordinate system given by

$$Q_{11} = \frac{E_1}{1 - \nu_{12}\nu_{21}}$$

$$Q_{12} = \frac{\nu_{12}E_2}{1 - \nu_{12}\nu_{21}}$$

$$Q_{22} = \frac{E_2}{1 - \nu_{12}\nu_{21}}$$

$$Q_{66} = G_{12}$$

The relation between the three-dimensional stiffness coefficient and reduced stiffness coefficient is given by [Chia, 1980]

$$Q_{ij} = C_{ij} - \frac{C_{i3}C_{j3}}{C_{33}} \quad (i, j = 1, 2, 6) \quad (2.17)$$

## Transformation of element stiffness matrix and force vector

It is often convenient to establish the characteristics of an individual element in a coordinate system which is different from that in which the external forces and displacements of the assembled structure or system will be measured. A different coordinate system may, in fact, be used for every element, to ease the computation. Clearly, it is necessary to do the transformation of coordinates to a common global system before the assembly of elements.

Let the common coordinate system denoted by  $xyz$  and the local coordinate system denoted by  $x'y'z'$ , refer to Figure 2.3. Define the nodal displacement vector of a node  $i$  as

$$\{a_i\} = \{u_i, v_i, w_i, \theta_{xi}, \theta_{yi}, \theta_{zi}\}^T$$

and the corresponding nodal force vector as

$$\{f_i\} = \{F_{xi}, F_{yi}, F_{zi}, M_{xi}, M_{yi}, M_{zi}\}^T$$

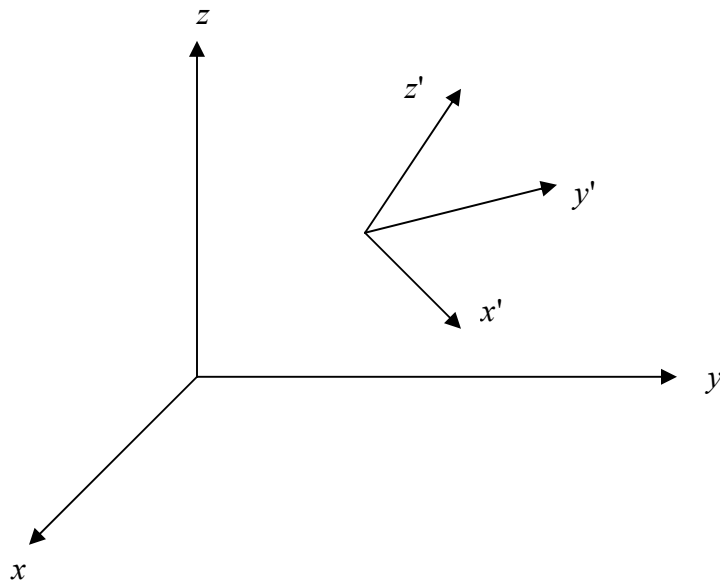


Figure 2.3 Cartesian coordinate systems  $xyz$  and  $x'y'z'$

The displacements and forces of a node  $i$  transform from the global, to the local system (shown by prime) by a matrix  $[T_i]$  given by

$$\{a'_i\} = [T_i]\{a_i\} \quad (2.18a)$$

where

$$[T_i] = \begin{bmatrix} [\lambda] & 0 \\ 0 & [\lambda] \end{bmatrix}$$

with  $[\lambda]$  being a  $3 \times 3$  matrix of direction cosines between the two sets of axes, that is,

$$[\lambda] = \begin{bmatrix} \cos(x',x) & \cos(x',y) & \cos(x',z) \\ \cos(y',x) & \cos(y',y) & \cos(y',z) \\ \cos(z',x) & \cos(z',y) & \cos(z',z) \end{bmatrix}$$

Therefore, the nodal displacements and forces of a three-node triangular plate bending element transform from the global to the local system by a matrix  $[T]$  given by

$$\{a'\} = [T]\{a\}, \quad \{f'\} = [T]\{f\} \quad (2.18b)$$

where

$$[T] = \begin{bmatrix} [T_1] & 0 & 0 \\ 0 & [T_2] & 0 \\ 0 & 0 & [T_3] \end{bmatrix}$$

Using the rules of orthogonal transformation, the inverse of  $[T]$  is given by its transpose, thus we have

$$\{a\} = [T]^T \{a'\}, \quad \{f\} = [T]^T \{f'\} \quad (2.19)$$

which permits the stiffness matrix of an element in the global coordinates to be computed as

$$[K] = [T]^T [K'] [T] \quad (2.20)$$

### 2.3 Area/Natural Coordinates and Shape Functions for Triangular Elements

As compared to other types of elements, a triangular element has one great advantage it can approximate to any boundary shape.

For studying the triangular element, area coordinates are more convenient than Cartesian



coordinates. Let us first define area coordinates. In Figure 2.4, an arbitrarily located point P divides triangle 1-2-3 into three sub-triangles. Area coordinates of the point P are defined as ratios of the area of these sub-triangles to that of the total triangle (For formulation of the area of the triangle, see appendix C):

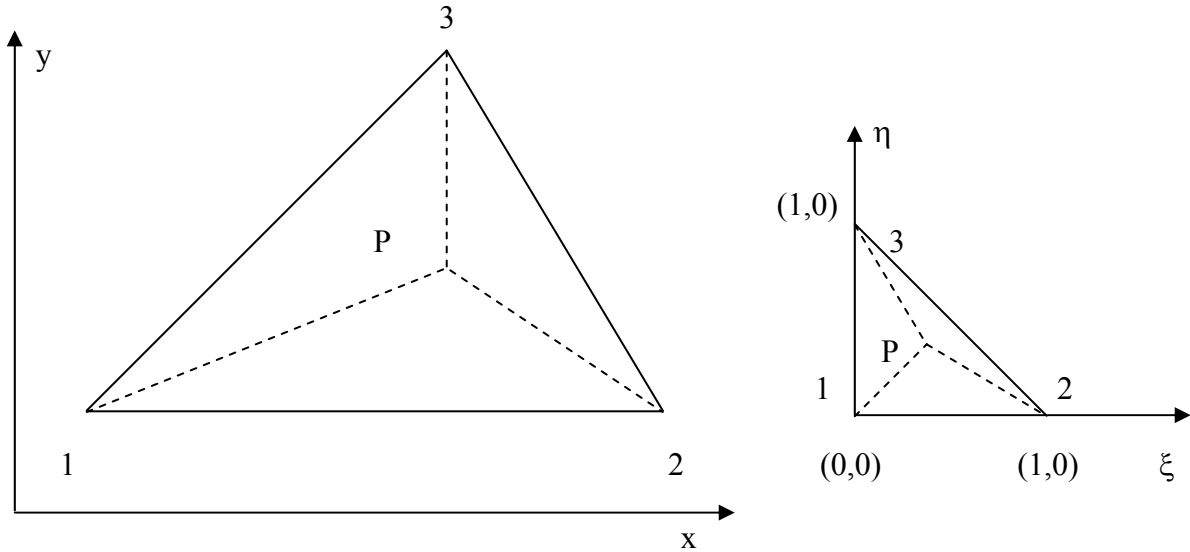


Figure 2.4 a) Area coordinates

b) Natural coordinates

$$\xi_1 = \frac{S_{\Delta P23}}{S_{\Delta 123}} = \frac{\frac{1}{2} \begin{vmatrix} 1 & x & y \\ 1 & x_2 & y_2 \\ 1 & x_3 & y_3 \end{vmatrix}}{\frac{1}{2} \begin{vmatrix} 1 & x_1 & y_1 \\ 1 & x_2 & y_2 \\ 1 & x_3 & y_3 \end{vmatrix}} = \frac{a_1 + b_1x + c_1y}{2A} \quad (2.21a)$$

$$\xi_2 = \frac{S_{\Delta P31}}{S_{\Delta 123}} = \frac{\frac{1}{2} \begin{vmatrix} 1 & x & y \\ 1 & x_3 & y_3 \\ 1 & x_1 & y_1 \end{vmatrix}}{A} = \frac{a_2 + b_2x + c_2y}{2A} \quad (2.21b)$$

$$\xi_3 = \frac{S_{\Delta P12}}{S_{\Delta 123}} = \frac{\frac{1}{2} \begin{vmatrix} 1 & x & y \\ 1 & x_1 & y_1 \\ 1 & x_2 & y_2 \end{vmatrix}}{A} = \frac{a_3 + b_3x + c_3y}{2A} \quad (2.21c)$$

where

$$a_1 = x_2 y_3 - x_3 y_2, \quad b_1 = y_2 - y_3, \quad c_1 = x_3 - x_2$$

$$a_2 = x_3 y_1 - x_1 y_3, \quad b_2 = y_3 - y_1, \quad c_2 = x_1 - x_3$$

$$a_3 = x_1 y_2 - x_2 y_1, \quad b_3 = y_1 - y_2, \quad c_3 = x_2 - x_1$$

$$A = S_{\Delta 123} = \frac{1}{2} \begin{vmatrix} 1 & x_1 & y_1 \\ 1 & x_2 & y_2 \\ 1 & x_3 & y_3 \end{vmatrix} = \frac{1}{2} (b_2 c_3 - c_2 b_3)$$

In the matrix form, we have,

$$\begin{Bmatrix} \xi_1 \\ \xi_2 \\ \xi_3 \end{Bmatrix} = \frac{1}{2A} \begin{bmatrix} a_1 & b_1 & c_1 \\ a_2 & b_2 & c_2 \\ a_3 & b_3 & c_3 \end{bmatrix} \begin{Bmatrix} 1 \\ x \\ y \end{Bmatrix} \quad (2.21d)$$

Because the total area of the triangle equals the sum of the areas of its three sub-triangles, we have

$$\xi_1 + \xi_2 + \xi_3 = 1 \quad (2.22a)$$

From the definition of area coordinates we can see that the Cartesian coordinates,  $x$  and  $y$ , of the point  $P$  have linear relations with the area coordinates. Here we have

$$x = \xi_1 x_1 + \xi_2 x_2 + \xi_3 x_3 \quad (2.22b)$$

$$y = \xi_1 y_1 + \xi_2 y_2 + \xi_3 y_3 \quad (2.22c)$$

because these relations holds at points 1, 2, and 3. The above relations can also be obtained from the geometry of a triangle (see Appendix D).

In the matrix form, we have,

$$\begin{Bmatrix} 1 \\ x \\ y \end{Bmatrix} = \begin{bmatrix} 1 & 1 & 1 \\ x_1 & x_2 & x_3 \\ y_1 & y_2 & y_3 \end{bmatrix} \begin{Bmatrix} \xi_1 \\ \xi_2 \\ \xi_3 \end{Bmatrix} \quad (2.22d)$$

The integral of a polynomial term in terms of area coordinates over the triangular region can

be exactly computed (see Appendix E).

Along a side of the triangle, the partial derivatives of area coordinates with respect to  $s$  are,

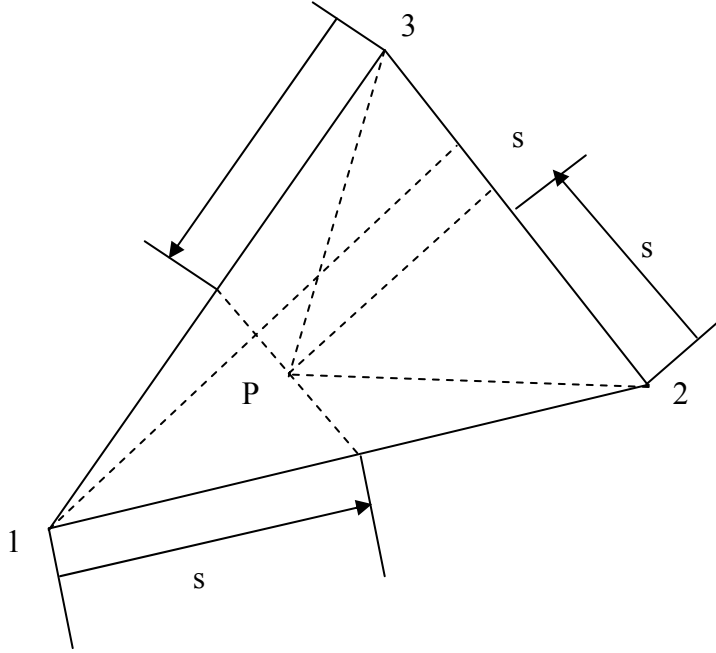


Figure 2.5 Area coordinates along the side of the triangle

Along the side 12,  $\xi_1 = \frac{S_{\Delta P23}}{S_{\Delta 123}} = 1 - \frac{s}{l_{12}}, \quad \left. \frac{\partial \xi_1}{\partial s} \right|_{side12} = -\frac{1}{l_{12}}$

Along the side 31,  $\xi_1 = \frac{S_{\Delta P23}}{S_{\Delta 123}} = \frac{s}{l_{31}}, \quad \left. \frac{\partial \xi_1}{\partial s} \right|_{side31} = \frac{1}{l_{31}}$

Similarly,

Along the side 12,  $\xi_2 = \frac{S_{\Delta P31}}{S_{\Delta 123}} = \frac{s}{l_{12}}, \quad \left. \frac{\partial \xi_2}{\partial s} \right|_{side12} = \frac{1}{l_{12}}$

Along the side 23,  $\xi_2 = \frac{S_{\Delta P31}}{S_{\Delta 123}} = 1 - \frac{s}{l_{23}}, \quad \left. \frac{\partial \xi_2}{\partial s} \right|_{side23} = -\frac{1}{l_{23}}$

Along the side 23,  $\xi_3 = \frac{S_{\Delta P12}}{S_{\Delta 123}} = \frac{s}{l_{23}}, \quad \left. \frac{\partial \xi_3}{\partial s} \right|_{side23} = \frac{1}{l_{23}}$

Along the side 31,  $\xi_3 = \frac{S_{\Delta P12}}{S_{\Delta 123}} = 1 - \frac{s}{l_{31}}, \quad \left. \frac{\partial \xi_3}{\partial s} \right|_{side31} = -\frac{1}{l_{31}}$



where  $l_i^l(\xi_1)$ , etc., are given by expression (2.23), with  $\xi_1$  taking the place of  $x$ , etc.

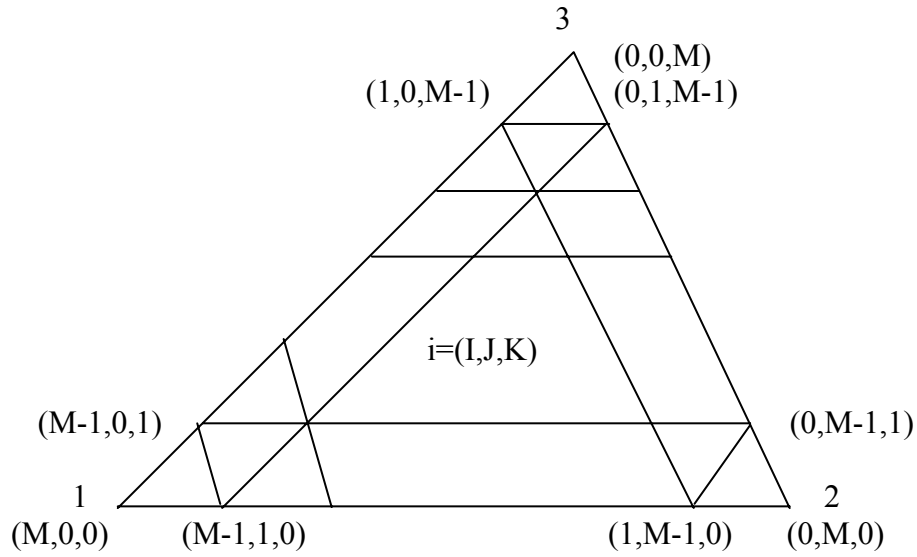


Figure 2.7 A general triangular element

Therefore, the shape functions for quadratic and cubic triangular elements can be generated as follows.

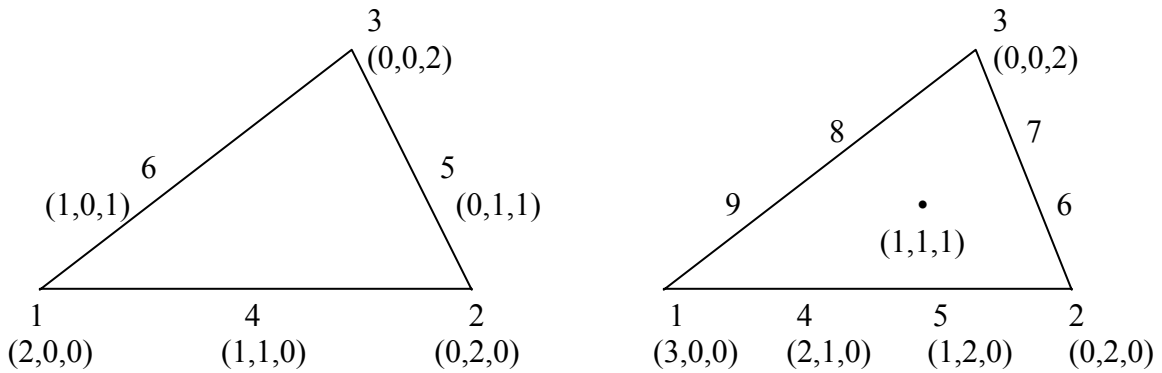


Figure 2.8 a) Quadratic triangular element      b) Cubic triangular element

**Quadratic triangular element (LST, linear strain triangular element)**

Corner nodes:

$$N_1 = \frac{(\xi_1 - 0)(\xi_1 - \frac{1}{2})}{(1 - 0)(1 - \frac{1}{2})} = \xi_1(2\xi_1 - 1)$$

$$N_2 = \frac{(\xi_2 - 0)(\xi_2 - \frac{1}{2})}{(1-0)(1-\frac{1}{2})} = \xi_2(2\xi_2 - 1)$$

$$N_3 = \frac{(\xi_3 - 0)(\xi_3 - \frac{1}{2})}{(1-0)(1-\frac{1}{2})} = \xi_3(2\xi_3 - 1)$$

Mid-side nodes:

$$N_4 = \frac{(\xi_1 - 0)(\xi_2 - 0)}{(\frac{1}{2} - 0)(\frac{1}{2} - 0)} = 4\xi_1\xi_2$$

$$N_5 = \frac{(\xi_2 - 0)(\xi_3 - 0)}{(\frac{1}{2} - 0)(\frac{1}{2} - 0)} = 4\xi_2\xi_3$$

$$N_6 = \frac{(\xi_1 - 0)(\xi_3 - 0)}{(\frac{1}{2} - 0)(\frac{1}{2} - 0)} = 4\xi_1\xi_3$$

### Cubic triangular element

Corner nodes:

$$N_1 = \frac{(\xi_1 - 0)(\xi_1 - \frac{1}{3})(\xi_1 - \frac{2}{3})}{(1-0)(1-\frac{1}{3})(1-\frac{2}{3})} = \frac{1}{2}\xi_1(3\xi_1 - 1)(3\xi_1 - 2)$$

similarly,

$$N_2 = \frac{1}{2}\xi_2(3\xi_2 - 1)(3\xi_2 - 2)$$

$$N_3 = \frac{1}{2}\xi_3(3\xi_3 - 1)(3\xi_3 - 2)$$

Mid-side nodes:

$$N_4 = \frac{(\xi_1 - 0)(\xi_1 - \frac{1}{3})(\xi_2 - 0)}{(\frac{2}{3} - 0)(\frac{2}{3} - \frac{1}{3})(\frac{1}{3} - 0)} = \frac{9}{2} \xi_1 \xi_2 (3\xi_1 - 1)$$

similarly

$$N_6 = \frac{9}{2} \xi_2 \xi_3 (3\xi_2 - 1)$$

$$N_8 = \frac{9}{2} \xi_1 \xi_3 (3\xi_3 - 1)$$

$$N_5 = \frac{(\xi_1 - 0)(\xi_2 - 0)(\xi_2 - \frac{1}{3})}{(\frac{1}{3} - 0)(\frac{2}{3} - 0)(\frac{2}{3} - \frac{1}{3})} = \frac{9}{2} \xi_1 \xi_2 (3\xi_2 - 1)$$

$$N_7 = \frac{9}{2} \xi_2 \xi_3 (3\xi_3 - 1)$$

$$N_9 = \frac{9}{2} \xi_1 \xi_3 (3\xi_1 - 1)$$

In practice, it is frequently expedient to use a natural coordinate system. It contains a right triangle of unit base and unit height, called a ‘parent’ element in the context of mapped elements. Using the natural coordinate system, we have

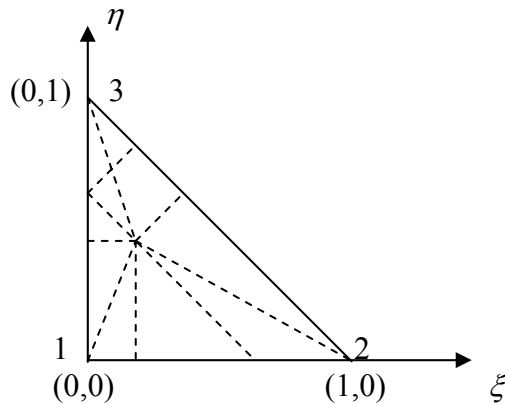


Figure 2.9 Relation between the area coordinates and natural coordinates

$$\xi_1 = 1 - \xi - \eta, \quad \xi_2 = \xi, \quad \xi_3 = \eta \quad (2.25)$$

It is easily seen that the ‘parent’ element will be mapped into an actual element by the following transformation.

$$x = (1 - \xi - \eta)x_1 + \xi x_2 + \eta x_3 \quad (2.26a)$$

$$y = (1 - \xi - \eta)y_1 + \xi y_2 + \eta y_3 \quad (2.26b)$$

where  $(x_1, y_1)$ ,  $(x_2, y_2)$ , and  $(x_3, y_3)$  are the coordinates of nodes 1, 2 and 3 of the actual element.

$$dxdy = |J|d\xi d\eta \quad (2.27)$$

where  $|J|$  is the determinant of the Jacobian matrix,

$$|J| = \begin{vmatrix} \frac{\partial x}{\partial \xi} & \frac{\partial y}{\partial \xi} \\ \frac{\partial x}{\partial \eta} & \frac{\partial y}{\partial \eta} \end{vmatrix} = \begin{vmatrix} x_2 - x_1 & y_2 - y_1 \\ x_3 - x_1 & y_3 - y_1 \end{vmatrix} = \begin{vmatrix} 1 & x_1 & y_1 \\ 1 & x_2 & y_2 \\ 1 & x_3 & y_3 \end{vmatrix} = 2A$$

where  $A$  is the area of triangle. Furthermore, all integrations are carried out over the natural coordinate, i.e., the  $\xi$  integration goes from 0 to 1 and the  $\eta$  integration goes from 0 to  $(1 - \xi)$ .

Using the chain rule, we have

$$\frac{\partial}{\partial x} = \frac{\partial}{\partial \xi} \frac{\partial \xi}{\partial x} + \frac{\partial}{\partial \eta} \frac{\partial \eta}{\partial x} \quad (2.28a)$$

$$\frac{\partial}{\partial y} = \frac{\partial}{\partial \xi} \frac{\partial \xi}{\partial y} + \frac{\partial}{\partial \eta} \frac{\partial \eta}{\partial y} \quad (2.28b)$$

To evaluate  $\frac{\partial \xi}{\partial x}$ ,  $\frac{\partial \xi}{\partial y}$ , etc., we note that

$$\begin{Bmatrix} d\xi \\ d\eta \end{Bmatrix} = \begin{bmatrix} \frac{\partial \xi}{\partial x} & \frac{\partial \xi}{\partial y} \\ \frac{\partial \eta}{\partial x} & \frac{\partial \eta}{\partial y} \end{bmatrix} \begin{Bmatrix} dx \\ dy \end{Bmatrix} \quad (2.29)$$

and



$$\begin{Bmatrix} dx \\ dy \end{Bmatrix} = \begin{bmatrix} \frac{\partial x}{\partial \xi} & \frac{\partial x}{\partial \eta} \\ \frac{\partial y}{\partial \xi} & \frac{\partial y}{\partial \eta} \end{bmatrix} \begin{Bmatrix} d\xi \\ d\eta \end{Bmatrix}$$

or

$$\begin{Bmatrix} d\xi \\ d\eta \end{Bmatrix} = \begin{bmatrix} \frac{\partial x}{\partial \xi} & \frac{\partial x}{\partial \eta} \\ \frac{\partial y}{\partial \xi} & \frac{\partial y}{\partial \eta} \end{bmatrix}^{-1} \begin{Bmatrix} dx \\ dy \end{Bmatrix} = \frac{1}{|J|} \begin{bmatrix} \frac{\partial y}{\partial \eta} & -\frac{\partial x}{\partial \eta} \\ -\frac{\partial y}{\partial \xi} & \frac{\partial x}{\partial \xi} \end{bmatrix} \begin{Bmatrix} dx \\ dy \end{Bmatrix} \quad (2.30)$$

A comparison of ( 2.29) and ( 2.30) yields

$$\frac{\partial \xi}{\partial x} = \frac{1}{|J|} \frac{\partial y}{\partial \eta}, \quad \frac{\partial \xi}{\partial y} = -\frac{1}{|J|} \frac{\partial x}{\partial \eta}, \quad \frac{\partial \eta}{\partial x} = -\frac{1}{|J|} \frac{\partial y}{\partial \xi}, \quad \frac{\partial \eta}{\partial y} = \frac{1}{|J|} \frac{\partial x}{\partial \xi}$$

$$\frac{\partial}{\partial x} = \frac{\partial}{\partial \xi} \frac{\partial \xi}{\partial x} + \frac{\partial}{\partial \eta} \frac{\partial \eta}{\partial x} = \frac{1}{|J|} \left( \frac{\partial}{\partial \xi} \frac{\partial y}{\partial \eta} - \frac{\partial}{\partial \eta} \frac{\partial y}{\partial \xi} \right)$$

$$\frac{\partial}{\partial y} = \frac{\partial}{\partial \xi} \frac{\partial \xi}{\partial y} + \frac{\partial}{\partial \eta} \frac{\partial \eta}{\partial y} = \frac{1}{|J|} \left( -\frac{\partial}{\partial \xi} \frac{\partial x}{\partial \eta} + \frac{\partial}{\partial \eta} \frac{\partial x}{\partial \xi} \right)$$

in matrix form,

$$\begin{Bmatrix} \frac{\partial}{\partial x} \\ \frac{\partial}{\partial y} \end{Bmatrix} = \frac{1}{|J|} \begin{bmatrix} \frac{\partial y}{\partial \eta} & -\frac{\partial y}{\partial \xi} \\ -\frac{\partial x}{\partial \eta} & \frac{\partial x}{\partial \xi} \end{bmatrix} \begin{Bmatrix} \frac{\partial}{\partial \xi} \\ \frac{\partial}{\partial \eta} \end{Bmatrix} = \frac{1}{2A} \begin{bmatrix} b_2 & b_3 \\ c_2 & c_3 \end{bmatrix} \begin{Bmatrix} \frac{\partial}{\partial \xi} \\ \frac{\partial}{\partial \eta} \end{Bmatrix} \quad (2.31)$$

$$\text{where } b_2 = y_3 - y_1, \quad b_3 = y_1 - y_2, \quad c_2 = x_1 - x_3, \quad c_3 = x_2 - x_1$$

The shape functions and their derivatives of linear strain triangular element (quadratic triangular element) in the natural coordinate system, see Appendix F.

## 2.4 Numerical Integration

In finite element analysis a large number of integrations are required, including the evaluation of the element stiffness matrix, mass matrix and force vector. To develop general finite element software, numerical integration is essential. Because the Gauss numerical

integration requires the least number of functional evaluations as compared with other methods, it is used almost exclusively in the finite element formulations.

With  $n$  sampling points Gauss integration can exactly integrate any polynomial of degree  $2n - 1$ . That is, if  $f(\xi)$  is any polynomial of degree less than  $2n$ , we have

$$\int_{-1}^1 f(\xi) d\xi = \sum_{i=1}^n W_i f(\xi_i) \quad (2.32a)$$

where  $\xi_i, i = 1, 2, \dots, n$ , are the roots of the Legendre polynomial of degree  $n$ , given by

$$P_n(\xi) = \frac{1}{2^n n!} \frac{d^n (\xi^2 - 1)^n}{d\xi^n} \quad (2.32b)$$

$W_i, i = 1, 2, \dots, n$ , are the corresponding weights given by

$$W_i = \int_{-1}^1 N_i(\xi) d\xi \quad (2.32c)$$

where  $N_i(\xi), i = 1, 2, \dots, n$ , are the corresponding Lagrange shape function given by

$$N_i(\xi) = \frac{(\xi - \xi_1) \cdots (\xi - \xi_{i-1})(\xi - \xi_{i+1}) \cdots (\xi - \xi_n)}{(\xi_i - \xi_1) \cdots (\xi_i - \xi_{i-1})(\xi_i - \xi_{i+1}) \cdots (\xi_i - \xi_n)} \quad (2.32d)$$

The weights and sampling points for integrating an even order polynomial on  $[-1, 1]$  are the same as that for the next odd order polynomial. The sampling points and the corresponding weights for  $n=1$  to 4 are given in Table 2.2[Yang, 1986]

Table 2.2 Sampling points and weights in Gauss integration  $\int_{-1}^1 f(\xi) d\xi = \sum_{i=1}^n W_i f(\xi_i)$

| $n$ | $\xi_i$                 | $W_i$             |
|-----|-------------------------|-------------------|
| 1   | 0                       | 2                 |
| 2   | $\pm 1/\sqrt{3}$        | 1                 |
| 3   | 0                       | 8/9               |
|     | $\pm\sqrt{0.6}$         | 5/9               |
| 4   | $\pm 0.339981043584856$ | 0.652145154862546 |
|     | $\pm 0.861136311594053$ | 0.347854845137454 |

Note: The third digit from the end in the number 0.861136311594053 in the Table was

mistyped to 9 in the Zienkiewicz's book.

The above Gauss integration can be easily extended to the rectangular region as follows

$$\int_{-1}^1 \int_{-1}^1 f(\xi, \eta) d\xi d\eta = \sum_{i=1}^m \sum_{j=1}^n W_i W_j f(\xi_i, \eta_j) \quad (2.33)$$

For the triangular region, the Gauss integration is

$$\int_0^1 \int_0^{1-\xi} f(\xi, \eta) d\xi d\eta = \frac{1}{2} \sum_{i=1}^n W_i f(\xi_i, \eta_i) \quad (2.34)$$

where the coefficient  $\frac{1}{2}$  represents the area of triangular integration region. The sum of

weights equals 1 because the formulation must be true when  $f(\xi, \eta) = 1$ .  $\xi_i$  and  $\eta_i$  are corresponding to the area coordinates  $\xi_2$  and  $\xi_3$ , respectively. The sampling points are symmetric with respect to the three area coordinates. That is, the sampling points occur only in groups of one, three or six points with equal weights in each group, in the form of

$\left(\frac{1}{3}, \frac{1}{3}, \frac{1}{3}\right)$ ,  $(a, b, b)$ ,  $(b, a, b)$ ,  $(b, b, a)$  or  $(a, b, c)$ ,  $(b, c, a)$ ,  $(c, a, b)$ ,  $(b, a, c)$ ,  $(c, b, a)$  and  $(a, c, b)$ ,

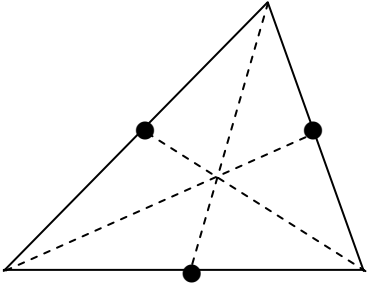
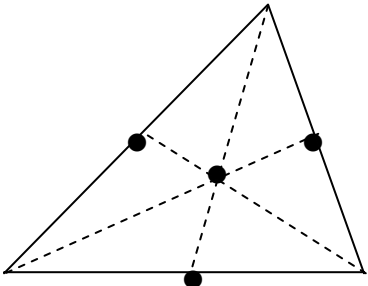
respectively. Note that the sum of three area coordinates equals one.

The choice of the order of numerical integration is important in practice. In theory, if a high enough order is used, all matrices will be evaluated very accurately. However, the cost of analysis increases when a high-order integration is employed. On the other hand, if the order of numerical integration is too low, the matrices may be evaluated very inaccurately and singularities may arise. The integration order required to evaluate a specific element matrix can be determined by studying the order of the function to be integrated. If the integrand is not a polynomial function, one should experiment with an increasing number of Gauss points till the difference between two successive values obtained is less than the acceptable tolerance. In general, the order of integration for the evaluation of the consistent mass matrix

is higher than that for the evaluation of the stiffness matrix because the mass matrix is obtained from the displacement interpolation functions, whereas the stiffness matrix is computed from the derivatives of the displacement functions. If the element geometric distortions are very large, and in nonlinear analysis, a higher order of the integration may be appropriate. For a reliable finite element analysis, full (exact) numerical integration should be used.

The sampling points and the corresponding weights for  $n=3$  to 4 are given in Table 2.3 [Yang, 1986]. For more comprehensive list, see the book [Yang, 1986] and papers [Hammer et al., 1956; Cowper, 1973; and Dunavant, 1985].

Table 2.3 Gauss Integration for the triangular region

| Number and Locations of Sampling Points  | $\xi_i$       | $\eta_i$      | Weights $W_i$   | Degree of Accuracy |
|--|---------------|---------------|-----------------|--------------------|
| n=3<br> | $\frac{1}{2}$ | 0             | $\frac{1}{3}$   | 2                  |
|  | $\frac{1}{2}$ | $\frac{1}{2}$ | $\frac{1}{3}$   |                    |
|  | 0             | $\frac{1}{2}$ | $\frac{1}{3}$   |                    |
| n=4<br> | $\frac{1}{3}$ | $\frac{1}{3}$ | $\frac{27}{48}$ | 3                  |
|  | $\frac{1}{5}$ | $\frac{1}{5}$ | $\frac{25}{48}$ |                    |
|  | $\frac{3}{5}$ | $\frac{1}{5}$ | $\frac{25}{48}$ |                    |
|  | $\frac{1}{5}$ | $\frac{3}{5}$ | $\frac{25}{48}$ |                    |

In the finite element history, the reduced/selective integration that mitigates the shear locking in the displacement-based plate/shell element should be viewed as merely an effective way to accurately compute the finite element matrices of the mixed formulation. The equivalence between the reduced/selective integration and the mixed formulation was first shown by Malkus and Hughes in 1978 and later in a general context by Zienkiewicz and Nakazawa in 1984.

## **2.5 Membrane Element**

### **Allman Triangular Element**

One way to improve the performance of elements is to add drilling d.o.f. A drilling d.o.f. in a plane element is a rotational d.o.f. whose vector is normal to the analysis plane. A benefit of the drilling d.o.f. is that they can enable elements having only corner nodes to provide acceptable performance while using fewer d.o.f. than elements having both corner and side nodes. For example, a triangular element having drilling d.o.f. and only vertex nodes performs much better than the six d.o.f. CST element, although not as well as the 12 d.o.f. LST element. The number of d.o.f. in a large 2D mesh is reduced by a factor of 5/8 comparing with using LST element. Another benefit of using drilling degrees of freedom lies in shell analysis. A shell element can easily be formed as the combination of a plane element and an element for plate bending. A shell element that uses all six d.o.f. at each node is perhaps best suited to analysis of folded plates, where many elements are coplanar. In modeling a continuously curved shell, drilling d.o.f. may interact unfavorably with bending deformation [MacNeal, 1994].

The LST element is known to give much improved estimates of displacements and stresses, for a given finite element mesh size, compared to the CST element. However, this

improvement in accuracy is achieved at a price of a big increase in the total degrees of freedom in the finite element model used to represent a structure. The Allman triangle, which has three nodes and three degrees of freedom at each node, combines the best features of the two elements, namely: compatible quadratic displacements with the degrees of freedom located at the vertices only.

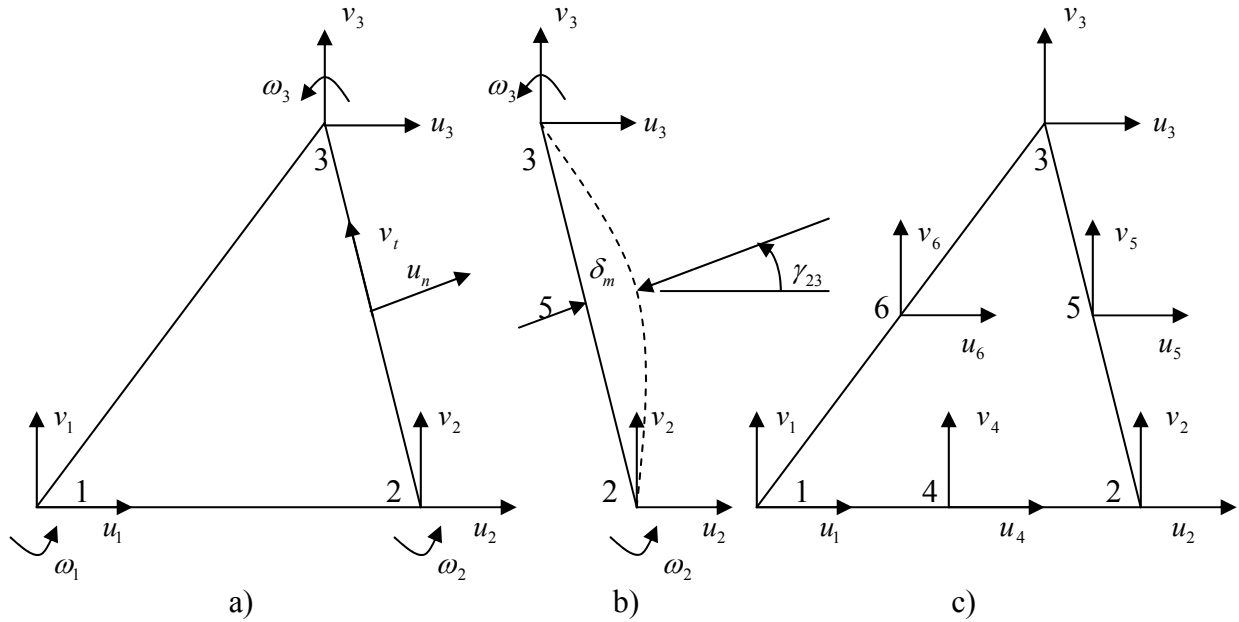


Figure 2.10 a) Nodal d.o.f. of the Allman triangle b) Parabolic edge displacement created by d.o.f.  $\omega_2$  and  $\omega_3$  c) D.o.f. of the linear strain triangle (LST).

In the Allman triangle, the normal and tangential displacements  $u_n$  and  $u_t$  along the side of triangle are assumed to be quadratic and linear, respectively. Consider a typical side of a plane element, Figure 2.10 (b), in which  $\delta_m$  is the mid-side normal displacement relative to the straight-side condition. Therefore, we have

$$u_n = \xi_2 u_{n2} + \xi_3 u_{n3} + 4\xi_2 \xi_3 \delta_m = \left(1 - \frac{s}{l_{23}}\right) u_{n2} + \frac{s}{l_{23}} u_{n3} + 4\left(1 - \frac{s}{l_{23}}\right) \frac{s}{l_{23}} \delta_m$$

$$u_t = \xi_2 u_{t2} + \xi_3 u_{t3} = \left(1 - \frac{s}{l_{23}}\right) u_{t2} + \left(\frac{s}{l_{23}}\right) u_{t3} \quad (2.35)$$

We can also write  $u_n = N_2 u_{n2} + N_3 u_{n3} + N_5 u_{n5} = \xi_2(2\xi_2 - 1)u_{n2} + \xi_3(2\xi_3 - 1)u_{n3} + 4\xi_2\xi_3 u_{n5}$ , but as long as we note  $u_{n5} = \frac{u_{n2} + u_{n3}}{2} + \delta_m$ , it reduces to eqn. (2.35).

Our objective is to express  $\delta_m$  by the vertex degrees of freedom. Using the following condition

$$\left. \frac{\partial u_n}{\partial s} \right|_{s=l_{23}} - \left. \frac{\partial u_n}{\partial s} \right|_{s=0} = -\omega_3 + \omega_2 \quad (2.36)$$

we get  $\delta_m$

$$\delta_m = \frac{l_{23}}{8}(\omega_3 - \omega_2) \quad (2.37)$$

Clearly,  $\omega_2$  and  $\omega_3$  are not true rotations as defined in the theory of elasticity and the quadratic term in the normal displacement  $u_n$  is caused by these drilling degrees of freedom.

We also note here that the use of eqn. (2.36) neither prevents the compatibility of the displacements nor constrains the change in the vertex angles of a triangular element.

Therefore, all constant states of strain can be represented exactly by the present formulation and convergence to an exact solution with consistent mesh refinement is thus assured.

Substituting eqn. (2.37) into (2.35) gives the boundary displacements along side 23 as

$$u_n = \xi_2 u_{n2} + \xi_3 u_{n3} + \frac{1}{2} l_{23} (\omega_3 - \omega_2) \xi_2 \xi_3 = \left(1 - \frac{s}{l_{23}}\right) u_{n2} + \frac{s}{l_{23}} u_{n3} + \frac{1}{2} s \left(1 - \frac{s}{l_{23}}\right) (\omega_3 - \omega_2)$$

$$u_t = \xi_2 u_{t2} + \xi_3 u_{t3} = \left(1 - \frac{s}{l_{23}}\right) u_{t2} + \left(\frac{s}{l_{23}}\right) u_{t3} \quad (2.38)$$

and the boundary displacements along sides 31 and 12 follow from a cyclic permutation of the indices in eqn (2.38).

Based on the eqns (2.38), Allman introduced the element displacement field as follows

$$\begin{aligned}
u &= u_1 \xi_1 + u_2 \xi_2 + u_3 \xi_3 + \frac{1}{2} l_{12} \cos \gamma_{12} (\omega_2 - \omega_1) \xi_1 \xi_2 \\
&\quad + \frac{1}{2} l_{23} \cos \gamma_{23} (\omega_3 - \omega_2) \xi_2 \xi_3 + \frac{1}{2} l_{31} \cos \gamma_{31} (\omega_1 - \omega_3) \xi_3 \xi_1 \\
v &= v_1 \xi_1 + v_2 \xi_2 + v_3 \xi_3 + \frac{1}{2} l_{12} \sin \gamma_{12} (\omega_2 - \omega_1) \xi_1 \xi_2 \\
&\quad + \frac{1}{2} l_{23} \sin \gamma_{23} (\omega_3 - \omega_2) \xi_2 \xi_3 + \frac{1}{2} l_{31} \sin \gamma_{31} (\omega_1 - \omega_3) \xi_3 \xi_1
\end{aligned} \tag{2.39}$$

where  $\sin \gamma_{12} = \frac{x_1 - x_2}{l_{12}}$ ,  $\cos \gamma_{12} = -\frac{y_1 - y_2}{l_{12}}$ , etc.

To verify that the displacement field eqn. (2.39) is corresponding to the boundary displacements eqn. (2.38), we note that along the side 23, for example,

$$\begin{aligned}
\xi_1 &= 0, \quad \xi_2 = 1 - \frac{s}{l_{23}}, \quad \xi_3 = \frac{s}{l_{23}} \\
u_n &= u \cos \gamma_{23} + v \sin \gamma_{23} \\
&= (u_2 \xi_2 + u_3 \xi_3 + \frac{1}{2} l_{23} \cos \gamma_{23} (\omega_3 - \omega_2) \xi_2 \xi_3) \cos \gamma_{23} \\
&\quad + (v_2 \xi_2 + v_3 \xi_3 + \frac{1}{2} l_{23} \sin \gamma_{23} (\omega_3 - \omega_2) \xi_2 \xi_3) \sin \gamma_{23} \\
&= \xi_2 (u_2 \cos \gamma_{23} + v_2 \sin \gamma_{23}) + \xi_3 (u_3 \cos \gamma_{23} + v_3 \sin \gamma_{23}) + \frac{1}{2} l_{23} (\omega_3 - \omega_2) \xi_2 \xi_3 \\
&= \xi_2 u_{n2} + \xi_3 u_{n3} + \frac{1}{2} l_{23} (\omega_3 - \omega_2) \xi_2 \xi_3 \\
&= (1 - \frac{s}{l_{23}}) u_{n2} + (\frac{s}{l_{23}}) u_{n3} + \frac{1}{2} s (1 - \frac{s}{l_{23}}) (\omega_3 - \omega_2) \\
u_t &= -u \sin \gamma_{23} + v \cos \gamma_{23} \\
&= -(u_2 \xi_2 + u_3 \xi_3 + \frac{1}{2} l_{23} \cos \gamma_{23} (\omega_3 - \omega_2) \xi_2 \xi_3) \sin \gamma_{23} \\
&\quad + (v_2 \xi_2 + v_3 \xi_3 + \frac{1}{2} l_{23} \sin \gamma_{23} (\omega_3 - \omega_2) \xi_2 \xi_3) \cos \gamma_{23} \\
&= \xi_2 (-u_2 \sin \gamma_{23} + v_2 \cos \gamma_{23}) + \xi_3 (-u_3 \sin \gamma_{23} + v_3 \cos \gamma_{23}) \\
&= \xi_2 u_{t2} + \xi_3 u_{t3} \\
&= (1 - \frac{s}{l_{23}}) u_{t2} + (\frac{s}{l_{23}}) u_{t3}
\end{aligned}$$



From the displacement field eqn. (2.39), Allman constructs the 9 by 9 element stiffness matrix. Tests show that the element performs much better than the CST element, although not as well as the LST element. However, in a large mesh the LST may produce more than twice as many d.o.f. One nodal  $\omega$  of the entire mesh must be set to zero to prevent an unusual type of zero energy mode in which all  $u_i$  and  $v_i$  are zero and all  $\omega_i$  are equal.

Cook noted that the Allman triangle can be regarded as the result of applying a coordinate transformation to an element that has mid-side nodes. From eqn. (2.39), we have the displacements at the mid-side nodes

$$u_4 = \frac{1}{2}u_1 + \frac{1}{2}u_2 + \frac{l_{12}}{8}(\omega_2 - \omega_1)\cos\gamma_{12} = \frac{1}{2}u_1 + \frac{1}{2}u_2 - \frac{y_1 - y_2}{8}(\omega_2 - \omega_1) = \frac{1}{2}u_1 + \frac{1}{2}u_2 - \frac{b_3}{8}(\omega_2 - \omega_1)$$

$$v_4 = \frac{1}{2}v_1 + \frac{1}{2}v_2 + \frac{l_{12}}{8}(\omega_2 - \omega_1)\sin\gamma_{12} = \frac{1}{2}v_1 + \frac{1}{2}v_2 - \frac{x_2 - x_1}{8}(\omega_2 - \omega_1) = \frac{1}{2}v_1 + \frac{1}{2}v_2 - \frac{c_3}{8}(\omega_2 - \omega_1)$$

$$u_5 = \frac{1}{2}u_2 + \frac{1}{2}u_3 + \frac{l_{23}}{8}(\omega_3 - \omega_2)\cos\gamma_{23} = \frac{1}{2}u_2 + \frac{1}{2}u_3 - \frac{y_2 - y_3}{8}(\omega_3 - \omega_2) = \frac{1}{2}u_2 + \frac{1}{2}u_3 - \frac{b_1}{8}(\omega_3 - \omega_2)$$

$$v_5 = \frac{1}{2}v_2 + \frac{1}{2}v_3 + \frac{l_{23}}{8}(\omega_3 - \omega_2)\sin\gamma_{23} = \frac{1}{2}v_2 + \frac{1}{2}v_3 - \frac{x_3 - x_2}{8}(\omega_3 - \omega_2) = \frac{1}{2}v_2 + \frac{1}{2}v_3 - \frac{c_1}{8}(\omega_3 - \omega_2)$$

$$u_6 = \frac{1}{2}u_3 + \frac{1}{2}u_1 + \frac{l_{31}}{8}(\omega_1 - \omega_3)\cos\gamma_{31} = \frac{1}{2}u_3 + \frac{1}{2}u_1 - \frac{y_3 - y_1}{8}(\omega_1 - \omega_3) = \frac{1}{2}u_3 + \frac{1}{2}u_1 - \frac{b_2}{8}(\omega_1 - \omega_3)$$

$$v_6 = \frac{1}{2}v_3 + \frac{1}{2}v_1 + \frac{l_{31}}{8}(\omega_1 - \omega_3)\sin\gamma_{31} = \frac{1}{2}v_3 + \frac{1}{2}v_1 - \frac{x_1 - x_3}{8}(\omega_1 - \omega_3) = \frac{1}{2}v_3 + \frac{1}{2}v_1 - \frac{c_2}{8}(\omega_1 - \omega_3)$$

Therefore, the coordinate transformation between the degrees of freedom of the LST and the Allman triangle is

$$\{a_{lst}\} = [T]\{a_{allman}\} \quad (2.40)$$

where

$$\{a_{lst}\} = \{u_1 \ v_1 \ u_2 \ v_2 \ u_3 \ v_3 \ u_4 \ v_4 \ u_5 \ v_5 \ u_6 \ v_6\}^T$$

$$\{a_{allman}\} = \{u_1 \ v_1 \ \omega_1 \ u_2 \ v_2 \ \omega_2 \ u_3 \ v_3 \ \omega_3\}^T$$

$$[T] = \begin{bmatrix} 1 & 0 & 0 & 0 & 0 & 0 & 0 & 0 & 0 \\ 0 & 1 & 0 & 0 & 0 & 0 & 0 & 0 & 0 \\ 0 & 0 & 0 & 1 & 0 & 0 & 0 & 0 & 0 \\ 0 & 0 & 0 & 0 & 1 & 0 & 0 & 0 & 0 \\ 0 & 0 & 0 & 0 & 0 & 0 & 1 & 0 & 0 \\ 0 & 0 & 0 & 0 & 0 & 0 & 0 & 1 & 0 \\ 0.5 & 0 & \frac{b_3}{8} & 0.5 & 0 & -\frac{b_3}{8} & 0 & 0 & 0 \\ 0 & 0.5 & \frac{c_3}{8} & 0 & 0.5 & -\frac{c_3}{8} & 0 & 0 & 0 \\ 0 & 0 & 0 & 0.5 & 0 & \frac{b_1}{8} & 0.5 & 0 & -\frac{b_1}{8} \\ 0 & 0 & 0 & 0 & 0.5 & \frac{c_1}{8} & 0 & 0.5 & -\frac{c_1}{8} \\ 0.5 & 0 & -\frac{b_2}{8} & 0 & 0 & 0 & 0.5 & 0 & \frac{b_2}{8} \\ 0 & 0.5 & -\frac{c_2}{8} & 0 & 0 & 0 & 0 & 0.5 & \frac{c_2}{8} \end{bmatrix}$$

where

$$b_1 = y_2 - y_3, \quad c_1 = x_3 - x_2$$

$$b_2 = y_3 - y_1, \quad c_2 = x_1 - x_3$$

$$b_3 = y_1 - y_2, \quad c_3 = x_2 - x_1$$

So the 9 by 9 stiffness matrix  $[k_A]$  of the Allman triangle is

$$[k_A] = [T]^T [k_{LST}] [T] \quad (2.41)$$

where  $[k_{LST}]$  is the 12 by 12 stiffness matrix of the corresponding LST element. Clearly, the transformation symbolized by eqn (2.40) can be applied to elements with more than three sides. Accordingly, various elements with nodal rotations can be produced from similar elements with midside nodes and straight edges merely by employing a coordinate transformation subroutine. Thus, Allman type elements can easily be added as an option to existing programs.

Next, we verify that the element obtained by the above transformation from the LST element is indeed the Allman triangle. The element displacement field is

$$\begin{aligned}
u &= \sum_{i=1}^6 N_i u_i \\
&= \xi_1 (2\xi_1 - 1)u_1 + \xi_2 (2\xi_2 - 1)u_2 + \xi_3 (2\xi_3 - 1)u_3 + 4\xi_1 \xi_2 \left( \frac{1}{2}u_1 + \frac{1}{2}u_2 + \frac{l_{12}}{8}(\omega_2 - \omega_1) \cos \gamma_{12} \right) \\
&\quad + 4\xi_2 \xi_3 \left( \frac{1}{2}u_2 + \frac{1}{2}u_3 + \frac{l_{23}}{8}(\omega_3 - \omega_2) \cos \gamma_{23} \right) + 4\xi_1 \xi_3 \left( \frac{1}{2}u_3 + \frac{1}{2}u_1 + \frac{l_{31}}{8}(\omega_1 - \omega_3) \cos \gamma_{31} \right) \\
&= (2\xi_1 (\xi_1 + \xi_2 + \xi_3) - \xi_1)u_1 + (2\xi_2 (\xi_1 + \xi_2 + \xi_3) - \xi_2)u_2 + (2\xi_3 (\xi_1 + \xi_2 + \xi_3) - \xi_3)u_3 \\
&\quad + \frac{l_{12}}{2}(\omega_2 - \omega_1) \cos \gamma_{12} \xi_1 \xi_2 + \frac{l_{23}}{2}(\omega_3 - \omega_2) \cos \gamma_{23} \xi_2 \xi_3 + \frac{l_{31}}{2}(\omega_1 - \omega_3) \cos \gamma_{31} \xi_3 \xi_1 \\
&= \xi_1 u_1 + \xi_2 u_2 + \xi_3 u_3 + \frac{l_{12}}{2}(\omega_2 - \omega_1) \cos \gamma_{12} \xi_1 \xi_2 + \frac{l_{23}}{2}(\omega_3 - \omega_2) \cos \gamma_{23} \xi_2 \xi_3 + \frac{l_{31}}{2}(\omega_1 - \omega_3) \cos \gamma_{31} \xi_3 \xi_1 \\
v &= \sum_{i=1}^6 N_i v_i \\
&= \xi_1 (2\xi_1 - 1)v_1 + \xi_2 (2\xi_2 - 1)v_2 + \xi_3 (2\xi_3 - 1)v_3 + 4\xi_1 \xi_2 \left( \frac{1}{2}u_1 + \frac{1}{2}u_2 + \frac{l_{12}}{8}(\omega_2 - \omega_1) \sin \gamma_{12} \right) \\
&\quad + 4\xi_2 \xi_3 \left( \frac{1}{2}u_2 + \frac{1}{2}u_3 + \frac{l_{23}}{8}(\omega_3 - \omega_2) \sin \gamma_{23} \right) + 4\xi_1 \xi_3 \left( \frac{1}{2}u_3 + \frac{1}{2}u_1 + \frac{l_{31}}{8}(\omega_1 - \omega_3) \sin \gamma_{31} \right) \\
&= (2\xi_1 (\xi_1 + \xi_2 + \xi_3) - \xi_1)v_1 + (2\xi_2 (\xi_1 + \xi_2 + \xi_3) - \xi_2)v_2 + (2\xi_3 (\xi_1 + \xi_2 + \xi_3) - \xi_3)v_3 \\
&\quad + \frac{l_{12}}{2}(\omega_2 - \omega_1) \sin \gamma_{12} \xi_1 \xi_2 + \frac{l_{23}}{2}(\omega_3 - \omega_2) \sin \gamma_{23} \xi_2 \xi_3 + \frac{l_{31}}{2}(\omega_1 - \omega_3) \sin \gamma_{31} \xi_3 \xi_1 \\
&= \xi_1 v_1 + \xi_2 v_2 + \xi_3 v_3 + \frac{l_{12}}{2}(\omega_2 - \omega_1) \sin \gamma_{12} \xi_1 \xi_2 + \frac{l_{23}}{2}(\omega_3 - \omega_2) \sin \gamma_{23} \xi_2 \xi_3 + \frac{l_{31}}{2}(\omega_1 - \omega_3) \sin \gamma_{31} \xi_3 \xi_1
\end{aligned} \tag{2.42}$$

Comparing eqn. (2.42) with eqn. (2.39), we can see that the element really has the same element displacement field as the Allman triangular element. Therefore, the element obtained by the above transformation from the LST element is indeed the Allman triangular element. In the displacement field of the Allman triangle, eqn. (2.39), the true rotation  $\Omega$  in the theory of elasticity is (The derivation, see Appendix G)

$$\Omega = \frac{1}{2} \left( \frac{\partial v}{\partial x} - \frac{\partial u}{\partial y} \right) = \Omega_0 + \frac{1}{4} \sum_{i=1}^3 (3\xi_i - 1) \omega_i \tag{2.43}$$

where  $\Omega_0$ , the rotation at the centroid  $\xi_1 = \xi_2 = \xi_3 = \frac{1}{3}$ , is

$$\Omega_0 = \frac{1}{4A} [(x_2 - x_3)u_1 + (x_3 - x_1)u_2 + (x_1 - x_2)u_3 + (y_2 - y_3)v_1 + (y_3 - y_1)v_2 + (y_1 - y_2)v_3]$$

From the eqn. (2.43), we have at the vertices

$$\Omega_1 = \Omega_0 + \frac{1}{4}(2\omega_1 - \omega_2 - \omega_3)$$

$$\Omega_2 = \Omega_0 + \frac{1}{4}(2\omega_2 - \omega_1 - \omega_3)$$

$$\Omega_3 = \Omega_0 + \frac{1}{4}(2\omega_3 - \omega_1 - \omega_2)$$

therefore,

$$\Omega_0 = \frac{1}{3}(\Omega_1 + \Omega_2 + \Omega_3)$$

Moreover, denoting  $\omega_0$  as the average value of the  $\omega_i$  connectors, thus

$$\omega_0 = \frac{1}{3}(\omega_1 + \omega_2 + \omega_3)$$

$$\Omega_i - \Omega_0 = \frac{3}{4}(\omega_i - \omega_0) \tag{2.44}$$

Eqs. (2.43) and (2.44) show that continuity of the true rotation field is not enforced in the Allman element either across element sides or at the nodes. It is to be noted that this level of continuity is not required for a correct application of the principle of minimum potential energy.

Notes:

(1)  $\omega$  true meaning. Though we get  $\delta_m = \frac{l_{23}}{8}(\omega_3 - \omega_2)$  from the condition

$\frac{\partial u_n}{\partial s} \Big|_{s=l_{23}} - \frac{\partial u_n}{\partial s} \Big|_{s=0} = -\omega_3 + \omega_2$ , we can not assume  $\omega = -\frac{\partial u_n}{\partial s}$ , concept wrong. Applying the

boundary conditions should include the drilling degrees when we choose the Allman element. Whether the drilling degrees  $\omega_i = 0$  or not should be based on whether  $\delta_m = 0$  or not.

(2)  $\omega$  is not true rotation, which is defined as  $(v_{,x} - u_{,y})/2$  in the theory of elasticity, but it is closely related to the true rotation as in eqn. (2.43) and (2.44).

(3) In addition to the rigid body motion, the Allman element also exhibits an unusual type of zero energy mode  $u_i = v_i = 0$  and  $\omega_i = c$ , a constant. The result is that a mesh of elements formulated in this way displays no strain energy if all drilling d.o.f. in the mesh are equal. Therefore, the structure stiffness matrix is singular even if the rigid body movements are constrained. One nodal  $\omega$  of the entire mesh must be set to zero to prevent this singularity.

(4) Because of the zero energy mode, the element has only 8 d.o.f. available to model deformation, despite having a total of 9 nodal d.o.f. Therefore, the element uses incomplete quadratic fields. The complete quadratic field in a triangular element needs 12 d.o.f to describe it, with each component having 6 d.o.fs as in the LST element.

## 2.6 Bending Element

Because of the high efficiency and accuracy of discrete Kirchhoff triangular (DKT) element for thin plate bending analysis but lack of document for its derivation we present the detail derivation for DKT element in this section.

### Discrete Kirchhoff Triangular (DKT) Element

The formulation of elements based on the discrete Kirchhoff theory for the bending of thin plates is obtained by first considering a theory of plates including transverse shear deformations. The independent variables are the deflection  $w$ , and the rotations  $\beta_x$  and  $\beta_y$ , and only  $C^0$  continuity requirements need to be satisfied. The transverse shear energy is

neglected altogether and the Kirchhoff hypothesis is introduced in a discrete way along the edges of the element to relate the rotations to the transverse displacements.

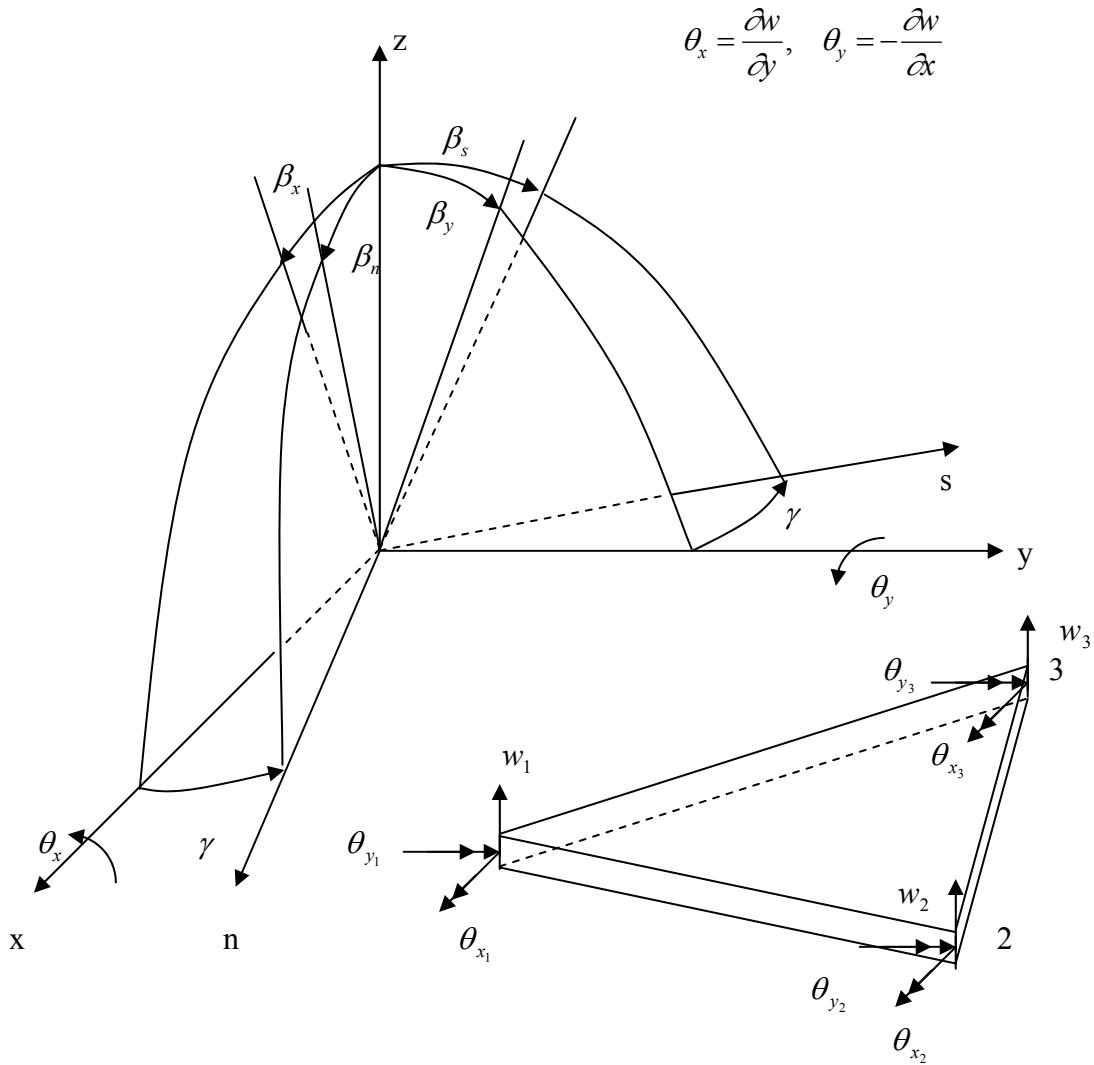


Figure 2.11 Definitions of variables in the formulation of the DKT element

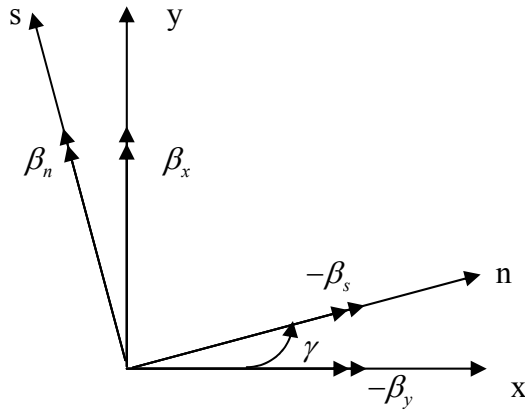


Figure 2.12 Relation between  $\beta_x$ ,  $\beta_y$  and  $\beta_n$ ,  $\beta_s$

Table 2.4 Direction cosines between the two sets of axes

|   | n             | s              |
|---|---------------|----------------|
| x | $\cos \gamma$ | $-\sin \gamma$ |
| y | $\sin \gamma$ | $\cos \gamma$  |

$$x = n \cos \gamma - s \sin \gamma$$

$$y = n \sin \gamma + s \cos \gamma$$

Using tensor transformation,

$$\begin{Bmatrix} -\beta_y \\ \beta_x \end{Bmatrix} = \begin{bmatrix} \cos \gamma & -\sin \gamma \\ \sin \gamma & \cos \gamma \end{bmatrix} \begin{Bmatrix} -\beta_s \\ \beta_n \end{Bmatrix}$$

that is,

$$\begin{Bmatrix} \beta_x \\ \beta_y \end{Bmatrix} = \begin{bmatrix} \cos \gamma & -\sin \gamma \\ \sin \gamma & \cos \gamma \end{bmatrix} \begin{Bmatrix} \beta_n \\ \beta_s \end{Bmatrix} \quad (2.45a)$$

or,

$$\begin{Bmatrix} \beta_n \\ \beta_s \end{Bmatrix} = \begin{bmatrix} \cos \gamma & \sin \gamma \\ -\sin \gamma & \cos \gamma \end{bmatrix} \begin{Bmatrix} \beta_x \\ \beta_y \end{Bmatrix} \quad (2.45b)$$

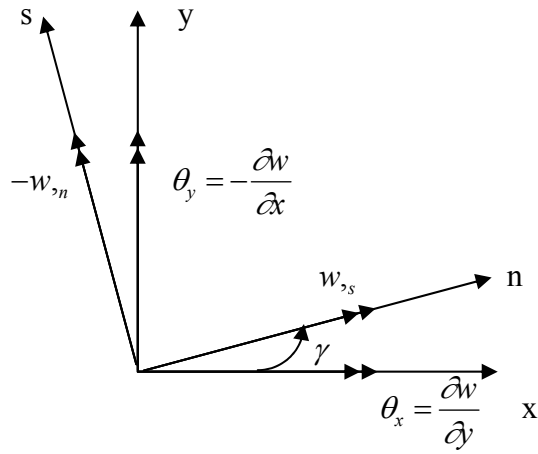


Figure 2.13 Relation between  $w_n$ ,  $w_s$  and  $\theta_x$ ,  $\theta_y$

Table 2.5 Direction cosines between the two sets of axes

|   | x              | y             |
|---|----------------|---------------|
| n | $\cos \gamma$  | $\sin \gamma$ |
| s | $-\sin \gamma$ | $\cos \gamma$ |

$$\begin{Bmatrix} w_{2s} \\ -w_{2n} \end{Bmatrix} = \begin{bmatrix} \cos \gamma & \sin \gamma \\ -\sin \gamma & \cos \gamma \end{bmatrix} \begin{Bmatrix} w_{2y} \\ -w_{2x} \end{Bmatrix} = \begin{bmatrix} \cos \gamma & \sin \gamma \\ -\sin \gamma & \cos \gamma \end{bmatrix} \begin{Bmatrix} \theta_x \\ \theta_y \end{Bmatrix}$$

that is,

$$\begin{Bmatrix} w_{2s} \\ w_{2n} \end{Bmatrix} = \begin{bmatrix} \cos \gamma & \sin \gamma \\ \sin \gamma & -\cos \gamma \end{bmatrix} \begin{Bmatrix} \theta_x \\ \theta_y \end{Bmatrix} \quad (2.46)$$

Another way,

$$w(x,y) = w(n,s)$$

so

$$w_{2n} = \frac{\partial w}{\partial n} = \frac{\partial w}{\partial x} \frac{\partial x}{\partial n} + \frac{\partial w}{\partial y} \frac{\partial y}{\partial n} = \cos \gamma \frac{\partial w}{\partial x} + \sin \gamma \frac{\partial w}{\partial y} = \sin \gamma \theta_x - \cos \gamma \theta_y$$

$$w_{2s} = \frac{\partial w}{\partial s} = \frac{\partial w}{\partial x} \frac{\partial x}{\partial s} + \frac{\partial w}{\partial y} \frac{\partial y}{\partial s} = -\sin \gamma \frac{\partial w}{\partial x} + \cos \gamma \frac{\partial w}{\partial y} = \cos \gamma \theta_x + \sin \gamma \theta_y$$



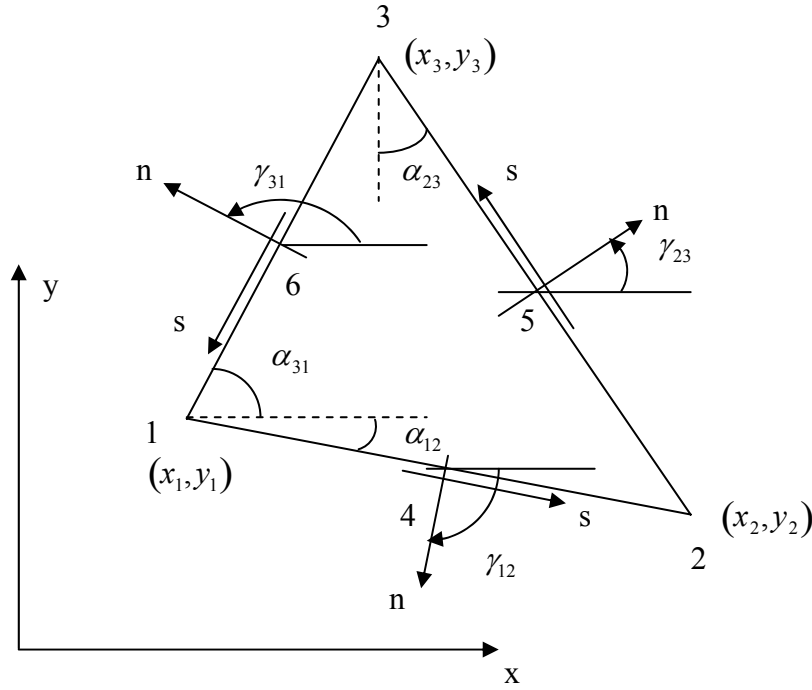


Figure 2.14 Geometry of the triangular element

$$\sin \gamma_{12} = \sin(-90 + \alpha_{12}) = -\cos \alpha_{12} = \frac{x_1 - x_2}{l_{12}} = \frac{x_{12}}{l_{12}}$$

$$\cos \gamma_{12} = \cos(-90 + \alpha_{12}) = -\sin \alpha_{12} = -\frac{y_1 - y_2}{l_{12}} = -\frac{y_{12}}{l_{12}}$$

$$\sin \gamma_{23} = \sin \alpha_{23} = \frac{x_2 - x_3}{l_{23}} = \frac{x_{23}}{l_{23}}$$

$$\cos \gamma_{23} = \cos \alpha_{23} = -\frac{y_2 - y_3}{l_{23}} = -\frac{y_{23}}{l_{23}}$$

$$\sin \gamma_{31} = \sin(90 + \alpha_{31}) = \cos \alpha_{31} = \frac{x_3 - x_1}{l_{31}} = \frac{x_{31}}{l_{31}}$$

$$\cos \gamma_{31} = \cos(90 + \alpha_{31}) = -\sin \alpha_{31} = -\frac{y_3 - y_1}{l_{31}} = -\frac{y_{31}}{l_{31}}$$

$$l_{ij} = \sqrt{x_{ij}^2 + y_{ij}^2}, \quad x_{ij} = x_i - x_j, \quad y_{ij} = y_i - y_j$$

$$\sin \gamma_{ij} = \frac{x_{ij}}{l_{ij}}, \quad \cos \gamma_{ij} = -\frac{y_{ij}}{l_{ij}}$$

$$x_k = \frac{1}{2}(x_i + x_j), \quad y_k = \frac{1}{2}(y_i + y_j)$$

where  $k = 4, 5, 6$  for the sides  $ij = 12, 23, 31$ , respectively.

The formulation of the DKT element is based on the following assumptions

(1)  $\beta_x$  and  $\beta_y$  are given by complete quadratic polynomials, i.e.

$$\beta_x = \sum_{i=1}^6 N_i \beta_{x_i}, \quad \beta_y = \sum_{i=1}^6 N_i \beta_{y_i} \quad (2.47)$$

Shape functions  $N_i$  are given in Appendix F.

(2) The Kirchhoff hypothesis is imposed at,

(a) the corner nodes

$$\gamma = \begin{cases} \beta_x + w_{,x} \\ \beta_y + w_{,y} \end{cases} = 0 \quad \text{at the nodes 1, 2, and 3} \quad (2.48)$$

(b) the mid-nodes (defined anticlockwise around the element boundary)

$$\beta_{s_k} + w_{,s_k} = 0 \quad k=4, 5, 6 \quad (2.49)$$

(3) The variation of  $w$  along the sides is cubic. The slope  $w_{,s}$  at the mid-nodes can be obtained from beam shape functions by differentiating once and evaluating at the mid-span( see Appendix H), i.e.

$$w_{,s_k} = -\frac{3}{2l_{ij}} w_i - \frac{1}{4} w_{,s_i} + \frac{3}{2l_{ij}} w_j - \frac{1}{4} w_{,s_j} \quad k = 4, 5, 6 \quad (2.50)$$

(4) The normal slope  $\beta_n$  along each side vary linearly. Therefore,

$$\beta_{n_k} = \frac{1}{2}(\beta_{n_i} + \beta_{n_j}) \quad k = 4, 5, 6 \quad (2.51)$$

where  $k = 4, 5, 6$  denotes the mid-node of the sides 12, 23 and 31, respectively.

$$\beta_x = \begin{bmatrix} H_{x_1} & H_{x_2} & H_{x_3} & H_{x_4} & H_{x_5} & H_{x_6} & H_{x_7} & H_{x_8} & H_{x_9} \end{bmatrix} \begin{Bmatrix} w_1 \\ \theta_{x_1} \\ \theta_{y_1} \\ w_2 \\ \theta_{x_2} \\ \theta_{y_2} \\ w \\ \theta_{x_3} \\ \theta_{y_3} \end{Bmatrix} = H_x^T \begin{Bmatrix} w_1 \\ \theta_{x_1} \\ \theta_{y_1} \\ w_2 \\ \theta_{x_2} \\ \theta_{y_2} \\ w \\ \theta_{x_3} \\ \theta_{y_3} \end{Bmatrix}$$

$$\beta_x = N_1\beta_{x_1} + N_2\beta_{x_2} + N_3\beta_{x_3} + N_4\beta_{x_4} + N_5\beta_{x_5} + N_6\beta_{x_6}$$

using (2.48) and (2.45a)

$$\begin{aligned} \beta_x = & -N_1w_{x_1} - N_2w_{x_2} - N_3w_{x_3} + N_4(\cos\gamma_{12}\beta_{n_4} - \sin\gamma_{12}\beta_{s_4}) \\ & + N_5(\cos\gamma_{23}\beta_{n_5} - \sin\gamma_{23}\beta_{s_5}) + N_6(\cos\gamma_{31}\beta_{n_6} - \sin\gamma_{31}\beta_{s_6}) \end{aligned}$$

using (2.49) and (2.51)

$$\begin{aligned} \beta_x = & N_1\theta_{y_1} + N_2\theta_{y_2} + N_3\theta_{y_3} + N_4\cos\gamma_{12}\frac{1}{2}(\beta_{n_1} + \beta_{n_2}) + N_4\sin\gamma_{12}w_{s_4} \\ & + N_5\cos\gamma_{23}\frac{1}{2}(\beta_{n_2} + \beta_{n_3}) + N_5\sin\gamma_{23}w_{s_5} + N_6\cos\gamma_{31}\frac{1}{2}(\beta_{n_3} + \beta_{n_1}) + N_6\sin\gamma_{31}w_{s_6} \end{aligned}$$

using (2.45b)

$$\begin{aligned} \beta_x = & N_1\theta_{y_1} + N_2\theta_{y_2} + N_3\theta_{y_3} \\ & + N_4\cos\gamma_{12}\frac{1}{2}(\cos\gamma_{12}\beta_{x_1} + \sin\gamma_{12}\beta_{y_1} + \cos\gamma_{12}\beta_{x_2} + \sin\gamma_{12}\beta_{y_2}) + N_4\sin\gamma_{12}w_{s_4} \\ & + N_5\cos\gamma_{23}\frac{1}{2}(\cos\gamma_{23}\beta_{x_2} + \sin\gamma_{23}\beta_{y_2} + \cos\gamma_{23}\beta_{x_3} + \sin\gamma_{23}\beta_{y_3}) + N_5\sin\gamma_{23}w_{s_5} \\ & + N_6\cos\gamma_{31}\frac{1}{2}(\cos\gamma_{31}\beta_{x_3} + \sin\gamma_{31}\beta_{y_3} + \cos\gamma_{31}\beta_{x_1} + \sin\gamma_{31}\beta_{y_1}) + N_6\sin\gamma_{31}w_{s_6} \end{aligned}$$

using (2.48)

$$\begin{aligned}
\beta_x &= N_1 \theta_{y_1} + N_2 \theta_{y_2} + N_3 \theta_{y_3} \\
&+ N_4 \cos \gamma_{12} \frac{1}{2} (\cos \gamma_{12} (-w_{x_1}) + \sin \gamma_{12} (-w_{y_1}) + \cos \gamma_{12} (-w_{x_2}) + \sin \gamma_{12} (-w_{y_2})) + N_4 \sin \gamma_{12} w_{s_4} \\
&+ N_5 \cos \gamma_{23} \frac{1}{2} (\cos \gamma_{23} (-w_{x_2}) + \sin \gamma_{23} (-w_{y_2}) + \cos \gamma_{23} (-w_{x_3}) + \sin \gamma_{23} (-w_{y_3})) + N_5 \sin \gamma_{23} w_{s_5} \\
&+ N_6 \cos \gamma_{31} \frac{1}{2} (\cos \gamma_{31} (-w_{x_3}) + \sin \gamma_{31} (-w_{y_3}) + \cos \gamma_{31} (-w_{x_1}) + \sin \gamma_{31} (-w_{y_1})) + N_6 \sin \gamma_{31} w_{s_6} \\
&= N_1 \theta_{y_1} + N_2 \theta_{y_2} + N_3 \theta_{y_3} \\
&+ N_4 \cos \gamma_{12} \frac{1}{2} (\cos \gamma_{12} \theta_{y_1} - \sin \gamma_{12} \theta_{x_1} + \cos \gamma_{12} \theta_{y_2} - \sin \gamma_{12} \theta_{x_2}) + N_4 \sin \gamma_{12} w_{s_4} \\
&+ N_5 \cos \gamma_{23} \frac{1}{2} (\cos \gamma_{23} \theta_{y_2} - \sin \gamma_{23} \theta_{x_2} + \cos \gamma_{23} \theta_{y_3} - \sin \gamma_{23} \theta_{x_3}) + N_5 \sin \gamma_{23} w_{s_5} \\
&+ N_6 \cos \gamma_{31} \frac{1}{2} (\cos \gamma_{31} \theta_{y_3} - \sin \gamma_{31} \theta_{x_3} + \cos \gamma_{31} \theta_{y_1} - \sin \gamma_{31} \theta_{x_1}) + N_6 \sin \gamma_{31} w_{s_6}
\end{aligned}$$

using (2.50)

$$\begin{aligned}
\beta_x &= N_1 \theta_{y_1} + N_2 \theta_{y_2} + N_3 \theta_{y_3} \\
&+ N_4 \cos \gamma_{12} \frac{1}{2} (\cos \gamma_{12} \theta_{y_1} - \sin \gamma_{12} \theta_{x_1} + \cos \gamma_{12} \theta_{y_2} - \sin \gamma_{12} \theta_{x_2}) \\
&+ N_4 \sin \gamma_{12} \left( -\frac{3}{2l_{12}} w_1 - \frac{1}{4} w_{s_1} + \frac{3}{2l_{12}} w_2 - \frac{1}{4} w_{s_2} \right) \\
&+ N_5 \cos \gamma_{23} \frac{1}{2} (\cos \gamma_{23} \theta_{y_2} - \sin \gamma_{23} \theta_{x_2} + \cos \gamma_{23} \theta_{y_3} - \sin \gamma_{23} \theta_{x_3}) \\
&+ N_5 \sin \gamma_{23} \left( -\frac{3}{2l_{23}} w_2 - \frac{1}{4} w_{s_2} + \frac{3}{2l_{23}} w_3 - \frac{1}{4} w_{s_3} \right) \\
&+ N_6 \cos \gamma_{31} \frac{1}{2} (\cos \gamma_{31} \theta_{y_3} - \sin \gamma_{31} \theta_{x_3} + \cos \gamma_{31} \theta_{y_1} - \sin \gamma_{31} \theta_{x_1}) \\
&+ N_6 \sin \gamma_{31} \left( -\frac{3}{2l_{31}} w_3 - \frac{1}{4} w_{s_3} + \frac{3}{2l_{31}} w_1 - \frac{1}{4} w_{s_1} \right)
\end{aligned}$$

using (2.46)

$$\begin{aligned}
\beta_x &= N_1 \theta_{y_1} + N_2 \theta_{y_2} + N_3 \theta_{y_3} \\
&+ N_4 \cos \gamma_{12} \frac{1}{2} (\cos \gamma_{12} \theta_{y_1} - \sin \gamma_{12} \theta_{x_1} + \cos \gamma_{12} \theta_{y_2} - \sin \gamma_{12} \theta_{x_2}) \\
&+ N_4 \sin \gamma_{12} \left( -\frac{3}{2l_{12}} w_1 - \frac{1}{4} (\cos \gamma_{12} \theta_{x_1} + \sin \gamma_{12} \theta_{y_1}) + \frac{3}{2l_{12}} w_2 - \frac{1}{4} (\cos \gamma_{12} \theta_{x_2} + \sin \gamma_{12} \theta_{y_2}) \right) \\
&+ N_5 \cos \gamma_{23} \frac{1}{2} (\cos \gamma_{23} \theta_{y_2} - \sin \gamma_{23} \theta_{x_2} + \cos \gamma_{23} \theta_{y_3} - \sin \gamma_{23} \theta_{x_3}) \\
&+ N_5 \sin \gamma_{23} \left( -\frac{3}{2l_{23}} w_2 - \frac{1}{4} (\cos \gamma_{23} \theta_{x_2} + \sin \gamma_{23} \theta_{y_2}) + \frac{3}{2l_{23}} w_3 - \frac{1}{4} (\cos \gamma_{23} \theta_{x_3} + \sin \gamma_{23} \theta_{y_3}) \right) \\
&+ N_6 \cos \gamma_{31} \frac{1}{2} (\cos \gamma_{31} \theta_{y_3} - \sin \gamma_{31} \theta_{x_3} + \cos \gamma_{31} \theta_{y_1} - \sin \gamma_{31} \theta_{x_1}) \\
&+ N_6 \sin \gamma_{31} \left( -\frac{3}{2l_{31}} w_3 - \frac{1}{4} (\cos \gamma_{31} \theta_{x_3} + \sin \gamma_{31} \theta_{y_3}) + \frac{3}{2l_{31}} w_1 - \frac{1}{4} (\cos \gamma_{31} \theta_{x_1} + \sin \gamma_{31} \theta_{y_1}) \right)
\end{aligned}$$

Collecting the coefficient of  $w_1$ ,  $\theta_{x_1}$ ,  $\theta_{y_1}$ , etc., we get the shape function

$$H_{x_1} = -N_4 \sin \gamma_{12} \frac{3}{2l_{12}} + N_6 \sin \gamma_{31} \frac{3}{2l_{31}} = -N_4 \frac{x_{12}}{l_{12}} \frac{3}{2l_{12}} + N_6 \frac{x_{31}}{l_{31}} \frac{3}{2l_{31}} = 1.5(a_4 N_4 - a_6 N_6)$$

$$H_{x_2} = -\frac{3}{4} N_4 \sin \gamma_{12} \cos \gamma_{12} - \frac{3}{4} N_6 \sin \gamma_{31} \cos \gamma_{31} = -\frac{3}{4} N_4 \frac{x_{12}}{l_{12}} \left( -\frac{y_{12}}{l_{12}} \right) - \frac{3}{4} N_6 \frac{x_{31}}{l_{31}} \left( -\frac{y_{31}}{l_{31}} \right) = b_4 N_4 + b_6 N_6$$

$$\begin{aligned}
H_{x_3} &= N_1 - \left( \frac{1}{4} \sin^2 \gamma_{12} - \frac{1}{2} \cos^2 \gamma_{12} \right) N_4 - \left( \frac{1}{4} \sin^2 \gamma_{31} - \frac{1}{2} \cos^2 \gamma_{31} \right) N_6 \\
&= N_1 - \left( \frac{1}{4} \left( \frac{x_{12}}{l_{12}} \right)^2 - \frac{1}{2} \left( -\frac{y_{12}}{l_{12}} \right)^2 \right) N_4 - \left( \frac{1}{4} \left( \frac{x_{31}}{l_{31}} \right)^2 - \frac{1}{2} \left( -\frac{y_{31}}{l_{31}} \right)^2 \right) N_6 \\
&= N_1 - c_4 N_4 - c_6 N_6
\end{aligned}$$

$$H_{x_4} = N_4 \sin \gamma_{12} \frac{3}{2l_{12}} - N_5 \sin \gamma_{23} \frac{3}{2l_{23}} = N_4 \frac{x_{12}}{l_{12}} \frac{3}{2l_{12}} - N_5 \frac{x_{23}}{l_{23}} \frac{3}{2l_{23}} = 1.5(a_5 N_5 - a_4 N_4)$$

$$H_{x_5} = -\frac{3}{4} N_4 \sin \gamma_{12} \cos \gamma_{12} - \frac{3}{4} N_5 \sin \gamma_{23} \cos \gamma_{23} = -\frac{3}{4} N_4 \frac{x_{12}}{l_{12}} \left( -\frac{y_{12}}{l_{12}} \right) - \frac{3}{4} N_5 \frac{x_{23}}{l_{23}} \left( -\frac{y_{23}}{l_{23}} \right) = b_4 N_4 + b_5 N_5$$

$$\begin{aligned}
H_{x_6} &= N_2 - \left( \frac{1}{4} \sin^2 \gamma_{12} - \frac{1}{2} \cos^2 \gamma_{12} \right) N_4 - \left( \frac{1}{4} \sin^2 \gamma_{23} - \frac{1}{2} \cos^2 \gamma_{23} \right) N_5 \\
&= N_2 - \left( \frac{1}{4} \left( \frac{x_{12}}{l_{12}} \right)^2 - \frac{1}{2} \left( -\frac{y_{12}}{l_{12}} \right)^2 \right) N_4 - \left( \frac{1}{4} \left( \frac{x_{23}}{l_{23}} \right)^2 - \frac{1}{2} \left( -\frac{y_{23}}{l_{23}} \right)^2 \right) N_5 \\
&= N_2 - c_4 N_4 - c_5 N_5
\end{aligned}$$

$$H_{x_7} = -N_6 \sin \gamma_{31} \frac{3}{2l_{31}} + N_5 \sin \gamma_{23} \frac{3}{2l_{23}} = -N_6 \frac{x_{31}}{l_{31}} \frac{3}{2l_{31}} + N_5 \frac{x_{23}}{l_{23}} \frac{3}{2l_{23}} = 1.5(a_6 N_6 - a_5 N_5)$$

$$H_{x_8} = -\frac{3}{4} N_5 \sin \gamma_{23} \cos \gamma_{23} - \frac{3}{4} N_6 \sin \gamma_{31} \cos \gamma_{31} = -\frac{3}{4} N_5 \frac{x_{23}}{l_{23}} \left(-\frac{y_{23}}{l_{23}}\right) - \frac{3}{4} N_6 \frac{x_{31}}{l_{31}} \left(-\frac{y_{31}}{l_{31}}\right) = b_5 N_5 + b_6 N_6$$

$$\begin{aligned} H_{x_9} &= N_3 - \left(\frac{1}{4} \sin^2 \gamma_{23} - \frac{1}{2} \cos^2 \gamma_{23}\right) N_5 - \left(\frac{1}{4} \sin^2 \gamma_{31} - \frac{1}{2} \cos^2 \gamma_{31}\right) N_6 \\ &= N_3 - \left(\frac{1}{4} \left(\frac{x_{23}}{l_{23}}\right)^2 - \frac{1}{2} \left(-\frac{y_{23}}{l_{23}}\right)^2\right) N_5 - \left(\frac{1}{4} \left(\frac{x_{31}}{l_{31}}\right)^2 - \frac{1}{2} \left(-\frac{y_{31}}{l_{31}}\right)^2\right) N_6 \\ &= N_3 - c_5 N_5 - c_6 N_6 \end{aligned}$$

where

$$a_4 = -x_{12}/l_{12}^2, \quad a_5 = -x_{23}/l_{23}^2, \quad a_6 = -x_{31}/l_{31}^2$$

$$b_4 = \frac{3}{4} \frac{x_{12}y_{12}}{l_{12}^2}, \quad b_5 = \frac{3}{4} \frac{x_{23}y_{23}}{l_{23}^2}, \quad b_6 = \frac{3}{4} \frac{x_{31}y_{31}}{l_{31}^2}$$

$$c_4 = \left(\frac{1}{4} x_{12}^2 - \frac{1}{2} y_{12}^2\right)/l_{12}^2, \quad c_5 = \left(\frac{1}{4} x_{23}^2 - \frac{1}{2} y_{23}^2\right)/l_{23}^2, \quad c_6 = \left(\frac{1}{4} x_{31}^2 - \frac{1}{2} y_{31}^2\right)/l_{31}^2$$

Similarly

$$\beta_y = \begin{bmatrix} H_{y_1} & H_{y_2} & H_{y_3} & H_{y_4} & H_{y_5} & H_{y_6} & H_{y_7} & H_{y_8} & H_{y_9} \end{bmatrix} \begin{Bmatrix} w_1 \\ \theta_{x_1} \\ \theta_{y_1} \\ w_2 \\ \theta_{x_2} \\ \theta_{y_2} \\ w \\ \theta_{x_3} \\ \theta_{y_3} \end{Bmatrix} = H_y^T \begin{Bmatrix} w_1 \\ \theta_{x_1} \\ \theta_{y_1} \\ w_2 \\ \theta_{x_2} \\ \theta_{y_2} \\ w \\ \theta_{x_3} \\ \theta_{y_3} \end{Bmatrix}$$

$$\beta_y = N_1 \beta_{y_1} + N_2 \beta_{y_2} + N_3 \beta_{y_3} + N_4 \beta_{y_4} + N_5 \beta_{y_5} + N_6 \beta_{y_6}$$

using (2.48) and (2.45a)

$$\begin{aligned} \beta_y &= -N_1 w_{y_1} - N_2 w_{y_2} - N_3 w_{y_3} + N_4 (\sin \gamma_{12} \beta_{n_4} + \cos \gamma_{12} \beta_{s_4}) \\ &\quad + N_5 (\sin \gamma_{23} \beta_{n_5} + \cos \gamma_{23} \beta_{s_5}) + N_6 (\sin \gamma_{31} \beta_{n_6} + \cos \gamma_{31} \beta_{s_6}) \end{aligned}$$

using (2.49) and (2.51)

$$\begin{aligned}\beta_y &= -N_1\theta_{x_1} - N_2\theta_{x_2} - N_3\theta_{x_3} + N_4 \sin \gamma_{12} \frac{1}{2}(\beta_{n_1} + \beta_{n_2}) - N_4 \cos \gamma_{12} w_{s_4} \\ &\quad + N_5 \sin \gamma_{23} \frac{1}{2}(\beta_{n_2} + \beta_{n_3}) - N_5 \cos \gamma_{23} w_{s_5} + N_6 \sin \gamma_{31} \frac{1}{2}(\beta_{n_3} + \beta_{n_1}) - N_6 \cos \gamma_{31} w_{s_6}\end{aligned}$$

using (2.45b)

$$\begin{aligned}\beta_y &= -N_1\theta_{x_1} - N_2\theta_{x_2} - N_3\theta_{x_3} \\ &\quad + N_4 \sin \gamma_{12} \frac{1}{2}(\cos \gamma_{12}\beta_{x_1} + \sin \gamma_{12}\beta_{y_1} + \cos \gamma_{12}\beta_{x_2} + \sin \gamma_{12}\beta_{y_2}) - N_4 \cos \gamma_{12} w_{s_4} \\ &\quad + N_5 \sin \gamma_{23} \frac{1}{2}(\cos \gamma_{23}\beta_{x_2} + \sin \gamma_{23}\beta_{y_2} + \cos \gamma_{23}\beta_{x_3} + \sin \gamma_{23}\beta_{y_3}) - N_5 \cos \gamma_{23} w_{s_5} \\ &\quad + N_6 \sin \gamma_{31} \frac{1}{2}(\cos \gamma_{31}\beta_{x_3} + \sin \gamma_{31}\beta_{y_3} + \cos \gamma_{31}\beta_{x_1} + \sin \gamma_{31}\beta_{y_1}) - N_6 \cos \gamma_{31} w_{s_6}\end{aligned}$$

using (2.48)

$$\begin{aligned}\beta_y &= -N_1\theta_{x_1} - N_2\theta_{x_2} - N_3\theta_{x_3} \\ &\quad + N_4 \sin \gamma_{12} \frac{1}{2}(\cos \gamma_{12}(-w_{x_1}) + \sin \gamma_{12}(-w_{y_1}) + \cos \gamma_{12}(-w_{x_2}) + \sin \gamma_{12}(-w_{y_2})) - N_4 \cos \gamma_{12} w_{s_4} \\ &\quad + N_5 \sin \gamma_{23} \frac{1}{2}(\cos \gamma_{23}(-w_{x_2}) + \sin \gamma_{23}(-w_{y_2}) + \cos \gamma_{23}(-w_{x_3}) + \sin \gamma_{23}(-w_{y_3})) - N_5 \cos \gamma_{23} w_{s_5} \\ &\quad + N_6 \sin \gamma_{31} \frac{1}{2}(\cos \gamma_{31}(-w_{x_3}) + \sin \gamma_{31}(-w_{y_3}) + \cos \gamma_{31}(-w_{x_1}) + \sin \gamma_{31}(-w_{y_1})) - N_6 \cos \gamma_{31} w_{s_6} \\ &= -N_1\theta_{x_1} - N_2\theta_{x_2} - N_3\theta_{x_3} \\ &\quad + N_4 \sin \gamma_{12} \frac{1}{2}(\cos \gamma_{12}\theta_{y_1} - \sin \gamma_{12}\theta_{x_1} + \cos \gamma_{12}\theta_{y_2} - \sin \gamma_{12}\theta_{x_2}) - N_4 \cos \gamma_{12} w_{s_4} \\ &\quad + N_5 \sin \gamma_{23} \frac{1}{2}(\cos \gamma_{23}\theta_{y_2} - \sin \gamma_{23}\theta_{x_2} + \cos \gamma_{23}\theta_{y_3} - \sin \gamma_{23}\theta_{x_3}) - N_5 \cos \gamma_{23} w_{s_5} \\ &\quad + N_6 \sin \gamma_{31} \frac{1}{2}(\cos \gamma_{31}\theta_{y_3} - \sin \gamma_{31}\theta_{x_3} + \cos \gamma_{31}\theta_{y_1} - \sin \gamma_{31}\theta_{x_1}) - N_6 \cos \gamma_{31} w_{s_6}\end{aligned}$$

using (2.50)

$$\begin{aligned}
\beta_y = & -N_1\theta_{x_1} - N_2\theta_{x_2} - N_3\theta_{x_3} \\
& + N_4 \sin \gamma_{12} \frac{1}{2} (\cos \gamma_{12}\theta_{y_1} - \sin \gamma_{12}\theta_{x_1} + \cos \gamma_{12}\theta_{y_2} - \sin \gamma_{12}\theta_{x_2}) \\
& - N_4 \cos \gamma_{12} \left( -\frac{3}{2l_{12}} w_1 - \frac{1}{4} w_{s_1} + \frac{3}{2l_{12}} w_2 - \frac{1}{4} w_{s_2} \right) \\
& + N_5 \sin \gamma_{23} \frac{1}{2} (\cos \gamma_{23}\theta_{y_2} - \sin \gamma_{23}\theta_{x_2} + \cos \gamma_{23}\theta_{y_3} - \sin \gamma_{23}\theta_{x_3}) \\
& - N_5 \cos \gamma_{23} \left( -\frac{3}{2l_{23}} w_2 - \frac{1}{4} w_{s_2} + \frac{3}{2l_{23}} w_3 - \frac{1}{4} w_{s_3} \right) \\
& + N_6 \sin \gamma_{31} \frac{1}{2} (\cos \gamma_{31}\theta_{y_3} - \sin \gamma_{31}\theta_{x_3} + \cos \gamma_{31}\theta_{y_1} - \sin \gamma_{31}\theta_{x_1}) \\
& - N_6 \cos \gamma_{31} \left( -\frac{3}{2l_{31}} w_3 - \frac{1}{4} w_{s_3} + \frac{3}{2l_{31}} w_1 - \frac{1}{4} w_{s_1} \right)
\end{aligned}$$

using (2.46)

$$\begin{aligned}
\beta_y = & -N_1\theta_{x_1} - N_2\theta_{x_2} - N_3\theta_{x_3} \\
& + N_4 \sin \gamma_{12} \frac{1}{2} (\cos \gamma_{12}\theta_{y_1} - \sin \gamma_{12}\theta_{x_1} + \cos \gamma_{12}\theta_{y_2} - \sin \gamma_{12}\theta_{x_2}) \\
& - N_4 \cos \gamma_{12} \left( -\frac{3}{2l_{12}} w_1 - \frac{1}{4} (\cos \gamma_{12}\theta_{x_1} + \sin \gamma_{12}\theta_{y_1}) + \frac{3}{2l_{12}} w_2 - \frac{1}{4} (\cos \gamma_{12}\theta_{x_2} + \sin \gamma_{12}\theta_{y_2}) \right) \\
& + N_5 \sin \gamma_{23} \frac{1}{2} (\cos \gamma_{23}\theta_{y_2} - \sin \gamma_{23}\theta_{x_2} + \cos \gamma_{23}\theta_{y_3} - \sin \gamma_{23}\theta_{x_3}) \\
& - N_5 \cos \gamma_{23} \left( -\frac{3}{2l_{23}} w_2 - \frac{1}{4} (\cos \gamma_{23}\theta_{x_2} + \sin \gamma_{23}\theta_{y_2}) + \frac{3}{2l_{23}} w_3 - \frac{1}{4} (\cos \gamma_{23}\theta_{x_3} + \sin \gamma_{23}\theta_{y_3}) \right) \\
& + N_6 \sin \gamma_{31} \frac{1}{2} (\cos \gamma_{31}\theta_{y_3} - \sin \gamma_{31}\theta_{x_3} + \cos \gamma_{31}\theta_{y_1} - \sin \gamma_{31}\theta_{x_1}) \\
& - N_6 \cos \gamma_{31} \left( -\frac{3}{2l_{31}} w_3 - \frac{1}{4} (\cos \gamma_{31}\theta_{x_3} + \sin \gamma_{31}\theta_{y_3}) + \frac{3}{2l_{31}} w_1 - \frac{1}{4} (\cos \gamma_{31}\theta_{x_1} + \sin \gamma_{31}\theta_{y_1}) \right)
\end{aligned}$$

collecting the coefficient of  $w_1$ ,  $\theta_{x_1}$ ,  $\theta_{y_1}$ , etc., we get the shape function

$$H_{y_1} = N_4 \cos \gamma_{12} \frac{3}{2l_{12}} - N_6 \cos \gamma_{31} \frac{3}{2l_{31}} = N_4 \left( -\frac{y_{12}}{l_{12}} \right) \frac{3}{2l_{12}} - N_6 \left( -\frac{y_{31}}{l_{31}} \right) \frac{3}{2l_{31}} = 1.5(d_4 N_4 - d_6 N_6)$$

$$\begin{aligned}
H_{y_2} = & -N_1 + \left( \frac{1}{4} \cos^2 \gamma_{12} - \frac{1}{2} \sin^2 \gamma_{12} \right) N_4 + \left( \frac{1}{4} \cos^2 \gamma_{31} - \frac{1}{2} \sin^2 \gamma_{31} \right) N_6 \\
= & -N_1 + \left( \frac{1}{4} \left( -\frac{y_{12}}{l_{12}} \right)^2 - \frac{1}{2} \left( \frac{x_{12}}{l_{12}} \right)^2 \right) N_4 + \left( \frac{1}{4} \left( -\frac{y_{31}}{l_{31}} \right)^2 - \frac{1}{2} \left( \frac{x_{31}}{l_{31}} \right)^2 \right) N_6 \\
= & -N_1 + e_4 N_4 + e_6 N_6
\end{aligned}$$



$$H_{y_3} = \frac{3}{4}N_4 \sin \gamma_{12} \cos \gamma_{12} + \frac{3}{4}N_6 \sin \gamma_{31} \cos \gamma_{31} = \frac{3}{4}N_4 \frac{x_{12}}{l_{12}} \left(-\frac{y_{12}}{l_{12}}\right) + \frac{3}{4}N_6 \frac{x_{31}}{l_{31}} \left(-\frac{y_{31}}{l_{31}}\right) = -b_4 N_4 - b_6 N_6 = -H_{x_2}$$

$$H_{y_4} = -N_4 \cos \gamma_{12} \frac{3}{2l_{12}} + N_5 \cos \gamma_{23} \frac{3}{2l_{23}} = -N_4 \left(-\frac{y_{12}}{l_{12}}\right) \frac{3}{2l_{12}} + N_5 \left(-\frac{y_{23}}{l_{23}}\right) \frac{3}{2l_{23}} = 1.5(d_5 N_5 - d_4 N_4)$$

$$\begin{aligned} H_{y_5} &= -N_2 + \left(\frac{1}{4} \cos^2 \gamma_{12} - \frac{1}{2} \sin^2 \gamma_{12}\right) N_4 + \left(\frac{1}{4} \cos^2 \gamma_{23} - \frac{1}{2} \sin^2 \gamma_{23}\right) N_5 \\ &= -N_2 + \left(\frac{1}{4} \left(-\frac{y_{12}}{l_{12}}\right)^2 - \frac{1}{2} \left(\frac{x_{12}}{l_{12}}\right)^2\right) N_4 + \left(\frac{1}{4} \left(-\frac{y_{23}}{l_{23}}\right)^2 - \frac{1}{2} \left(\frac{x_{23}}{l_{23}}\right)^2\right) N_5 \\ &= -N_2 + e_4 N_4 + e_5 N_5 \end{aligned}$$

$$H_{y_6} = \frac{3}{4}N_4 \sin \gamma_{12} \cos \gamma_{12} + \frac{3}{4}N_5 \sin \gamma_{23} \cos \gamma_{23} = \frac{3}{4}N_4 \frac{x_{12}}{l_{12}} \left(-\frac{y_{12}}{l_{12}}\right) + \frac{3}{4}N_5 \frac{x_{23}}{l_{23}} \left(-\frac{y_{23}}{l_{23}}\right) = -b_4 N_4 - b_5 N_5 = -H_{x_5}$$

$$H_{y_7} = -N_5 \cos \gamma_{23} \frac{3}{2l_{23}} + N_6 \cos \gamma_{31} \frac{3}{2l_{31}} = -N_5 \left(-\frac{y_{23}}{l_{23}}\right) \frac{3}{2l_{23}} + N_6 \left(-\frac{y_{31}}{l_{31}}\right) \frac{3}{2l_{31}} = 1.5(d_6 N_6 - d_5 N_5)$$

$$\begin{aligned} H_{y_8} &= -N_3 + \left(\frac{1}{4} \cos^2 \gamma_{23} - \frac{1}{2} \sin^2 \gamma_{23}\right) N_5 + \left(\frac{1}{4} \cos^2 \gamma_{31} - \frac{1}{2} \sin^2 \gamma_{31}\right) N_6 \\ &= -N_3 + \left(\frac{1}{4} \left(-\frac{y_{23}}{l_{23}}\right)^2 - \frac{1}{2} \left(\frac{x_{23}}{l_{23}}\right)^2\right) N_5 + \left(\frac{1}{4} \left(-\frac{y_{31}}{l_{31}}\right)^2 - \frac{1}{2} \left(\frac{x_{31}}{l_{31}}\right)^2\right) N_6 \\ &= -N_3 + e_5 N_5 + e_6 N_6 \end{aligned}$$

$$H_{y_9} = \frac{3}{4}N_5 \sin \gamma_{23} \cos \gamma_{23} + \frac{3}{4}N_6 \sin \gamma_{31} \cos \gamma_{31} = \frac{3}{4}N_5 \frac{x_{23}}{l_{23}} \left(-\frac{y_{23}}{l_{23}}\right) + \frac{3}{4}N_6 \frac{x_{31}}{l_{31}} \left(-\frac{y_{31}}{l_{31}}\right) = -b_5 N_5 - b_6 N_6 = -H_{x_8}$$

where

$$b_4 = \frac{3}{4} \frac{x_{12} y_{12}}{l_{12}^2}, \quad b_5 = \frac{3}{4} \frac{x_{23} y_{23}}{l_{23}^2}, \quad b_6 = \frac{3}{4} \frac{x_{31} y_{31}}{l_{31}^2}$$

$$d_4 = -y_{12}/l_{12}^2, \quad d_5 = -y_{23}/l_{23}^2, \quad d_6 = -y_{31}/l_{31}^2$$

$$e_4 = \left(\frac{1}{4} y_{12}^2 - \frac{1}{2} x_{12}^2\right)/l_{12}^2, \quad e_5 = \left(\frac{1}{4} y_{23}^2 - \frac{1}{2} x_{23}^2\right)/l_{23}^2, \quad e_6 = \left(\frac{1}{4} y_{31}^2 - \frac{1}{2} x_{31}^2\right)/l_{31}^2$$

For a summary of the shape functions and their derivatives of the Discrete Kirchhoff

Triangular (DKT) Element, see Appendix I.

$$\begin{aligned}
\kappa &= \begin{Bmatrix} \beta_{x,x} \\ \beta_{y,y} \\ \beta_{x,y} + \beta_{y,x} \end{Bmatrix} = \begin{bmatrix} H_{x,x}^T \\ H_{y,y}^T \\ H_{x,y}^T + H_{y,x}^T \end{bmatrix} \begin{Bmatrix} w_1 \\ \theta_{x1} \\ \theta_{y1} \\ w_2 \\ \theta_{x2} \\ \theta_{y2} \\ w_3 \\ \theta_{x3} \\ \theta_{y3} \end{Bmatrix} = \begin{bmatrix} \frac{\partial H_x^T}{\partial \xi} \frac{\partial \xi}{\partial x} + \frac{\partial H_x^T}{\partial \eta} \frac{\partial \eta}{\partial x} \\ \frac{\partial H_y^T}{\partial \xi} \frac{\partial \xi}{\partial y} + \frac{\partial H_y^T}{\partial \eta} \frac{\partial \eta}{\partial y} \\ \left( \frac{\partial H_x^T}{\partial \xi} \frac{\partial \xi}{\partial y} + \frac{\partial H_x^T}{\partial \eta} \frac{\partial \eta}{\partial y} \right) + \left( \frac{\partial H_y^T}{\partial \xi} \frac{\partial \xi}{\partial x} + \frac{\partial H_y^T}{\partial \eta} \frac{\partial \eta}{\partial x} \right) \end{bmatrix} \begin{Bmatrix} w_1 \\ \theta_{x1} \\ \theta_{y1} \\ w_2 \\ \theta_{x2} \\ \theta_{y2} \\ w_3 \\ \theta_{x3} \\ \theta_{y3} \end{Bmatrix} \\
&= \frac{1}{2A} \begin{bmatrix} y_{31}H_{x,\xi}^T + y_{12}H_{x,\eta}^T \\ -x_{31}H_{y,\xi}^T - x_{12}H_{y,\eta}^T \\ -x_{31}H_{x,\xi}^T - x_{12}H_{x,\eta}^T + y_{31}H_{y,\xi}^T + y_{12}H_{y,\eta}^T \end{bmatrix} \begin{Bmatrix} w_1 \\ \theta_{x1} \\ \theta_{y1} \\ w_2 \\ \theta_{x2} \\ \theta_{y2} \\ w_3 \\ \theta_{x3} \\ \theta_{y3} \end{Bmatrix} = B(\xi, \eta)U
\end{aligned}$$

(2.52)

where

$$\begin{aligned}
B &= \frac{1}{2A} \begin{bmatrix} y_{31}H_{x,\xi}^T + y_{12}H_{x,\eta}^T \\ -x_{31}H_{y,\xi}^T - x_{12}H_{y,\eta}^T \\ -x_{31}H_{x,\xi}^T - x_{12}H_{x,\eta}^T + y_{31}H_{y,\xi}^T + y_{12}H_{y,\eta}^T \end{bmatrix}_{3 \times 9} = \frac{1}{2A} \begin{bmatrix} b_2H_{x,\xi}^T + b_3H_{x,\eta}^T \\ c_2H_{y,\xi}^T + c_3H_{y,\eta}^T \\ c_2H_{x,\xi}^T + c_3H_{x,\eta}^T + b_2H_{y,\xi}^T + b_3H_{y,\eta}^T \end{bmatrix}_{3 \times 9} \\
b_2 &= y_{31} = y_3 - y_1, \quad b_3 = y_{12} = y_1 - y_2, \quad c_2 = -x_{31} = x_1 - x_3, \quad c_3 = -x_{12} = x_2 - x_1
\end{aligned}$$

$$\begin{aligned}
U_b &= \frac{1}{2} \iiint_V \begin{pmatrix} \varepsilon_x & \varepsilon_y & \gamma_{xy} \end{pmatrix} \begin{Bmatrix} \sigma_x \\ \sigma_y \\ \tau_{xy} \end{Bmatrix} dV = \frac{1}{2} \iint_A \begin{pmatrix} \beta_{x,x} & \beta_{y,y} & \beta_{x,y} + \beta_{y,x} \end{pmatrix} D_b \begin{Bmatrix} \beta_{x,x} \\ \beta_{y,y} \\ \beta_{x,y} + \beta_{y,x} \end{Bmatrix} dx dy \\
&= \frac{1}{2} U^T \iint_A B^T D_b B dx dy U \\
&= \frac{1}{2} U^T k_{DKT} U
\end{aligned}$$

$$k_{DKT} = \iint_A B^T D_b B dx dy = \int_0^1 \int_0^{1-\xi} B^T D_b B |J| d\xi d\eta \quad (2.53)$$

$$|J| = \begin{vmatrix} \frac{\partial x}{\partial \xi} & \frac{\partial y}{\partial \xi} \\ \frac{\partial x}{\partial \eta} & \frac{\partial y}{\partial \eta} \end{vmatrix} = \begin{vmatrix} x_2 - x_1 & y_2 - y_1 \\ x_3 - x_1 & y_3 - y_1 \end{vmatrix} = \begin{vmatrix} 1 & x_1 & y_1 \\ 1 & x_2 & y_2 \\ 1 & x_3 & y_3 \end{vmatrix} = 2A$$

$$k_{DKT} = \int_0^1 \int_0^{1-\xi} B^T D_b B |J| d\xi d\eta = 2A \int_0^1 \int_0^{1-\xi} B^T D_b B d\xi d\eta$$

$$D_b = \frac{1}{3} \sum_{i=1}^n \begin{vmatrix} \bar{Q}_{11} & \bar{Q}_{12} & \bar{Q}_{16} \\ \bar{Q}_{21} & \bar{Q}_{22} & \bar{Q}_{26} \\ \bar{Q}_{16} & \bar{Q}_{26} & \bar{Q}_{66} \end{vmatrix} (h_{i+1}^3 - h_i^3)$$

It is helpful to note the following points (Batoz, et al., 1980),

- (1) From the relations (2.47)-(2.51) it is seen that the relation between the rotations and the transverse displacement  $w$  is given by equation (2.49) by assuming a cubic variation of  $w$  along the sides (or a quadratic variation of  $w_{,s}$ ).
- (2) There is no need to define an interpolation function for  $w$  on the element (but the assumption of a cubic variation of  $w$  along the sides is the property of a cubic polynomial on the element).
- (3) Since  $w$  varies cubically along the sides,  $w_{,s}$  varies quadratically and so does  $\beta_s$ .  
Since  $w_{,s}$  matches  $\beta_s$  at the three points along each side, the Kirchhoff hypothesis ( $\gamma_s = \beta_s + w_{,s} = 0$ ) is satisfied along the entire boundary.
- (4) Convergence towards the classical thin plate solution is obtained because the transverse shear strain energy is neglected, equation (2.53), and because the Kirchhoff hypothesis is satisfied along the element boundary.
- (5) It follows from equations (2.47-2.51) that  $w$ ,  $w_{,s}$ ,  $\beta_s$  and  $\beta_n$  are compatible (inter-element continuous) along the sides (note that  $w_{,n}$  has not been introduced since  $w$  is not defined in the interior).

- (6) With the restriction imposed on  $\beta_n$  in equation (2.51),  $\beta_x$  and  $\beta_y$  are given by complete polynomials of degree one in the element. The global discretization error in the energy is  $o(l^2)$ , where  $l$  is the measure of the size of the element.
- (7) When the formulation is applied to a one-dimensional beam, the exact stiffness matrix of a thin beam (with a cubic polynomial  $w$ ) is obtained.

It is also noted that lateral deflection  $w$  is defined only on element sides, using d.o.f. of vertex nodes. On each side  $w$  is a cubic in the side-tangent coordinate  $s$ . Because  $w$  is defined only along element sides, consistent formulations for an element load vector and an elastic foundation stiffness matrix are not available. It is helpful that there is an alternative formulation of the DKT element that defines  $w$  within the element [Crisfield, 1986]. The nine term cubic polynomial in area coordinates given by Specht (1988) was also used to represent the transverse displacement by Kapania and Mohan (1996) to compute the mass matrix for free vibration analysis.

## **2.7 Shell Element**

### **Flat Triangular Shell Element**

#### **Local coordinates and direction cosines for a triangular element arbitrarily orientated in space**

When we use triangular elements to model an arbitrary shell, we will face the problem of how to define local coordinates and their direction cosines. Because the direction of one of the local axes is arbitrary, the local coordinates are not unique to choose. In our study, we will define them as followed from vector algebra.

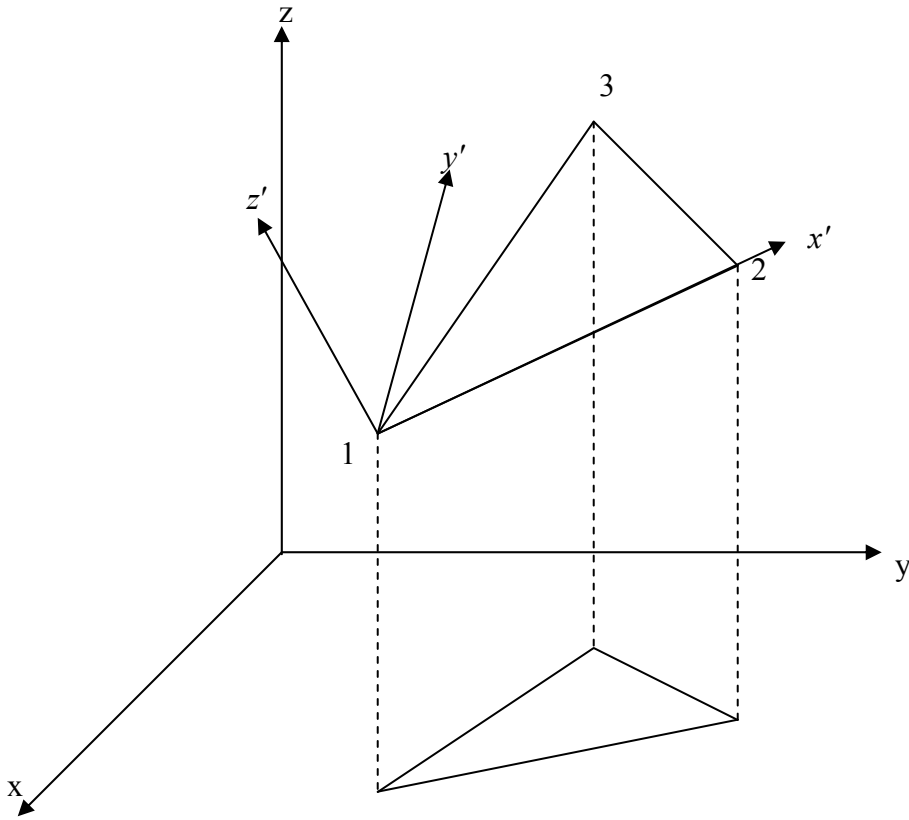


Figure 2.15 Local and global coordinate systems for a triangular element

The local  $x'$  axis is chosen to be directed along the side 12 of the triangle. The vector  $\vec{V}_{21}$  defines this side and in terms of global coordinates we have

$$\vec{V}_{x'} = \vec{V}_{21} = \begin{Bmatrix} x_2 - x_1 \\ y_2 - y_1 \\ z_2 - z_1 \end{Bmatrix} = \begin{Bmatrix} x_{21} \\ y_{21} \\ z_{21} \end{Bmatrix}$$

The  $z'$  direction is normal to the plane of the triangle. We choose this direction by means of cross-product of the two vectors  $\vec{V}_{21}$  and  $\vec{V}_{31}$  formed by the two sides of the triangle. The

vector  $\vec{V}_{31}$  is

$$\vec{V}_{31} = \begin{Bmatrix} x_3 - x_1 \\ y_3 - y_1 \\ z_3 - z_1 \end{Bmatrix} = \begin{Bmatrix} x_{31} \\ y_{31} \\ z_{31} \end{Bmatrix}$$

Thus, we have

$$\vec{V}_{z'} = \vec{V}_{21} \times \vec{V}_{31} = \begin{vmatrix} \vec{i} & \vec{j} & \vec{k} \\ x_{21} & y_{21} & z_{21} \\ x_{31} & y_{31} & z_{31} \end{vmatrix} = \begin{Bmatrix} y_{21}z_{31} - z_{21}y_{31} \\ z_{21}x_{31} - x_{21}z_{31} \\ x_{21}y_{31} - y_{21}x_{31} \end{Bmatrix} = \begin{Bmatrix} V_{z'1} \\ V_{z'2} \\ V_{z'3} \end{Bmatrix}$$

The  $y'$  direction can be obtained from the cross-product of two vectors  $\vec{V}_{z'}$  and  $\vec{V}_{x'}$ ,

$$\vec{V}_{y'} = \vec{V}_{z'} \times \vec{V}_{x'} = \begin{vmatrix} \vec{i} & \vec{j} & \vec{k} \\ V_{z'1} & V_{z'2} & V_{z'3} \\ x_{21} & y_{21} & z_{21} \end{vmatrix} = \begin{Bmatrix} V_{z'2}z_{21} - V_{z'3}y_{21} \\ V_{z'3}x_{21} - V_{z'1}z_{21} \\ V_{z'1}y_{21} - V_{z'2}x_{21} \end{Bmatrix} = \begin{Bmatrix} V_{y'1} \\ V_{y'2} \\ V_{y'3} \end{Bmatrix}$$

The direction cosines are given by dividing the components of each vector by its length, that is, defining a vector of unit length

$$\vec{v}_{x'} = \begin{Bmatrix} \lambda_{x'x} \\ \lambda_{x'y} \\ \lambda_{x'z} \end{Bmatrix} = \frac{1}{l_{12}} \begin{Bmatrix} x_{21} \\ y_{21} \\ z_{21} \end{Bmatrix} \quad (2.54a)$$

$$\vec{v}_{y'} = \begin{Bmatrix} \lambda_{y'x} \\ \lambda_{y'y} \\ \lambda_{y'z} \end{Bmatrix} = \frac{1}{l_{y'}} \begin{Bmatrix} V_{z'2}z_{21} - V_{z'3}y_{21} \\ V_{z'3}x_{21} - V_{z'1}z_{21} \\ V_{z'1}y_{21} - V_{z'2}x_{21} \end{Bmatrix} \quad (2.54b)$$

$$\vec{v}_{z'} = \begin{Bmatrix} \lambda_{z'x} \\ \lambda_{z'y} \\ \lambda_{z'z} \end{Bmatrix} = \frac{1}{l_{z'}} \begin{Bmatrix} y_{21}z_{31} - z_{21}y_{31} \\ z_{21}x_{31} - x_{21}z_{31} \\ x_{21}y_{31} - y_{21}x_{31} \end{Bmatrix} \quad (2.54c)$$

where

$$l_{12} = \sqrt{x_{21}^2 + y_{21}^2 + z_{21}^2}$$

$$l_{y'} = \sqrt{V_{y'1}^2 + V_{y'2}^2 + V_{y'3}^2}$$

$$l_{z'} = 2\Delta = \sqrt{V_{z'1}^2 + V_{z'2}^2 + V_{z'3}^2}, \quad \text{with } \Delta \text{ representing the area of the triangle.}$$

### Derivation of a consistent plate/shell model

The term “consistent plate model” comes from the assumption of consistent deformations in the actuators and substructures. The strain distribution is assumed to result from a linear combination of in-plane extensional (constant strain through the thickness) and bending (linearly varying through the thickness) displacements. This assumed strain distribution, in contrast to several other possibilities, has been found to most accurately represent the actual behavior, even in the case of discrete surface bonded actuators [Crawley and Lazarus, 1991]. In this section we will use the principle of virtual work to derive the equations of finite element. It is assumed that the solution for the configuration  $C_0$  at time  $t = 0$  is available and that a new configuration  $C_\tau$  at time  $t = \tau$  has to be determined. The principle of virtual work can be expressed for a single element as follows:

$$\delta W_i = \delta W_e \quad (2.55)$$

where  $\delta W_i$  is the virtual work done by internal forces and  $\delta W_e$  is the virtual work done by external forces. The internal virtual work is given by

$$\delta W_i = \int_{C_0} \delta\{\boldsymbol{\varepsilon}\}^T \{\boldsymbol{s}\} dV \quad (2.56)$$

where  $V$  is the volume of the element in  $C_0$ ,  $\{\boldsymbol{\varepsilon}\}$  is the vector of incremental Green-Lagrange strains and  $\{\boldsymbol{s}\}$  is the vector of second Piola-Kirchhoff (PK2) stresses. Under infinitesimal strain condition the stress and strain reduce to the engineering stress and strain [Shames and Dym, 1985]. The components of the Green-Lagrange strains and second Piola-Kirchhoff stresses do not change under rigid body motions including rigid body translation or rigid body rotation. This fundamental fact implies that any material description which has been developed for infinitesimal displacement analysis using engineering stress and strain measures can directly be employed for large displacement, large rotation but small strain analysis by simply substituting Green-Lagrange strains and second Piola-Kirchhoff stresses

for the engineering strains and stresses. In updated Lagrangian formulation, the PK2 stresses at any time  $0 < t < \tau$  during the solution process can be decomposed as

$$\{s\} = \{\sigma\} + \{\Delta s\} \quad (2.57)$$

where  $\{\sigma\}$  is the vector of Cauchy stresses in  $C_0$  at time  $t = 0$  and  $\{\Delta s\}$  is the vector of incremental PK2 stresses. The basic difference between the Cauchy stresses and the PK2 stresses is that the Cauchy stresses are measured in the current configuration, whereas the PK2 stresses are measured in the reference configuration. The term “current configuration” is used to denote any configuration between  $C_0$  and  $C_\tau$  obtained during the solution process. The incremental Green-Lagrange strains and PK2 stresses are related by the constitutive equations

$$\{\Delta s\} = [\overline{Q}]\{\varepsilon\} \quad (2.58)$$

where  $[\overline{Q}]$  is the transformed reduced stiffness matrix of the plate or one of its plies in the local element coordinate system and is given by

$$[\overline{Q}] = \begin{bmatrix} c^2 & s^2 & -2cs \\ s^2 & c^2 & 2cs \\ cs & -cs & c^2 - s^2 \end{bmatrix} \begin{bmatrix} Q_{11} & Q_{12} & 0 \\ Q_{12} & Q_{22} & 0 \\ 0 & 0 & Q_{66} \end{bmatrix} \begin{bmatrix} c^2 & s^2 & -2cs \\ s^2 & c^2 & 2cs \\ cs & -cs & c^2 - s^2 \end{bmatrix}^T \quad (2.59)$$

where

$$Q_{11} = \frac{E_1}{1 - \nu_{12}\nu_{21}}$$

$$Q_{12} = \frac{\nu_{12}E_2}{1 - \nu_{12}\nu_{21}}$$

$$Q_{22} = \frac{E_2}{1 - \nu_{12}\nu_{21}}$$

$$Q_{66} = G_{12}$$



$$s = \sin \theta, \quad c = \cos \theta$$

$E_1, E_2, \nu_{12}, G_{12}$  are the properties in the principal material directions and  $\theta$  is the angle which the  $E_1$  direction makes with the local x-axis, measured counter clock wise from the local x-axis.

$E_i$  = Young's moduli in the  $i^{\text{th}}$  principal material direction,

$\nu_{ij}$  = Poisson's ration for transverse strain in the j-direction when stressed in the i-direction,

that is,

$$\nu_{ij} = -\frac{\varepsilon_j}{\varepsilon_i}$$

Because of the symmetric property of the compliance matrix

$$\frac{\nu_{ij}}{E_i} = \frac{\nu_{ji}}{E_j}$$

$G_{12}$  = shear modulus in the 1-2 plane

At the end of the current step ( $t = \tau$ ), the PK2 stresses in  $C_0$ , computed using Eqs. 2.57

and 2.58, are converted to Cauchy stresses in  $C_\tau$  by the following transformation,

$$\sigma_{mn} = \frac{\rho_t}{\rho_0} {}^t x_{m,i} {}^t x_{n,j} s_{ij} \quad (2.60a)$$

or in matrix form,

$$[\sigma] = \frac{\rho_t}{\rho_0} [{}^t X][s][{}^t X]^T \quad (2.60b)$$

where  $\rho_0$  and  $\rho_t$  are the mass density of the structure at time 0 and  $t$ , respectively. They

are related by the deformation gradient  $[{}^t X]$  as follows,

$$\rho_t = \frac{\rho_0}{|{}^t X|}$$

The deformation gradient  ${}^t_0X$  is defined as

$${}^t_0X = \begin{bmatrix} \frac{\partial x_1}{\partial^0 x_1} & \frac{\partial x_1}{\partial^0 x_2} & \frac{\partial x_1}{\partial^0 x_3} \\ \frac{\partial x_2}{\partial^0 x_1} & \frac{\partial x_2}{\partial^0 x_2} & \frac{\partial x_2}{\partial^0 x_3} \\ \frac{\partial x_3}{\partial^0 x_1} & \frac{\partial x_3}{\partial^0 x_2} & \frac{\partial x_3}{\partial^0 x_3} \end{bmatrix} = \begin{bmatrix} {}^t x_{1,1} & {}^t x_{1,2} & {}^t x_{1,3} \\ {}^t x_{2,1} & {}^t x_{2,2} & {}^t x_{2,3} \\ {}^t x_{3,1} & {}^t x_{3,2} & {}^t x_{3,3} \end{bmatrix} \quad (2.61)$$

where  ${}^0 x_1$ ,  ${}^0 x_2$ , and  ${}^0 x_3$  are the coordinates of a typical point P in the structure at time 0 and  ${}^t x_1$ ,  ${}^t x_2$ , and  ${}^t x_3$  are the coordinates of the new position of P at time t.

Under mechanical, thermal and electric loads, the variation of strain through the thickness can be expressed as

$$\{\varepsilon\} = \{\varepsilon^0\} + z\{\kappa\} - \{\varepsilon\}_E - \{\varepsilon\}_T \quad (2.62)$$

where  $\{\varepsilon^0\}$  and  $\{\kappa\}$  are the vectors of incremental membrane strains and bending strains, respectively.

$$\{\varepsilon^0\} = \begin{Bmatrix} \varepsilon_x^0 \\ \varepsilon_y^0 \\ \gamma_{xy}^0 \end{Bmatrix} = \begin{Bmatrix} u_{,x} + \frac{1}{2}(u_{,x}^2 + v_{,x}^2 + w_{,x}^2) \\ v_{,y} + \frac{1}{2}(u_{,y}^2 + v_{,y}^2 + w_{,y}^2) \\ u_{,y} + v_{,x} + u_{,x}u_{,y} + v_{,x}v_{,y} + w_{,x}w_{,y} \end{Bmatrix} \quad (2.63)$$

$$\{\kappa\} = \begin{Bmatrix} \kappa_x \\ \kappa_y \\ \kappa_{xy} \end{Bmatrix} = \begin{Bmatrix} \frac{\partial \beta_x}{\partial x} \\ \frac{\partial \beta_y}{\partial y} \\ \frac{\partial \beta_x}{\partial y} + \frac{\partial \beta_y}{\partial x} \end{Bmatrix} \quad (2.64)$$

where  $u$ ,  $v$ , and  $w$  are the incremental displacements of the mid-plane of the element,  $\beta_x$  and  $\beta_y$  are the incremental rotations of the normal to the undeformed mid-plane in the local x-z and y-z planes, respectively.

$\{\varepsilon\}_E$  and  $\{\varepsilon\}_T$  are actuation strains and thermal strains, respectively, and given by

$$\{\varepsilon\}_E = \begin{Bmatrix} \varepsilon_x \\ \varepsilon_y \\ \gamma_{xy} \end{Bmatrix}_E = \begin{bmatrix} 0 & 0 & \bar{d}_{31} \\ 0 & 0 & \bar{d}_{32} \\ 0 & 0 & \bar{d}_{36} \end{bmatrix} \begin{Bmatrix} E_x \\ E_y \\ E_z \end{Bmatrix} = \begin{Bmatrix} \bar{d}_{31} \\ \bar{d}_{32} \\ \bar{d}_{36} \end{Bmatrix} E_z = \begin{bmatrix} c^2 & s^2 & -cs \\ s^2 & c^2 & cs \\ 2cs & -2cs & c^2 - s^2 \end{bmatrix} \begin{Bmatrix} d_{31} \\ d_{32} \\ d_{36} \end{Bmatrix} E_3 \quad (2.65)$$

$$\{\varepsilon\}_T = \begin{Bmatrix} \varepsilon_x \\ \varepsilon_y \\ \gamma_{xy} \end{Bmatrix}_T = \begin{Bmatrix} \alpha_x \\ \alpha_y \\ \alpha_{xy} \end{Bmatrix} \Delta T = \begin{bmatrix} c^2 & s^2 & -cs \\ s^2 & c^2 & cs \\ 2cs & -2cs & c^2 - s^2 \end{bmatrix} \begin{Bmatrix} \alpha_1 \\ \alpha_2 \\ \alpha_{12} \end{Bmatrix} \Delta T \quad (2.66)$$

where  $E_i$  is the applied electric field in volts/meter, and  $d_{ij}$  is piezoelectric coefficients in meters/volt.  $\alpha_x$ ,  $\alpha_y$  and  $\alpha_{xy}$  are the coefficients of thermal expansion with respect to the element local coordinate system.  $\alpha_1$ ,  $\alpha_2$  and  $\alpha_{12}$  are the coefficients of thermal expansion with respect to the principal material coordinate system in 1/degrees Kelvin,  $\Delta T$  is the prescribed temperature increment.

Under mechanical, thermal and electric loads, the incremental Green-Lagrange strains and PK2 stresses are related by

$$\{\Delta s\} = [\overline{Q}]\{\varepsilon\} = [\overline{Q}]\{\{\varepsilon^0\} + z\{\kappa\} - \{\varepsilon\}_E - \{\varepsilon\}_T\} = [\overline{Q}]\{\{\varepsilon^0\} + z\{\kappa\}\} - [\overline{Q}]\{\varepsilon\}_E - [\overline{Q}]\{\varepsilon\}_T \quad (2.67)$$

where the second term  $[\overline{Q}]\{\varepsilon\}_E$  in Eq. ( 2.67) represents the equivalent stress created as a result of the actuation strains. The actuation strain vector  $\{\varepsilon\}_E$  contains in-plane normal and shear strain components, and enters into the elasticity equations in the same manner as does thermal strain. Actuation strain is the strain that physically causes induced strains to be produced, and can be due to thermal expansion, piezoelectricity, electrostriction, etc. The last term  $[\overline{Q}]\{\varepsilon\}_T$  in Eq. ( 2.67 ) represents the equivalent stress created as a result of the thermal strains.

The internal force and moment resultants are defined by

$$\{N\} = \int_t \{s\} dz, \quad \{M\} = \int_t \{s\} z dz \quad (2.68)$$

where  $h$  is the thickness of the element. Substituting Eqs. (2.57) and (2.67) into Eqs. (2.68) and integrating through the thickness  $t$  of the plate, we can get the plate load deformation relations as follows

$$\begin{Bmatrix} N \\ M \end{Bmatrix} = \begin{Bmatrix} N_I \\ M_I \end{Bmatrix} + \begin{bmatrix} A & B \\ B & D \end{bmatrix} \begin{Bmatrix} \varepsilon^0 \\ \kappa \end{Bmatrix} - \begin{Bmatrix} N_E \\ M_E \end{Bmatrix} - \begin{Bmatrix} N_T \\ M_T \end{Bmatrix} \quad (2.69)$$

where the initial force and moment resultants are

$$\{N_I\} = \begin{Bmatrix} N_{xl} \\ N_{yl} \\ N_{xyl} \end{Bmatrix} = \int_t \sigma dz, \quad \{M_I\} = \begin{Bmatrix} M_{xl} \\ M_{yl} \\ M_{xyl} \end{Bmatrix} = \int_t \sigma z dz \quad (2.70)$$

The matrices A, B, and D are the usual extensional, coupling and bending stiffnesses of the plate.

$$A = \int_t \bar{Q} dz = \begin{bmatrix} A_{11} & A_{12} & A_{16} \\ A_{12} & A_{22} & A_{26} \\ A_{16} & A_{26} & A_{66} \end{bmatrix}, \quad A_{ij} = \sum_{k=1}^N (\bar{Q}_{ij})_k (h_k - h_{k-1})$$

$$B = \int_t \bar{Q} z dz = \begin{bmatrix} B_{11} & B_{12} & B_{16} \\ B_{12} & B_{22} & B_{26} \\ B_{16} & B_{26} & B_{66} \end{bmatrix}, \quad B_{ij} = \sum_{k=1}^N (\bar{Q}_{ij})_k \left( \frac{h_k^2 - h_{k-1}^2}{2} \right)$$

$$D = \int_t \bar{Q} z^2 dz = \begin{bmatrix} D_{11} & D_{12} & D_{16} \\ D_{12} & D_{22} & D_{26} \\ D_{16} & D_{26} & D_{66} \end{bmatrix}, \quad D_{ij} = \sum_{k=1}^N (\bar{Q}_{ij})_k \left( \frac{h_k^3 - h_{k-1}^3}{3} \right)$$

The equivalent actuator forces  $N_E$  and moments  $M_E$  per unit length are

$$\{N_E\} = \int_t \bar{Q} \{\varepsilon_E\} dz, \quad \{M_E\} = \int_t \bar{Q} \{\varepsilon_E\} z dz \quad (2.71)$$

The equivalent thermal forces  $N_T$  and moments  $M_T$  per unit length are

$$\{N_T\} = \int_t \bar{Q} \{\varepsilon_T\} dz, \quad \{M_T\} = \int_t \bar{Q} \{\varepsilon_T\} z dz \quad (2.72)$$

Care must be taken in performing the necessary integrations to obtain the correct stiffness, actuator and thermal forcing terms. Both actuator and substrate plies contribute to the stiffness matrices A, B, and D and the thermal forcing vectors  $N_T$  and  $M_T$ , whereas only actuator plies contribute to the actuator forcing vectors  $N_E$  and  $M_E$ , which are dependent on the mode of actuation (prescribed actuation strains). Extensional actuation is produced by prescribing actuation strains that are symmetric about the neutral axis, while bending actuation results when the actuation strains in the actuators above the neutral axis are prescribed to be in a direction opposite (180 deg out of phase) to those below the neutral axis. Equation (2.69) relates the resultant total strains and curvatures found in the actuator/substrate system to the actuation strains, thermal strains, external loads, and stiffness properties of the system in a general and compact form. The presence of numerous coupling terms shows that it is possible to create a variety of deformations (e.g., bending or twisting) using several different actuation modes (e.g., extension or bending). Thus, by careful selection of the laminate ply orientations, an actuator/substrate system can be designed to effect control for a variety of applications. In addition, various couplings may be introduced by the boundary conditions, as would be the case for a swept cantilever wing.

The internal virtual work can now be expressed as

$$\begin{aligned}
\delta W_i &= \int_{C_0} \delta\{\varepsilon\}^T \{s\} dV = \int_{C_0} \left\{ \delta\{\varepsilon^0\}^T + z\delta\{\kappa\}^T \right\} \{s\} dV \\
&= \int_{C_0} \left\{ \delta\{\varepsilon^0\}^T \int_i \{s\} dz + \delta\{\kappa\}^T \int_i \{s\} z dz \right\} dA \\
&= \int_{C_0} \left\{ \delta\{\varepsilon^0\}^T \{N\} + \delta\{\kappa\}^T \{M\} \right\} dA
\end{aligned} \tag{2.73}$$

The variation of the membrane strains can be expressed as

$$\{\delta\varepsilon^0\} = \left\{ \begin{array}{c} \delta u_{,x} + u_{,x}\delta u_{,x} + v_{,x}\delta v_{,x} + w_{,x}\delta w_{,x} \\ \delta v_{,y} + u_{,y}\delta u_{,y} + v_{,y}\delta v_{,y} + w_{,y}\delta w_{,y} \\ \delta u_{,y} + \delta v_{,x} + u_{,x}\delta u_{,y} + u_{,y}\delta u_{,x} + v_{,x}\delta v_{,y} + v_{,y}\delta v_{,x} + w_{,x}\delta w_{,y} + w_{,y}\delta w_{,x} \end{array} \right\} \quad (2.74a)$$

$$= [G_1] \{\delta u_{,x} \quad \delta u_{,y} \quad \delta v_{,x} \quad \delta v_{,y} \quad \delta w_{,x} \quad \delta w_{,y}\}^T$$

where

$$[G_1] = \begin{bmatrix} 1+u_{,x} & 0 & v_{,x} & 0 & w_{,x} & 0 \\ 0 & u_{,y} & 0 & 1+v_{,y} & 0 & w_{,y} \\ u_{,y} & 1+u_{,x} & 1+v_{,y} & v_{,x} & w_{,y} & w_{,x} \end{bmatrix} \quad (2.74b)$$

Noting that the coordinate transformation between the degrees of freedom of the LST element and Allman triangle element, the in-plane Allman displacement field  $u$  and  $v$  can be expressed in terms of the shape function of the LST element and the nodal degrees of freedom of the shell element  $\{a\}$  as follows,

$$\begin{aligned} \begin{Bmatrix} u \\ v \end{Bmatrix} &= \begin{bmatrix} \{N\}^T & 0 \\ 0 & \{N\}^T \end{bmatrix} \{u_1, u_2, u_3, u_4, u_5, u_6, v_1, v_2, v_3, v_4, v_5, v_6\}^T \\ &= \begin{bmatrix} \{N\}^T & 0 \\ 0 & \{N\}^T \end{bmatrix} [T_{lst}] \{a\} \end{aligned} \quad (2.75)$$

where  $\{N\}$  is the vector of the shape functions of the LST element in the natural coordinates (Appendix F),  $\{a\}$  is the nodal degrees of freedom of the shell element,

$$\{a\} = \{u_1, v_1, w_1, \theta_{x1}, \theta_{y1}, \theta_{z1}, u_2, v_2, w_2, \theta_{x2}, \theta_{y2}, \theta_{z2}, u_3, v_3, w_3, \theta_{x3}, \theta_{y3}, \theta_{z3}\}^T$$

$[T_{lst}]$  is transformation matrix between the degrees of freedom of the LST element and

Allman triangle element

$$[T_{lst}] = \begin{bmatrix} 1 & 0 & 0 & 0 & 0 & 0 & 0 & 0 & 0 & 0 & 0 & 0 & 0 & 0 & 0 & 0 & 0 \\ 0 & 0 & 0 & 0 & 0 & 0 & 1 & 0 & 0 & 0 & 0 & 0 & 0 & 0 & 0 & 0 & 0 \\ 0 & 0 & 0 & 0 & 0 & 0 & 0 & 0 & 0 & 0 & 0 & 0 & 1 & 0 & 0 & 0 & 0 \\ 0.5 & 0 & 0 & 0 & 0 & \frac{b_3}{8} & 0.5 & 0 & 0 & 0 & 0 & -\frac{b_3}{8} & 0 & 0 & 0 & 0 & 0 \\ 0 & 0 & 0 & 0 & 0 & 0 & 0.5 & 0 & 0 & 0 & 0 & \frac{b_1}{8} & 0.5 & 0 & 0 & 0 & 0 & -\frac{b_1}{8} \\ 0.5 & 0 & 0 & 0 & 0 & -\frac{b_2}{8} & 0 & 0 & 0 & 0 & 0 & 0 & 0.5 & 0 & 0 & 0 & 0 & \frac{b_2}{8} \\ 0 & 1 & 0 & 0 & 0 & 0 & 0 & 0 & 0 & 0 & 0 & 0 & 0 & 0 & 0 & 0 & 0 & 0 \\ 0 & 0 & 0 & 0 & 0 & 0 & 0 & 1 & 0 & 0 & 0 & 0 & 0 & 0 & 0 & 0 & 0 & 0 \\ 0 & 0 & 0 & 0 & 0 & 0 & 0 & 0 & 0 & 0 & 0 & 0 & 0 & 1 & 0 & 0 & 0 & 0 \\ 0 & 0.5 & 0 & 0 & 0 & \frac{c_3}{8} & 0 & 0.5 & 0 & 0 & 0 & -\frac{c_3}{8} & 0 & 0 & 0 & 0 & 0 & 0 \\ 0 & 0 & 0 & 0 & 0 & 0 & 0 & 0.5 & 0 & 0 & 0 & \frac{c_1}{8} & 0 & 0.5 & 0 & 0 & 0 & 0 & -\frac{c_1}{8} \\ 0 & 0.5 & 0 & 0 & 0 & -\frac{c_2}{8} & 0 & 0 & 0 & 0 & 0 & 0 & 0 & 0.5 & 0 & 0 & 0 & 0 & \frac{c_2}{8} \end{bmatrix}$$

The derivatives of the in-plane displacements are given by

$$\begin{Bmatrix} u_{,x} \\ u_{,y} \\ v_{,x} \\ v_{,y} \end{Bmatrix} = \begin{bmatrix} \frac{\partial \{N\}^T}{\partial x} & 0 \\ \frac{\partial \{N\}^T}{\partial y} & 0 \\ 0 & \frac{\partial \{N\}^T}{\partial x} \\ 0 & \frac{\partial \{N\}^T}{\partial y} \end{bmatrix} [T_{lst}] \{a\} = \frac{1}{2A} \begin{bmatrix} b_2 \{N_{,\xi}\}^T + b_3 \{N_{,\eta}\}^T & 0 \\ c_2 \{N_{,\xi}\}^T + c_3 \{N_{,\eta}\}^T & 0 \\ 0 & b_2 \{N_{,\xi}\}^T + b_3 \{N_{,\eta}\}^T \\ 0 & c_2 \{N_{,\xi}\}^T + c_3 \{N_{,\eta}\}^T \end{bmatrix} [T_{lst}] \{a\} \\ = [B_{lst}] \{a\} \quad (2.76a)$$

where  $[B_{lst}]$  is strain-displacement matrix

$$[B_{lst}] = \frac{1}{2A} \begin{bmatrix} b_2 \{N_{,\xi}\}^T + b_3 \{N_{,\eta}\}^T & 0 \\ c_2 \{N_{,\xi}\}^T + c_3 \{N_{,\eta}\}^T & 0 \\ 0 & b_2 \{N_{,\xi}\}^T + b_3 \{N_{,\eta}\}^T \\ 0 & c_2 \{N_{,\xi}\}^T + c_3 \{N_{,\eta}\}^T \end{bmatrix} [T_{lst}] \quad (2.76b)$$

$\{N_{,\xi}\}$  and  $\{N_{,\eta}\}$  are the vectors of derivatives of the LST shape functions with respect to the natural coordinates  $\xi$  and  $\eta$

$$\{N_{,\xi}\} = \frac{\partial\{N\}}{\partial\xi} = \begin{Bmatrix} \frac{\partial N_1}{\partial\xi} \\ \frac{\partial N_2}{\partial\xi} \\ \frac{\partial N_3}{\partial\xi} \\ \frac{\partial N_4}{\partial\xi} \\ \frac{\partial N_5}{\partial\xi} \\ \frac{\partial N_6}{\partial\xi} \end{Bmatrix} = \begin{Bmatrix} 4\xi + 4\eta - 3 \\ 4\xi - 1 \\ 0 \\ 4 - 8\xi - 4\eta \\ 4\eta \\ -4\eta \end{Bmatrix} \quad \{N_{,\eta}\} = \frac{\partial\{N\}}{\partial\eta} = \begin{Bmatrix} \frac{\partial N_1}{\partial\eta} \\ \frac{\partial N_2}{\partial\eta} \\ \frac{\partial N_3}{\partial\eta} \\ \frac{\partial N_4}{\partial\eta} \\ \frac{\partial N_5}{\partial\eta} \\ \frac{\partial N_6}{\partial\eta} \end{Bmatrix} = \begin{Bmatrix} 4\xi + 4\eta - 3 \\ 0 \\ 4\eta - 1 \\ -4\xi \\ 4\xi \\ 4 - 4\xi - 8\eta \end{Bmatrix} \quad (2.76c)$$

The transverse displacement  $w$  is not defined explicitly in the DKT formulation. Farfard et al. in 1989 have shown that evaluating the derivatives  $w_{,x}$  and  $w_{,y}$  at the integration points from the linear interpolation for  $w$  gives better results than from the linear interpolation for the derivatives in terms of the nodal values. If the linear interpolation for  $w$  is used, that is,  $w(\xi, \eta) = (1 - \xi - \eta)w_1 + \xi w_2 + \eta w_3$ , the derivatives  $w_{,x}$  and  $w_{,y}$  can be obtained as

$$\begin{Bmatrix} w_{,x} \\ w_{,y} \end{Bmatrix} = \frac{1}{2A} \begin{bmatrix} -b_2 - b_3 & b_2 & b_3 \\ -c_2 - c_3 & c_2 & c_3 \end{bmatrix} \begin{Bmatrix} w_1 \\ w_2 \\ w_3 \end{Bmatrix} = \frac{1}{2A} \begin{bmatrix} -b_2 - b_3 & b_2 & b_3 \\ -c_2 - c_3 & c_2 & c_3 \end{bmatrix} [T_w] \{a\} = [B_w] \{a\} \quad (2.77a)$$

where the transformation matrix  $[T_w]$  is used to express  $\{w_1, w_2, w_3\}^T$  in terms of the degrees of freedom of the shell element and given by

$$[T_w] = \begin{bmatrix} 0 & 0 & 1 & 0 & 0 & 0 & 0 & 0 & 0 & 0 & 0 & 0 & 0 & 0 & 0 & 0 & 0 \\ 0 & 0 & 0 & 0 & 0 & 0 & 0 & 0 & 1 & 0 & 0 & 0 & 0 & 0 & 0 & 0 & 0 \\ 0 & 0 & 0 & 0 & 0 & 0 & 0 & 0 & 0 & 0 & 0 & 0 & 0 & 0 & 1 & 0 & 0 \end{bmatrix} \quad (2.77b)$$

$[B_w]$  is strain-displacement matrix and given by

$$[B_w] = \frac{1}{2A} \begin{bmatrix} -b_2 - b_3 & b_2 & b_3 \\ -c_2 - c_3 & c_2 & c_3 \end{bmatrix} [T_w] \quad (2.77c)$$

Combining the variations of Eqs. (2.40) and (2.41), we have



$$\{\delta u_{,x} \quad \delta u_{,y} \quad \delta v_{,x} \quad \delta v_{,y} \quad \delta w_{,x} \quad \delta w_{,y}\}^T = \begin{bmatrix} [B_{lst}] \\ [B_w] \end{bmatrix} \{\delta a\} = [G_2] \{\delta a\} \quad (2.78a)$$

where  $[G_2]$  is a matrix of size 6 by 18 with the first 4 rows made of  $[B_{lst}]$  and the last 2 rows made of  $[B_w]$ , that is,

$$[G_2] = \begin{bmatrix} [B_{lst}] \\ [B_w] \end{bmatrix} \quad (2.78b)$$

Substituting (2.42) into (2.38), the variation of the membrane strains can be expressed as

$$\{\delta \varepsilon^0\} = [G_1][G_2] \{\delta a\} \quad (2.79)$$

The normal rotations  $\beta_x$  and  $\beta_y$  can be expressed in terms of the nodal degrees of freedom of the DKT element as

$$\beta_x = \{H_x\}^T \{a_{dkt}\}, \quad \beta_y = \{H_y\}^T \{a_{dkt}\} \quad (2.80)$$

where  $\{H_x\}$  and  $\{H_y\}$  are the vectors of the shape functions of the DKT element (Appendix I),  $\{a_{dkt}\}$  is the vector of nodal degrees of freedom of the DKT element given by

$$\{a_{dkt}\}^T = \{w_1, \theta_{x1}, \theta_{y1}, w_2, \theta_{x2}, \theta_{y2}, w_3, \theta_{x3}, \theta_{y3}\}$$

The first variation of the bending strains can be expressed as

$$\{\delta \kappa\} = \frac{1}{2A} \begin{bmatrix} y_{31} \{H_{x,\xi}\}^T + y_{12} \{H_{x,\eta}\}^T \\ -x_{31} \{H_{y,\xi}\}^T - x_{12} \{H_{y,\eta}\}^T \\ -x_{31} \{H_{x,\xi}\}^T - x_{12} \{H_{x,\eta}\}^T + y_{31} \{H_{y,\xi}\}^T + y_{12} \{H_{y,\eta}\}^T \end{bmatrix} [T_{dkt}] \{\delta a\} = [B_{dkt}] \{\delta a\} \quad (2.81)$$

where  $\{H_{x,\xi}\}$ ,  $\{H_{x,\eta}\}$ ,  $\{H_{y,\xi}\}$ ,  $\{H_{y,\eta}\}$  are the derivatives of the shape functions with respect to the natural coordinates (Appendix I).

The transformation matrix  $[T_{dkt}]$  is used to express the nodal degrees of freedom of the DKT element  $\{a_{dkt}\}$  in terms of the nodal degrees of freedom of the shell element  $\{a\}$  as

$\{a_{dkt}\} = [T_{dkt}]\{a\}$  and given by

$$[T_{dkt}] = \begin{bmatrix} 0 & 0 & 1 & 0 & 0 & 0 & 0 & 0 & 0 & 0 & 0 & 0 & 0 & 0 & 0 & 0 & 0 \\ 0 & 0 & 0 & 1 & 0 & 0 & 0 & 0 & 0 & 0 & 0 & 0 & 0 & 0 & 0 & 0 & 0 \\ 0 & 0 & 0 & 0 & 1 & 0 & 0 & 0 & 0 & 0 & 0 & 0 & 0 & 0 & 0 & 0 & 0 \\ 0 & 0 & 0 & 0 & 0 & 0 & 0 & 0 & 1 & 0 & 0 & 0 & 0 & 0 & 0 & 0 & 0 \\ 0 & 0 & 0 & 0 & 0 & 0 & 0 & 0 & 0 & 1 & 0 & 0 & 0 & 0 & 0 & 0 & 0 \\ 0 & 0 & 0 & 0 & 0 & 0 & 0 & 0 & 0 & 0 & 1 & 0 & 0 & 0 & 0 & 0 & 0 \\ 0 & 0 & 0 & 0 & 0 & 0 & 0 & 0 & 0 & 0 & 0 & 0 & 0 & 1 & 0 & 0 & 0 \\ 0 & 0 & 0 & 0 & 0 & 0 & 0 & 0 & 0 & 0 & 0 & 0 & 0 & 0 & 0 & 1 & 0 \\ 0 & 0 & 0 & 0 & 0 & 0 & 0 & 0 & 0 & 0 & 0 & 0 & 0 & 0 & 0 & 0 & 1 \end{bmatrix}$$

$[B_{dkt}]$  is strain-displacement matrix and given by

$$[B_{dkt}] = \frac{1}{2A} \begin{bmatrix} y_{31}\{H_{x,\xi}\}^T + y_{12}\{H_{x,\eta}\}^T \\ -x_{31}\{H_{y,\xi}\}^T - x_{12}\{H_{y,\eta}\}^T \\ -x_{31}\{H_{x,\xi}\}^T - x_{12}\{H_{x,\eta}\}^T + y_{31}\{H_{y,\xi}\}^T + y_{12}\{H_{y,\eta}\}^T \end{bmatrix} [T_{dkt}]$$

Substituting the Eqs. (2.79) and (2.81) into Eqs. (2.73), the internal virtual work can be written as

$$\begin{aligned} \delta W_i &= \int_{C_0} \left\{ [G_1][G_2]\{\delta a\}\}^T \{N\} + [B_{dkt}]\{\delta a\}\}^T \{M\} \right\} dA \\ &= \{\delta a\}^T \int_{C_0} \left\{ [G_2]^T [G_1]^T \{N\} + [B_{dkt}]^T \{M\} \right\} dA \\ &= \{\delta a\}^T \{q\} \end{aligned}$$

where  $\{q\}$  is the element internal force vector given by

$$\{q\} = \int_{C_0} \left\{ [G_2]^T [G_1]^T \{N\} + [B_{dkt}]^T \{M\} \right\} dA \quad (2.82)$$

The external virtual work can be expressed as

$$\delta W_e = \{\delta a\}^T \{f\} \quad (2.83)$$

where  $\{f\}$  is the element external force vector due to mechanical loads. The equations of equilibrium at the element level can be expressed as

$$\{g\} = \{q\} - \{f\} = 0 \quad (2.84)$$

The element tangent stiffness matrix  $[k] = \frac{\partial\{q\}}{\partial\{a\}}$  can be obtained by taking the first variation

of the element internal force vector  $\{q\}$  in Eq. (2.82) and using the relation  $\delta\{q\} = \frac{\partial\{q\}}{\partial\{a\}}\delta\{a\}$ .

The first variation of the element internal force vector  $\{q\}$  is

$$\begin{aligned} \delta\{q\} &= \int_{C_0} \left\{ \delta\left([G_2]^T [G_1]^T \{N\}\right) + \delta\left([B_{dkt}]^T \{M\}\right) \right\} dA \\ &= \int_{C_0} \left\{ [G_2]^T \left( \delta[G_1]^T \right) \{N\} + [G_2]^T [G_1]^T \delta\{N\} + [B_{dkt}]^T \delta\{M\} \right\} dA \end{aligned} \quad (2.85)$$

$$\begin{aligned} (\delta[G_1]^T)\{N\} &= \begin{bmatrix} \delta u_{,x} & 0 & \delta u_{,y} \\ 0 & \delta u_{,y} & \delta u_{,x} \\ \delta v_{,x} & 0 & \delta v_{,y} \\ 0 & \delta v_{,y} & \delta v_{,x} \\ \delta w_{,x} & 0 & \delta w_{,y} \\ 0 & \delta w_{,y} & \delta w_{,x} \end{bmatrix} \begin{Bmatrix} N_x \\ N_y \\ N_{xy} \end{Bmatrix} = \begin{bmatrix} N_x & N_{xy} & 0 & 0 & 0 & 0 \\ N_{xy} & N_y & 0 & 0 & 0 & 0 \\ 0 & 0 & N_x & N_{xy} & 0 & 0 \\ 0 & 0 & N_{xy} & N_y & 0 & 0 \\ 0 & 0 & 0 & 0 & N_x & N_{xy} \\ 0 & 0 & 0 & 0 & N_{xy} & N_y \end{bmatrix} \begin{Bmatrix} \delta u_{,x} \\ \delta u_{,y} \\ \delta v_{,x} \\ \delta v_{,y} \\ \delta w_{,x} \\ \delta w_{,y} \end{Bmatrix} \\ &= \begin{bmatrix} \hat{N} & 0 & 0 \\ 0 & \hat{N} & 0 \\ 0 & 0 & \hat{N} \end{bmatrix} [G_2] \{\delta a\} \end{aligned} \quad (2.86)$$

$$\delta\{N\} = [A]\{\delta\varepsilon^0\} + [B]\{\delta\kappa\} = [A][G_1][G_2]\{\delta a\} + [B][B_{dkt}]\{\delta a\} \quad (2.87)$$

$$\delta\{M\} = [B]\{\delta\varepsilon^0\} + [D]\{\delta\kappa\} = [B][G_1][G_2]\{\delta a\} + [D][B_{dkt}]\{\delta a\} \quad (2.88)$$

Substituting (2.86), (2.87) and (2.88) into (2.85), we get the first variation of the element internal force vector  $\{q\}$

$$\delta\{q\} = [k]\{\delta a\} \quad (2.89)$$

where  $[k]$  is the element tangent stiffness matrix given by

$$\begin{aligned}
[k] &= \int_{C_1} \left( [G_2]^T [G_1]^T [A][G_1][G_2] + [B_{dkt}]^T [D][B_{dkt}] + [G_2]^T [G_1]^T [B][B_{dkt}] \right. \\
&\quad \left. + [B_{dkt}]^T [B][G_1][G_2] + [G_2]^T \begin{bmatrix} \hat{N} & 0 & 0 \\ 0 & \hat{N} & 0 \\ 0 & 0 & \hat{N} \end{bmatrix} [G_2] \right) dA \\
&= [k_a] + [k_{dkt}] + [k_{mb}] + [k_{bm}] + [k_n]
\end{aligned} \tag{2.90a}$$

where the first term  $[k_a]$  is the Allman membrane stiffness,

$$[k_a] = \int_{C_1} [G_2]^T [G_1]^T [A][G_1][G_2] dA \tag{2.90b}$$

The second  $[k_{dkt}]$  is the DKT bending stiffness,

$$[k_{dkt}] = \int_{C_1} [B_{dkt}]^T [D][B_{dkt}] dA \tag{2.90c}$$

The third  $[k_{mb}]$  is the membrane-bending coupling stiffness, associated with in-plane forces resulting from bending deformation,

$$[k_{mb}] = \int_{C_1} [G_2]^T [G_1]^T [B][B_{dkt}] dA \tag{2.90d}$$

The fourth  $[k_{bm}]$  is the bending-membrane coupling stiffness, associated with bending moment resulting from in-plane deformation,

$$[k_{bm}] = \int_{C_1} [B_{dkt}]^T [B][G_1][G_2] dA \tag{2.90e}$$

Obviously, this matrix is simply the transpose of the membrane-bending coupling stiffness.

That is,

$$[k_{bm}] = [k_{mb}]^T \tag{2.90f}$$

The last is the contribution from the geometrically nonlinear terms in the membrane strains due to the large deformation,

$$[k_n] = \int_{C_1} [G_2]^T \begin{bmatrix} \hat{N} & 0 & 0 \\ 0 & \hat{N} & 0 \\ 0 & 0 & \hat{N} \end{bmatrix} [G_2] dA \tag{2.90g}$$

From the derivation this term is zero matrix in the case of linear analysis.

In the case of linear analysis, we can easily get the corresponding linear formulation from the above. For example, the in-plane strain-displacement matrix  $[G_1]$ ,  $[G_2]$  and element stiffness  $[k]$  become

$$[G_1] = \begin{bmatrix} 1 & 0 & 0 & 0 & 0 & 0 \\ 0 & 0 & 0 & 1 & 0 & 0 \\ 0 & 1 & 1 & 0 & 0 & 0 \end{bmatrix}$$

$$[G_2] = \begin{bmatrix} [B_{lst}]_{4 \times 18} \\ [0]_{2 \times 18} \end{bmatrix}$$

$$[k] = \int_{C_1} \left( [G_2]^T [G_1]^T [A][G_1][G_2] + [B_{dkt}]^T [D][B_{dkt}] + [G_2]^T [G_1]^T [B][B_{dkt}] + [B_{dkt}]^T [B][G_1][G_2] \right) dA$$

Of course, we can get the above linear element stiffness using the total potential energy of the system as follows

$$\Pi = \frac{1}{2} \int_A \left\{ \begin{matrix} \varepsilon^{0T} & \kappa^T \end{matrix} \right\} \begin{bmatrix} A & B \\ B & D \end{bmatrix} \left\{ \begin{matrix} \varepsilon^0 \\ \kappa \end{matrix} \right\} dA - \int_A \left\{ \begin{matrix} N_E & M_E \end{matrix} \right\} \left\{ \begin{matrix} \varepsilon^0 \\ \kappa \end{matrix} \right\} dA - \int_A \left\{ \begin{matrix} N_T & M_T \end{matrix} \right\} \left\{ \begin{matrix} \varepsilon^0 \\ \kappa \end{matrix} \right\} dA$$

Derivation of the thermal load vector

The virtual work done by thermal load is given by

$$\begin{aligned} \delta W_T &= \int_{C_0} \left\{ \delta \left\{ \varepsilon^0 \right\}^T \left\{ N_T \right\} + \delta \left\{ \kappa \right\}^T \left\{ M_T \right\} \right\} dA \\ &= \left\{ \delta a \right\}^T \int_{C_0} \left\{ [G_2]^T [G_1]^T \left\{ N_T \right\} + [B_{dkt}]^T \left\{ M_T \right\} \right\} dA \end{aligned} \quad (2.91)$$

From which the thermal load can be identified as

$$\left\{ f_T \right\} = \int_{C_0} \left\{ [G_2]^T [G_1]^T \left\{ N_T \right\} + [B_{dkt}]^T \left\{ M_T \right\} \right\} dA \quad (2.92)$$

Substituting Eqs. (2.59), (2.66) and (2.72) into Eq. (2.92),

$$\left\{ f_T \right\} = \int_{C_0} \left( [G_2]^T [G_1]^T + z [B_{dkt}]^T \right) [Q] \left\{ \varepsilon_T \right\} dV \quad (2.93)$$

Using Eqs. (2.59) and (2.66),

$$\begin{aligned} [\bar{Q}]\{\varepsilon_T\} &= \begin{bmatrix} c^2 & s^2 & -2cs \\ s^2 & c^2 & 2cs \\ cs & -cs & c^2 - s^2 \end{bmatrix} \begin{bmatrix} Q_{11} & Q_{12} & 0 \\ Q_{12} & Q_{22} & 0 \\ 0 & 0 & Q_{66} \end{bmatrix} \begin{bmatrix} c^2 & s^2 & -2cs \\ s^2 & c^2 & 2cs \\ cs & -cs & c^2 - s^2 \end{bmatrix}^T \begin{bmatrix} c^2 & s^2 & -cs \\ s^2 & c^2 & cs \\ 2cs & -2cs & c^2 - s^2 \end{bmatrix} \begin{Bmatrix} \alpha_1 \\ \alpha_2 \\ \alpha_{12} \end{Bmatrix} \Delta T \\ &= \begin{bmatrix} c^2 & s^2 & -2cs \\ s^2 & c^2 & 2cs \\ cs & -cs & c^2 - s^2 \end{bmatrix} \begin{bmatrix} Q_{11} & Q_{12} & 0 \\ Q_{12} & Q_{22} & 0 \\ 0 & 0 & Q_{66} \end{bmatrix} \begin{Bmatrix} \alpha_1 \\ \alpha_2 \\ \alpha_{12} \end{Bmatrix} \Delta T = \begin{Bmatrix} \bar{\lambda}_x \\ \bar{\lambda}_y \\ \bar{\lambda}_{xy} \end{Bmatrix} \Delta T \end{aligned}$$

where

$$\begin{Bmatrix} \bar{\lambda}_x \\ \bar{\lambda}_y \\ \bar{\lambda}_{xy} \end{Bmatrix} = \begin{bmatrix} c^2 & s^2 & -2cs \\ s^2 & c^2 & 2cs \\ cs & -cs & c^2 - s^2 \end{bmatrix} \begin{bmatrix} Q_{11} & Q_{12} & 0 \\ Q_{12} & Q_{22} & 0 \\ 0 & 0 & Q_{66} \end{bmatrix} \begin{Bmatrix} \alpha_1 \\ \alpha_2 \\ \alpha_{12} \end{Bmatrix} \quad (2.94)$$

Therefore, the thermal load vector can be written as

$$\{f_T\} = \int_{C_0} \left( [G_2]^T [G_1]^T + z [B_{dkt}]^T \right) \begin{Bmatrix} \bar{\lambda}_x \\ \bar{\lambda}_y \\ \bar{\lambda}_{xy} \end{Bmatrix} \Delta T dV \quad (2.95)$$

The temperature distribution at any point  $(\xi, \eta, z)$  within the element is given by

$$\begin{aligned} \Delta T &= \frac{1}{2} (T_u(\xi, \eta) + T_l(\xi, \eta)) + \frac{z}{h} (T_u(\xi, \eta) - T_l(\xi, \eta)) \\ &= T_m(\xi, \eta) + \frac{z}{h} T_d(\xi, \eta) \end{aligned} \quad (2.96a)$$

where

$$T_m(\xi, \eta) = \frac{1}{2} (T_u(\xi, \eta) + T_l(\xi, \eta)), \quad T_d(\xi, \eta) = T_u(\xi, \eta) - T_l(\xi, \eta) \quad (2.96b)$$

$T_u(\xi, \eta)$  and  $T_l(\xi, \eta)$  are the temperatures at the top and bottom surfaces of the laminate, respectively. They are represented in terms of the nodal quantities  $T_{u1}$ ,  $T_{u2}$ ,  $T_{u3}$ , and  $T_{l1}$ ,  $T_{l2}$ ,

$T_{l3}$  using linear interpolation functions in the natural coordinates as follows

$$T_u(\xi, \eta) = T_{u1} + T_{u21}\xi + T_{u31}\eta, \quad T_l(\xi, \eta) = T_{l1} + T_{l21}\xi + T_{l31}\eta \quad (2.96c)$$

where  $T_{u21} = T_{u2} - T_{u1}$ ,  $T_{u31} = T_{u3} - T_{u1}$ ,  $T_{l21} = T_{l2} - T_{l1}$ ,  $T_{l31} = T_{l3} - T_{l1}$

Substituting Eq. (2.96) into (2.95) and integrating over the thickness, the thermal load vector can be expressed as

$$\begin{aligned} \{f_T\} = & \iint_{\Delta} [G_2]^T [G_1]^T \begin{Bmatrix} n_{t11} \\ n_{t12} \\ n_{t13} \end{Bmatrix} T_m(\xi, \eta) dA + \iint_{\Delta} [G_2]^T [G_1]^T \begin{Bmatrix} n_{t21} \\ n_{t22} \\ n_{t23} \end{Bmatrix} T_d(\xi, \eta) dA \\ & + \iint_{\Delta} [B_{dkt}]^T \begin{Bmatrix} m_{t11} \\ m_{t12} \\ m_{t13} \end{Bmatrix} T_m(\xi, \eta) dA + \iint_{\Delta} [B_{dkt}]^T \begin{Bmatrix} m_{t21} \\ m_{t22} \\ m_{t23} \end{Bmatrix} T_d(\xi, \eta) dA \end{aligned} \quad (2.97)$$

where

$$\begin{Bmatrix} n_{t11} \\ n_{t12} \\ n_{t13} \end{Bmatrix} = \int_t \begin{Bmatrix} \bar{\lambda}_x \\ \bar{\lambda}_y \\ \bar{\lambda}_{xy} \end{Bmatrix}_k dz = \sum_k \begin{Bmatrix} \bar{\lambda}_x \\ \bar{\lambda}_y \\ \bar{\lambda}_{xy} \end{Bmatrix}_k (z_{k+1} - z_k), \quad \begin{Bmatrix} n_{t21} \\ n_{t22} \\ n_{t23} \end{Bmatrix} = \int_t \begin{Bmatrix} \bar{\lambda}_x \\ \bar{\lambda}_y \\ \bar{\lambda}_{xy} \end{Bmatrix}_k \frac{z}{h} dz = \sum_k \begin{Bmatrix} \bar{\lambda}_x \\ \bar{\lambda}_y \\ \bar{\lambda}_{xy} \end{Bmatrix}_k \frac{1}{2h} (z_{k+1}^2 - z_k^2)$$

$$\begin{Bmatrix} m_{t11} \\ m_{t12} \\ m_{t13} \end{Bmatrix} = \int_t \begin{Bmatrix} \bar{\lambda}_x \\ \bar{\lambda}_y \\ \bar{\lambda}_{xy} \end{Bmatrix}_k z dz = \sum_k \begin{Bmatrix} \bar{\lambda}_x \\ \bar{\lambda}_y \\ \bar{\lambda}_{xy} \end{Bmatrix}_k \frac{1}{2} (z_{k+1}^2 - z_k^2), \quad \begin{Bmatrix} m_{t21} \\ m_{t22} \\ m_{t23} \end{Bmatrix} = \int_t \begin{Bmatrix} \bar{\lambda}_x \\ \bar{\lambda}_y \\ \bar{\lambda}_{xy} \end{Bmatrix}_k \frac{z^2}{h} dz = \sum_k \begin{Bmatrix} \bar{\lambda}_x \\ \bar{\lambda}_y \\ \bar{\lambda}_{xy} \end{Bmatrix}_k \frac{1}{3h} (z_{k+1}^3 - z_k^3)$$

Derivation of the electric load vector

The virtual work done by electric load is given by

$$\begin{aligned} \delta W_E = & \int_{C_0} \left\{ \delta \{\varepsilon^0\}^T \{N_E\} + \delta \{\kappa\}^T \{M_E\} \right\} dA \\ = & \{\delta \alpha\}^T \int_{C_0} \left\{ [G_2]^T [G_1]^T \{N_E\} + [B_{dkt}]^T \{M_E\} \right\} dA \end{aligned} \quad (2.98)$$

From which the electric load can be identified as

$$\{f_E\} = \int_{C_0} \left\{ [G_2]^T [G_1]^T \{N_E\} + [B_{dkt}]^T \{M_E\} \right\} dA \quad (2.99)$$

Substituting Eqs. (2.59), (2.65) and (2.71) into Eq. (2.99),

$$\{f_E\} = \int_{C_0} \left( [G_2]^T [G_1]^T + z [B_{dkt}]^T \right) [\bar{Q}] \{\varepsilon_E\} dV \quad (2.100)$$

Using Eqs. (2.59) and (2.65),

$$\begin{aligned} [\overline{Q}]\{\varepsilon_E\} &= \begin{bmatrix} c^2 & s^2 & -2cs \\ s^2 & c^2 & 2cs \\ cs & -cs & c^2 - s^2 \end{bmatrix} \begin{bmatrix} Q_{11} & Q_{12} & 0 \\ Q_{12} & Q_{22} & 0 \\ 0 & 0 & Q_{66} \end{bmatrix} \begin{bmatrix} c^2 & s^2 & -2cs \\ s^2 & c^2 & 2cs \\ cs & -cs & c^2 - s^2 \end{bmatrix}^T \begin{bmatrix} c^2 & s^2 & -cs \\ s^2 & c^2 & cs \\ 2cs & -2cs & c^2 - s^2 \end{bmatrix} \begin{Bmatrix} d_{31} \\ d_{32} \\ d_{36} \end{Bmatrix} E_3 \\ &= \begin{bmatrix} c^2 & s^2 & -2cs \\ s^2 & c^2 & 2cs \\ cs & -cs & c^2 - s^2 \end{bmatrix} \begin{bmatrix} Q_{11} & Q_{12} & 0 \\ Q_{12} & Q_{22} & 0 \\ 0 & 0 & Q_{66} \end{bmatrix} \begin{Bmatrix} d_{31} \\ d_{32} \\ d_{36} \end{Bmatrix} E_3 = \begin{Bmatrix} \bar{e}_{31} \\ \bar{e}_{32} \\ \bar{e}_{36} \end{Bmatrix} E_3 \end{aligned}$$

where

$$\begin{Bmatrix} \bar{e}_{31} \\ \bar{e}_{32} \\ \bar{e}_{36} \end{Bmatrix} = \begin{bmatrix} c^2 & s^2 & -2cs \\ s^2 & c^2 & 2cs \\ cs & -cs & c^2 - s^2 \end{bmatrix} \begin{bmatrix} Q_{11} & Q_{12} & 0 \\ Q_{12} & Q_{22} & 0 \\ 0 & 0 & Q_{66} \end{bmatrix} \begin{Bmatrix} d_{31} \\ d_{32} \\ d_{36} \end{Bmatrix} \quad (2.101)$$

Therefore, the electric load vector can be written as

$$\{f_E\} = \int_{c_0} \left( [G_2]^T [G_1]^T + z[B_{dkt}]^T \right) \begin{Bmatrix} \bar{e}_{31} \\ \bar{e}_{32} \\ \bar{e}_{36} \end{Bmatrix} E_3 dV \quad (2.102)$$

Integrating over the thickness, the electric load vector can be expressed as

$$\{f_E\} = \iint_{\Delta} [G_2]^T [G_1]^T \begin{Bmatrix} n_{e1} \\ n_{e2} \\ n_{e3} \end{Bmatrix} dA + \iint_{\Delta} [B_{dkt}]^T \begin{Bmatrix} m_{e1} \\ m_{e2} \\ m_{e3} \end{Bmatrix} dA \quad (2.103)$$

where

$$\begin{Bmatrix} n_{e1} \\ n_{e2} \\ n_{e3} \end{Bmatrix} = \int_t \begin{Bmatrix} \bar{e}_{31} \\ \bar{e}_{32} \\ \bar{e}_{36} \end{Bmatrix}_k E_3 dz = \sum_k \begin{Bmatrix} \bar{e}_{31} \\ \bar{e}_{32} \\ \bar{e}_{36} \end{Bmatrix}_k (E_3)_k (z_{k+1} - z_k)$$

$$\begin{Bmatrix} m_{e1} \\ m_{e2} \\ m_{e3} \end{Bmatrix} = \int_t \begin{Bmatrix} \bar{e}_{31} \\ \bar{e}_{32} \\ \bar{e}_{36} \end{Bmatrix}_k E_3 z dz = \sum_k \begin{Bmatrix} \bar{e}_{31} \\ \bar{e}_{32} \\ \bar{e}_{36} \end{Bmatrix}_k \frac{1}{2} (E_3)_k (z_{k+1}^2 - z_k^2)$$

Integrating the stiffness matrix, thermal load and electric load vector by Gauss numerical integration, we have, respectively



The Allman membrane stiffness  $[k_a]$ ,

$$\begin{aligned} [k_a] &= \int_0^1 \int_0^{1-\xi} [G_2]^T [G_1]^T [A][G_1][G_2] J d\xi d\eta \\ &= \frac{1}{2} \sum_{i=1}^n W_i [G_2]^T [G_1]^T [A][G_1][G_2] J \end{aligned} \quad (2.104a)$$

The DKT bending stiffness  $[k_{dkt}]$ ,

$$\begin{aligned} [k_{dkt}] &= \int_0^1 \int_0^{1-\xi} [B_{dkt}]^T [D][B_{dkt}] J d\xi d\eta \\ &= \frac{1}{2} \sum_{i=1}^n W_i [B_{dkt}]^T [D][B_{dkt}] J \end{aligned} \quad (2.104b)$$

The membrane-bending coupling stiffness  $[k_{mb}]$ ,

$$\begin{aligned} [k_{mb}] &= \int_0^1 \int_0^{1-\xi} [G_2]^T [G_1]^T [B][B_{dkt}] J d\xi d\eta \\ &= \frac{1}{2} \sum_{i=1}^n W_i [G_2]^T [G_1]^T [B][B_{dkt}] J \end{aligned} \quad (2.104c)$$

The contribution from the geometrically nonlinear terms in the membrane strains  $[k_n]$ ,

$$\begin{aligned} [k_n] &= \int_0^1 \int_0^{1-\xi} [G_2]^T \begin{bmatrix} \hat{N} & 0 & 0 \\ 0 & \hat{N} & 0 \\ 0 & 0 & \hat{N} \end{bmatrix} [G_2] J d\xi d\eta \\ &= \frac{1}{2} \sum_{i=1}^n W_i [G_2]^T \begin{bmatrix} \hat{N} & 0 & 0 \\ 0 & \hat{N} & 0 \\ 0 & 0 & \hat{N} \end{bmatrix} [G_2] J \end{aligned}$$

The thermal load vector can be computed as

$$\begin{aligned}
\{f_T\} &= \int_0^1 \int_0^{1-\xi} [G_2]^T [G_1]^T \begin{Bmatrix} n_{t11} \\ n_{t12} \\ n_{t13} \end{Bmatrix} T_m(\xi, \eta) |J| d\xi d\eta + \int_0^1 \int_0^{1-\xi} [G_2]^T [G_1]^T \begin{Bmatrix} n_{t21} \\ n_{t22} \\ n_{t23} \end{Bmatrix} T_d(\xi, \eta) |J| d\xi d\eta \\
&+ \int_0^1 \int_0^{1-\xi} [B_{dkt}]^T \begin{Bmatrix} m_{t11} \\ m_{t12} \\ m_{t13} \end{Bmatrix} T_m(\xi, \eta) |J| d\xi d\eta + \int_0^1 \int_0^{1-\xi} [B_{dkt}]^T \begin{Bmatrix} m_{t21} \\ m_{t22} \\ m_{t23} \end{Bmatrix} T_d(\xi, \eta) |J| d\xi d\eta \\
&= \frac{1}{2} \sum_{i=1}^n W_i [G_2]^T [G_1]^T \begin{Bmatrix} n_{t11} \\ n_{t12} \\ n_{t13} \end{Bmatrix} T_m(\xi, \eta) |J| + \frac{1}{2} \sum_{i=1}^n W_i [G_2]^T [G_1]^T \begin{Bmatrix} n_{t21} \\ n_{t22} \\ n_{t23} \end{Bmatrix} T_d(\xi, \eta) |J| \\
&+ \frac{1}{2} \sum_{i=1}^n W_i [B_{dkt}]^T \begin{Bmatrix} m_{t11} \\ m_{t12} \\ m_{t13} \end{Bmatrix} T_m(\xi, \eta) |J| + \frac{1}{2} \sum_{i=1}^n W_i [B_{dkt}]^T \begin{Bmatrix} m_{t21} \\ m_{t22} \\ m_{t23} \end{Bmatrix} T_d(\xi, \eta) |J|
\end{aligned} \tag{2.105}$$

The electric load vector can be computed as

$$\begin{aligned}
\{f_E\} &= \int_0^1 \int_0^{1-\xi} [G_2]^T [G_1]^T \begin{Bmatrix} n_{e1} \\ n_{e2} \\ n_{e3} \end{Bmatrix} |J| d\xi d\eta + \int_0^1 \int_0^{1-\xi} [B_{dkt}]^T \begin{Bmatrix} m_{e1} \\ m_{e2} \\ m_{e3} \end{Bmatrix} |J| d\xi d\eta \\
&= \frac{1}{2} \sum_{i=1}^n W_i [G_2]^T [G_1]^T \begin{Bmatrix} n_{e1} \\ n_{e2} \\ n_{e3} \end{Bmatrix} |J| + \frac{1}{2} \sum_{i=1}^n W_i [B_{dkt}]^T \begin{Bmatrix} m_{e1} \\ m_{e2} \\ m_{e3} \end{Bmatrix} |J|
\end{aligned} \tag{2.106}$$

where  $|J|$  is the determinant of the Jacobian matrix given by

$$|J| = 2A$$

$W_i$  is the weight corresponding to the sampling point.  $n$  is the number of the sampling points. Because the integrand is quadratic polynomial in  $\xi$  and  $\eta$ , the 3-point Gauss integration is used.

## Chapter 3. Genetic Algorithms for the Optimization of Piezoelectric

### Actuator Locations

#### 3.1 Abstract

Genetic algorithms ( GAs ) are becoming increasingly popular due to their ability to solve large complex optimization problems which can't be solved by any other method. GAs are robust stochastic global search techniques based on the mechanism of natural selection and natural genetics. In this paper, the advantages and disadvantages of GAs are presented. An improved GA (termed Version 2), developed by changing the mechanism that preserves the best solution and making the population size variable, from an existing version (termed Version 1) is employed to study an important issue in the design of smart structures: The selection of piezoelectric actuator location for shape control. The problem is to find both an optimal placement and optimal voltages for 30 piezoelectric actuators, selected from a maximum of 193 candidate locations, to obtain the best correction to the surface thermal distortions of a thin hexagonal spherical primary mirror. The mirror considered is a representative of the mirrors to be used in the next generation astronomical telescopes. Four different types of thermal distortions are considered. Two optimization problems are considered: (i) to find the optimal locations and optimal voltages suitable for only one type of thermal loads at a time, and (ii) to determine just one set of actuator locations which will reduce the distortion caused by all the four types of thermal loads. Although both these problems are large, difficult and computationally intensive, combinatorial and continuous optimization problems, the latter is a more challenging, multi-criterion optimization problem. A recently developed laminated triangular shell element is used to model the mirror. The

---

This chapter contains the materials presented at *AIAA/ASME/ASCE/AHS/AHC 41<sup>st</sup> SDM Conference* (in MDO session) and published by the conference proceedings and *AIAA Journal*, Vol. 39, No. 9, 2001, pp. 1818-1822.

results reveal an important phenomenon in the application of GAs to practical problems, namely that the convergence may occur to a non-optimal solution. The improved GAs are found to be more flexible and can get modestly better results than the DeLorenzo algorithm and the computational cost of the GA is found to be less than DeLorenzo's algorithm for the case of 30 actuators. Moreover, using GAs, it is possible to determine one set of actuator locations that reduces distortions caused by all the four different thermal loads.

### **3.2 Introduction**

Placement of sensors/actuators in an optimal fashion has drawn significant attention recently due to its importance in many applications such as shape control, vibration control, acoustic control, buckling control, aeroelastic control, and health monitoring of structures. Various methods have been used to address this issue, including the method of placing piezoelectric actuators in the region of high average strain and away from areas of zero strain,<sup>1</sup> heuristic integer programming,<sup>2</sup> tabu search,<sup>3</sup> simulated annealing,<sup>4</sup> and genetic algorithms,<sup>5</sup> etc.

The problem in this study is that given a set of 193 candidate piezoelectric actuator locations, find a subset of 30 locations and corresponding voltages that provide the best performance i.e. obtain the best correction to the surface thermal distortions of a thin hexagonal spherical primary mirror in the next generation of astronomical telescopes under four different types of thermal loads (Figure 3.1 a) ). This is a very large, difficult and computationally intensive optimization problem with more than  $1.28 \times 10^{35}$  candidate schemes for the placement of piezoelectric actuators. Kapania, Mohan, and Jakubowski studied the above problem using DeLorenzo algorithm.<sup>2</sup> The solution obtained by such an approach may be a local minimum.

Genetic algorithms ( GAs ) have attracted considerable attention due to their ability to solve large complex optimization problems. Genetic algorithms are also very general optimization methods which can be applied to virtually any optimization problem. However, implementing GAs for practical problems in an effective way is not easy. When one wants to apply GAs to a particular problem, especially a large complex practical problem, one faces a huge number of choices about how to proceed, with little theoretical guidance on how to make the most appropriate choice. There are a number of questions which must be answered. For example, which encoding scheme should be used? Which is the best selection scheme? Which is the best crossover scheme? How to set the values for the various parameters such as population size, crossover rate, and mutation rate? There are no conclusive answers to these questions. Besides these, one must choose what number of generations or evaluations GAs should run because GAs are not generally allowed to run until the convergence is reached but instead are halted after a certain time. If these issues are not addressed properly, solutions which are of both low quality and are costly may result.

As a first step, the present authors successfully applied genetic algorithms to the large-scale complex optimization problem, the selection of piezoelectric actuator location from more than  $1.28 \times 10^{35}$  candidate schemes in the case of 30 actuators and more than  $1.38 \times 10^{54}$  candidate schemes in the case of 121 actuators to obtain the best correction to the surface distortion of the primary mirror caused by one type of thermal loads. However, the GAs (termed Version 1) used in that study got results that were only slightly better than DeLorenzo algorithm. Also the cost of the GA was found to be less than that for the DeLorenzo's algorithm for the case of 30 actuators but was more than that for the DeLorenzo's algorithm for the case of 121 actuators. Four different types of temperature

distributions are considered in the present study. In general, the optimal locations determined for one type of thermal loads are not optimal for the others. Here, we use the improved GAs not only to find optimal actuator location for each of the four types of thermal loads considered but also to find a single set of actuator location, but with different voltage in a given actuator for each thermal load, that will reduce the thermal distortions caused by all the four different types of thermal loads.

### **3.3 Genetic Algorithms**

Genetic algorithms ( GAs ) are robust stochastic global optimization techniques based on the mechanism of natural selection and natural genetics. Genetic algorithms were invented by Holland in the 1960s.<sup>10</sup> They are population-based search algorithms with selection, crossover, mutation, and inversion operations. They work with a population of strings or chromosomes which represent potential solutions from one generation to another until some criteria are satisfied. These population-based search techniques distinguish GAs from traditional point-by-point engineering optimization techniques. Point-by-point search moves from a single point in the search space to the next, using some decision rule such as gradient information in the steepest descent algorithm to decide how to reach the next point in the design space. This point-by-point method may at times be highly inaccurate because it often locates a false peak in a search space with multiple peaks, almost the case in practical problems. But genetic algorithms work with a population of points simultaneously climbing many peaks in parallel, thus are less likely to get trapped at a false peak.

Selection is a bias operation much like Darwinian survival of the fittest, through which the better solutions will be retained and the worse ones will be discarded. Crossover exchanges subparts of two strings much like swapping genes of two chromosomes. Mutation randomly

changes the genes of some locations in the chromosome. Inversion reverses the order of a contiguous section of the chromosome, thus rearranging the order in which genes are arrayed.

Genetic algorithms have been developed by a large number of researchers. There are as many different GAs as there are GA projects. But, the basic idea is the same and is based on the mechanism of natural selection and natural genetics. There are two kinds of operations: one is evolution operation i.e. selection operation; the other is genetic operations such as crossover, mutation and the like. GAs have the following advantages and disadvantages:

Advantages:

- very general optimization techniques which can be applied to virtually any optimization problem.
- applicable to either continuous or discrete or both types of optimization problems.
- applicable to either linear or nonlinear or both types of optimization problems.
- robust stochastic global optimization techniques.
- population-based search techniques.
- require only objective function evaluations, not the gradient or sensitivity information.
- can find many optimal or near-optimal solutions.
- can solve large, complex optimization problems which can't be solved by any other method.
- can get better results than or at least the same results as any other method.

Disadvantages:

- not fully understood even now
- computation cost would be prohibitive if the effective GAs could not be developed.

To get an insight into the power of genetic algorithms we need to understand the concept of schemas (or schemata) introduced by Holland.<sup>8</sup> A schema is a set of bit strings that can be described by a template made up of ones, zeros, and asterisks, the asterisks representing wild cards or don't care symbols. For example, the schema  $H=1101^{**}01$  represents the set of four strings  $\{11011001, 11010001, 11011101, 11010101\}$ . It is easy to see that a schema with  $k$  asterisks represents the set of  $2^k$  strings. On the other hand, a string of length  $L$  is matched by  $2^L$  schemata. For example, the string 1101 is matched by sixteen schemata  $\{1101, *101, 1*01, 11*1, 110*, **01, *1*1, *10*, 1**1, 1*0*, 11**, ***1, **0*, *1**, 1***, ****\}$ . The largest region which contains many wild cards will typically be sampled by a large fraction of all the strings in a population. Thus, genetic algorithms that manipulate a population of strings actually sample a vastly large number of regions. This implicit parallelism gives genetic algorithms one of their central advantages over other optimization schemes.

In the field of shape control, noise and vibration control, buckling control, and aeroelastic control of smart structures, the effectiveness of the control system strongly depends on the actuator locations. In this paper, the improved GA (termed Version 2), developed by changing the mechanism that preserves the best solution and making the population size variable (as opposed to being fixed), from our preliminary study (termed Version 1), a micro-genetic algorithm, is employed to solve an important problem in the design of smart structures, namely, the selection of actuator locations. Genetic algorithms usually run with a large population. The low convergence rate of GAs is partially due to evaluating the large population, especially in large complex practical problems. Goldberg noted that a small population could be used successfully with GAs ( hence called micro-genetic algorithms ) if the population is restarted a sufficient number of times.<sup>7</sup> This is mainly due to the fact that



genetic algorithms using smaller populations converge in fewer generations than the ones with large populations. In this study, encoding scheme is the same as that used in Version 1, which is, the string would contain a 1 or 0 in the bits corresponding to the presence or absence of actuators. The selection scheme is the same as that used in Version 1, which is, the tournament selection. Crossover scheme is also the same as that used in Version 1, and is the uniform crossover with a rate of 0.5. The main differences between the previous and the present versions are as follows:

--- First, the mechanism that preserves the best solution is different. In Version 1, a randomly selected individual in the population is replaced by the best solution, but in Version 2, the worst individual in the population is replaced by the best solution.

--- Second, there are two important issues in the design of GAs: population diversity and selective pressure. Both of these are influenced by the size of the population. In Version 1, the size of the population is fixed, but in Version 2, the population size can vary during evolution.

### **3.4 Problem Definition**

In the design of next generation astronomical telescopes, one of the most stringent requirements is the maintenance of high surface accuracy of the primary mirror during their operation. A promising method is to use a certain number of piezoelectric actuators bonded onto the rear surface of the primary mirror to correct its distortions without imposing a significant weight penalty. The problem is how to find the optimal location of piezoelectric actuators to maximize their effectiveness. Our problem is as follows:

With 30 piezoelectric actuators, determine from a total of 193 candidate locations an optimal placement, and corresponding optimal voltage for each actuator, to obtain the best

correction to the surface thermal distortions of a thin hexagonal spherical primary mirror subjected to four different types of thermal loads (Figure 3.1 a ). There are two kinds of optimization problems: one is to find a set of locations and corresponding voltages that get the best correction to the surface thermal distortions under each of the four types of thermal loads; the other is to find one set of locations and corresponding voltages that provide the best possible correction to the four surface thermal distortions caused by the four different thermal loads. Note that, for the second case, while the actuator locations are same for all the four cases, the corresponding voltages may not be. The second problem is a multi-criterion problem and obviously is a more challenging problem.

These are very large, difficult and computationally intensive combinatorial optimization problems. Total number of different candidate sets are:

$${}_{193}C_{30} = \binom{193}{30} = \frac{193!}{30!(193-30)!} = 1.28866 * 10^{35}$$

The geometry and material properties of the mirror and piezoelectric actuators are given in Table 3.1. The temperature distribution at the lower surface of the mirror is assumed to be in the form of linear combination of the first few terms of the Zernike series expressed in terms of Cartesian coordinates  $x$  and  $y$  with the origin at the center of the mirror. The Cartesian coordinates used to express the temperature distributions are normalized such that they are in the range  $[-1,1]$ . The temperature distributions that are considered in this study are given in Table 3.2, where the constant  $C$  is used to scale the temperature distributions such that the upper, light-reflecting surface is at a lower temperature than the lower one, with a constant temperature difference  $\Delta T_z$  °C, taken as 0.2°C. The maximum temperature difference between any two grid points across the lower surface of the mirror,  $\Delta T_{xy}$  °C, is taken as 0.5°C.

Table 3.1: Properties and geometry of the mirror and piezoelectric actuators

|                                       | Mirror<br>(beryllium) | Piezoelectric strips |
|---------------------------------------|-----------------------|----------------------|
| Young's modulus, GPa                  | 293                   | 63                   |
| Poisson's ratio                       | 0.1                   | 0.3                  |
| Coefficient of thermal expansion, /°C | 11.5E-6               | 0.9E-6               |
| $d_{31}, d_{32}$ , m/V                |                       | 254E-12              |
| Radius, m                             | 10                    |                      |
| Side of the hexagon, m                | 0.5                   | 0.04166              |
| Thickness, m                          | 0.012                 | 0.25E-3              |

Table 3.2: Temperature distributions at the lower surface of the mirror

|    | Temperature distribution      |
|----|-------------------------------|
| T1 | $C[2(x^2 + y^2) - 1]$         |
| T2 | $C[(x + y)(3x^2 + 3y^2 - 2)]$ |
| T3 | $C(\sum_{i=1}^{i=9} K_i Z_i)$ |
| T4 | $C[x + y + 2xy]$              |

### 3.5 Finite Element Modeling

A recently developed laminated triangular shell element in Chapter 2 is used to model the mirror. The element is a combination of the DKT plate bending element and a membrane element derived from the linear strain triangular element with a total of 18 degrees-of-freedom (3 translations and 3 rotations per node). The piezoelectric strips are assumed to be perfectly bonded on the lower surface of the mirror and are modeled as a separate layer. The finite element model consists of 864 flat shell elements, 469 grid points (Figure 3.1 b). The mirror segment is assumed to be simple-supported at the six vertices 1, 13, 223, 247, 457, and 469.

### 3.6 Control Algorithms

The surface thermal distortions or the transverse displacements  $w$  of the mirror segment are corrected by applying the voltage across the thickness of the strip, which induces a distributed strain in the strip and hence in the mirror. In this study, the thermal deformation  $w$

due to any one type of thermal loads is computed by the finite element analysis. The finite element formulation suggested in Chapter 2 is capable of analyzing panels under thermal loads.

The deformations considered are so small (of order of a few micrometers) that the correction  $u_i$  at any point can be assumed to be:

$$u_i = \sum_{j=1}^n \alpha_{ij} V_j$$

where the control input  $V_j$  is the voltage applied across the  $j$ th piezoelectric strip and the influence coefficient  $\alpha_{ij}$  is defined as the deformation caused at node  $i$  due to a unit voltage applied across the  $j$ th piezoelectric strip alone.

A matrix of influence coefficients of size  $m \times n$  ( where  $m$  represents the total number of grid points in the FEM model,  $n$  represents the given number of piezoelectric actuators ) is obtained from the finite element model by applying a unit voltage across each of the piezoelectric strips, one at a time. A measure of the overall deviation or the RMS error is given by

$$E = \sqrt{\frac{1}{m} \sum_{i=1}^m (w_i + u_i)^2} = \sqrt{\frac{1}{m} \sum_{i=1}^m (w_i + \sum_{j=1}^n \alpha_{ij} V_j)^2}$$

To obtain the best correction, setting  $\partial E / \partial V_k = 0$  gives

$$\sum_{i=1}^m (w_i + \sum_{j=1}^n \alpha_{ij} V_j) \alpha_{ik} = 0$$

i.e.  $[A]\{V\} = \{b\}$ , where  $A_{kj} = \sum_{i=1}^m \alpha_{ij} \alpha_{ik}$ ,  $b_k = -\sum_{i=1}^m w_i \alpha_{ik}$

For each set of locations we can get the optimal voltages to minimize RMS error. Different settings of actuator location have different optimal voltages and corresponding minimum RMS error. Thus, **the first optimization problem** is to find a set of locations and

corresponding voltages that minimizes the minimum RMS error for a given type of distortions i.e. of the form,

$$E = \underset{L}{\text{Min}} \underset{V}{\text{Min}} E(T, L, V)$$

**the second optimization problem** is to find a set of locations and corresponding voltages that minimizes the maximum of the minimum RMS error for all the four different distortions i.e. of the form,

$$E = \underset{L}{\text{Min}} \underset{T}{\text{Max}} \underset{V}{\text{Min}} E(T, L, V)$$

### 3.7 Results and Discussion

In this section, the results obtained by using the improved GAs to solve the above two kinds of optimization problems are presented. To show the effectiveness of Version 2, the corresponding results obtained by DeLorenzo algorithm and Version 1 are also presented.

Following parameters were used:

Version 1: Population size 5, restart control parameter diffrac=0.06.

Version 2: run1 -- Initial population size 10, population size 5, scale=0.5, random=0, restart control parameter diffrac=0.06.

Version 2: run2 -- Initial population size 10, population size 5, scale=0.5, random=0, restart control parameter diffrac=0.0.

Note: The new parameters Initial population size, scale, and random were introduced in Version 2. The parameter scale is used to adjust the selective pressure. The parameter random is used to control whether the initial population size and population size are randomly generated or not. When the parameter random equals 0, the initial population size and population size equal the preset values respectively; otherwise, they equal the numbers generated randomly. The parameter diffrac is used to check the convergence of population.

When this value is less than the preset value, the new population are randomly generated.

The number of evaluations for the case of 30 strips using DeLorenzo algorithm is 18256. Note that DA in Figure 3.3 to Figure 3.6 represents the results by using DeLorenzo algorithm. The performance of the GAs on different types of thermal loads versus the number of evaluations is shown in Figure 3.2 a) to d) and Figure 3.7 a). Version 2 outperforms Version 1. Results for optimal actuator locations for various cases of thermal loads considered are presented in Figure 3.3 to Figure 3.9. For example, Figure 3.3 a) indicates the actuator locations as obtained using DeLorenzo algorithm to minimize the distortions caused by the type 1 (T1) of thermal loads. It is of interest to see how the optimal locations, obtained to minimize a given type of thermal loads, perform for other types of thermal distortions. In general, it was seen that this performance of the actuators deteriorates (substantially, in some cases) when used for any other type of thermal loads. For example, the actuator location obtained to minimize distortions for the type 1 thermal load, Figure 3.3 a), is not as effective for reducing the other types of thermal distortions. Using this set of actuator location, the RMS error for the type 1 distortions reduces to 0.204 (see top left corner of Figure 3.3 a) ), whereas the corresponding number is 0.272 for type 2 (top right corner in Figure 3.3 a) ); 0.359 for type 3 (bottom left corner in Figure 3.3 a) ); and 0.323 for type 4 (bottom right corner in Figure 3.3 a) ). Indeed, it was this deterioration in the performance of a given set of actuator locations for other types of thermal loads that led to the present authors to seek one set of actuator locations that will give acceptable distortion reduction for all the four types of thermal distortions (the second optimization problem). Figure 3.7 shows the one set of actuator locations that can be used for all the four types of thermal distortions. The number of evaluations using genetic algorithms is limited to 15000

except for results shown in Figure 3.8 and Figure 3.9. Figure 3.8 presents the results for the first optimization problem obtained using Version 2 with 30000 evaluations. Figure 3.9 presents the results for the second optimization problem obtained using Version 2 with 20000 evaluations.

The optimal voltages corresponding to this location under each type of thermal loads are shown in Table 3.3 to Table 3.6. The negative sign indicates that the voltage is applied in the direction opposite to the direction of polarization of the piezoelectric material. The voltages shown on some actuators may be too high to generate in space. Several promising methods can be used to lower the control voltages: one is using the piezoelectric materials with higher strain constant as actuators; another is using more piezoelectric actuators; the third is to optimize the design of composite mirror so that result in the smallest thermal deformations and hence reduce the control voltages, and so on. One of the most practical methods is to optimize the actuator location and corresponding voltages by applying constraints to electric voltages such as given the maximum voltages that can be provided. This is another different large and difficult optimization problem.

Table 3.3: Optimal voltages corresponding to optimal location (see Figure 3.9) for thermal load type T1.

| Strip Loc. | Voltage V | Strip Loc. | Voltage V | Strip Loc. | Voltage V |
|------------|-----------|------------|-----------|------------|-----------|
| 6          | -1017     | 65         | 350       | 126        | -201      |
| 7          | 723       | 74         | -474      | 138        | -659      |
| 11         | -357      | 79         | -1075     | 141        | -368      |
| 23         | -497      | 80         | 567       | 145        | -191      |
| 28         | -1011     | 88         | -456      | 156        | -471      |
| 29         | 502       | 89         | 188       | 159        | -641      |
| 40         | -699      | 93         | -587      | 161        | -34       |
| 47         | -293      | 98         | -222      | 164        | -87       |
| 59         | -502      | 119        | -351      | 176        | -483      |
| 64         | -420      | 121        | -313      | 179        | -175      |

Table 3.4: Optimal voltages corresponding to optimal location (see Figure 3.9) for thermal load type T2.

| Strip Loc. | Voltage V | Strip Loc. | Voltage V | Strip Loc. | Voltage V |
|------------|-----------|------------|-----------|------------|-----------|
| 6          | -1656     | 65         | 388       | 126        | 30        |
| 7          | 961       | 74         | -647      | 138        | -276      |
| 11         | -749      | 79         | -1417     | 141        | -218      |
| 23         | -688      | 80         | 836       | 145        | -37       |
| 28         | -1322     | 88         | -774      | 156        | -199      |
| 29         | 595       | 89         | 511       | 159        | -380      |
| 40         | -921      | 93         | -685      | 161        | -81       |
| 47         | -469      | 98         | -349      | 164        | -11       |
| 59         | -779      | 119        | -44       | 176        | -303      |
| 64         | -586      | 121        | -121      | 179        | -181      |



Table 3.5: Optimal voltages corresponding to optimal location (see Figure 3.9) for thermal load type T3.

| Strip Loc. | Voltage V | Strip Loc. | Voltage V | Strip Loc. | Voltage V |
|------------|-----------|------------|-----------|------------|-----------|
| 6          | -1744     | 65         | 983       | 126        | -109      |
| 7          | 732       | 74         | -192      | 138        | -66       |
| 11         | -1111     | 79         | -1306     | 141        | 190       |
| 23         | -967      | 80         | 1156      | 145        | -143      |
| 28         | -1594     | 88         | -797      | 156        | -139      |
| 29         | 826       | 89         | 772       | 159        | 20        |
| 40         | -270      | 93         | -539      | 161        | 222       |
| 47         | -102      | 98         | -266      | 164        | -222      |
| 59         | -527      | 119        | 53        | 176        | -50       |
| 64         | -843      | 121        | 213       | 179        | 197       |

Table 3.6: Optimal voltages corresponding to optimal location (see Figure 3.9) for thermal load type T4.

| Strip Loc. | Voltage V | Strip Loc. | Voltage V | Strip Loc. | Voltage V |
|------------|-----------|------------|-----------|------------|-----------|
| 6          | -1791     | 65         | 338       | 126        | -208      |
| 7          | 817       | 74         | -930      | 138        | -322      |
| 11         | -1103     | 79         | -1626     | 141        | -146      |
| 23         | -799      | 80         | 695       | 145        | -129      |
| 28         | -1608     | 88         | -771      | 156        | -245      |
| 29         | 964       | 89         | 154       | 159        | -258      |
| 40         | -49       | 93         | -988      | 161        | 120       |
| 47         | 73        | 98         | -571      | 164        | -133      |
| 59         | -387      | 119        | -268      | 176        | -113      |
| 64         | -389      | 121        | -166      | 179        | 129       |

### 3.8 Conclusions

In this study, a version of GAs (Version 2) obtained by changing the mechanism that preserves the best solution and making the population size variable from an existing version (Version 1) were used to solve two kinds of combinatorial and continuous optimization problems in the design of a thin hexagonal spherical primary mirror to be used in the next

generation of astronomical telescopes. One type of optimization problem is to find a set of locations and the corresponding voltages that gives us the best correction to the surface thermal distortions of the primary mirror under a given type of thermal loads; the other is to find one set of locations and corresponding voltages which provide the best correction to all the surface thermal distortions caused by each of the four different thermal loads. The second type is a difficult and computationally intensive multi-criterion optimization problem. The results show that both types of problems are multi-modal optimization problems, that is, there are more than one optimal or near optimal solution. This feature provides a great flexibility in the placement of piezoelectric actuators. The results reveal an important phenomenon in the application of GAs to a practical problem, namely that the convergence to a solution may occur without reaching an optimal or near-optimal solution. This study shows that the improved GAs are more flexible and can get modestly better results than DeLorenzo algorithm and that the cost of the GAs is still less than DeLorenzo's algorithm for the case of 30 actuators. Moreover, a very good solution to the optimization of one set of actuator locations applicable for the correction to all the thermal distortions under each of four different thermal loads has been found. The research shows that the improved GAs are effective in solving optimization problems of determining actuator locations for thermal distortion control.

### **Acknowledgments**

The work was performed under a subcontract from University of Texas at Arlington; themselves working under a grant from the National Science Foundation. We would like to thank Dr. Bernard Grossman, Department Head, Aerospace and Ocean Engineering, for providing considerable computational resources.

## References

1. Crawley, E. F. and de Luis, J., "Use of Piezoelectric Actuators as Elements of Intelligent Structures," *AIAA Journal*, Vol. 25, No. 10, 1987, pp. 1373-1385.
2. Kapania, R. K., Mohan, P., and Jakubowski, A., "Control of Thermal Deformations of Spherical Mirror Segment," Paper AIAA-96-4145, *Journal of Spacecraft and Rockets*, Vol. 35, No. 2, 1998, pp. 156-162.
3. Padula, S. L. and Palumbo, D. L., "Optimal Sensor/Actuator Locations for Active Structural Acoustic Control," Paper AIAA-98-1865.
4. Chen, G. S., Bruno, R. J., and Salama, M., "Optimal Placement of Active/Passive Members in Truss Structures Using Simulated Annealing," *AIAA Journal*, Vol. 29, No. 8, 1991, pp.1327-1334.
5. Rao, S. S., Pan, T. S., and Venkayya, V. B., "Optimal Placement of Actuators in Actively Controlled Structures Using Genetic Algorithms," *AIAA Journal*, Vol. 29, No. 6, 1991, pp. 942-943.
6. Kapania, R. K. and Mohan, P., "Static, Free Vibration and Thermal Analysis of Composite Plates and Shells Using a Flat Triangular Shell Element," *Computational Mechanics: An International Journal*, Vol. 17, No. 5, 1996, pp. 343-357.
7. Goldberg, D. E., "Sizing Populations for Serial and Parallel Genetic Algorithms," in *Proceedings of the 3rd International Conference on Genetic Algorithms*, edited by J. D. Schaffer, Morgan Kaufmann, 1989, pp. 70-79.
8. Goldberg, D. E., *Genetic Algorithms in Search, Optimization, and Machine Learning*, Addison-Wesley, 1989.
9. Holland, J. H., "Genetic algorithms," *Scientific American*, July, 1992, pp. 66-72.

10. Mitchell, M., *An Introduction to Genetic Algorithms*, MIT Press, 1996.
11. D. Dasgupta, and Z. Michalewicz (Editors), *Evolutionary Algorithms in Engineering Applications*, Springer, 1997.
12. David. L. Carroll's FORTRAN Genetic Algorithm Driver.

<http://www.aic.nrl.navy.mil:80/galist/src/#fortran>

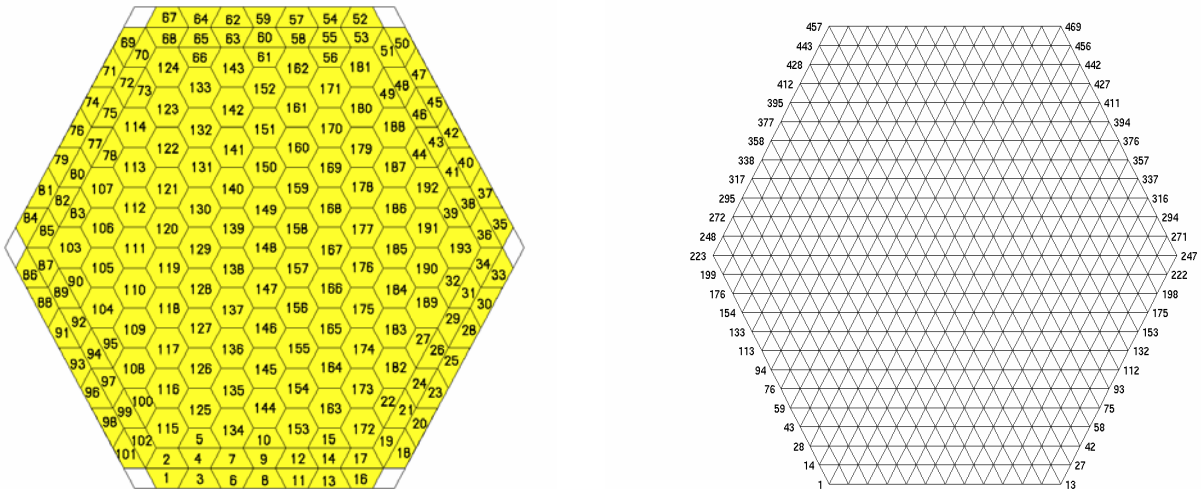


Figure 3.1 a) Piezoelectric actuator candidate locations b) Finite element mesh

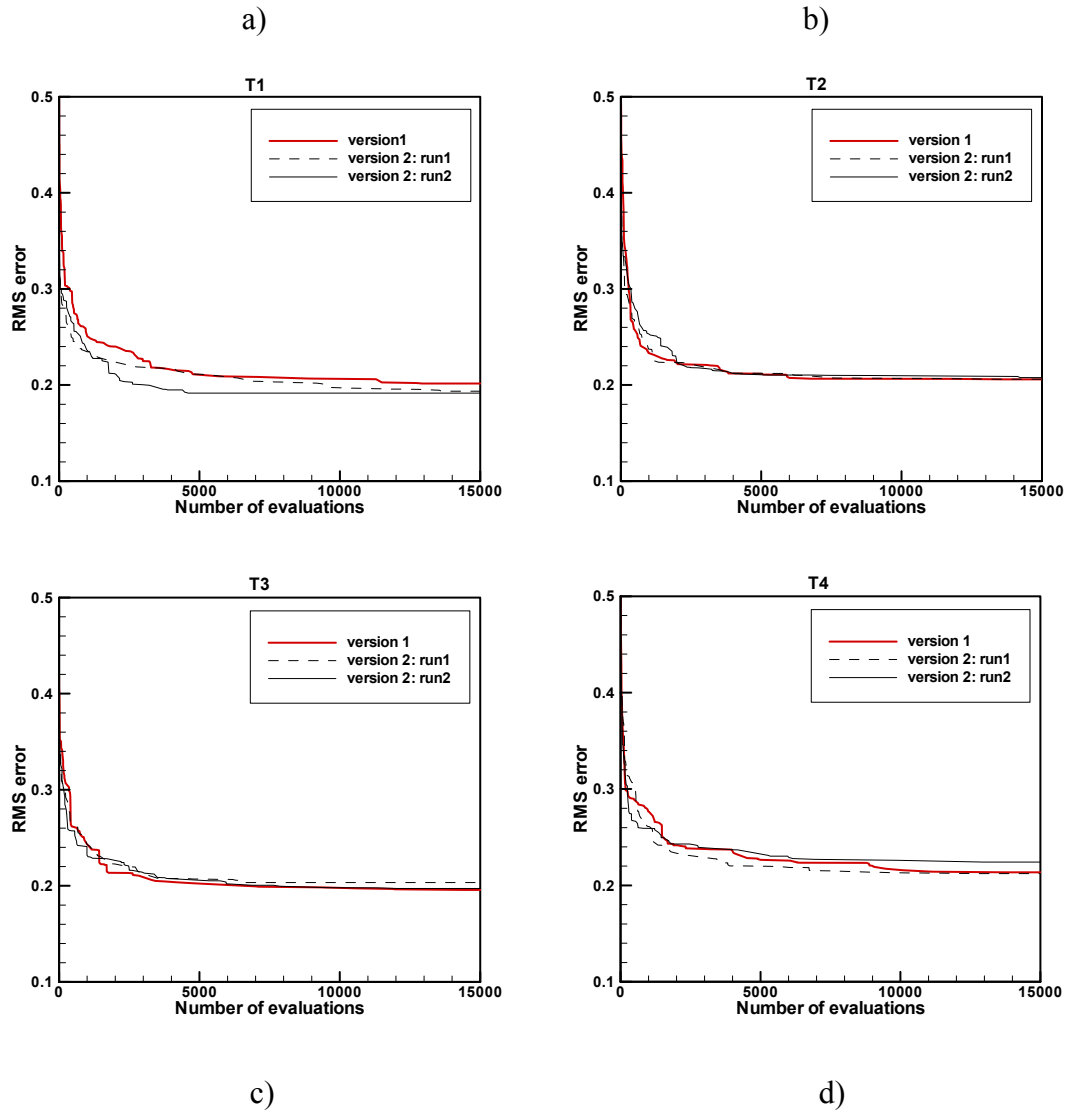


Figure 3.2 Performance of the GAs versus the number of evaluations on a) thermal load T1; b) thermal load T2; c) thermal load T3; and d) thermal load T4.

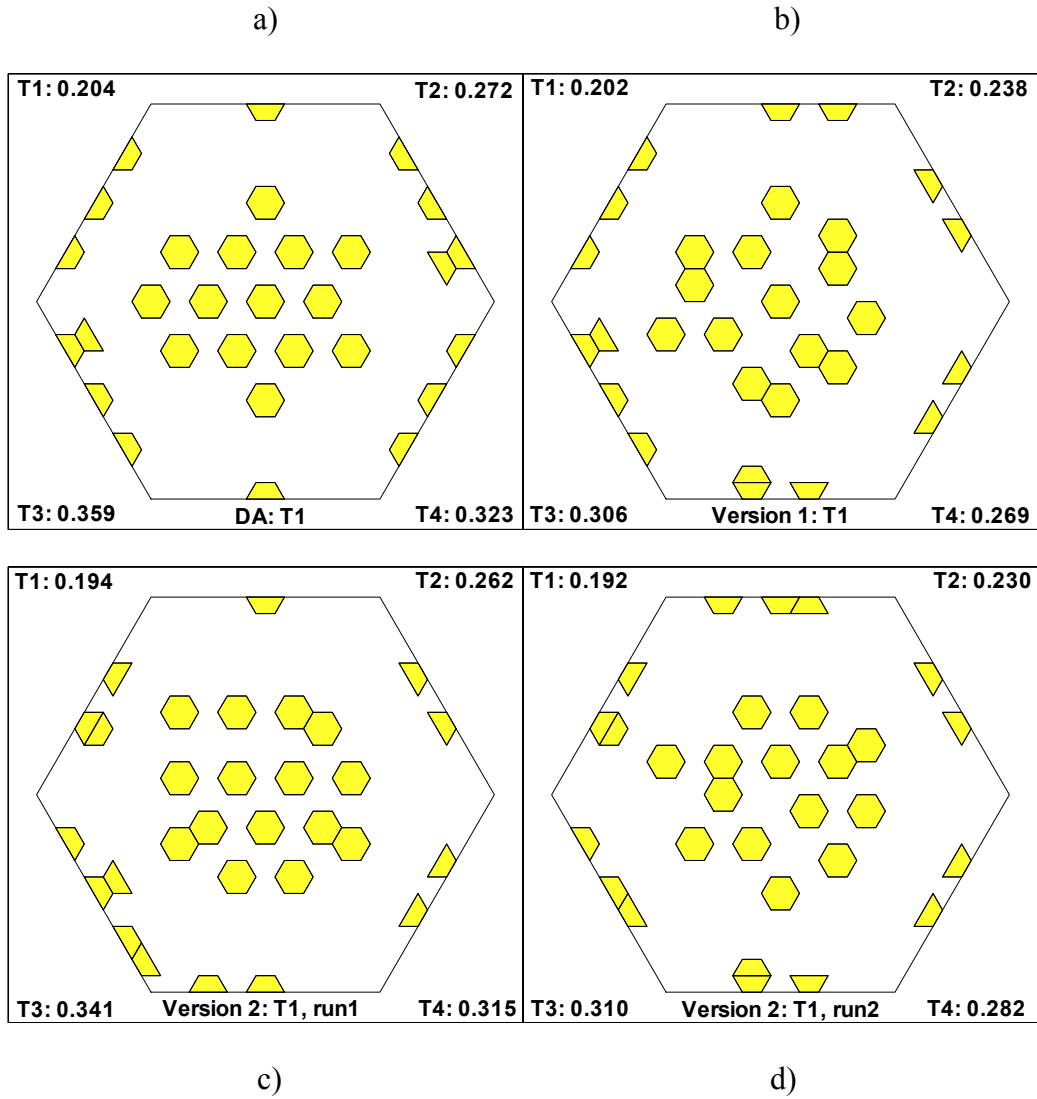


Figure 3.3 Optimal location for the thermal load T1 obtained by a) DeLorenzo algorithm; b) GA Version 1; c) GA Version 2, run1; and d) GA Version 2, run2.

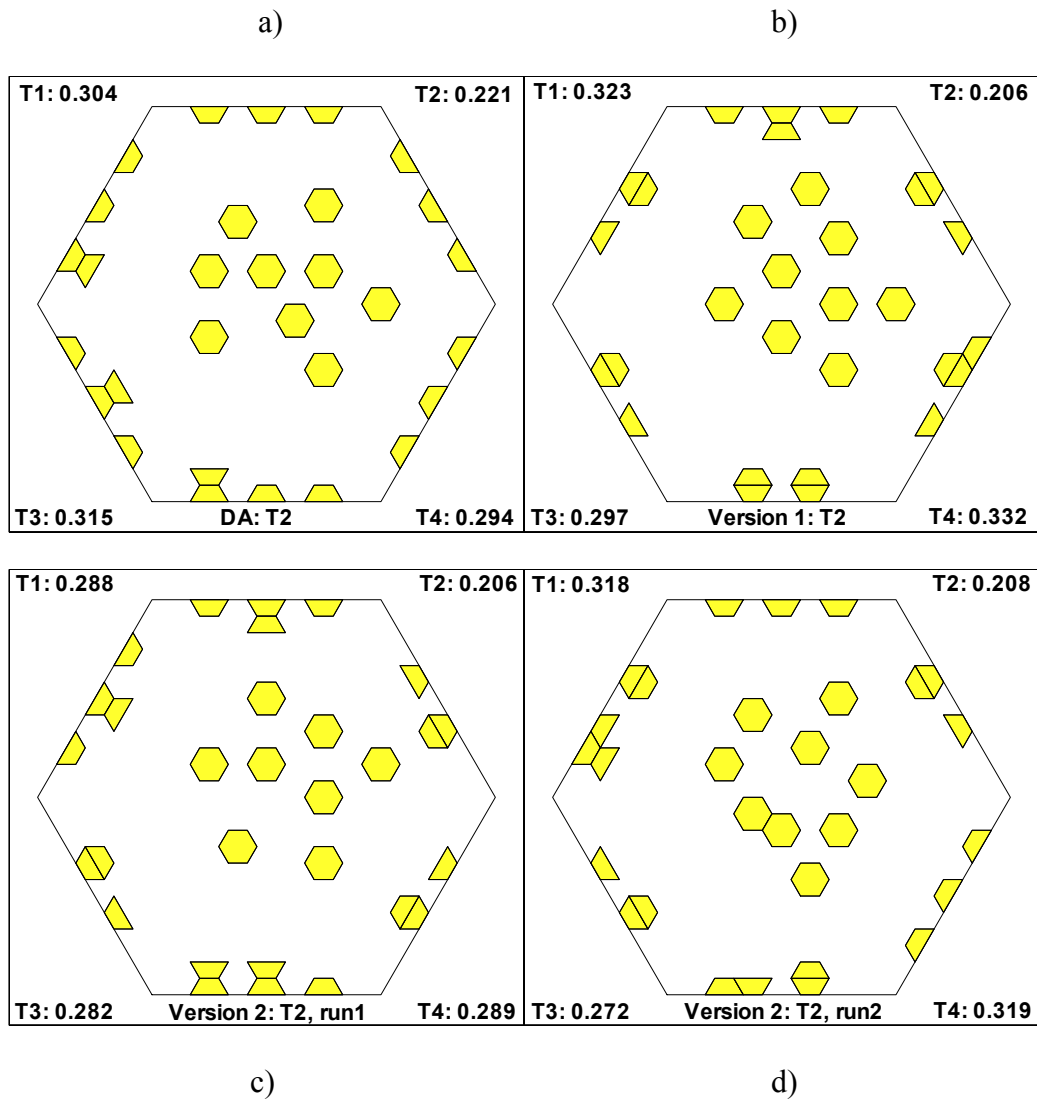


Figure 3.4 Optimal location for the thermal load T2 obtained by a) DeLorenzo algorithm; b) GA Version 1; c) GA Version 2, run1; and d) GA Version 2, run2.

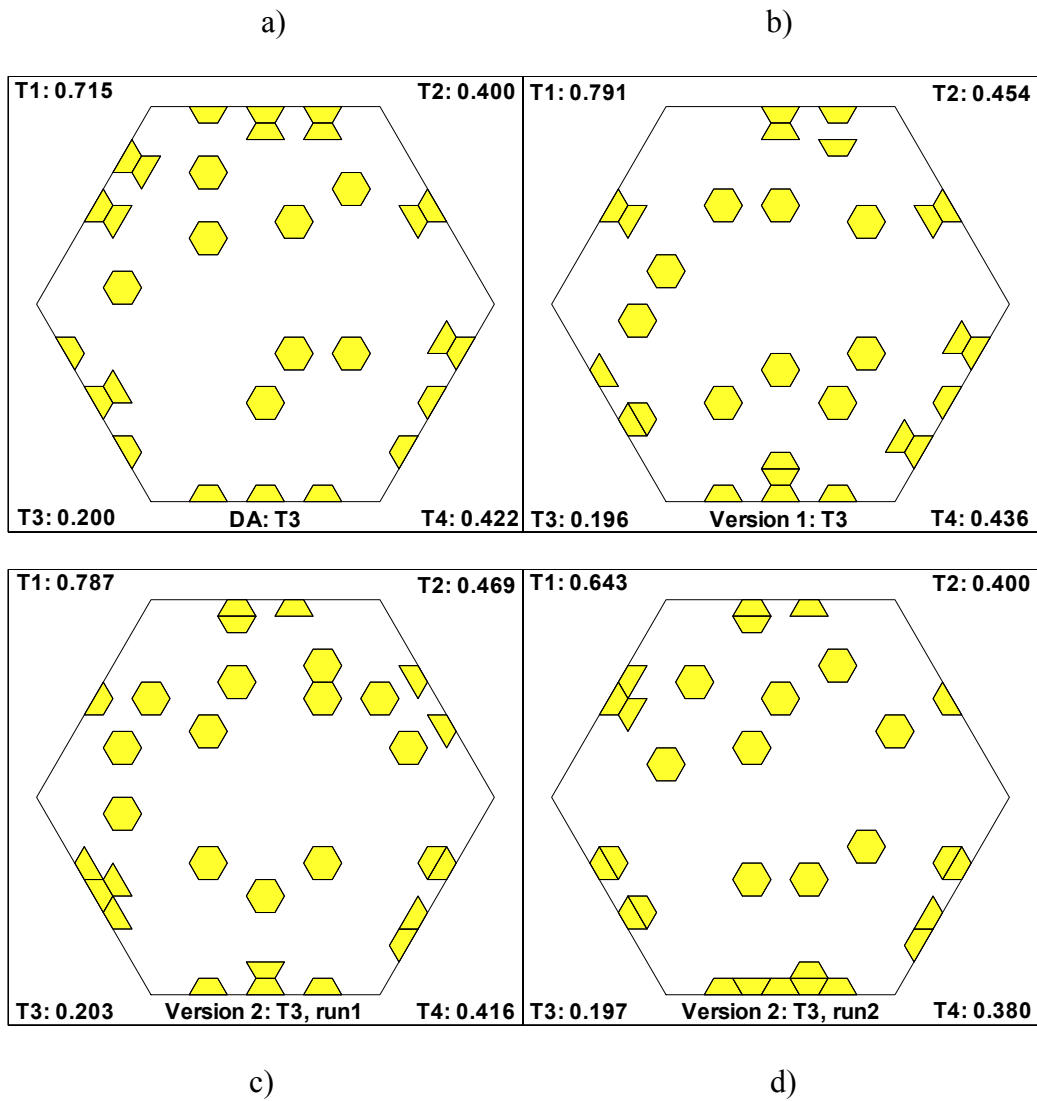


Figure 3.5 Optimal location for the thermal load T3 obtained by a) DeLorenzo algorithm; b) GA Version 1; c) GA Version 2, run1; and d) GA Version 2, run2.



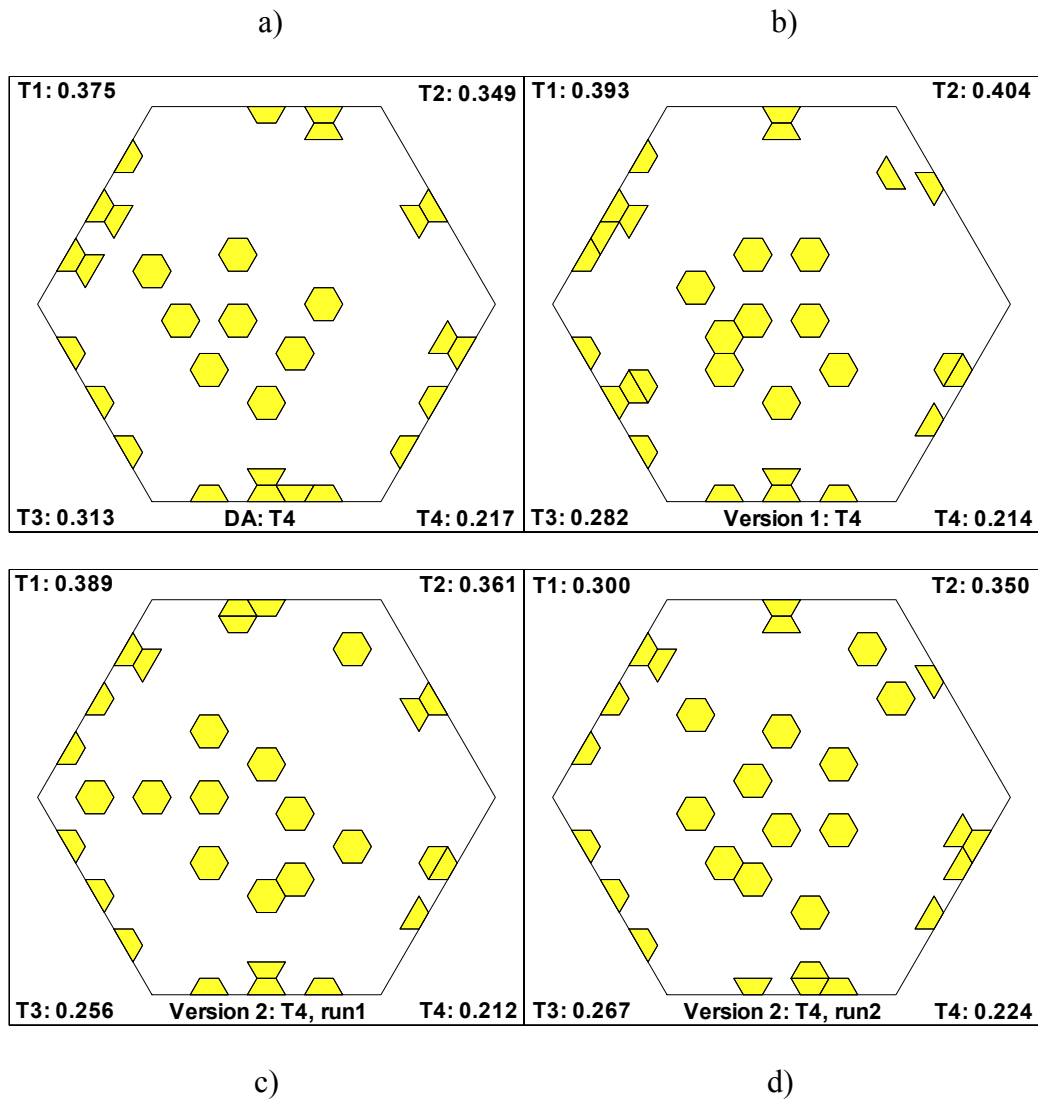


Figure 3.6 Optimal location for the thermal load T4 obtained by a) DeLorenzo algorithm; b) GA Version 1; c) GA Version 2, run1; and d) GA Version 2, run2.

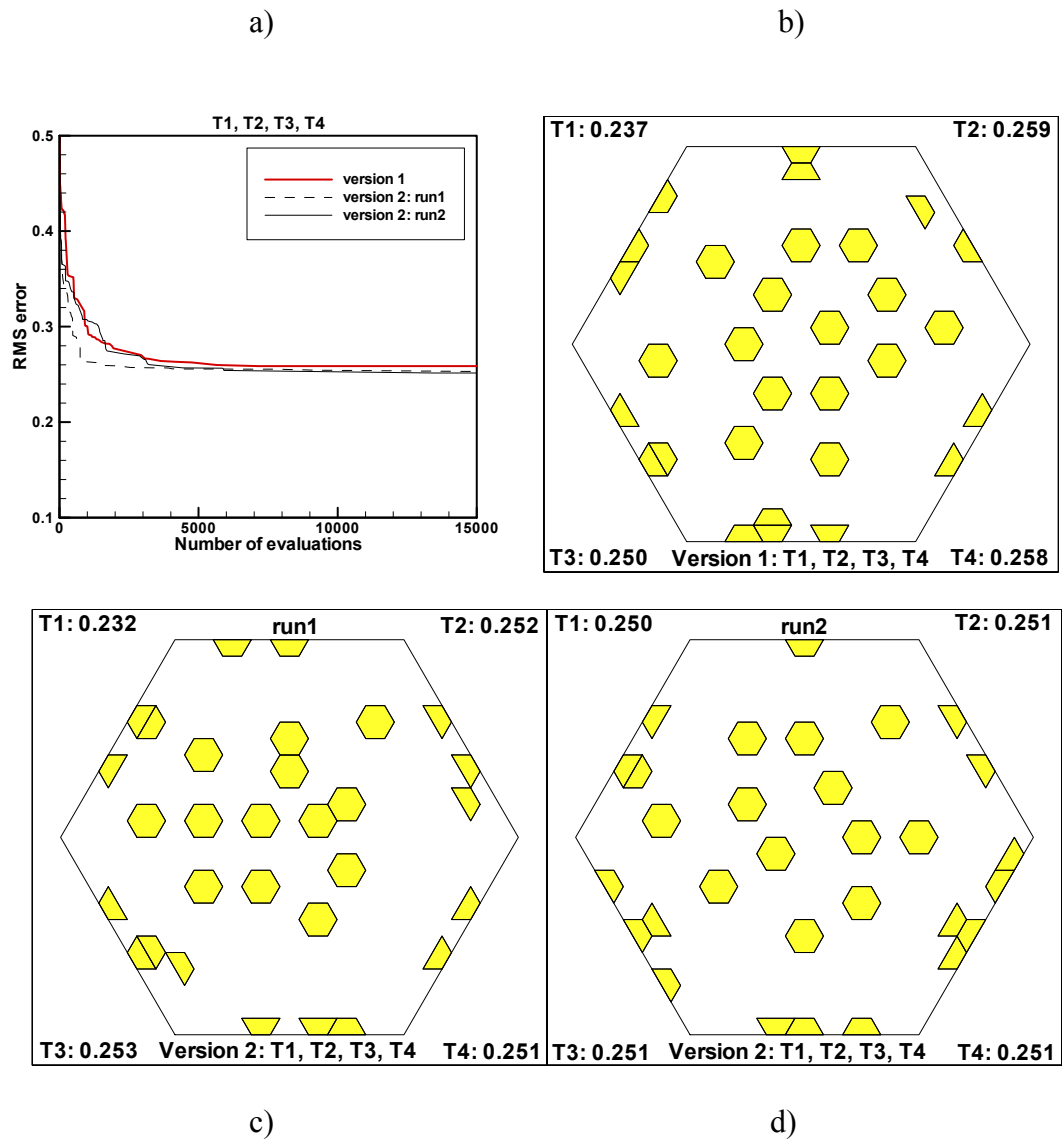


Figure 3.7 Performance of the GAs versus the number of evaluations a) and Optimal location for the thermal loads T1, T2, T3, and T4 obtained by b) GA Version 1; c) GA Version 2, run1; and d) GA Version 2, run2.

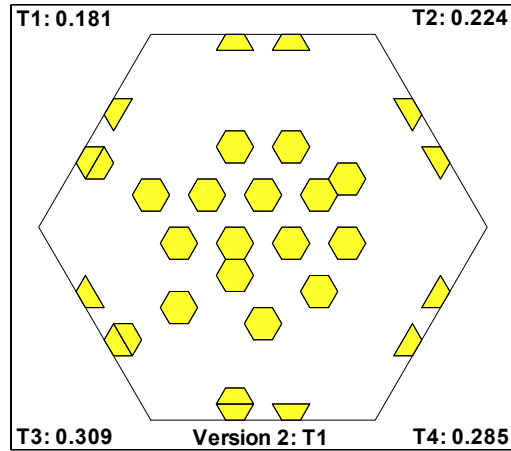


Figure 3.8 Optimal location for the thermal load T1 obtained using Version 2 with 30000 evaluations. Note that for the thermal load T1, the RMS error has reduced by 11.3%.

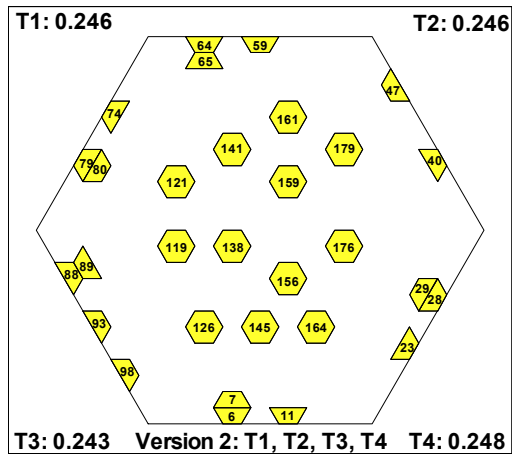


Fig 3.9 Optimal location for the thermal loads T1, T2, T3, and T4 obtained using Version 2 with 20000 evaluations

## Chapter 4. Toward More Effective Genetic Algorithms for the Optimization of Piezoelectric Actuator Locations

### 4.1 Abstract

Genetic algorithms ( GAs ), inspired by natural evolution, have drawn considerable attention during the past two decades due to their ability to solve large complex optimization problems that may be difficult to solve using conventional gradient-based optimization techniques. In our previous paper, some advantages and disadvantages of GAs were presented, and two versions of GA's ( termed GA Version 1 and GA Version 2) were used to solve two kinds of difficult, computationally intensive, combinatorial and continuous large-scale optimization problems. The problems consisted of finding both an optimal placement and optimal voltages of 30 piezoelectric actuators, from 193 candidate locations, with more than  $1.28 \times 10^{35}$  possible solutions, to obtain the best correction to the surface thermal distortions of a thin hexagonal spherical primary mirror. The thermal distortions were caused by four different types of spatial temperature distributions. The first problem was the one in which a set of actuator locations corresponding to each of the four types of thermal loads was obtained and in the other one set of actuator location was obtained for controlling thermal distortions caused by all the four types of thermal loads. The latter is a more challenging, multi-criterion optimization problem. A laminated triangular shell element was used to model the mirror. In this paper, an improved GA, termed GA Version 3, is developed from the GA Version 2 and is employed to resolve the problems studied in our previous paper and even larger problems. Two key differences between the GA Version 3 and the earlier GA Version 2 are: (i) to apply random-mutation hill climbing to elitists, and

---

This chapter contains the materials presented at *AIAA/ASME/ASCE/AHS/AHC 42<sup>nd</sup> SDM Conference* (in MDO session) and published by the conference proceedings and *AIAA Journal*, Vol. 40, No. 6, 2002, pp. 1246-1250.

(ii) to apply mutation to micro-genetic algorithms. For the problem of interest in this study, it is seen that the above two modifications significantly improve the performance of GAs. The results of using same parameter settings of the GA Version 3 to even a larger problem, that is, choosing a set of 121 piezoelectric actuator locations from 193 candidate locations with more than  $1.38 \times 10^{54}$  possible solutions, are also reported. The results show that the RMS error, for the first type of problem, for the 121- piezoelectric actuator case obtained using the GA Version 3, is basically the same as that obtained using the DeLorenzo's algorithm, but a different setting of piezoelectric actuator locations is obtained. Moreover, a very good setting of 121 actuators for the second optimization problem is found.

## 4.2 Introduction

Due to the well-known advantages of adaptive structures over traditional structures, significant research has been conducted in this field in the past two decades. The performance of such systems strongly depends on piezoelectric actuator locations. In our previous paper,<sup>1</sup> various methods addressing this issue were mentioned and some advantages and disadvantages of GAs were presented.

In the previous studies, the present authors successfully applied two versions of GA's (termed GA Version 1 and GA Version 2), developed by the present authors from Carroll's FORTRAN Genetic Algorithm Driver<sup>2</sup>, to solve two kinds of large-scale optimization problems. These problems entailed choosing a set of 30 piezoelectric actuator locations, from 193 possible candidate locations, and with more than  $1.28 \times 10^{35}$  possible solutions, to correct the thermal distortions of a thin hexagonal spherical primary mirror (Figure 4.1 a)). The thermal distortions were generated from four different thermal load distributions. The two types of optimization problems considered in the earlier study were: (i) to individually find

the optimal locations and optimal voltages suitable for each type of thermal loads; (ii) to determine just one set of actuator locations which will reduce the distortion caused by all the four types of thermal loads. Both these problems are difficult and computationally intensive. The latter type is a more challenging, multi-criterion optimization problem. A laminated triangular shell element developed in Chapter 2 was used to model the mirror. The first problem was studied by Kapania, Mohan, and Jakubowski<sup>4</sup> using DeLorenzo algorithm. The solution obtained by such an approach may be a local minimum. The main conclusions from our previous studies are as follows:

- The design search space is highly multi-modal.
- GA Version 1 got only slightly better results than the DeLorenzo algorithm and the computation cost was less than that of the DeLorenzo's algorithm for the case of 30 piezoelectric actuators but higher for the case of 121 piezoelectric actuators.
- Both GA Version 1 and GA Version 2 are robust for the optimization of piezoelectric actuator locations.
- The GA Version 2 has more flexibility than GA Version 1.
- The GA Version 2 can get modestly better results than DeLorenzo algorithm for both optimization problems for the case of 30 piezoelectric actuators.
- The convergence to a solution may occur without reaching an optimal or near-optimal solution.
- More than one sub-optimal solution to each problem were found.
- Optimal location obtained for one type of thermal loads may perform poorly for other types of thermal loads.
- GAs can determine one set of actuator locations which is good for all the four types of

thermal loads considered for these studies. The needed voltages will be different for different thermal loads.

In the present paper, an improved GA, termed GA Version 3, developed by modifying the GA Version 2, is employed to solve the two problems studied in Ref. 1 and also an even larger problem. Two key differences between GA Version 3 and GA Version 2 are:

- (i) Application of random-mutation hill climbing to elitists, and
- (ii) Application of mutation to micro-genetic algorithms.

From the results of running GA Version 3, for the problem of interest in this study, it can be seen that the above two modifications significantly improve the performance of GAs. The results of using same parameter settings of GA Version 3 to even larger problems of choosing a set of 121 piezoelectric actuator locations from 193 possible candidate locations with more than  $1.38 \times 10^{54}$  possible solutions are also reported.

### **4.3 Genetic Algorithms**

Genetic algorithms ( GAs ) are robust stochastic global search techniques based on the mechanics of natural selection and genetics. GAs were invented by Holland in the 1960s,<sup>5</sup> and later developed by De Jong, Goldberg, and many others. These algorithms evolve a population of chromosomes using selection and genetic operations such as crossover, mutation, and so on from one generation to another, hopefully to get a better solution. The selection operation is based on the Darwinian principle of the survival of the fittest. Genetic algorithms use only one very general assumption, namely: better individuals can reproduce better offspring more probably than the worst individuals. The concept's simplicity, flexibility and robust performance makes GAs one of the most exciting fields in evolutionary computation.

In the field of shape control, noise and vibration control, buckling control, and aeroelastic control of smart structures, the effectiveness of the control system strongly depends on the actuator locations. In this paper, the improved GA (termed Version 3), developed by the present authors from an earlier GA, the GA Version 2, is employed to solve an important problem in the design of smart structures, namely, the selection of actuator locations. Two key differences between GA Version 3 and GA Version 2 are as follows:

- (i) to apply random-mutation hill climbing to elitists,
- (ii) to apply mutation to micro-genetic algorithms.

---First, random-mutation hill climbing was applied to elitists – the best individuals. This came from our initial intuition that if we don't know which individual can reproduce a better offspring (we need to recall from Ref.6, p.201, “ in their purest form, genetic algorithms are blind search procedures ”, but in practical form GAs are directed search techniques not completely blind.), choosing the best one generally gets the highest probability. Random-mutation hill climbing outperformed the steepest-ascent hill climbing and next-ascent hill climbing (Ref. 5, p.129).

---Second, mutation was applied to micro-genetic algorithms. The micro-genetic algorithms here are the same as the genetic algorithms in the commonly used sense except that they include restart function in the outer loop and usually use a small population size in order to get the effect of faster convergence rate than the large population size usually used in genetic algorithms. In the literature, mutation rate was set 0.0 in most cases whenever the micro-genetic algorithms were used. This is probably due to traditional view of the negative effect of mutation – namely that the use of mutation slows down convergence. Recent advances in genetic algorithms show that the mutation operation also has some positive effects –



speeding up convergence as well as providing the diversity of population, thereby avoiding a premature convergence to a local optimum.

#### **4.4 Problem Definition**

In the design of next generation of astronomical telescopes, one of the most stringent requirements will be the maintenance of high surface accuracy of the primary mirror during their operation. A promising method is to use a certain number of piezoelectric actuators bonded onto the rear surface of the primary mirror to correct its distortions without imposing a significant weight penalty. The problem is how to find the optimal location of piezoelectric actuators to maximize their effectiveness. Our problem is as follows:

With,  $n$ , the number of piezoelectric actuators available, determine from a total of 193 candidate locations an optimal placement, and corresponding optimal voltage for each actuator, to obtain the best correction to the surface thermal distortions of a thin hexagonal spherical primary mirror subjected to four different types of thermal loads (Figure 4.1 a)). There are two kinds of optimization problems: one is to find a set of locations and corresponding voltages that get the best correction to the surface thermal distortions under each of the four types of thermal loads; the other is to find one set of locations and corresponding voltages that provide the best possible correction to the surface thermal distortions caused by all the four types of thermal loads. Note that, for the second problem, while the actuator locations are the same for all the four thermal distortions, the corresponding voltages may not be. The second problem is a multi-criterion problem and obviously is a more challenging problem.

These are very large, difficult and computationally intensive combinatorial optimization problems. Total number of different candidate sets are:

$${}^{193}C_n = \binom{193}{n} = \frac{193!}{n!(193-n)!}$$

So, for the case of 30 and 121 piezoelectric actuators, the number of different candidate sets are respectively,

$${}^{193}C_{30} = 1.28866 * 10^{35}$$

$${}^{193}C_{121} = 1.38231 * 10^{54}$$

The geometry and material properties of the mirror and piezoelectric actuators are given in Table 4.1. The temperature distribution at the lower surface of the mirror is assumed to be in the form of linear combination of the first few terms of the Zernike series expressed in terms of Cartesian coordinates  $x$  and  $y$  with the origin at the center of the mirror. The Cartesian coordinates used to express the temperature distributions are normalized such that they are in the range  $[-1,1]$ . The temperature distributions that are considered in this study are given in Table 2, where the constant  $C$  is used to scale the temperature distributions such that the upper, light-reflecting surface is at a lower temperature than the lower surface, with a constant temperature difference  $\Delta T_z$  °C, taken as 0.2°C. The maximum temperature difference between any two grid points across the lower surface of the mirror,  $\Delta T_{xy}$  °C, is taken as 0.5°C.

#### 4.5 Finite Element Modeling

A laminated triangular shell element developed in Chapter 2 is used to model the mirror. The element is a combination of the DKT plate bending element and a membrane element derived from the linear strain triangular element with a total of 18 degrees-of-freedom (3 translations and 3 rotations per node). The piezoelectric strips are assumed to be perfectly

bonded on the lower surface of the mirror and are modeled as a separate layer. The finite element model consists of 864 flat shell elements, 469 grid points (Figure 4.1 b)). The mirror segment is assumed to be simple-supported at the six vertices 1, 13, 223, 247, 457, and 469.

#### 4.6 Control Algorithms

The surface thermal distortions or the transverse displacements  $w$  of the mirror segment are corrected by applying the voltage across the thickness of the strip, which induces a distributed strain in the strip and hence in the mirror. In this study, the thermal deformation  $w$  due to any one type of thermal loads is computed by the finite element analysis. The finite element formulation suggested in Chapter 2 is capable of analyzing panels under thermal loads.

The deformations considered are so small (of order of a few micrometers) that the correction  $u_i$  at any point can be assumed to be:

$$u_i = \sum_{j=1}^n \alpha_{ij} V_j$$

where the control input  $V_j$  is the voltage applied across the  $j$ th piezoelectric strip and the influence coefficient  $\alpha_{ij}$  is defined as the deformation caused at node  $i$  due to a unit voltage applied across the  $j$ th piezoelectric strip alone.

A matrix of influence coefficients of size  $m \times n$  ( where  $m$  represents the total number of grid points in the FEM model,  $n$  represents the given number of piezoelectric actuators ) is obtained from the finite element model by applying a unit voltage across each of the piezoelectric strips, one at a time. A measure of the overall deviation or the RMS error is given by

$$E = \sqrt{\frac{1}{m} \sum_{i=1}^m (w_i + u_i)^2} = \sqrt{\frac{1}{m} \sum_{i=1}^m (w_i + \sum_{j=1}^n \alpha_{ij} V_j)^2}$$

To obtain the best correction, setting  $\partial E/\partial V_k = 0$  gives

$$\sum_{i=1}^m (w_i + \sum_{j=1}^n \alpha_{ij} V_j) \alpha_{ik} = 0$$

i.e.  $[A]\{V\} = \{b\}$ , where  $A_{kj} = \sum_{i=1}^m \alpha_{ij} \alpha_{ik}$ ,  $b_k = -\sum_{i=1}^m w_i \alpha_{ik}$

For each set of locations we can get the optimal voltages to minimize RMS error. Different settings of actuator location have different optimal voltages and corresponding minimum RMS error. Thus, **the first optimization problem** is to find a set of locations and corresponding voltages that minimizes the minimum RMS error for one type of distortions i.e. of the form,

$$E = \underset{L}{\text{Min}} \underset{V}{\text{Min}} E(T, L, V)$$

**the second optimization problem** is to find a set of locations and corresponding voltages that minimizes the maximum of the minimum RMS error for all the four different distortions i.e. of the form,

$$E = \underset{L}{\text{Min}} \underset{T}{\text{Max}} \underset{V}{\text{Min}} E(T, L, V)$$

Obviously, the second problem is a more realistic, but computationally very challenging problem.

## 4.7 Results and Discussion

In this section, the results obtained by using the GA Version 3 developed by the present authors from the GA Version 2<sup>1</sup> to solve the above two kinds of optimization problems are presented. Following parameters were used:

Version 1: Population size 5, crossover rate = 0.5, mutation rate = 0.0, restart control parameter difffrac = 0.06.

Version 2: run1 -- Initial population size 10, population size 5, scale=0.5, random=0, crossover rate =0.5, mutation rate=0.0, restart control parameter diffrac=0.06.

Version 2: run2 -- Initial population size 10, population size 5, scale=0.5, random=0, crossover rate =0.5, mutation rate=0.0, restart control parameter diffrac=0.0.

Version 3: run1 -- Initial population size 10, population size 5, scale=0.5, random=0, crossover rate =0.5, mutation rate=0.01, No\_of\_max\_generation\_inner\_loop=15, No\_of\_best\_mutation\_bits=2.

Version 3: run2 -- Initial population size 10, population size 5, scale=0.5, random=0, crossover rate =0.5, mutation rate=0.01, No\_of\_max\_generation\_inner\_loop=10, No\_of\_best\_mutation\_bits=2.

Note: The new parameter No\_of\_best\_mutation\_bits which represents mutation bits for elitists in each generation was introduced in Version 3. The parameter scale is used to adjust the selective pressure. The parameter random is used to control whether the initial population size and population size are randomly generated or not. When the parameter random equals 0, the initial population size and population size equal the preset values respectively; otherwise, they equal the numbers generated randomly. The parameter diffrac is used to check the convergence of population. When this value is less than the preset value, the new population are randomly generated.

In this study, the number of evaluations using genetic algorithms is limited to 15000. For 30 piezoelectric actuators, the performance of different versions of the GAs for the two kinds of optimization problems is shown in Figure 4.2 and Figure 4.3, respectively. Figure 4.2 shows the performance of the GAs versus the number of evaluations for the first optimization problems for each of the four types of thermal loads; Figure 4.3 shows the performance of

the GAs with respect to the number of evaluations for the second optimization problem. The optimal actuator locations obtained by the two runs of the GA version 3 for the two kinds of optimization problems are presented in Figure 4.4 and 4.5, respectively. Figure 4.4 presents the results for the first kind of optimization problems for each of the four types of thermal loads; Figure 4.5 presents the results for the second kind of optimization problem for all the four types of thermal loads. The number in each corner in Figure 4.4 and Figure 4.5 represents the RMS error corresponding to that type of thermal distortion. The set of actuator locations, shown in the top-left corner of Figure 4.4, was obtained to minimize the error due to thermal load T1. The RMS error under thermal load T1 becomes 0.191; the error under T2, T3 and T4 becomes 0.245, 0.332 and 0.326, respectively. Hence it is seen that this set of actuator locations, while best for T1, may perform poorly when used for other types of thermal loads.

The optimal voltages corresponding to the optimization location (Figure 4.5 b)) for each type of thermal loads are listed in Tables 4.3 to 4.6. The negative sign indicates that the voltage is applied in the direction opposite to the direction of polarization of the piezoelectric material.

Regarding the performance of GAs (Figures 4.2 and 4.3), GA Version 3 not only approached near optimal solution very fast, but also found the best solution. For example, when used for the second kind of optimization problem – the multi-criterion optimization problem (Figure 4.3), GA Version 3 run1 approached a near-optimal solution, with distortion RMS error value of 0.251, in less than 2000 evaluations and GA Version 3 run2 obtained the same RMS error in less than 5000 evaluations. Moreover, the latter obtained the best solution, with a distortion RMS error value of 0.230 at the end of 15000 evaluations, but GA

Version 2 run2 did not reach a near-optimal solution, with a distortion RMS error of 0.251 until more than 13000 evaluations. The GA Version 2 run1 and GA Version 1 did not even reach any near-optimal solution with the level of distortion RMS error of 0.251, at the end of stipulated 15000 evaluations. The research shows that the GA Version 3 is more effective than previous versions in solving optimization problem of determining actuator locations for thermal distortion control.

**Results for 121 actuators:** Figure 4.6 to Figure 4.10 and Table 4.7 to Table 4.10 present the results for the two kinds of optimization problems for the case of 121 piezoelectric actuators. The performance of GA version 3 for the two kinds of optimization problems is shown in Figure 4.6 and Figure 4.7, respectively. We can see from these figures that the GA version 3 still reaches near-optimal solutions very fast even though the search space of  $1.38 \times 10^{54}$  different sets of actuator locations for this case is much larger than that for the case of 30 piezoelectric actuators. Figure 4.8 presents the actuator location for the first kind of optimization problems and corresponding RMS errors obtained using the DeLorenzo's algorithm. Figure 4.9 and Figure 4.10 present the actuator location for the two kinds of optimization problems and corresponding RMS errors obtained by the two runs of the GA version 3. For the case of 121 actuators, we can see in Figure 4.8 and Figure 4.9 that the RMS errors for the first kind of optimization problems for each of the four different types of thermal loads obtained by the two runs of GA version 3 are basically the same as those obtained by the DeLorenzo's algorithm but different sets of actuator locations are found. It is of interest to note that the performance, of a set of actuator locations determined to be best for a given type of thermal loads, does not deteriorate as much for other loads as it did in the case of 30 actuators. This implies that if one can employ a larger number of actuators, the

performance will be better for a large variation in the thermal loads. A large number of actuators will thus provide a more robust set of locations. Moreover, the magnitude of the RMS error reduces as one employs a larger number of actuators. We can see that the RMS error in the worst case T4 for the set of actuator locations in Figure 4.10 a) for the second kind of optimization problem is as good as that in the best case T4 in Figure 4.8 or Figure 4.9 for the first kind of optimization problem. This demonstrates that the search space is highly multi-modal and that the GA version 3 is very powerful to search the solution as good as possible for the multi-criterion optimization problem. The optimal voltages corresponding to the optimization location (Figure 4.10 a)) for each type of thermal loads are listed in Table 4.7 to Table 4.10. We can see that even though the optimal voltages for this case are lower than those for the case of 30 actuators they may be still too high to generate in space. Some promising methods can be used to lower the control voltages. For example, one can select the piezoelectric materials with higher strain constant as actuators or optimize the actuator location and corresponding voltages by applying constraints to electric voltages such as given the maximum voltages that can be provided. The latter is another different large and computationally intensive optimization problem.

#### **4.8 Conclusions**

In this study, an improved version of GAs (Version 3) developed from the GA Version 2 by applying random-mutation hill climbing to elitists and applying mutation to micro-genetic algorithms, was used to solve two kinds of combinatorial and continuous large-scale optimization problems for two cases – selecting 30 and 121 actuator locations from 193 candidate locations in the design of a thin hexagonal spherical primary mirror to be used in the next generation of astronomical telescopes (Figure 4.1). One type of optimization



problem is to find a set of locations and the corresponding voltages that gives us the best correction to the surface thermal distortions of the primary mirror under a given type of thermal loads; the other is to find one set of locations and corresponding voltages which provide the best correction to the surface thermal distortions caused by all the four different kinds of thermal loads. The two types of problems are difficult and computationally intensive. The second type is a more challenging, multi-criterion optimization problem. The search space for these problems is highly multi-modal and conventional point-by-point optimization techniques usually get stuck at the local optimum, but population-based GAs are very good at searching such space and more likely get better results than the traditional techniques. The search space of  $1.38 \times 10^{54}$  different sets of actuator locations for the case of 121 piezoelectric actuators is much larger than that for the case of 30 piezoelectric actuators, but the GA version 3 still converged very fast and finally found a very good set of actuator locations which can be used to reduce all the four kinds of thermal distortions. The results show that the two modifications employed in this study significantly improve the performance of GAs. The current version of GAs are more effective than the previous versions in solving optimization problems of determining actuator locations for thermal distortion control.

The problems for this study are computationally intensive. Getting one solution using the GAs with the limit of 15000 evaluations for the second optimization problem took more than a week. GAs are very general and robust optimization methods which can be applied to virtually any optimization problem. Parallel GAs can significantly reduce the time and be more natural to imitate the evolution of the nature, so our current research is to develop parallel GAs.

## Acknowledgments

The work was performed under a subcontract from University of Texas at Arlington; themselves working under a grant from the National Science Foundation. We would like to thank the College of engineering for providing computational resources for this research.

## References

1. Sheng, L. and Kapania, R. K., “Genetic Algorithms for the Optimization of Piezoelectric Actuator Locations,” Presented as Paper AIAA-2000-1581, Proceedings of *AIAA/ASME/ASCE/AHS/AHC 41<sup>st</sup> Structures, Structural Dynamics and Materials Conference*, Atlanta, GA, April 3-6, 2000. To appear in the AIAA Journal.
2. David. L. Carroll’s FORTRAN Genetic Algorithm Driver.  
<http://www.aic.nrl.navy.mil:80/galist/src/#fortran>
3. Kapania, R. K. and Mohan, P., “Static, Free Vibration and Thermal Analysis of Composite Plates and Shells Using a Flat Triangular Shell Element,” *Computational Mechanics: An International Journal* , Vol. 17, No. 5, 1996, pp. 343-357.
4. Kapania, R. K., Mohan, P., and Jakubowski, A., “Control of Thermal Deformations of Spherical Mirror Segment,” Paper AIAA-96-4145, *Journal of Spacecraft and Rockets*, Vol. 35, No. 2, 1998, pp. 156-162.
5. Mitchell, M., *An Introduction to Genetic Algorithms*, MIT Press, 1996.
6. Goldberg, D. E., *Genetic Algorithms in Search, Optimization, and Machine Learning*, Addison-Wesley, 1989.
7. Pearson, E., and Stepp, L., “ Response of Large Optical Mirrors to Thermal Distributions,” *Proceedings of SPIE—The International Society for Optical Engineering*, Vol. 748, 1987, pp. 215-228.

8. Holland, J. H., "Genetic algorithms," *Scientific American*, July, 1992, pp. 66-72.
9. Michalewicz, Z., *Genetic Algorithms + Data Structures = Evolution Programs*, 3rd ed., Springer, 1996
10. Dasgupta, D. and Michalewicz, Z., "Evolutionary Algorithms—An Overview," in *Evolutionary Algorithms in Engineering Applications*, Dasgupta, D. and Michalewicz, Z. (eds.), Springer, 1997.
11. De Jong, K., "Evolutionary Computation: Recent Developments and Open Issues," in *Evolutionary Algorithms in Engineering and Computer Science*, Miettinen, K., Neittaanmaki, P., and etc. (eds.) John Wiley & Sons, Ltd, 1999.
12. Fogel, D., B., "Some Recent Important Foundational Results in Evolutionary Computation," in *Evolutionary Algorithms in Engineering and Computer Science*, Miettinen, K., Neittaanmaki, P., and etc. (eds.) John Wiley & Sons, Ltd, 1999.
13. Gen, M., and Cheng, R., *Genetic Algorithms & Engineering Optimization*, Chapter 1, John Wiley & Sons, Inc., 2000.

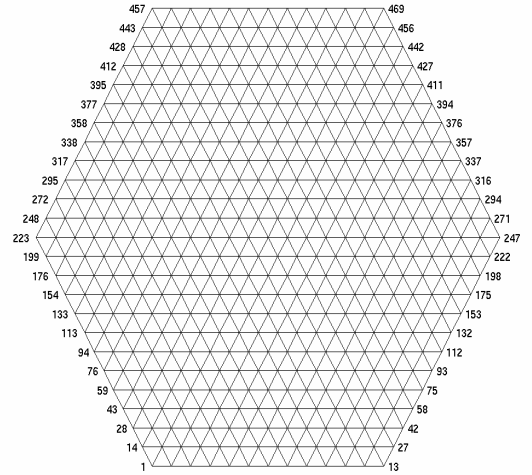
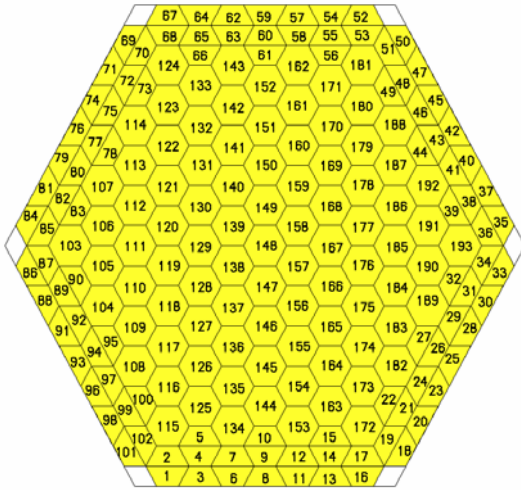


Figure 4.1 a) Piezoelectric actuator candidate locations

b) Finite element mesh

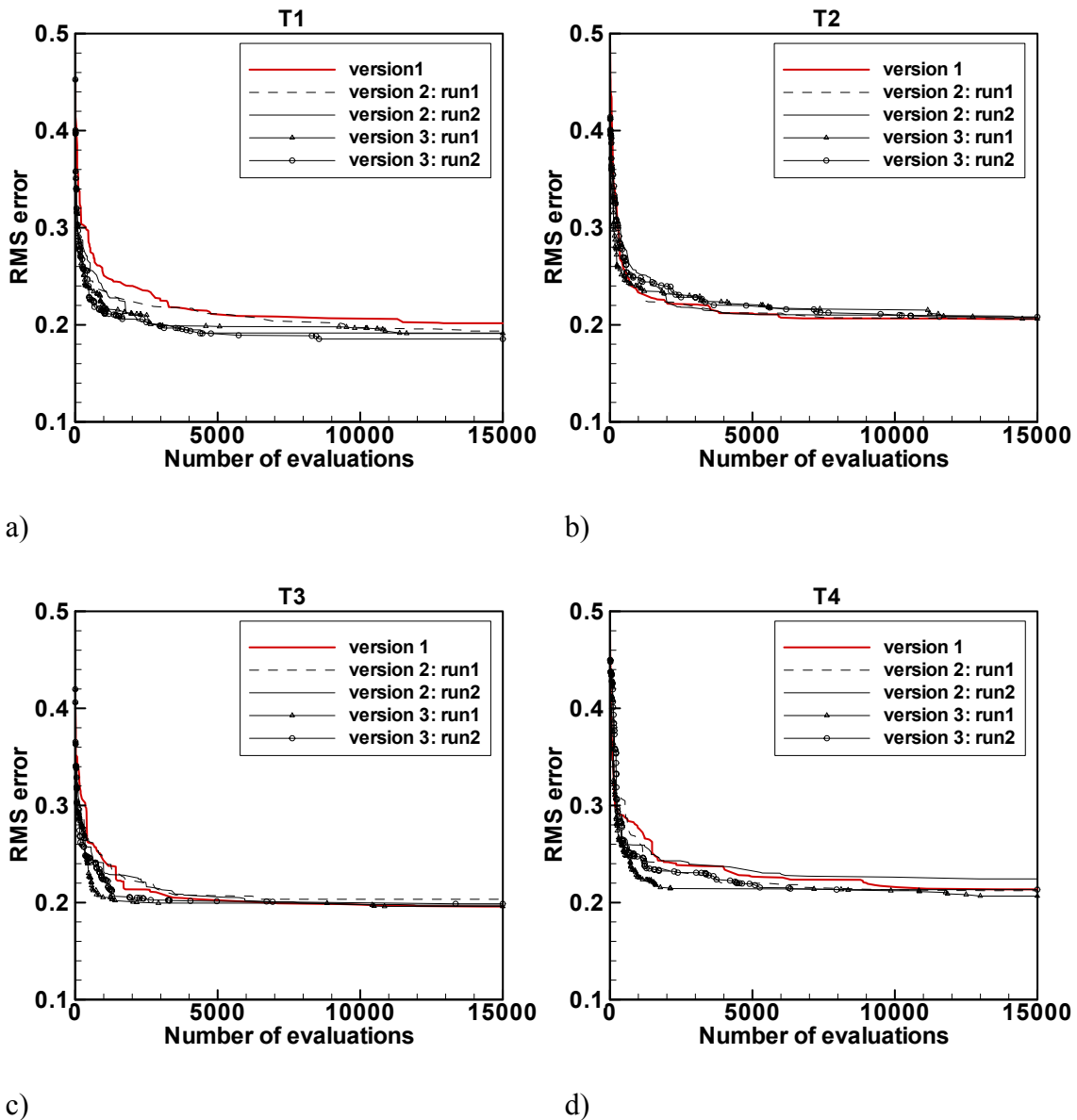


Figure 4.2 Performance of the GAs: The RMS error vs the number of evaluations for the first optimization problem for the case of, a) thermal load T1, b) thermal load T2, c) thermal load T3, and d) thermal load T4 ( 30 actuators ).

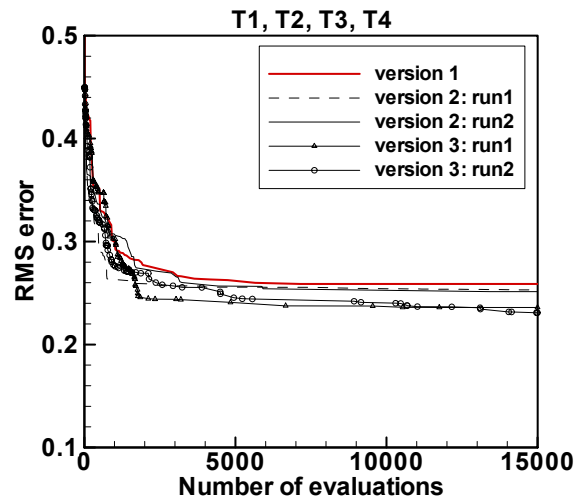


Figure 4.3 Performance of the GAs: Maximum of the four minimum RMS errors vs. the number of evaluations for the second optimization problem ( 30 actuators ).

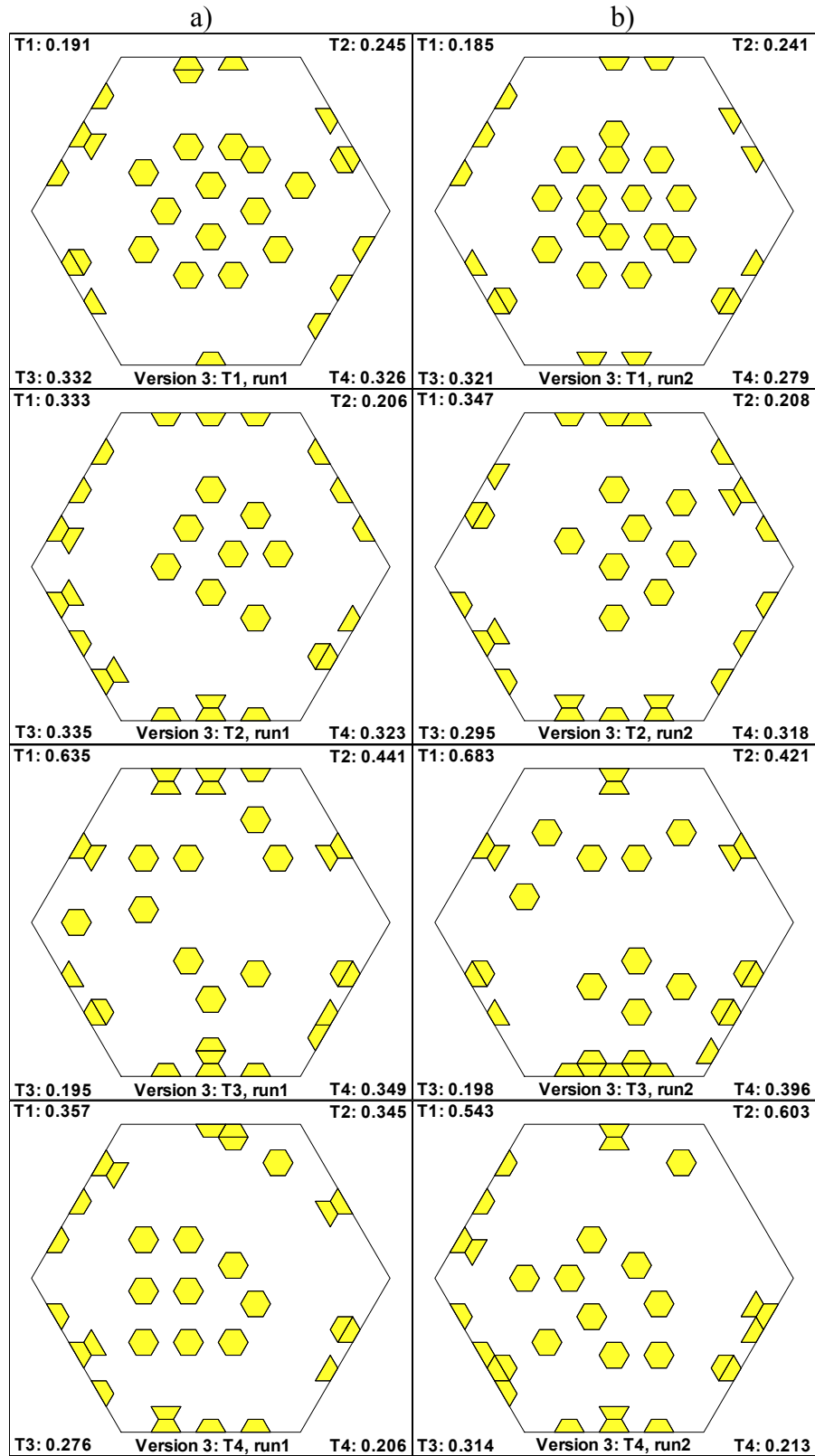


Figure 4.4 Optimal location, obtained by a) GA Version 3, run1; b) GA Version 3, run2 ( 30 actuators), for the first optimization problem for each of the four thermal loads.

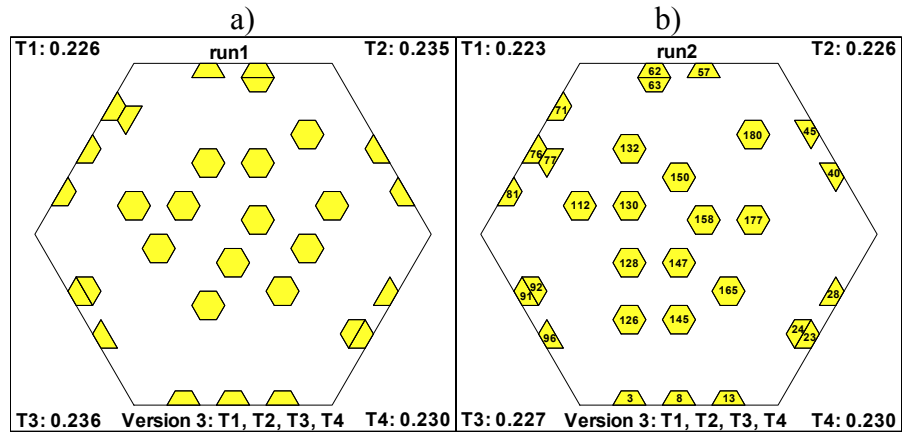
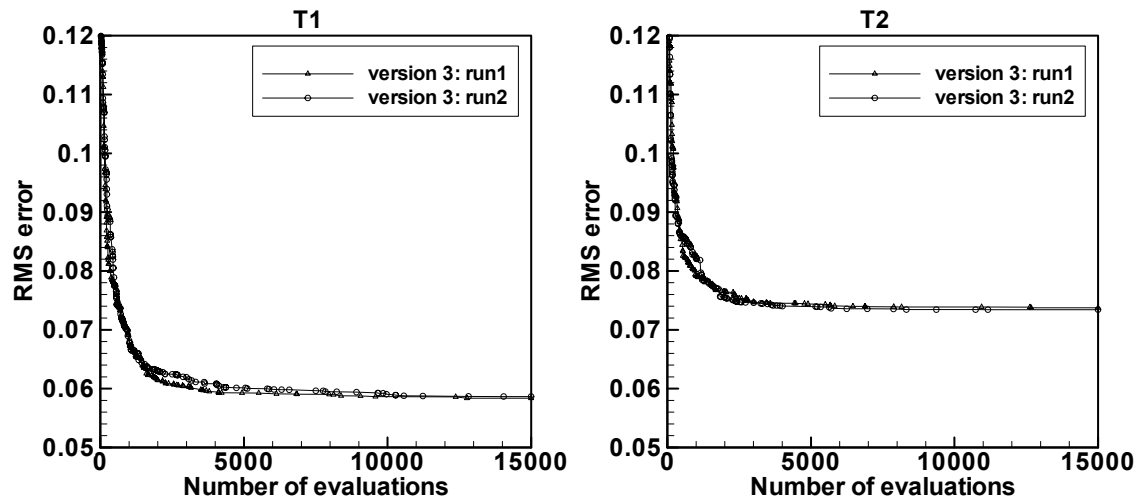


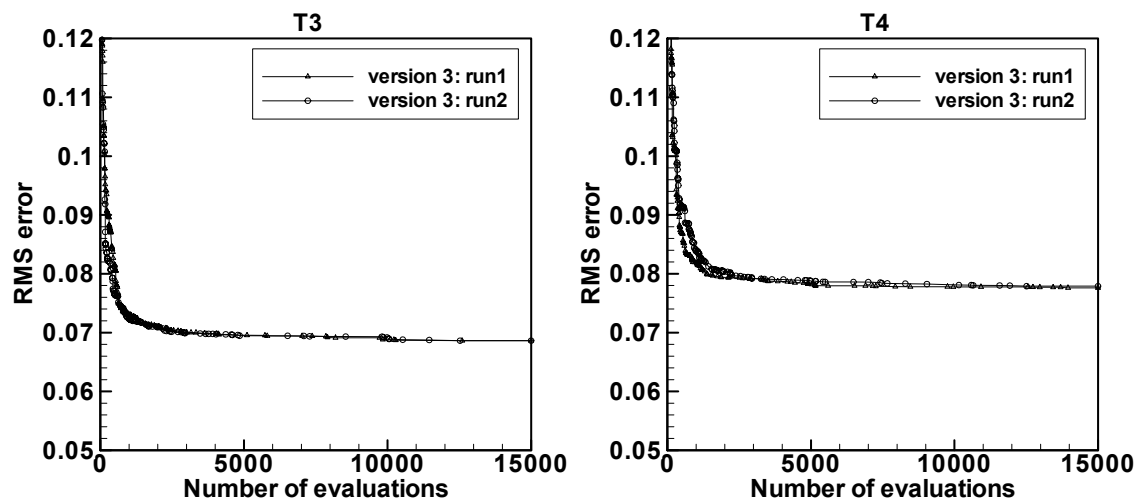
Figure 4.5 Optimal location for the second optimization problem obtained by a) GA Version 3, run1; b) GA Version 3, run2 ( 30 actuators ).





a)

b)



c)

d)

Figure 4.6 Performance of the GAs: The RMS error vs the number of evaluations for the first optimization problem for the case of, a) thermal load T1, b) thermal load T2, c) thermal load T3, and d) thermal load T4 ( 121 actuators ).

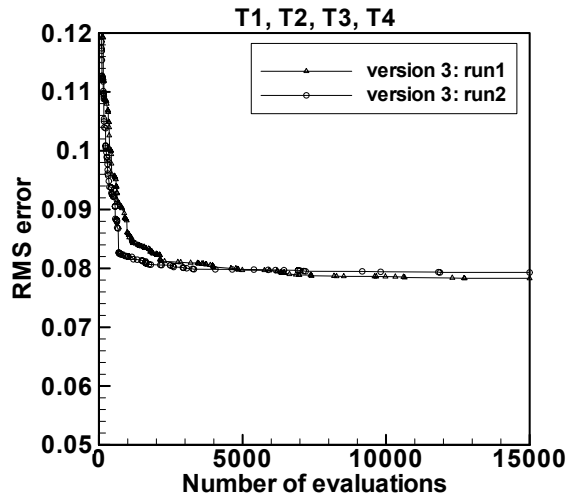


Figure 4.7 Performance of the GAs: Maximum of the four minimum RMS errors vs the number of evaluations for the second optimization problem ( 121 actuators ).

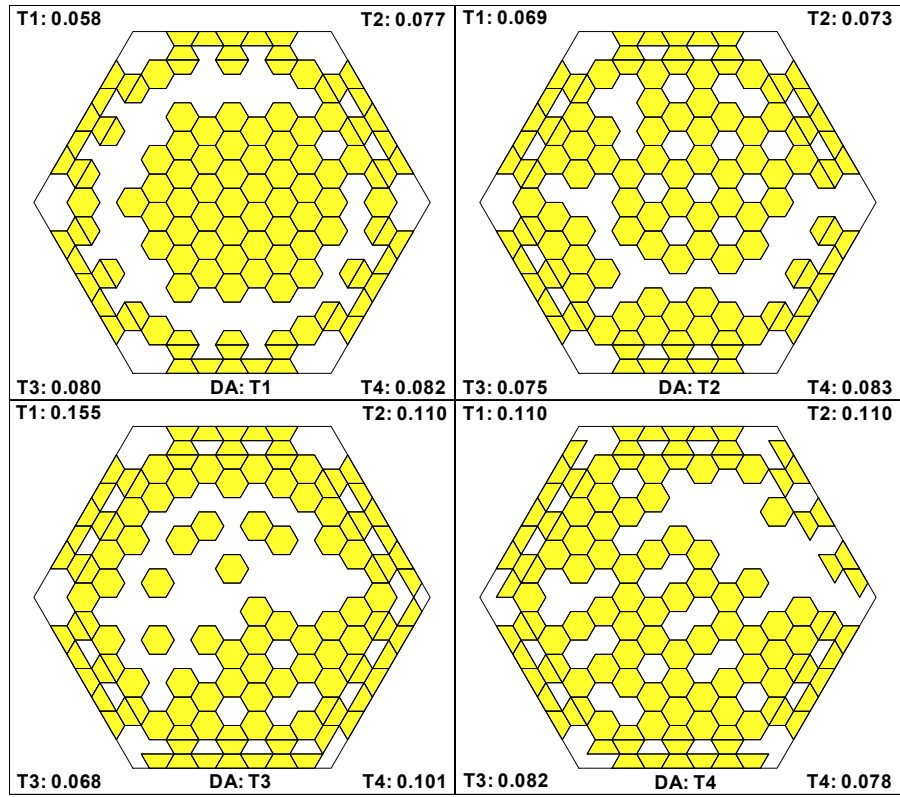


Figure 4.8 Optimal location, obtained by the DeLorenzo's algorithm (121 actuators), for the first optimization problem for each of the four thermal loads.

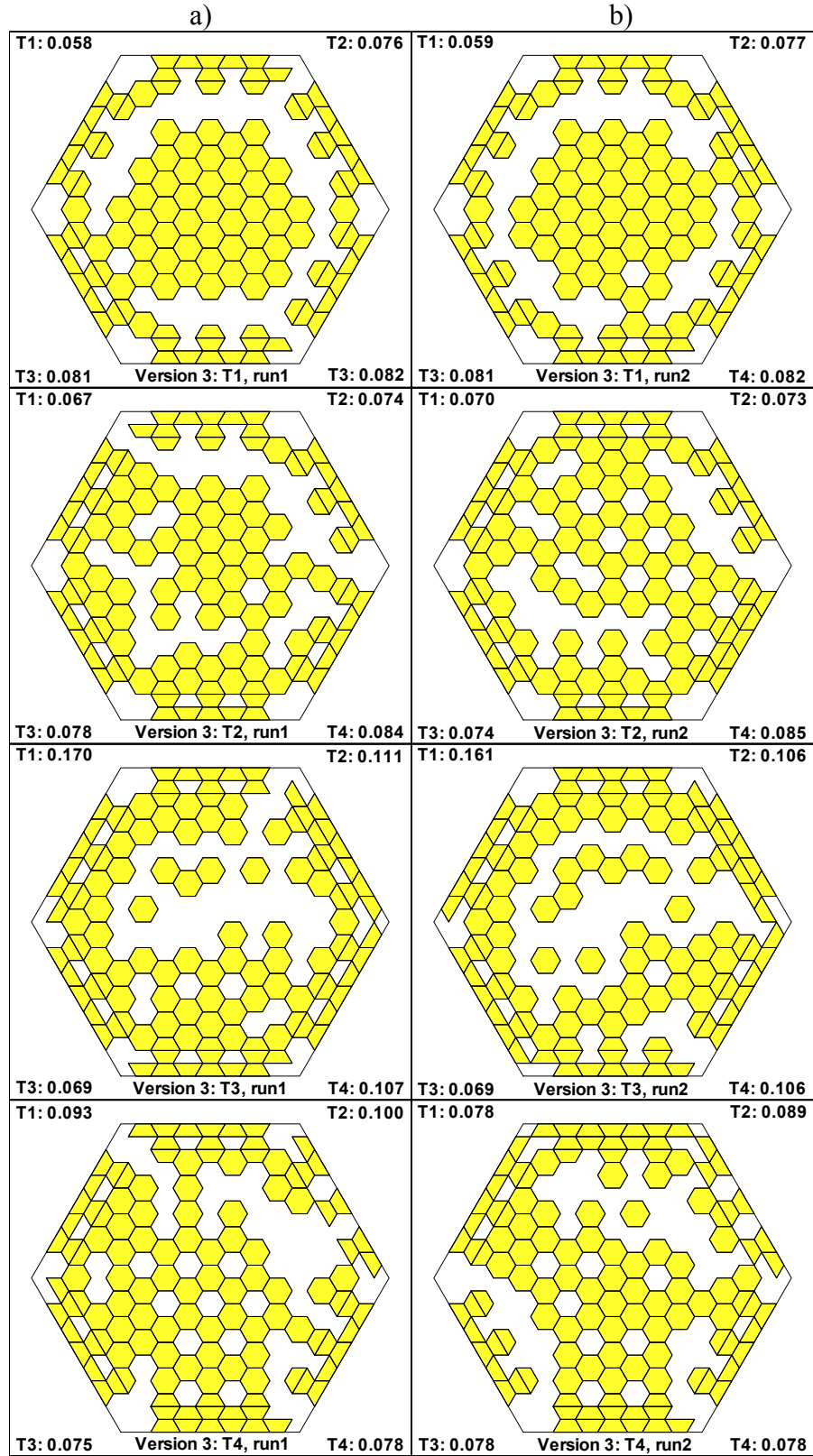


Figure 4.9 Optimal location, obtained by a) GA Version 3, run1; b) GA Version 3, run2 (121 actuators), for the first optimization problems for each of four thermal loads.

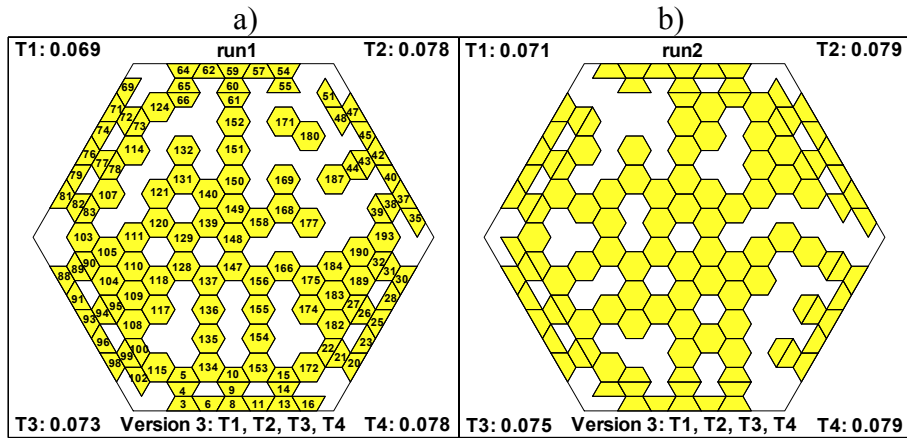


Figure 4.10 Optimal location for the second optimization problem obtained by a) GA Version 3, run1; b) GA Version 3, run2 ( 121 actuators ).

Table 4.1: Properties and geometry of the mirror and piezoelectric actuators

|                                       | Mirror<br>(beryllium) | Piezoelectric strips |
|---------------------------------------|-----------------------|----------------------|
| Young's modulus, GPa                  | 293                   | 63                   |
| Poisson's ratio                       | 0.1                   | 0.3                  |
| Coefficient of thermal expansion, /°C | 11.5E-6               | 0.9E-6               |
| $d_{31}$ , $d_{32}$ , m/V             |                       | 254E-12              |
| Radius, m                             | 10                    |                      |
| Side of the hexagon, m                | 0.5                   | 0.04166              |
| Thickness, m                          | 0.012                 | 0.25E-3              |

Table 4.2: Temperature distributions at the lower surface of the mirror

|    | Temperature distribution        |
|----|---------------------------------|
| T1 | $C[2(x^2 + y^2) - 1]$           |
| T2 | $C[(x + y)(3x^2 + 3y^2 - 2)]$   |
| T3 | $C(\sum_{i=1}^{i=9} K_i Z_i)^*$ |
| T4 | $C[x + y + 2xy]$                |

\*  $K_i$ , from Table 2 (back surface),  $Z_i$ , terms of Zernike series (p. 216) of Ref. 7.

Table 4.3: Optimal voltages corresponding to optimal location (see Figure 4.5 b)) for thermal load type T1.

| Strip Loc. | Voltage V | Strip Loc. | Voltage V | Strip Loc. | Voltage V |
|------------|-----------|------------|-----------|------------|-----------|
| 3          | -111      | 63         | 474       | 128        | -485      |
| 8          | -422      | 71         | -246      | 130        | -394      |
| 13         | -157      | 76         | -903      | 132        | -151      |
| 23         | -933      | 77         | 471       | 145        | -189      |
| 24         | 470       | 81         | -267      | 147        | -430      |
| 28         | -573      | 91         | -926      | 150        | -491      |
| 40         | -541      | 92         | 367       | 158        | -453      |
| 45         | -460      | 96         | -466      | 165        | -406      |
| 57         | -398      | 112        | -209      | 177        | -443      |
| 62         | -813      | 126        | -137      | 180        | -107      |

Table 4.4: Optimal voltages corresponding to optimal location (see Figure 4.5 b)) for thermal load type T2.

| Strip Loc. | Voltage V | Strip Loc. | Voltage V | Strip Loc. | Voltage V |
|------------|-----------|------------|-----------|------------|-----------|
| 3          | -372      | 63         | 564       | 128        | -118      |
| 8          | -769      | 71         | -368      | 130        | -164      |
| 13         | -400      | 76         | -1112     | 132        | -97       |
| 23         | -1357     | 77         | 544       | 145        | -15       |
| 24         | 721       | 81         | -345      | 147        | -191      |
| 28         | -784      | 91         | -1614     | 150        | -330      |
| 40         | -734      | 92         | 1026      | 158        | -240      |
| 45         | -645      | 96         | -607      | 165        | -177      |
| 57         | -619      | 112        | -20       | 177        | -318      |
| 62         | -1125     | 126        | 57        | 180        | -130      |

Table 4.5: Optimal voltages corresponding to optimal location (see Figure 4.5 b)) for thermal load type T3.

| Strip Loc. | Voltage V | Strip Loc. | Voltage V | Strip Loc. | Voltage V |
|------------|-----------|------------|-----------|------------|-----------|
| 3          | -579      | 63         | 1337      | 128        | -15       |
| 8          | -1040     | 71         | -123      | 130        | 35        |
| 13         | -716      | 76         | -902      | 132        | 240       |
| 23         | -1517     | 77         | 678       | 145        | -207      |
| 24         | 556       | 81         | -79       | 147        | -98       |
| 28         | -788      | 91         | -1433     | 150        | 193       |
| 40         | -125      | 92         | 1110      | 158        | -25       |
| 45         | -369      | 96         | -480      | 165        | -261      |
| 57         | -312      | 112        | 195       | 177        | 64        |
| 62         | -1606     | 126        | -48       | 180        | 317       |

Table 4.6: Optimal voltages corresponding to optimal location (see Figure 4.5 b)) for thermal load type T4.

| Strip Loc. | Voltage V | Strip Loc. | Voltage V | Strip Loc. | Voltage V |
|------------|-----------|------------|-----------|------------|-----------|
| 3          | -563      | 63         | 837       | 128        | -301      |
| 8          | -1021     | 71         | -576      | 130        | -216      |
| 13         | -682      | 76         | -1394     | 132        | -44       |
| 23         | -1534     | 77         | 615       | 145        | -168      |
| 24         | 765       | 81         | -559      | 147        | -213      |
| 28         | -667      | 91         | -1569     | 150        | -129      |
| 40         | 50        | 92         | 527       | 158        | -212      |
| 45         | -136      | 96         | -958      | 165        | -230      |
| 57         | -268      | 112        | -188      | 177        | -23       |
| 62         | -1097     | 126        | -142      | 180        | 207       |



Table 4.7: Optimal voltages corresponding to optimal location (see Figure 4.10 a)) for thermal load type T1.

| Strip Loc. | Voltage V | Strip Loc. | Voltage V | Strip Loc. | Voltage V |
|------------|-----------|------------|-----------|------------|-----------|
| 3          | -380      | 62         | -185      | 121        | -127      |
| 4          | 498       | 64         | -385      | 124        | 59        |
| 5          | -259      | 65         | 482       | 128        | -154      |
| 6          | -201      | 66         | -186      | 129        | -155      |
| 8          | -551      | 69         | 17        | 131        | -113      |
| 9          | 647       | 71         | -490      | 132        | -103      |
| 10         | -348      | 72         | 557       | 134        | 67        |
| 11         | -188      | 73         | -250      | 135        | -87       |
| 13         | -402      | 74         | -225      | 136        | -162      |
| 14         | 493       | 76         | -682      | 137        | -128      |
| 15         | -256      | 77         | 756       | 139        | -181      |
| 16         | 37        | 78         | -356      | 140        | -115      |
| 20         | -461      | 79         | -230      | 147        | -219      |
| 21         | 551       | 81         | -490      | 148        | -121      |
| 22         | -286      | 82         | 577       | 149        | -56       |
| 23         | -245      | 83         | -273      | 150        | -181      |
| 25         | -659      | 88         | -485      | 151        | -152      |
| 26         | 784       | 89         | 583       | 152        | -8        |
| 27         | -495      | 90         | -314      | 153        | 66        |
| 28         | -254      | 91         | -242      | 154        | -86       |
| 30         | -465      | 93         | -674      | 155        | -165      |
| 31         | 527       | 94         | 788       | 156        | -101      |
| 32         | -249      | 95         | -474      | 158        | -267      |
| 35         | 14        | 96         | -238      | 166        | -241      |
| 37         | -506      | 98         | -478      | 168        | -53       |
| 38         | 586       | 99         | 548       | 169        | -237      |
| 39         | -279      | 100        | -287      | 171        | -64       |
| 40         | -219      | 102        | 21        | 172        | 68        |
| 42         | -687      | 103        | 56        | 174        | -134      |
| 43         | 706       | 104        | 53        | 175        | -48       |
| 44         | -238      | 105        | 25        | 177        | -237      |
| 45         | -215      | 107        | 13        | 180        | -41       |
| 47         | -467      | 108        | 74        | 182        | 77        |
| 48         | 360       | 109        | 55        | 183        | 58        |
| 51         | 74        | 110        | -94       | 184        | -146      |
| 54         | -361      | 111        | -97       | 187        | -61       |
| 55         | 370       | 114        | 21        | 189        | 83        |
| 57         | -202      | 115        | 68        | 190        | -23       |
| 59         | -558      | 117        | -127      | 193        | 55        |
| 60         | 631       | 118        | -89       |            |           |
| 61         | -236      | 120        | -109      |            |           |

Table 4.8: Optimal voltages corresponding to optimal location (see Figure 4.10 a)) for thermal load type T2.

| Strip Loc. | Voltage V | Strip Loc. | Voltage V | Strip Loc. | Voltage V |
|------------|-----------|------------|-----------|------------|-----------|
| 3          | -693      | 62         | -255      | 121        | -51       |
| 4          | 708       | 64         | -558      | 124        | 51        |
| 5          | -351      | 65         | 586       | 128        | -42       |
| 6          | -356      | 66         | -224      | 129        | -58       |
| 8          | -932      | 69         | -10       | 131        | -67       |
| 9          | 975       | 71         | -594      | 132        | -63       |
| 10         | -501      | 72         | 639       | 134        | 97        |
| 11         | -366      | 73         | -296      | 135        | -15       |
| 13         | -661      | 74         | -305      | 136        | -45       |
| 14         | 703       | 76         | -818      | 137        | -42       |
| 15         | -349      | 77         | 869       | 139        | -84       |
| 16         | -35       | 78         | -418      | 140        | -57       |
| 20         | -638      | 79         | -299      | 147        | -94       |
| 21         | 660       | 81         | -584      | 148        | -50       |
| 22         | -320      | 82         | 632       | 149        | -37       |
| 23         | -323      | 83         | -283      | 150        | -112      |
| 25         | -888      | 88         | -631      | 151        | -127      |
| 26         | 980       | 89         | 702       | 152        | 9         |
| 27         | -586      | 90         | -371      | 153        | 92        |
| 28         | -332      | 91         | -314      | 154        | -30       |
| 30         | -644      | 93         | -864      | 155        | -66       |
| 31         | 667       | 94         | 955       | 156        | -42       |
| 32         | -328      | 95         | -526      | 158        | -155      |
| 35         | -8        | 96         | -333      | 166        | -128      |
| 37         | -614      | 98         | -606      | 168        | -29       |
| 38         | 666       | 99         | 672       | 169        | -189      |
| 39         | -305      | 100        | -305      | 171        | -70       |
| 40         | -293      | 102        | -56       | 172        | 75        |
| 42         | -850      | 103        | 63        | 174        | -74       |
| 43         | 859       | 104        | 77        | 175        | -33       |
| 44         | -328      | 105        | 52        | 177        | -174      |
| 45         | -298      | 107        | 64        | 180        | -54       |
| 47         | -570      | 108        | 85        | 182        | 83        |
| 48         | 411       | 109        | 60        | 183        | 61        |
| 51         | 24        | 110        | -45       | 184        | -113      |
| 54         | -497      | 111        | -25       | 187        | -51       |
| 55         | 406       | 114        | 55        | 189        | 84        |
| 57         | -277      | 115        | 98        | 190        | -7        |
| 59         | -773      | 117        | -27       | 193        | 41        |
| 60         | 824       | 118        | -25       |            |           |
| 61         | -352      | 120        | -39       |            |           |

Table 4.9: Optimal voltages corresponding to optimal location (see Figure 4.10 a)) for thermal load type T3.

| Strip Loc. | Voltage V | Strip Loc. | Voltage V | Strip Loc. | Voltage V |
|------------|-----------|------------|-----------|------------|-----------|
| 3          | -866      | 62         | -188      | 121        | 73        |
| 4          | 839       | 64         | -502      | 124        | 79        |
| 5          | -447      | 65         | 466       | 128        | -24       |
| 6          | -433      | 66         | -29       | 129        | 12        |
| 8          | -1138     | 69         | 38        | 131        | 7         |
| 9          | 1161      | 71         | -405      | 132        | 108       |
| 10         | -652      | 72         | 457       | 134        | 81        |
| 11         | -462      | 73         | -170      | 135        | -81       |
| 13         | -818      | 74         | -202      | 136        | -88       |
| 14         | 855       | 76         | -522      | 137        | -39       |
| 15         | -483      | 77         | 600       | 139        | 3         |
| 16         | -70       | 78         | -262      | 140        | 34        |
| 20         | -753      | 79         | -202      | 147        | -52       |
| 21         | 759       | 81         | -332      | 148        | -12       |
| 22         | -414      | 82         | 456       | 149        | 8         |
| 23         | -375      | 83         | -198      | 150        | 43        |
| 25         | -1017     | 88         | -505      | 151        | 46        |
| 26         | 1098      | 89         | 617       | 152        | 122       |
| 27         | -663      | 90         | -333      | 153        | 78        |
| 28         | -363      | 91         | -247      | 154        | -106      |
| 30         | -746      | 93         | -695      | 155        | -110      |
| 31         | 789       | 94         | 807       | 156        | -49       |
| 32         | -418      | 95         | -452      | 158        | -7        |
| 35         | 77        | 96         | -259      | 166        | -71       |
| 37         | -373      | 98         | -465      | 168        | -11       |
| 38         | 391       | 99         | 550       | 169        | 67        |
| 39         | -53       | 100        | -265      | 171        | 65        |
| 40         | -115      | 102        | -12       | 172        | 37        |
| 42         | -571      | 103        | 111       | 174        | -132      |
| 43         | 631       | 104        | 84        | 175        | -35       |
| 44         | -203      | 105        | 53        | 177        | -20       |
| 45         | -122      | 107        | 124       | 180        | 56        |
| 47         | -381      | 108        | 74        | 182        | 76        |
| 48         | 331       | 109        | 63        | 183        | 81        |
| 51         | 96        | 110        | -37       | 184        | -90       |
| 54         | -447      | 111        | 37        | 187        | 80        |
| 55         | 405       | 114        | 126       | 189        | 69        |
| 57         | -200      | 115        | 53        | 190        | 61        |
| 59         | -719      | 117        | -69       | 193        | 33        |
| 60         | 782       | 118        | -8        |            |           |
| 61         | -275      | 120        | 8         |            |           |

Table 4.10: Optimal voltages corresponding to optimal location (see Figure 4.10 a)) for thermal load type T4.

| Strip Loc. | Voltage V | Strip Loc. | Voltage V | Strip Loc. | Voltage V |
|------------|-----------|------------|-----------|------------|-----------|
| 3          | -828      | 62         | -173      | 121        | -83       |
| 4          | 841       | 64         | -390      | 124        | 68        |
| 5          | -474      | 65         | 457       | 128        | -94       |
| 6          | -439      | 66         | -137      | 129        | -89       |
| 8          | -1136     | 69         | -73       | 131        | -62       |
| 9          | 1164      | 71         | -784      | 132        | -44       |
| 10         | -647      | 72         | 814       | 134        | 91        |
| 11         | -474      | 73         | -399      | 135        | -89       |
| 13         | -833      | 74         | -421      | 136        | -117      |
| 14         | 865       | 76         | -1060     | 137        | -81       |
| 15         | -473      | 77         | 1088      | 139        | -88       |
| 16         | -86       | 78         | -540      | 140        | -57       |
| 20         | -665      | 79         | -384      | 147        | -114      |
| 21         | 690       | 81         | -763      | 148        | -62       |
| 22         | -359      | 82         | 766       | 149        | -23       |
| 23         | -336      | 83         | -356      | 150        | -62       |
| 25         | -920      | 88         | -827      | 151        | -53       |
| 26         | 1009      | 89         | 839       | 152        | 53        |
| 27         | -594      | 90         | -475      | 153        | 88        |
| 28         | -331      | 91         | -405      | 154        | -82       |
| 30         | -683      | 93         | -1097     | 155        | -110      |
| 31         | 736       | 94         | 1176      | 156        | -60       |
| 32         | -383      | 95         | -707      | 158        | -104      |
| 35         | 101       | 96         | -431      | 166        | -110      |
| 37         | -260      | 98         | -769      | 168        | -31       |
| 38         | 300       | 99         | 833       | 169        | -43       |
| 39         | -15       | 100        | -437      | 171        | 19        |
| 40         | -42       | 102        | -82       | 172        | 60        |
| 42         | -388      | 103        | 17        | 174        | -102      |
| 43         | 456       | 104        | 57        | 175        | -28       |
| 44         | -106      | 105        | 52        | 177        | -60       |
| 45         | -41       | 107        | 34        | 180        | 42        |
| 47         | -244      | 108        | 81        | 182        | 81        |
| 48         | 258       | 109        | 79        | 183        | 73        |
| 51         | 141       | 110        | -95       | 184        | -87       |
| 54         | -374      | 111        | -83       | 187        | 49        |
| 55         | 383       | 114        | 53        | 189        | 75        |
| 57         | -171      | 115        | 74        | 190        | 57        |
| 59         | -579      | 117        | -123      | 193        | 37        |
| 60         | 654       | 118        | -68       |            |           |
| 61         | -229      | 120        | -66       |            |           |

## **Chapter 5. Extensive Experiments on Genetic Algorithms for the Optimization of Piezoelectric Actuator Locations through Parallel Computation**

### **5.1 Abstract**

For investigating the shape control of smart structures, we have developed a series of genetic algorithms ( GAs ) for an optimal placement of the piezoelectric actuators --- an important issue in the design of smart structures. In this paper, we report results from extensive numerical experiments on the GAs. These numerical experiments were conducted using a course-grain parallel computing not only to answer some concerns expressed by a reviewer of one of our previous publications in the AIAA Journal about some of our findings based on limited runs, but also to determine the extent to which the solution quality is enhanced by incorporating our several ideas into a modified micro-genetic algorithm. We will address the following topics through a thorough comparison of solution quality as obtained by our latest micro-GAs version 3, running on a high performance Sun machine with 17 processors.

1. What is the effect of a different random number seed, specifically a comparison between the results obtained using a small seed and a large seed.
2. What is the effect of restart criteria in micro-GAs, specifically the two parameters --- number of generations used for the inner loop and the level of diversity in the population on the solution quality.
3. What is the effect on the solution quality as the number of actuators changes from 30 and 121 to 15, 60, and 90.

Using these extended studies, we not only got some better layouts of piezoelectric actuators

---

This chapter contains the materials submitted to *AIAA/ASME/ASCE/AHS/AHC 46<sup>th</sup> SDM Conference* (in 1<sup>st</sup> *AIAA MDO Specialist Conference*). (already accepted, Paper Number: AIAA-2005-1899)

than the ones reported in our previous publications, but also achieved a better understanding of the performance of the genetic algorithms, especially, the micro-genetic algorithms that were already shown to be more efficient than the commonly used genetic algorithms. Specifically, we look at how they work, what their nature is -- random in nature, what robustness means, how to choose appropriate genetic algorithms, the way to get better results if it becomes necessary, advantages of micro-GAs, how to tune micro-GAs, and the effect of different restart criteria in micro-GAs on the solution quality. Therefore, we can provide an efficient, reliable and robust optimization tool for the challenging problem of choosing optimal location for the large number of actuators or sensors in the design of next generation of smart structures. Our research will be useful for those involved with the application of genetic algorithms to other areas, such as damage identification in structural health monitoring, medical imaging and wing design.

The high performance Sun machine with 17 processors is chosen to run multiple jobs at the same time in order to shorten the investigation time.

## **5.2 Introduction**

During the last two decades, research and development of smart structures has received great attention from both university and industry researchers.<sup>1-7</sup> An example is the design of next generation of astronomical telescopes. One of the most stringent requirements for these telescopes is the maintenance of high surface accuracy of the primary mirror during their operation. A promising method is to use a certain number of piezoelectric actuators bonded onto the rear surface of the primary mirror to correct its distortions without imposing a significant weight penalty. The critical issue is how to arrange these actuators to maximize their benefit. If the number of actuators is small, we could easily solve the problem by using

the exhaustively enumerative search method, that is, by checking every possible solution in the search space. But this is not the case. Usually, a large number of actuators are needed for the structure to operate properly, so there are an extremely large number of possible schedules for placing these actuators. In our previous studies,<sup>9-10</sup> we developed a methodology of combining the finite element method and genetic algorithms to solve this challenging problem. We successfully developed a series of GAs, including regular GA and micro-GAs, termed Version 1, 2, and 3, from Carroll's FORTRAN Genetic Algorithm Driver.<sup>11</sup> With limited runs, we showed some very promising results produced by the latest version of our micro-GA codes – Version 3. As pointed out to us by a reviewer, because genetic algorithms are random in nature, the results may be a matter of chance, and thus must be verified by performing a large number of runs. In this paper, we will study these GAs by performing such an extensive numerical verification. With this study using a large number of runs, we aim to get a better understanding of genetic algorithms, which have emerged as a leading global search method for actuator placement. Our research shows that the most distinct natures of genetic algorithms are random and robust. With a few of runs with the number of 15000 evaluations GA version 3 can found a nearly optimal solution from the order of  $10^{21} \sim 10^{56}$  possible solutions in all of our test cases. However, to get the highest quality of solution a large number of runs using different seeds are necessary. Overall, the software GA version 3 is reliable and effective in solving the optimal placement of a large number of piezoelectric actuators in the design of next generation of smart structures.

### **5.3 Genetic Algorithms**

Genetic algorithms ( GAs ), inspired by biology and population genetics, have been definitely accepted as an efficient optimization method to solve a wide variety of problems as

shown by the ever-growing number of scientific papers and conferences dedicated to this subject. Even though there are various GAs proposed, they can be simply classified into two categories: regular GAs and micro-GAs. In their structure the micro-GAs are the same as the regular GAs except that they include an automatically restart function when the population converges to a solution according to some convergence criterion. The significant difference between regular GAs and micro-GAs is that the micro-GAs usually use a much smaller population size in order to achieve a faster convergence rate than the regular GAs that use a large population size. In the GA literature, regular GAs have received more thorough studies in respect to general choice of various parameters than micro-GAs. However, our experiences show that micro-GAs are much more efficient than regular GAs. Moreover, micro-GAs also benefit from the mutation operation. In this paper, we will study these GAs by extensive numerical experiments and further demonstrate that the GA version 3 is an efficient, reliable and robust optimization tool for the challenging problem of choosing optimal location for a large number of actuators or sensors in the design of next generation of smart structures. The results by running our latest micro-GA version 3 on the high performance Sun machine with 17 processors are reported in this paper.

The flow chart for the micro-GAs is shown in Figure 5.1.

The main differences among the regular GAs, micro-GAs version 1, micro-GAs version 2 and micro-GAs version 3 are shown in Table 5.1.



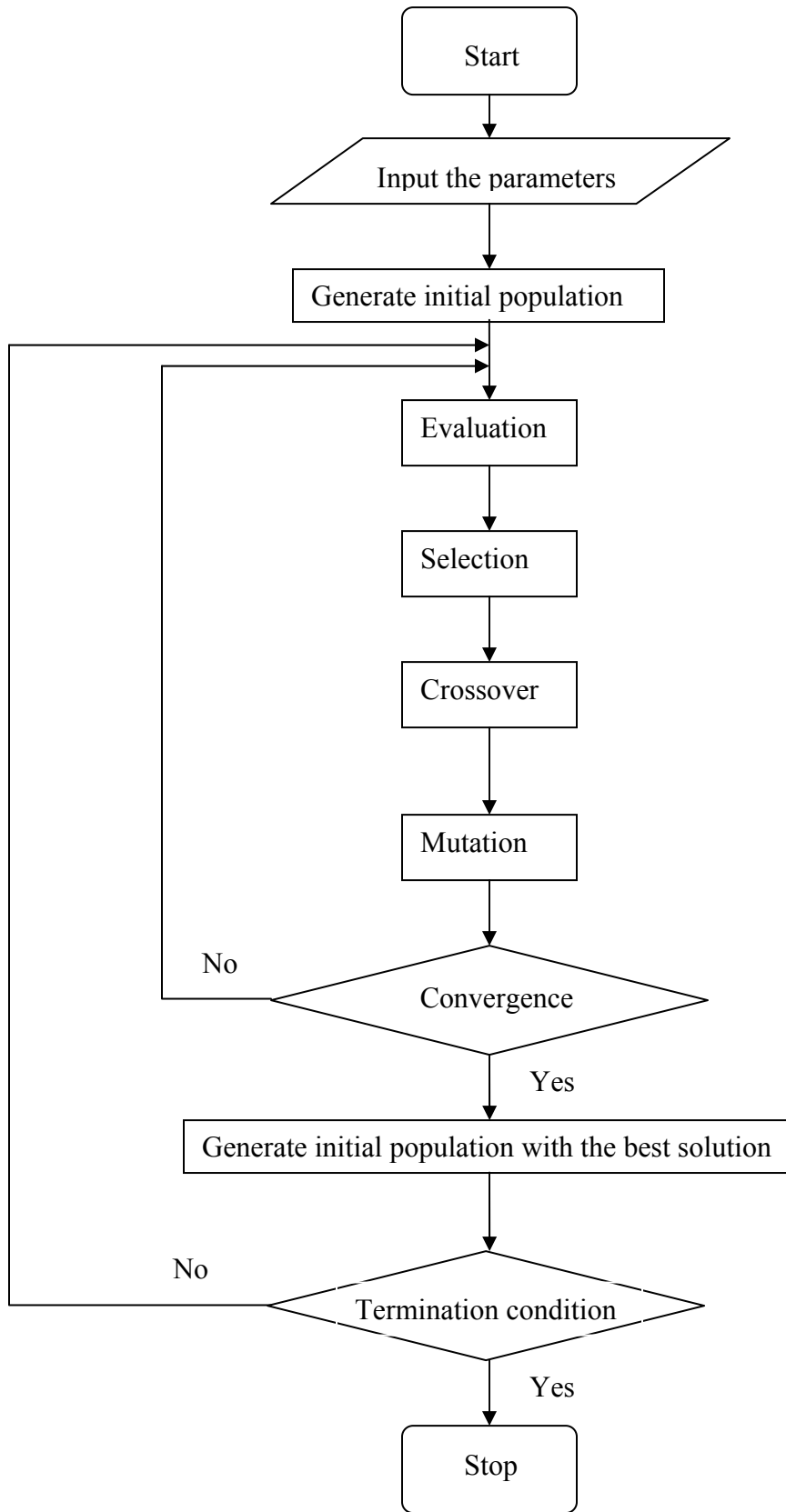


Figure 5.1 The flow chart for the micro-GAs

Table 5.1 The main differences among the regular GAs, micro-GAs version 1, micro-GAs version 2 and micro-GAs version 3

|  | Regular GAs  | Micro_GAs version 1          | Micro-GAs version 2  | Micro-GAs version 3  |
|--|--------------|------------------------------|----------------------|----------------------|
| Restart function                         | No           | Yes                          | Yes                  | Yes                  |
| crossover                                | Yes          | Yes                          | Yes                  | Yes                  |
| mutation                                 | Yes          | No                           | No                   | Yes                  |
| Individual replaced by the best solution | N/A          | Randomly-selected individual | The worst individual | The worst individual |
| Size of population                       | Large, fixed | Small, fixed                 | Small, variable      | Small, variable      |
| Hill-climbing                            | N/A          | No                           | No                   | Yes                  |

#### 5.4 Problem Definition

The problem in this study is as follows:

With N piezoelectric actuators, the problem is to find an optimal placement from a possible 193 candidate locations to get the best correction to the surface thermal distortions under combining four different types of thermal loads in a thin hexagonal spherical mirror segment to be used in the next generation of astronomical telescopes (Figure 5.2 a)). This is, the problem is to find only one set of locations and corresponding voltages that provide us the best correction for all the four different thermal distortions. Note that only the locations are same for all the four types of loads, not their voltages. This is a challenging multi-criterion optimization problem. Total number of different candidate sets can be computed by the following formula:

$${}^{193}C_n = \binom{193}{n} = \frac{193!}{n!(193-n)!}$$

In order to test the stability, reliability and to better understand the performance of our GA version 3, a set of the number of actuators will be tested. We will test the following cases, respectively,

Case 1: N=30,

$${}^{193}C_{30} = 1.28866 * 10^{35}$$

Case 2: N=121,

$${}^{193}C_{121} = 1.38231 * 10^{54}$$

Case 3: N=15,

$${}^{193}C_{15} = 8.4 * 10^{21}$$

Case 4: N=60,

$${}^{193}C_{60} = 5.53626 * 10^{50}$$

Case 5: N=90,

$${}^{193}C_{90} = 4.65676 * 10^{56}$$

It is clearly seen that it is impossible to use the enumeration method to find the solution from so huge a number of candidate sets even with the most advanced computer in the world.

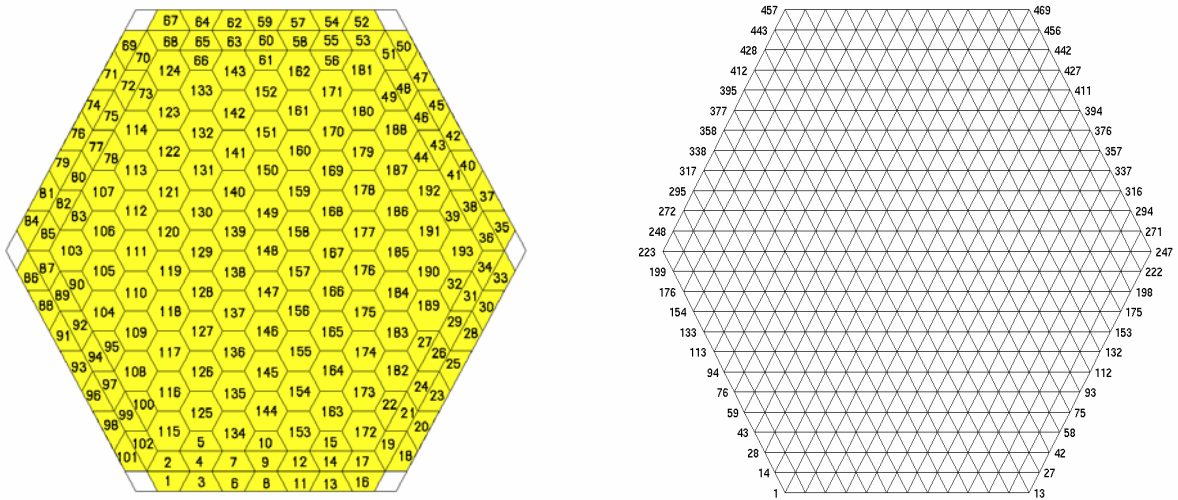


Figure 5.2 a) Piezoelectric actuator candidate locations b) Finite element mesh

The geometry and material properties of the mirror and piezoelectric actuators are given in Table 5.2. The temperature distribution at the lower surface of the mirror is assumed to be in the form of linear combination of the first few terms of the Zernike series expressed in terms of Cartesian coordinates  $x$  and  $y$  with the origin at the center of the mirror. The Cartesian coordinates used to express the temperature distributions are normalized such that they are in the range  $[-1,1]$ . The temperature distributions that are considered in this study are given in Table 5.3, where the constant  $C$  is used to scale the temperature distributions such that the upper, light-reflecting surface is at a lower temperature than the lower surface, with a constant temperature difference  $\Delta T_z$  °C, and the maximum temperature difference between any two grid points across the lower surface of the mirror is  $\Delta T_{xy}$  °C. In this study  $\Delta T_z=0.2$  °C and  $\Delta T_{xy}=0.5$  °C. The graphics of these thermal loads are shown in Figure 5.3.

Table 5.2 Properties and geometry of the mirror and piezoelectric actuators

|                                       | Mirror<br>(beryllium) | Piezoelectric strips |
|---------------------------------------|-----------------------|----------------------|
| Young's modulus, GPa                  | 293                   | 63                   |
| Poisson's ratio                       | 0.1                   | 0.3                  |
| Coefficient of thermal expansion, /°C | 11.5E-6               | 0.9E-6               |
| $d_{31}, d_{32}$ , m/V                |                       | 254E-12              |
| Radius, m                             | 10                    |                      |
| Side of the hexagon, m                | 0.5                   | 0.04166              |
| Thickness, m                          | 0.012                 | 0.25E-3              |

Table 5.3 Temperature distributions at the lower surface of the mirror

|    | Temperature distribution        |
|----|---------------------------------|
| T1 | $C[2(x^2 + y^2) - 1]$           |
| T2 | $C[(x + y)(3x^2 + 3y^2 - 2)]$   |
| T3 | $C(\sum_{i=1}^{i=9} K_i Z_i)$ * |
| T4 | $C[x + y + 2xy]$                |

\*  $K_i$ , from Table 2 (back surface),  $Z_i$ , terms of Zernike series (p. 216) of the reference [Pearson, et al. 1987].

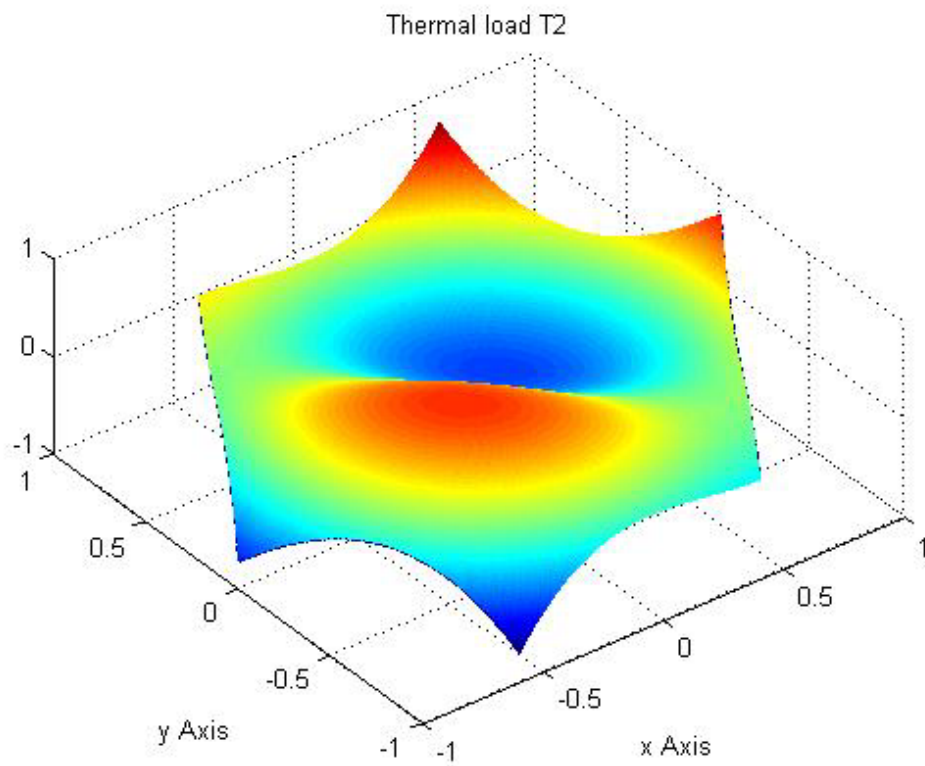
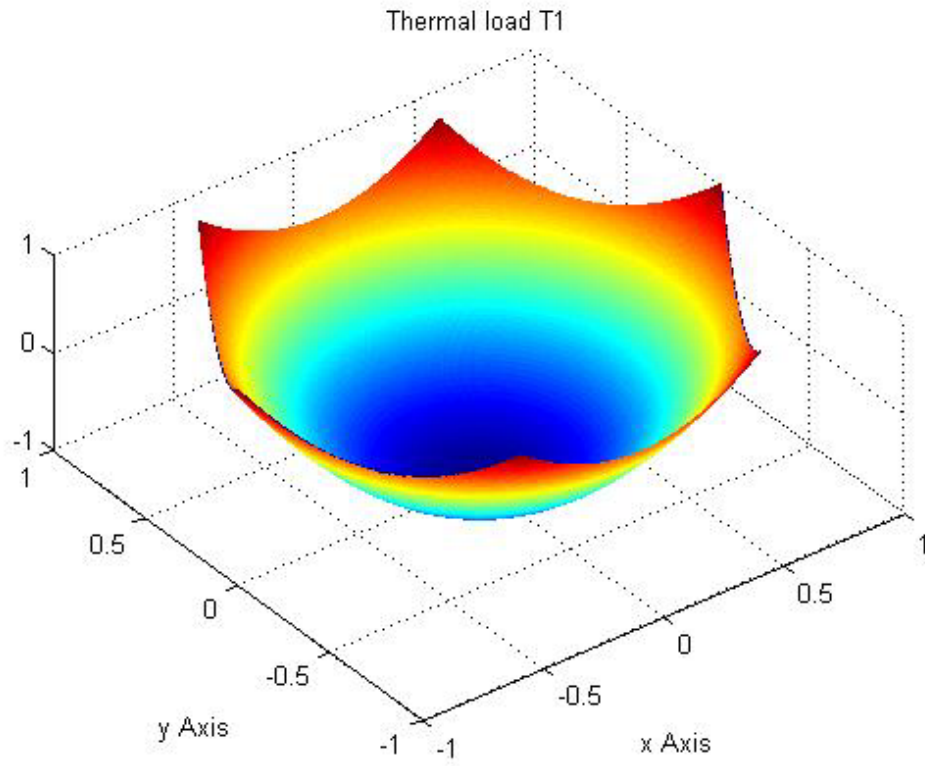


Figure 5.3 a) The thermal loads T1 and T2

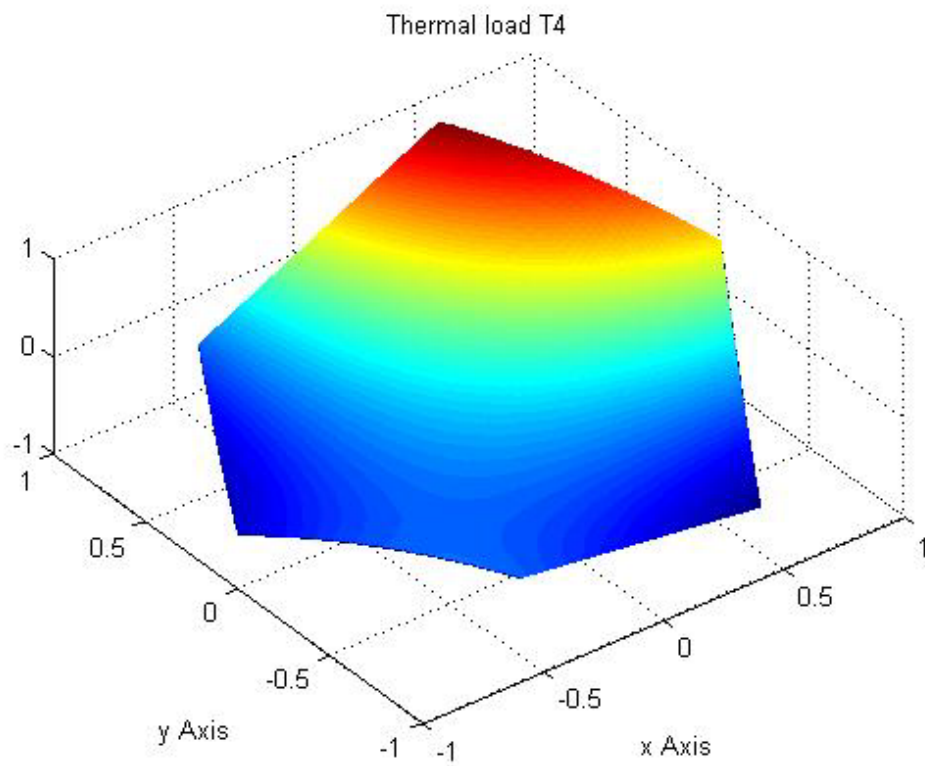
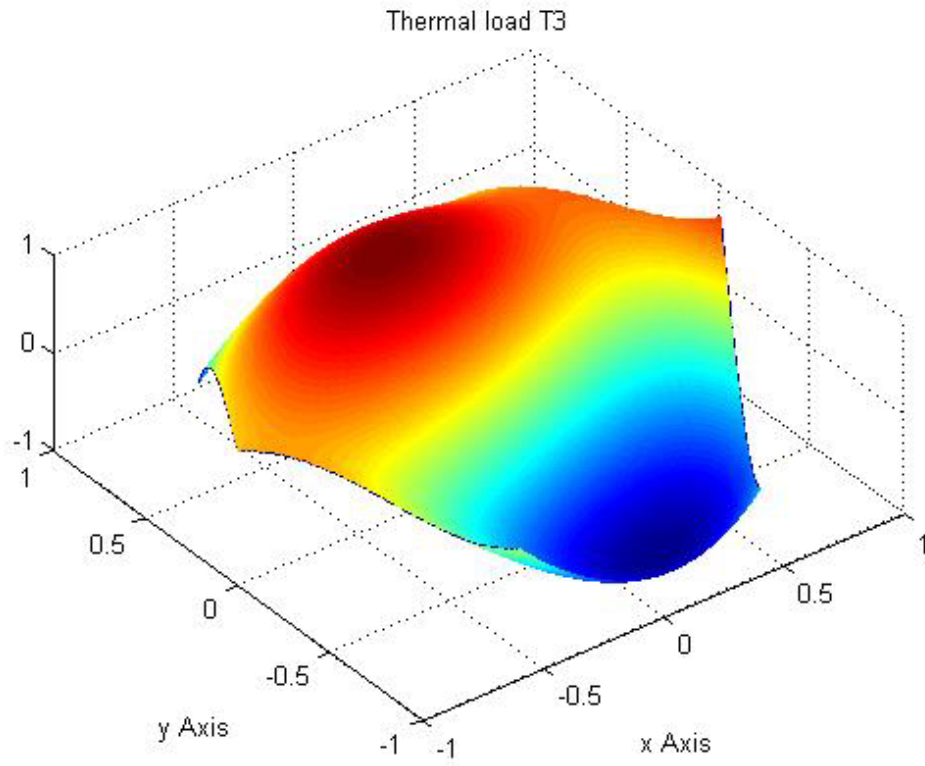


Figure 5.3 b) The thermal loads T3 and T4

## 5.5 Finite Element Modeling

A laminated triangular shell element developed in Chapter 2 is used to model the mirror. The element is a combination of the DKT plate bending element and a membrane element derived from the linear strain triangular element with a total of 18 degrees of freedom (3 translations and 3 rotations per node). The piezoelectric strips are assumed to be perfectly bonded to the lower surface of the mirror and are modeled as a separate layer. The finite element model consists of 864 flat shell elements, 469 grid points (Figure 5.2 b)). The mirror segment is assumed to be simple-supported at the six vertices 1, 13, 223, 247, 457, and 469.

## 5.6 Control Algorithms

The surface thermal distortions or the transverse displacements  $w$  of the mirror segment are corrected by applying the voltage across the thickness of the strip, which induces a distributed strain in the strip and hence in the mirror. In this study, the thermal deformation  $w$  due to a given type of thermal loads is computed by the finite element analysis. The finite element formulation suggested in Ref. 12 is capable of analyzing panels under thermal loads. The deformations considered are so small (of order of a few micrometers) that the correction  $u_i$  at any point can be assumed

$$u_i = \sum_{j=1}^n \alpha_{ij} V_j$$

where the control input  $V_j$  is the voltage applied across the  $j$ th piezoelectric strip and the influence coefficient  $\alpha_{ij}$  is defined as the deformation caused at node  $i$  due to a unit voltage applied across the  $j$ th piezoelectric strip alone.

A matrix of influence coefficients of size  $m \times n$  ( where  $m$  represents the total number of grid points in the FEM model,  $n$  represents the given number of piezoelectric actuators ) is obtained from the finite element model by applying a unit voltage across each of the

piezoelectric strips, one at a time. A measure of the overall deviation or the RMS error is given by

$$E = E(T, L, V) = \sqrt{\frac{1}{m} \sum_{i=1}^m (w_i + u_i)^2} = \sqrt{\frac{1}{m} \sum_{i=1}^m (w_i + \sum_{j=1}^n \alpha_{ij} V_j)^2}$$

To obtain the best correction, setting  $\partial E / \partial V_k = 0$  gives

$$\sum_{i=1}^m (w_i + \sum_{j=1}^n \alpha_{ij} V_j) \alpha_{ik} = 0$$

i.e.  $[A]\{V\} = \{b\}$ , where  $A_{kj} = \sum_{i=1}^m \alpha_{ij} \alpha_{ik}$      $b_k = -\sum_{i=1}^m w_i \alpha_{ik}$

For each set of locations we can get the optimal voltages to minimize RMS error. Different settings have different optimal voltages and corresponding minimum RMS error. For one type of thermal distortion we can find a set of locations and corresponding voltages that minimizes the minimum RMS error i.e. of the form,

$$E = \underset{L}{\text{Min}} \underset{V}{\text{Min}} E(T, L, V)$$

The optimization problem is to find a set of locations and corresponding voltages that minimizes the maximum of the minimum RMS error for all the four different distortions i.e. of the form,

$$E = \underset{L}{\text{Min}} \underset{T}{\text{Max}} \underset{V}{\text{Min}} E(T, L, V)$$

## 5.7 Results and Discussions

In this section, the performance of our latest micro-GA version 3 was thoroughly studied through extensive numerical experiments. A high performance Sun machine with 17 processors was used to do this research through parallel computation in order to shorten the time of investigation. The results corresponding to the cases of 30, 121, 15, 60 and 90 actuators are presented in the following.



The number of evaluations is limited to 15000 for all the runs.

**Case 1: N=30 actuators**

Micro-GA Version 3: Initial population size 10, population size 5, scale=0.5, random=0,

crossover rate =0.5, mutation rate=0.01, restart control parameter different level=0.0

No\_of\_best\_mutation\_bits=2.

Table 5.4 RMS errors corresponding to optimal placement (30 actuators)

| Generations of inner loop | RMS for initial evaluation |         | RMS for 5000 evaluations |                | RMS for 10000 evaluations |                | RMS for 15000 evaluations |                |
|---------------------------|----------------------------|---------|--------------------------|----------------|---------------------------|----------------|---------------------------|----------------|
|                           | Seed #1                    | Seed #2 | Seed #1                  | Seed #2        | Seed #1                   | Seed #2        | Seed #1                   | Seed #2        |
| 8                         | 0.87205                    | 0.61079 | 0.25069                  | 0.24362        | 0.24022                   | <b>0.23622</b> | 0.24022                   | 0.23455        |
| 9                         |                            |         | <b>0.23541</b>           | 0.25342        | <b>0.23130</b>            | 0.25026        | 0.22943                   | 0.24451        |
| 10                        |                            |         | 0.24551                  | 0.24459        | 0.24102                   | 0.23923        | 0.23093                   | 0.23399        |
| 11                        |                            |         | 0.23865                  | 0.25410        | 0.23581                   | 0.25116        | 0.23186                   | 0.25083        |
| 12                        |                            |         | 0.23831                  | 0.25208        | 0.23709                   | 0.25020        | 0.23709                   | 0.24594        |
| 13                        |                            |         | 0.24040                  | 0.24958        | 0.23924                   | 0.24892        | 0.23538                   | 0.24764        |
| 14                        |                            |         | 0.25305                  | 0.24685        | 0.23455                   | 0.24328        | 0.23304                   | 0.24243        |
| 15                        |                            |         | 0.24089                  | 0.25215        | 0.23744                   | 0.24655        | 0.23604                   | 0.24417        |
| 16                        |                            |         | 0.26163                  | 0.25954        | 0.25789                   | 0.24619        | 0.24962                   | 0.24241        |
| 17                        |                            |         | 0.24749                  | 0.25167        | 0.24473                   | 0.24938        | 0.24399                   | 0.24938        |
| 18                        |                            |         | 0.25494                  | 0.25040        | 0.24657                   | 0.24971        | 0.24657                   | 0.24971        |
| 19                        |                            |         | 0.24287                  | <b>0.24162</b> | 0.24175                   | 0.24162        | 0.24175                   | <b>0.23277</b> |
| 20                        |                            |         | 0.25131                  | 0.25439        | 0.23615                   | 0.25130        | <b>0.22882</b>            | 0.24636        |

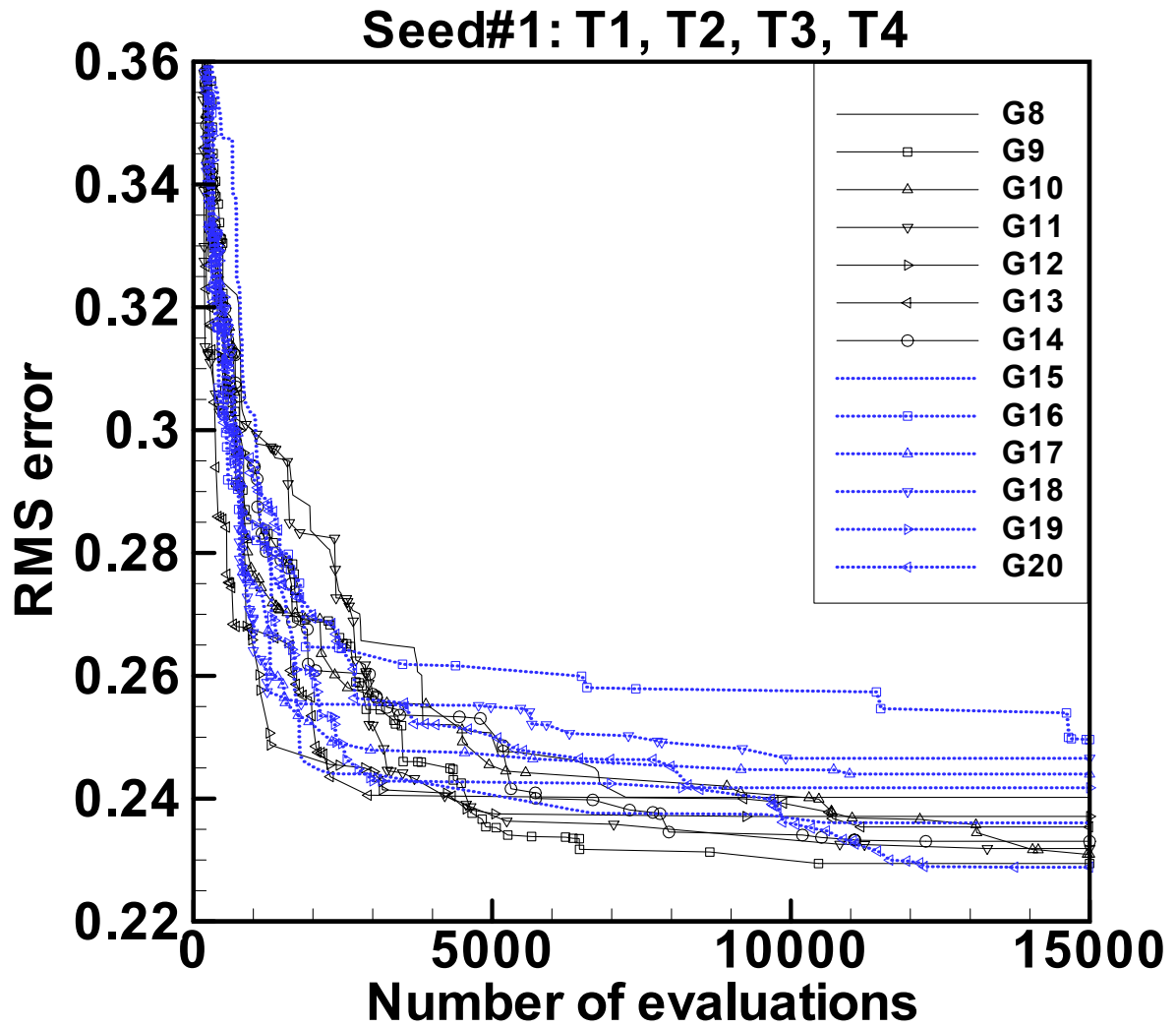


Figure 5.4 a) Performance of the GAs: Maximum of the four minimum RMS errors vs. the number of evaluations ( 30 actuators, seed#1 ).

Note: It is the optimization problem in which one set of actuators is chosen for all four thermal distortions.

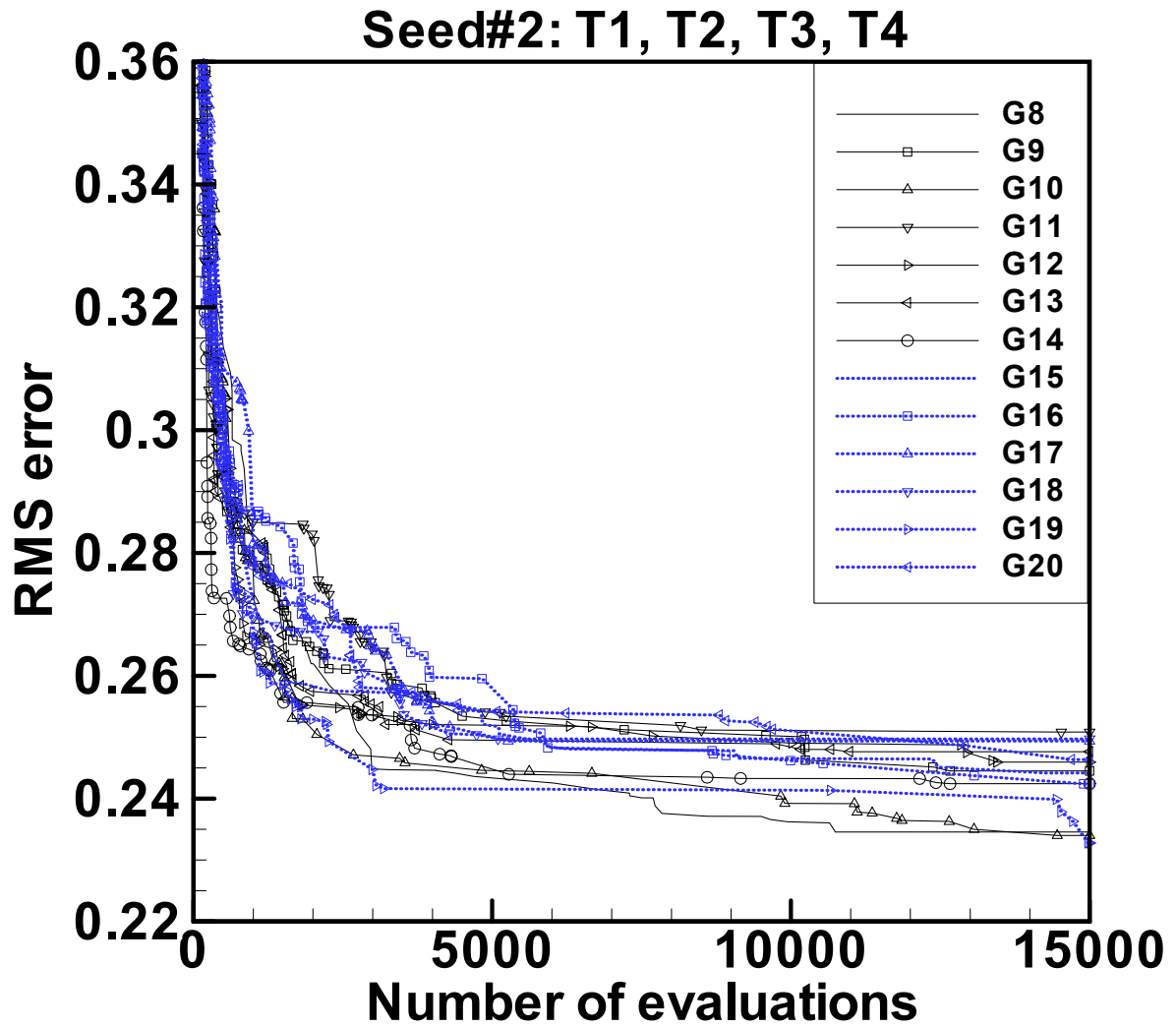


Figure 5.4 b) Performance of the GAs: Maximum of the four minimum RMS errors vs. the number of evaluations ( 30 actuators, seed#2 ).

Note: It is the optimization problem in which one set of actuators is chosen for all four thermal distortions.

For this case (nstrip=30)

Observation 1: Seed #1 is better than Seed #2 for all the three numbers of evaluations used for termination.

Observation 2: The best number of generations of inner loop is dependent on the number of evaluations used for termination. For example, if 5000 evaluations is chosen as termination condition, the best number of generations of inner loop is 9, but if 15000 evaluations is chosen as termination condition, the best number of generations of inner loop is 20.

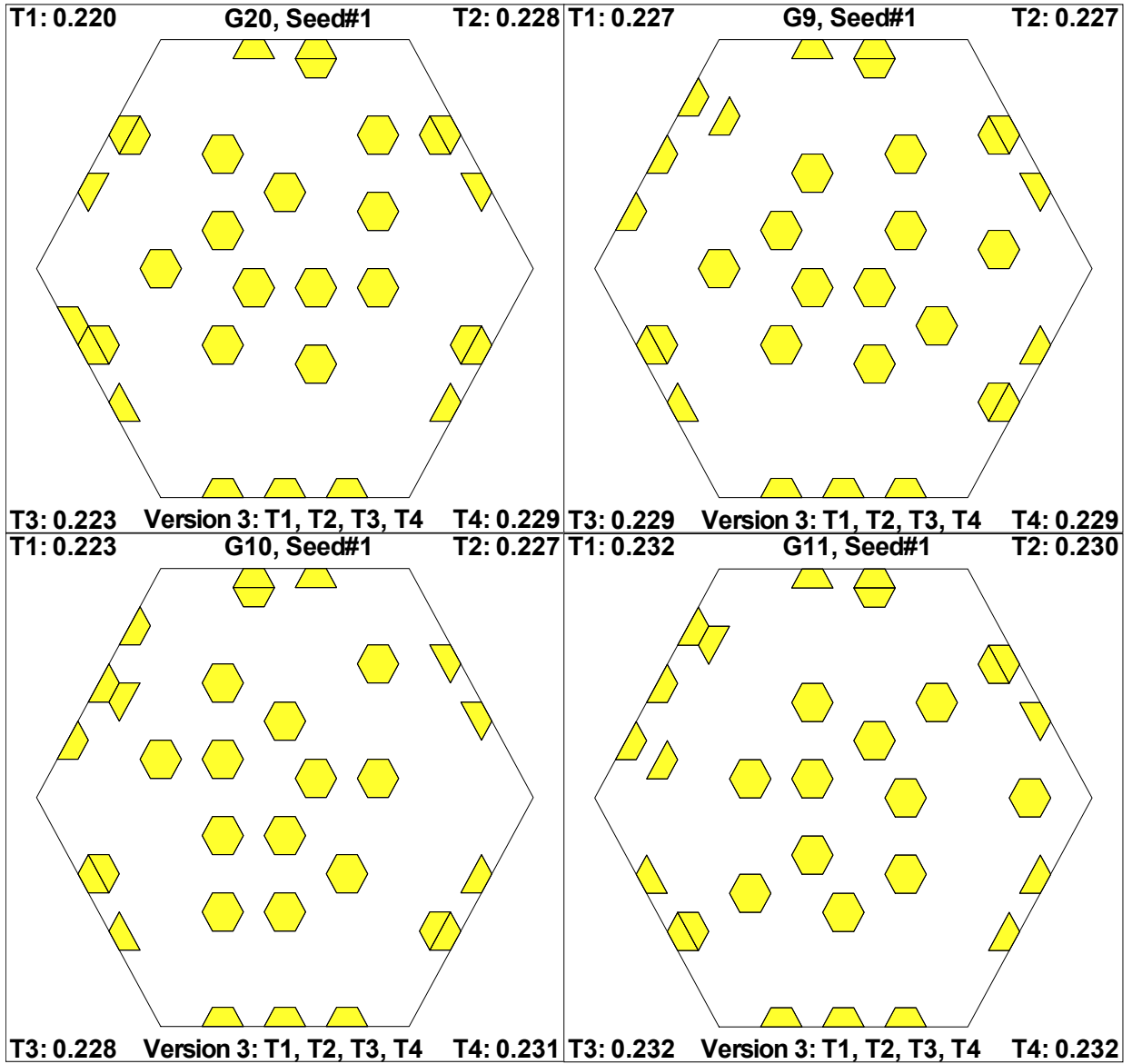


Figure 5.5 RMS error and Optimal location of piezoelectric actuators obtained by GA

Version 3 ( 30 actuators )

Note: The number in each corner in the Figure represents the RMS error corresponding to the specified type of the thermal load.

Table 5.5 Optimal voltages corresponding to optimal location (see Figure 5.5 upper left) for thermal load type T1 (30 actuators)

| Strip Loc. | Voltage V | Strip Loc. | Voltage V | Strip Loc. | Voltage V |
|------------|-----------|------------|-----------|------------|-----------|
| 3          | -157      | 58         | 427       | 127        | -394      |
| 8          | -452      | 62         | -385      | 130        | -386      |
| 13         | -133      | 74         | -1039     | 132        | -152      |
| 23         | -503      | 75         | 541       | 138        | -445      |
| 28         | -900      | 79         | -535      | 150        | -570      |
| 29         | -359      | 88         | -53       | 155        | -402      |
| 40         | -532      | 91         | -994      | 157        | -423      |
| 45         | -1229     | 92         | 540       | 176        | -358      |
| 46         | -834      | 96         | -497      | 178        | -356      |
| 57         | -843      | 111        | -247      | 180        | -121      |

Table 5.6 Optimal voltages corresponding to optimal location (see Figure 5.5 upper left) for thermal load type T2 (30 actuators)

| Strip Loc. | Voltage V | Strip Loc. | Voltage V | Strip Loc. | Voltage V |
|------------|-----------|------------|-----------|------------|-----------|
| 3          | -328      | 58         | 459       | 127        | -9        |
| 8          | -758      | 62         | -624      | 130        | -142      |
| 13         | -358      | 74         | -1375     | 132        | -98       |
| 23         | -646      | 75         | 733       | 138        | -194      |
| 28         | -1293     | 79         | -637      | 150        | -362      |
| 29         | 523       | 88         | -117      | 155        | -86       |
| 40         | -750      | 91         | -1483     | 157        | -267      |
| 45         | -1403     | 92         | 967       | 176        | -230      |
| 46         | 823       | 96         | -590      | 178        | -261      |
| 57         | -1089     | 111        | -14       | 180        | -160      |

Table 5.7 Optimal voltages corresponding to optimal location (see Figure 5.5 upper left) for thermal load type T3 (30 actuators)

| Strip Loc. | Voltage V | Strip Loc. | Voltage V | Strip Loc. | Voltage V |
|------------|-----------|------------|-----------|------------|-----------|
| 3          | -610      | 58         | 1305      | 127        | -136      |
| 8          | -1071     | 62         | -375      | 130        | 72        |
| 13         | -689      | 74         | -1366     | 132        | 275       |
| 23         | -993      | 75         | 1168      | 138        | -41       |
| 28         | -1542     | 79         | -190      | 150        | 178       |
| 29         | 747       | 88         | -4        | 155        | -353      |
| 40         | -217      | 91         | -1353     | 157        | -58       |
| 45         | -1004     | 92         | 963       | 176        | -106      |
| 46         | 676       | 96         | -485      | 178        | 130       |
| 57         | -1592     | 111        | 194       | 180        | 168       |

Table 5.8 Optimal voltages corresponding to optimal location (see Figure 5.5 upper left) for thermal load type T4 (30 actuators)

| Strip Loc. | Voltage V | Strip Loc. | Voltage V | Strip Loc. | Voltage V |
|------------|-----------|------------|-----------|------------|-----------|
| 3          | -615      | 58         | 882       | 127        | -309      |
| 8          | -1051     | 62         | -338      | 130        | -211      |
| 13         | -635      | 74         | -1700     | 132        | -64       |
| 23         | -789      | 75         | 741       | 138        | -220      |
| 28         | -1602     | 79         | -958      | 150        | -164      |
| 29         | 926       | 88         | -311      | 155        | -298      |
| 40         | -20       | 91         | -1295     | 157        | -240      |
| 45         | -796      | 92         | 584       | 176        | -98       |
| 46         | 713       | 96         | -1041     | 178        | -23       |
| 57         | -1132     | 111        | -195      | 180        | 108       |

**Case 2: N=121 actuators**

Micro-GA Version 3: Initial population size 10, population size 5, scale=0.5, random=0, crossover rate =0.5, mutation rate=0.01, restart control parameter different level=0.0

No\_of\_best\_mutation\_bits=2.

Table 5.9 RMS errors corresponding to optimal placement (121 actuators)

| Generations of inner loop | RMS for initial evaluation |         | RMS for 5000 evaluations |                | RMS for 10000 evaluations |                | RMS for 15000 evaluations |                |
|---------------------------|----------------------------|---------|--------------------------|----------------|---------------------------|----------------|---------------------------|----------------|
|                           | Seed #1                    | Seed #2 | Seed #1                  | Seed #2        | Seed #1                   | Seed #2        | Seed #1                   | Seed #2        |
| 8                         | 0.20413                    | 0.18827 | 0.07880                  | 0.08017        | 0.07825                   | 0.07891        | 0.07802                   | 0.07864        |
| 9                         |                            |         | 0.07930                  | 0.07933        | 0.07845                   | 0.07874        | 0.07817                   | 0.07831        |
| 10                        |                            |         | 0.07982                  | 0.07894        | 0.07942                   | 0.07822        | 0.07931                   | 0.07810        |
| 11                        |                            |         | 0.07927                  | 0.07951        | 0.07862                   | 0.07843        | 0.07824                   | 0.07813        |
| 12                        |                            |         | 0.07866                  | 0.07872        | 0.07828                   | 0.07812        | 0.07805                   | 0.07797        |
| 13                        |                            |         | 0.07881                  | 0.07850        | <b>0.07802</b>            | 0.07817        | <b>0.07788</b>            | 0.07809        |
| 14                        |                            |         | 0.07897                  | 0.07918        | 0.07854                   | 0.07868        | 0.07851                   | 0.07853        |
| 15                        |                            |         | 0.07970                  | 0.07902        | 0.07860                   | 0.07826        | 0.07831                   | 0.07815        |
| 16                        |                            |         | 0.07903                  | 0.07879        | 0.07871                   | 0.07855        | 0.07857                   | 0.07822        |
| 17                        |                            |         | 0.07893                  | 0.07860        | 0.07840                   | 0.07822        | 0.07810                   | 0.07809        |
| 18                        |                            |         | 0.07898                  | 0.07892        | 0.07858                   | 0.07870        | 0.07832                   | 0.07857        |
| 19                        |                            |         | <b>0.07861</b>           | 0.07839        | 0.07852                   | 0.07831        | 0.07790                   | 0.07813        |
| 20                        |                            |         | 0.07908                  | <b>0.07833</b> | 0.07888                   | <b>0.07799</b> | 0.07877                   | <b>0.07795</b> |



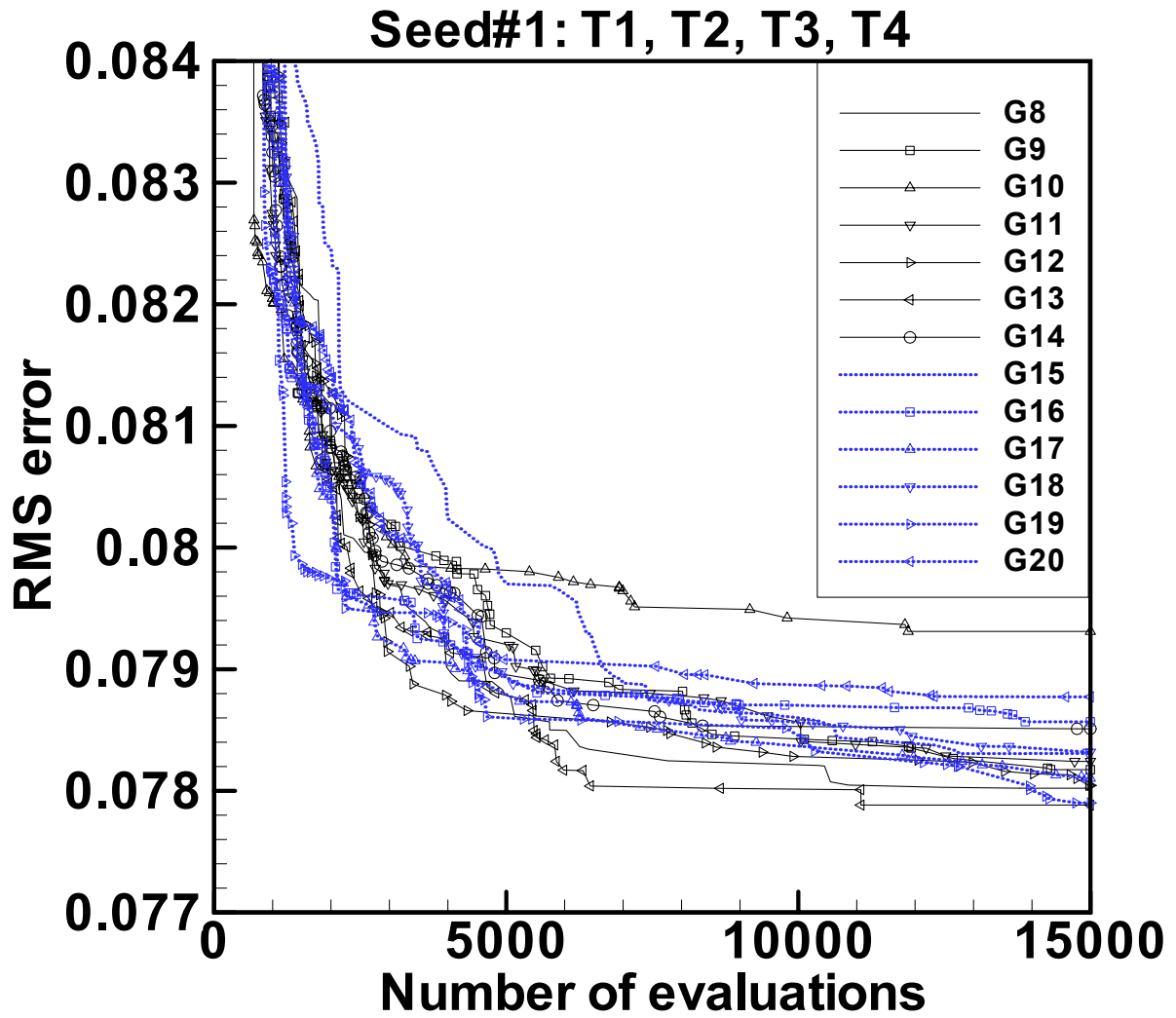


Figure 5.6 a) Performance of the GAs: Maximum of the four minimum RMS errors vs. the number of evaluations ( 121 actuators, seed#1 ).

Note: It is the optimization problem in which one set of actuators is chosen for all four thermal distortions.

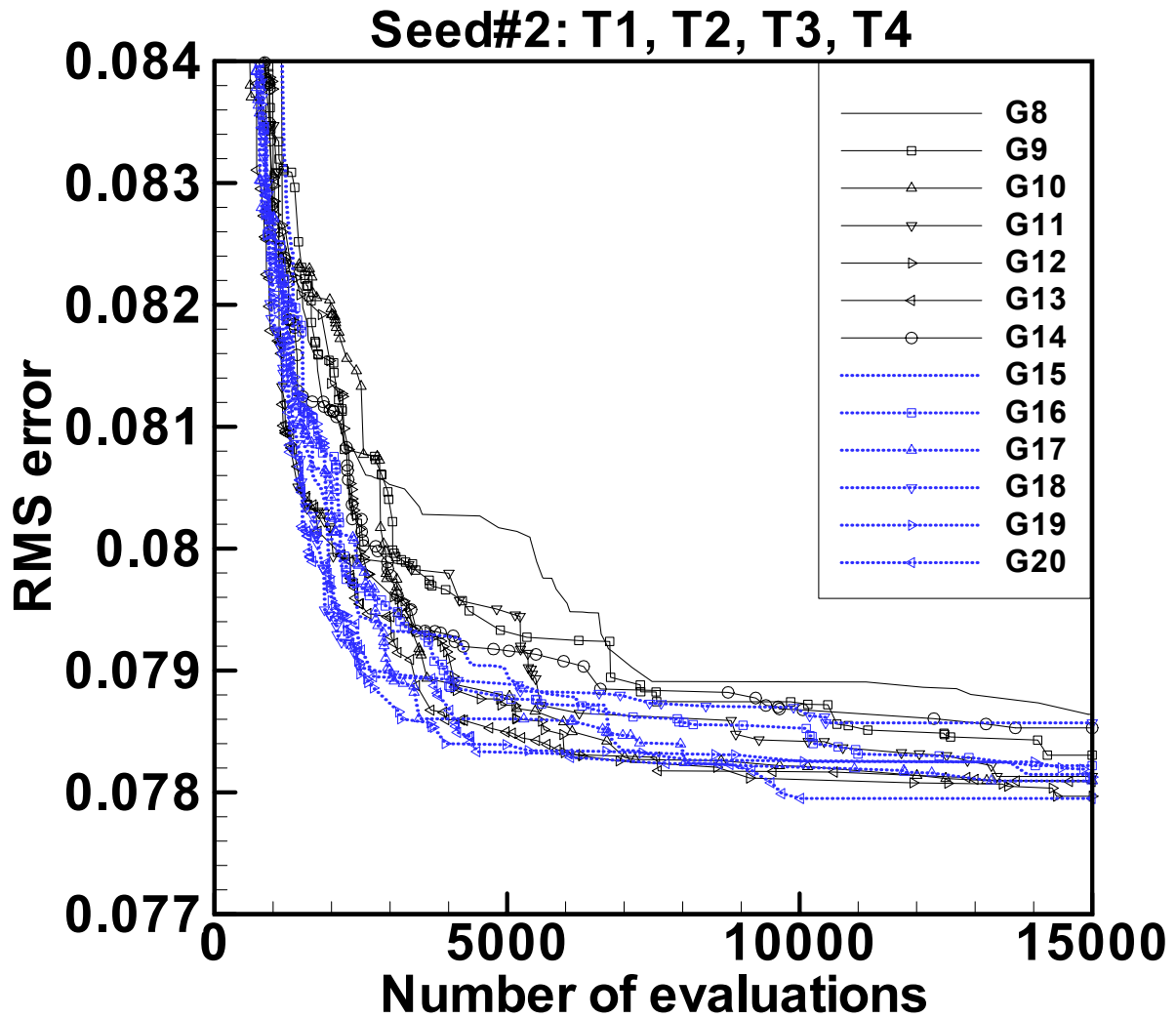


Figure 5.6 b) Performance of the GAs: Maximum of the four minimum RMS errors vs. the number of evaluations ( 121 actuators, seed#2 ).

Note: It is the optimization problem in which one set of actuators is chosen for all four thermal distortions.

For this case (nstrip=121)

Observation 1: Which seed is better depends on the number of evaluations used for termination. For example, if 5000 or 10000 evaluations are chosen as termination condition,

Seed #2 is better than Seed #1, but if 15000 evaluations are chosen as the termination condition, the conclusion is reverse. However, the differences between the results obtained from two seeds are not substantially different.

Observation 2: The best number of generations of inner loop is dependent on the number of evaluations used for termination. For example, If 5000 or 10000 evaluations are performed for termination, the best number of generations of inner loop is 20, but If 15000 evaluations are performed as the termination condition, the best number of generations of inner loop is 13.

The computation time in the case of 121 actuators is about one week per job running on one processor of the Sun machine. The advantage of using the Sun machine is that we can submit multiple jobs running on different processors simultaneously, so we can study the performance of GAs with different parameter settings at the same time and significantly reduce the time of investigation.

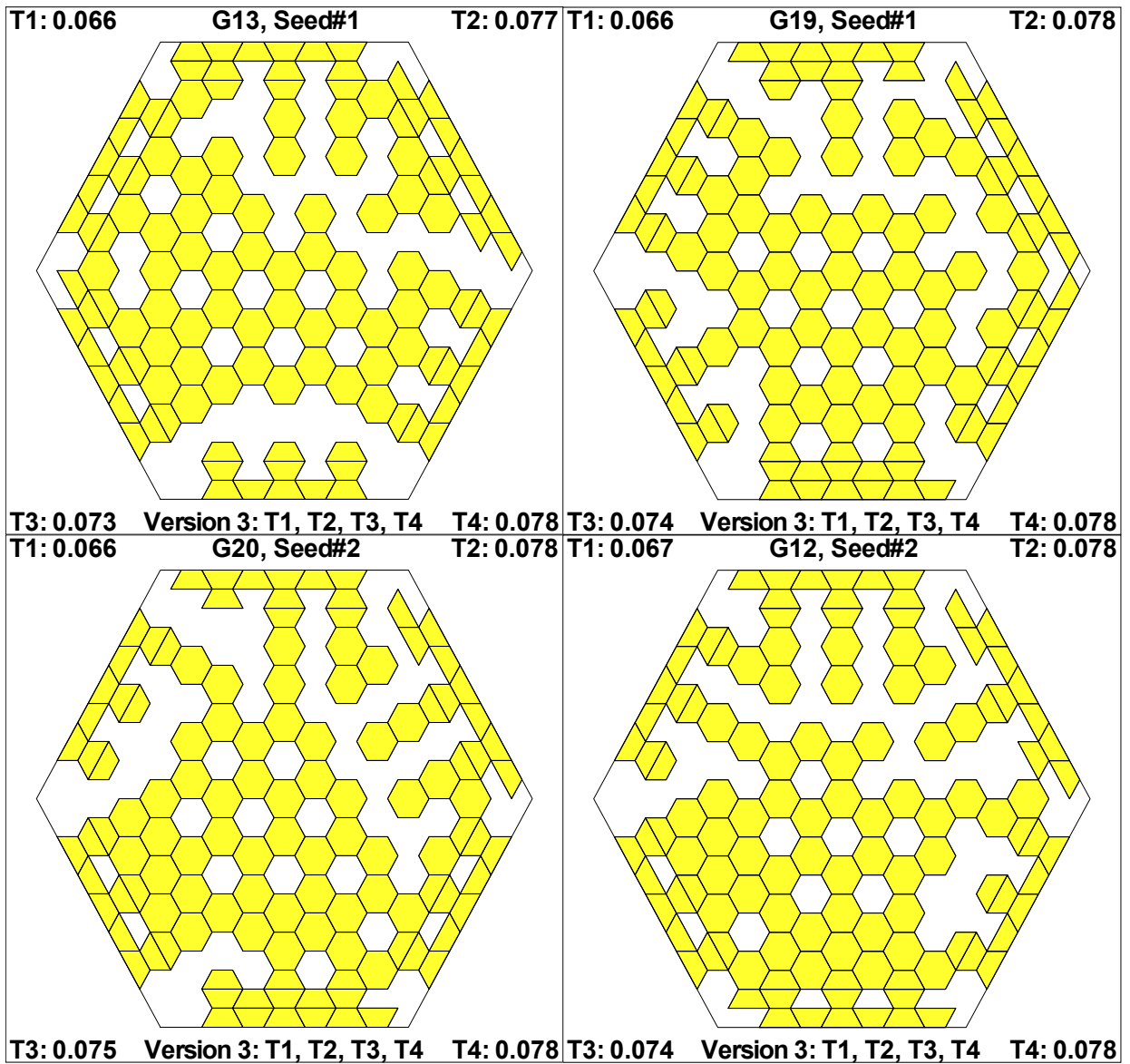


Figure 5.7 RMS error and Optimal location of piezoelectric actuators obtained by GA

Version 3 ( 121 actuators )

Note: The number in each corner in the Figure represents the RMS error corresponding to the specified type of the thermal load.

Table 5.10 Optimal voltages corresponding to optimal location (see Figure 5.7 upper left) for thermal load type T1 (121 actuators)

| Strip Loc. | Voltage V | Strip Loc. | Voltage V | Strip Loc. | Voltage V |
|------------|-----------|------------|-----------|------------|-----------|
| 3          | -373      | 62         | -165      | 120        | -104      |
| 4          | 485       | 64         | -419      | 121        | -102      |
| 5          | -126      | 65         | 483       | 122        | -31       |
| 6          | -218      | 66         | -186      | 124        | 60        |
| 8          | -537      | 67         | 48        | 126        | -96       |
| 9          | 638       | 68         | -13       | 128        | -135      |
| 10         | -261      | 71         | -460      | 129        | -172      |
| 11         | -217      | 72         | 541       | 131        | -74       |
| 13         | -373      | 73         | -253      | 132        | -105      |
| 14         | 484       | 74         | -239      | 136        | -99       |
| 15         | -127      | 76         | -662      | 137        | -163      |
| 20         | -479      | 77         | 742       | 139        | -133      |
| 21         | 581       | 78         | -379      | 140        | -238      |
| 22         | -212      | 79         | -240      | 145        | -119      |
| 23         | -247      | 81         | -480      | 147        | -155      |
| 25         | -675      | 82         | 562       | 148        | -218      |
| 26         | 766       | 83         | -282      | 151        | -219      |
| 27         | -369      | 87         | 7         | 152        | 37        |
| 28         | -239      | 88         | -482      | 155        | -96       |
| 30         | -485      | 89         | 548       | 156        | -170      |
| 31         | 595       | 90         | -269      | 158        | -102      |
| 32         | -271      | 91         | -246      | 159        | -279      |
| 35         | 41        | 93         | -666      | 164        | -100      |
| 37         | -472      | 94         | 775       | 166        | -108      |
| 38         | 364       | 95         | -428      | 167        | -233      |
| 40         | -203      | 96         | -255      | 170        | -155      |
| 42         | -699      | 98         | -475      | 171        | 33        |
| 43         | 777       | 99         | 583       | 173        | 47        |
| 44         | -353      | 100        | -228      | 174        | -71       |
| 45         | -219      | 103        | 60        | 175        | -129      |
| 47         | -486      | 104        | 52        | 178        | -218      |
| 48         | 533       | 107        | 45        | 181        | 48        |
| 49         | -220      | 108        | 23        | 183        | 56        |
| 51         | 28        | 109        | 49        | 184        | -57       |
| 54         | -394      | 110        | -89       | 185        | -160      |
| 55         | 510       | 111        | -70       | 187        | 39        |
| 56         | -233      | 112        | -42       | 188        | 8         |
| 57         | -180      | 114        | 44        | 190        | 53        |
| 59         | -581      | 116        | 45        | 192        | -36       |
| 60         | 667       | 117        | -82       |            |           |
| 61         | -298      | 118        | -106      |            |           |

Table 5.11 Optimal voltages corresponding to optimal location (see Figure 5.7 upper left) for thermal load type T2 (121 actuators)

| Strip Loc. | Voltage V | Strip Loc. | Voltage V | Strip Loc. | Voltage V |
|------------|-----------|------------|-----------|------------|-----------|
| 3          | -699      | 62         | -252      | 120        | -45       |
| 4          | 661       | 64         | -576      | 121        | -38       |
| 5          | -152      | 65         | 623       | 122        | -19       |
| 6          | -334      | 66         | -243      | 124        | 71        |
| 8          | -951      | 67         | 63        | 126        | -10       |
| 9          | 900       | 68         | -79       | 128        | -38       |
| 10         | -276      | 71         | -583      | 129        | -64       |
| 11         | -332      | 72         | 638       | 131        | -41       |
| 13         | -690      | 73         | -320      | 132        | -68       |
| 14         | 668       | 74         | -308      | 136        | -35       |
| 15         | -184      | 76         | -807      | 137        | -53       |
| 20         | -649      | 77         | 863       | 139        | -56       |
| 21         | 705       | 78         | -437      | 140        | -133      |
| 22         | -291      | 79         | -304      | 145        | -16       |
| 23         | -306      | 81         | -579      | 147        | -63       |
| 25         | -912      | 82         | 632       | 148        | -107      |
| 26         | 962       | 83         | -313      | 151        | -165      |
| 27         | -456      | 87         | -43       | 152        | 39        |
| 28         | -306      | 88         | -612      | 155        | -45       |
| 30         | -667      | 89         | 671       | 156        | -77       |
| 31         | 724       | 90         | -309      | 158        | -52       |
| 32         | -341      | 91         | -332      | 159        | -186      |
| 35         | 7         | 93         | -863      | 164        | -42       |
| 37         | -559      | 94         | 961       | 166        | -49       |
| 38         | 393       | 95         | -525      | 167        | -146      |
| 40         | -276      | 96         | -327      | 170        | -143      |
| 42         | -863      | 98         | -630      | 171        | 29        |
| 43         | 925       | 99         | 707       | 173        | 65        |
| 44         | -430      | 100        | -315      | 174        | -52       |
| 45         | -299      | 103        | 97        | 175        | -86       |
| 47         | -609      | 104        | 85        | 178        | -176      |
| 48         | 653       | 107        | 85        | 181        | 44        |
| 49         | -288      | 108        | 58        | 183        | 76        |
| 51         | 14        | 109        | 72        | 184        | -42       |
| 54         | -547      | 110        | -43       | 185        | -126      |
| 55         | 624       | 111        | 4         | 187        | 38        |
| 56         | -299      | 112        | -21       | 188        | 6         |
| 57         | -258      | 114        | 72        | 190        | 51        |
| 59         | -781      | 116        | 70        | 192        | -39       |
| 60         | 836       | 117        | -52       |            |           |
| 61         | -380      | 118        | -23       |            |           |

Table 5.12 Optimal voltages corresponding to optimal location (see Figure 5.7 upper left) for thermal load type T3 (121 actuators)

| Strip Loc. | Voltage V | Strip Loc. | Voltage V | Strip Loc. | Voltage V |
|------------|-----------|------------|-----------|------------|-----------|
| 3          | -877      | 62         | -185      | 120        | -3        |
| 4          | 826       | 64         | -525      | 121        | 62        |
| 5          | -331      | 65         | 494       | 122        | 13        |
| 6          | -410      | 66         | -46       | 124        | 94        |
| 8          | -1172     | 67         | 32        | 126        | -68       |
| 9          | 1157      | 68         | -31       | 128        | -21       |
| 10         | -546      | 71         | -378      | 129        | 15        |
| 11         | -407      | 72         | 471       | 131        | 0         |
| 13         | -875      | 73         | -184      | 132        | 106       |
| 14         | 841       | 74         | -214      | 136        | -48       |
| 15         | -405      | 76         | -521      | 137        | -48       |
| 20         | -751      | 77         | 605       | 139        | -5        |
| 21         | 757       | 78         | -253      | 140        | 64        |
| 22         | -374      | 79         | -198      | 145        | -109      |
| 23         | -344      | 81         | -333      | 147        | -43       |
| 25         | -1032     | 82         | 445       | 148        | -6        |
| 26         | -1064     | 83         | -184      | 151        | 60        |
| 27         | -525      | 87         | -2        | 152        | 110       |
| 28         | -340      | 88         | -495      | 155        | -61       |
| 30         | -750      | 89         | 551       | 156        | -68       |
| 31         | 776       | 90         | -236      | 158        | -18       |
| 32         | -336      | 91         | -252      | 159        | 52        |
| 35         | 100       | 93         | -692      | 164        | -109      |
| 37         | -354      | 94         | 796       | 166        | -42       |
| 38         | 325       | 95         | -421      | 167        | -26       |
| 40         | -138      | 96         | -259      | 170        | 56        |
| 42         | -536      | 98         | -472      | 171        | 80        |
| 43         | 642       | 99         | 572       | 173        | 39        |
| 44         | -303      | 100        | -251      | 174        | -65       |
| 45         | -166      | 103        | 118       | 175        | -72       |
| 47         | -372      | 104        | 87        | 178        | 12        |
| 48         | 419       | 107        | 110       | 181        | 55        |
| 49         | -128      | 108        | 45        | 183        | 76        |
| 51         | 61        | 109        | 50        | 184        | -48       |
| 54         | -494      | 110        | -15       | 185        | -32       |
| 55         | 572       | 111        | 50        | 187        | 52        |
| 56         | -192      | 112        | 17        | 188        | 84        |
| 57         | -189      | 114        | 115       | 190        | 74        |
| 59         | -726      | 116        | 40        | 192        | 39        |
| 60         | 761       | 117        | -44       |            |           |
| 61         | -238      | 118        | -19       |            |           |

Table 5.13 Optimal voltages corresponding to optimal location (see Figure 5.7 upper left) for thermal load type T4 (121 actuators)

| Strip Loc. | Voltage V | Strip Loc. | Voltage V | Strip Loc. | Voltage V |
|------------|-----------|------------|-----------|------------|-----------|
| 3          | -841      | 62         | -150      | 120        | -70       |
| 4          | 806       | 64         | -447      | 121        | -53       |
| 5          | -328      | 65         | 518       | 122        | -33       |
| 6          | -404      | 66         | -151      | 124        | 77        |
| 8          | -1176     | 67         | 195       | 126        | -88       |
| 9          | 1142      | 68         | -180      | 128        | -84       |
| 10         | -504      | 71         | -779      | 129        | -98       |
| 11         | -409      | 72         | 785       | 131        | -48       |
| 13         | -900      | 73         | -411      | 132        | -39       |
| 14         | 838       | 74         | -401      | 136        | -71       |
| 15         | -353      | 76         | -1041     | 137        | -99       |
| 20         | -659      | 77         | 1068      | 139        | -72       |
| 21         | 698       | 78         | -571      | 140        | -103      |
| 22         | -315      | 79         | -392      | 145        | -99       |
| 23         | -309      | 81         | -752      | 147        | -86       |
| 25         | -933      | 82         | 778       | 148        | -99       |
| 26         | 981       | 83         | -428      | 151        | -81       |
| 27         | -463      | 87         | -95       | 152        | 66        |
| 28         | -308      | 88         | -798      | 155        | -64       |
| 30         | -685      | 89         | 853       | 156        | -93       |
| 31         | 727       | 90         | -438      | 158        | -51       |
| 32         | -302      | 91         | -438      | 159        | -88       |
| 35         | 128       | 93         | -1097     | 164        | -84       |
| 37         | -259      | 94         | 1170      | 166        | -53       |
| 38         | 285       | 95         | -684      | 167        | -84       |
| 40         | -66       | 96         | -407      | 170        | -16       |
| 42         | -360      | 98         | -799      | 171        | 64        |
| 43         | 477       | 99         | 824       | 173        | 52        |
| 44         | -212      | 100        | -427      | 174        | -57       |
| 45         | -78       | 103        | 79        | 175        | -70       |
| 47         | -223      | 104        | 70        | 178        | -45       |
| 48         | 283       | 107        | 76        | 181        | 48        |
| 49         | -65       | 108        | 49        | 183        | 82        |
| 51         | 102       | 109        | 69        | 184        | -46       |
| 54         | -405      | 110        | -88       | 185        | -46       |
| 55         | 505       | 111        | -48       | 187        | 43        |
| 56         | -177      | 112        | -45       | 188        | 65        |
| 57         | -152      | 114        | 79        | 190        | 82        |
| 59         | -588      | 116        | 54        | 192        | 39        |
| 60         | 652       | 117        | -90       |            |           |
| 61         | -237      | 118        | -81       |            |           |



**Case 3: N=15 actuators**

Micro-GA Version 3: Initial population size 10, population size 5, scale=0.5, random=0,

crossover rate =0.5, mutation rate=0.01, restart control parameter different level=0.0

No\_of\_best\_mutation\_bits=2.

Table 5.14 RMS errors corresponding to optimal placement (15 actuators)

| Generations of inner loop | RMS for initial evaluation |         | RMS for 5000 evaluations |                | RMS for 10000 evaluations |                | RMS for 15000 evaluations |                |
|---------------------------|----------------------------|---------|--------------------------|----------------|---------------------------|----------------|---------------------------|----------------|
|                           | Seed #1                    | Seed #2 | Seed #1                  | Seed #2        | Seed #1                   | Seed #2        | Seed #1                   | Seed #2        |
| 8                         | 1.66981                    | 1.13175 | 0.42783                  | 0.41276        | 0.41357                   | 0.40926        | 0.40345                   | 0.40905        |
| 9                         |                            |         | 0.40495                  | <b>0.39477</b> | 0.40010                   | <b>0.38528</b> | 0.39804                   | <b>0.38188</b> |
| 10                        |                            |         | <b>0.39957</b>           | 0.47201        | 0.39087                   | 0.44066        | 0.38581                   | 0.43244        |
| 11                        |                            |         | 0.40130                  | 0.43442        | <b>0.38671</b>            | 0.41774        | 0.38314                   | 0.38577        |
| 12                        |                            |         | 0.41044                  | 0.42707        | 0.39972                   | 0.42327        | <b>0.38018</b>            | 0.41599        |
| 13                        |                            |         | 0.41505                  | 0.44012        | 0.40725                   | 0.41871        | 0.40618                   | 0.41636        |
| 14                        |                            |         | 0.40621                  | 0.44519        | 0.39955                   | 0.38707        | 0.39951                   | 0.38342        |
| 15                        |                            |         | 0.41498                  | 0.43830        | 0.41037                   | 0.43830        | 0.40985                   | 0.42657        |
| 16                        |                            |         | 0.40793                  | 0.44148        | 0.40190                   | 0.42044        | 0.40159                   | 0.41474        |
| 17                        |                            |         | 0.41550                  | 0.41523        | 0.40134                   | 0.41455        | 0.39573                   | 0.40850        |
| 18                        |                            |         | 0.41861                  | 0.43983        | 0.40661                   | 0.41402        | 0.40340                   | 0.41295        |
| 19                        |                            |         | 0.41356                  | 0.41859        | 0.41084                   | 0.40415        | 0.40651                   | 0.40415        |
| 20                        |                            |         | 0.41257                  | 0.41963        | 0.40811                   | 0.40114        | 0.39851                   | 0.39657        |

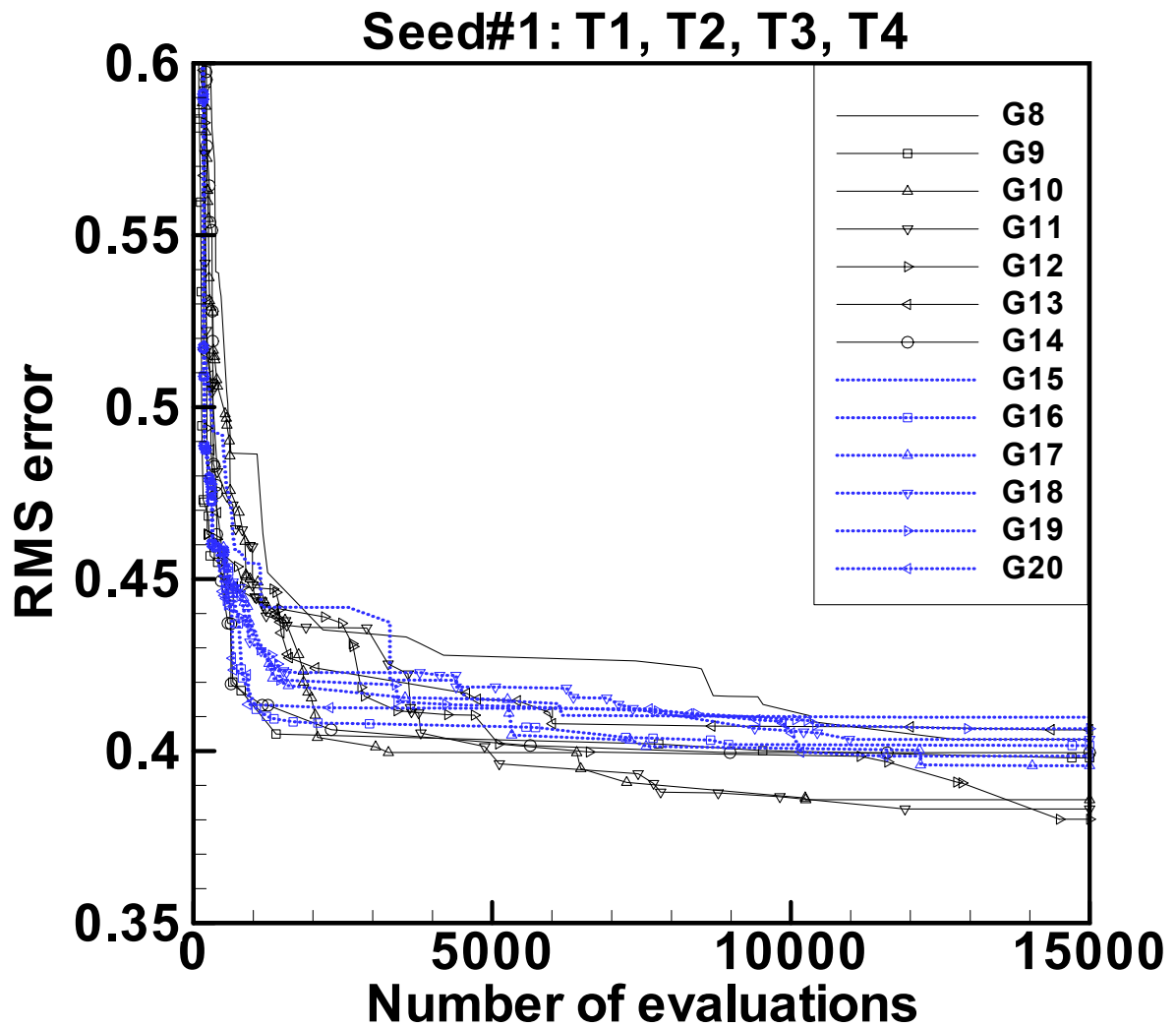


Figure 5.8 a) Performance of the GAs: Maximum of the four minimum RMS errors vs. the number of evaluations ( 15 actuators, seed#1 ).

Note: It is the optimization problem in which one set of actuators is chosen for all four thermal distortions.

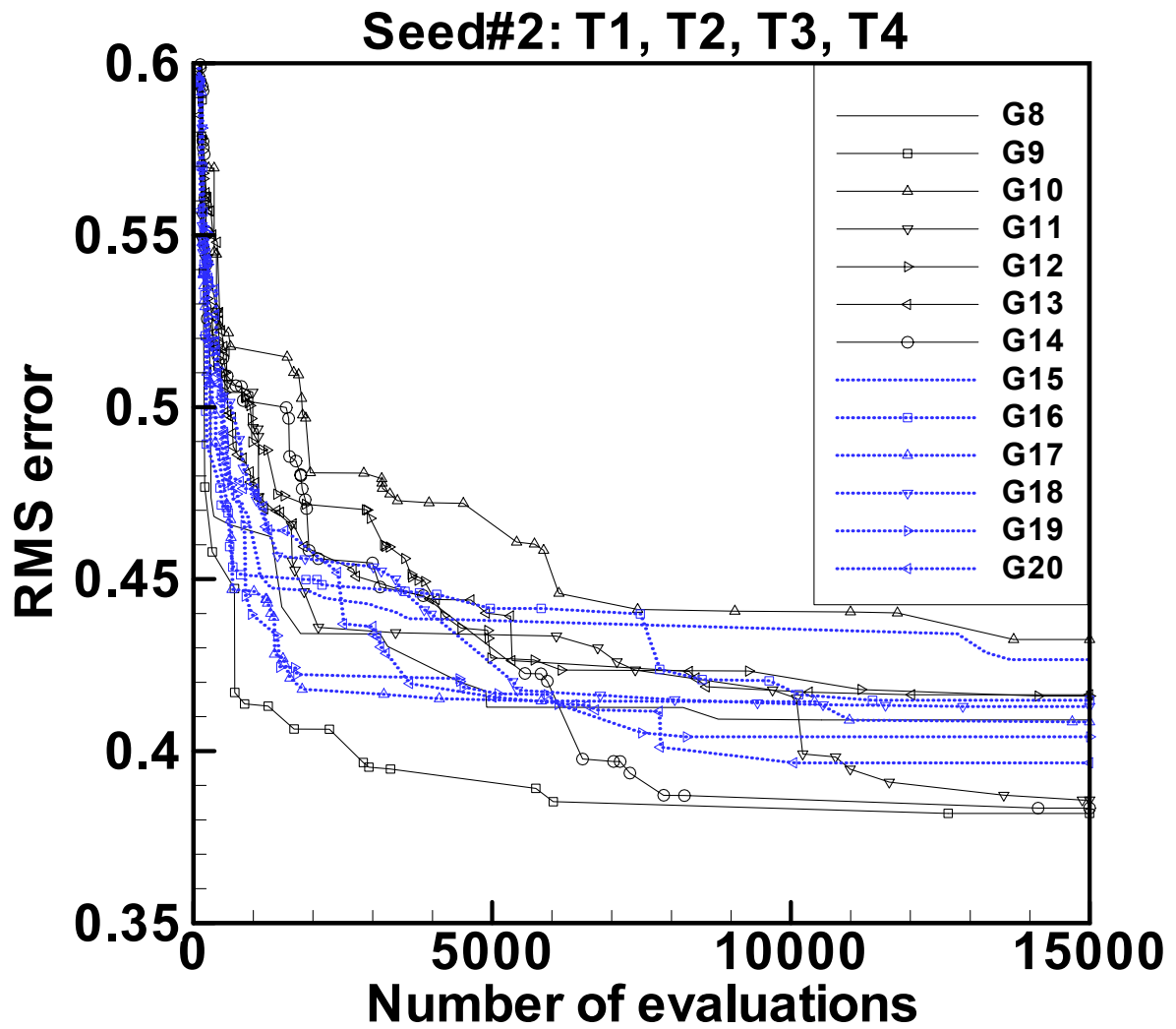


Figure 5.8 b) Performance of the GAs: Maximum of the four minimum RMS errors vs. the number of evaluations ( 15 actuators, seed#2 ).

Note: It is the optimization problem in which one set of actuators is chosen for all four thermal distortions.

For this case (nstrip=15), following observations are made:

- 1) Which seed is better depends on the number of evaluations used for termination. For example, if 5000 or 10000 evaluations are chosen as termination condition, Seed #2 is better than Seed #1, but if 15000 evaluations are chosen as the termination condition, the conclusion is reverse.
- 2) The best number of generations in the inner loop for each seed is different and maybe dependent on the number of evaluations used for termination. For example, for Seed#1, the best number of generations in the inner loop is 10, 11 and 12 corresponding to the 5000, 10000, and 15000 evaluations as the termination condition, respectively; for Seed#2, the best number of generations in the inner loop is consistently 9 for all the three termination conditions.
- 3) The best number of generations in the inner loop is less than 14 for all the three termination conditions.
- 4) The range of the RMS errors for Seed#2 is obviously larger than that for Seed#1.

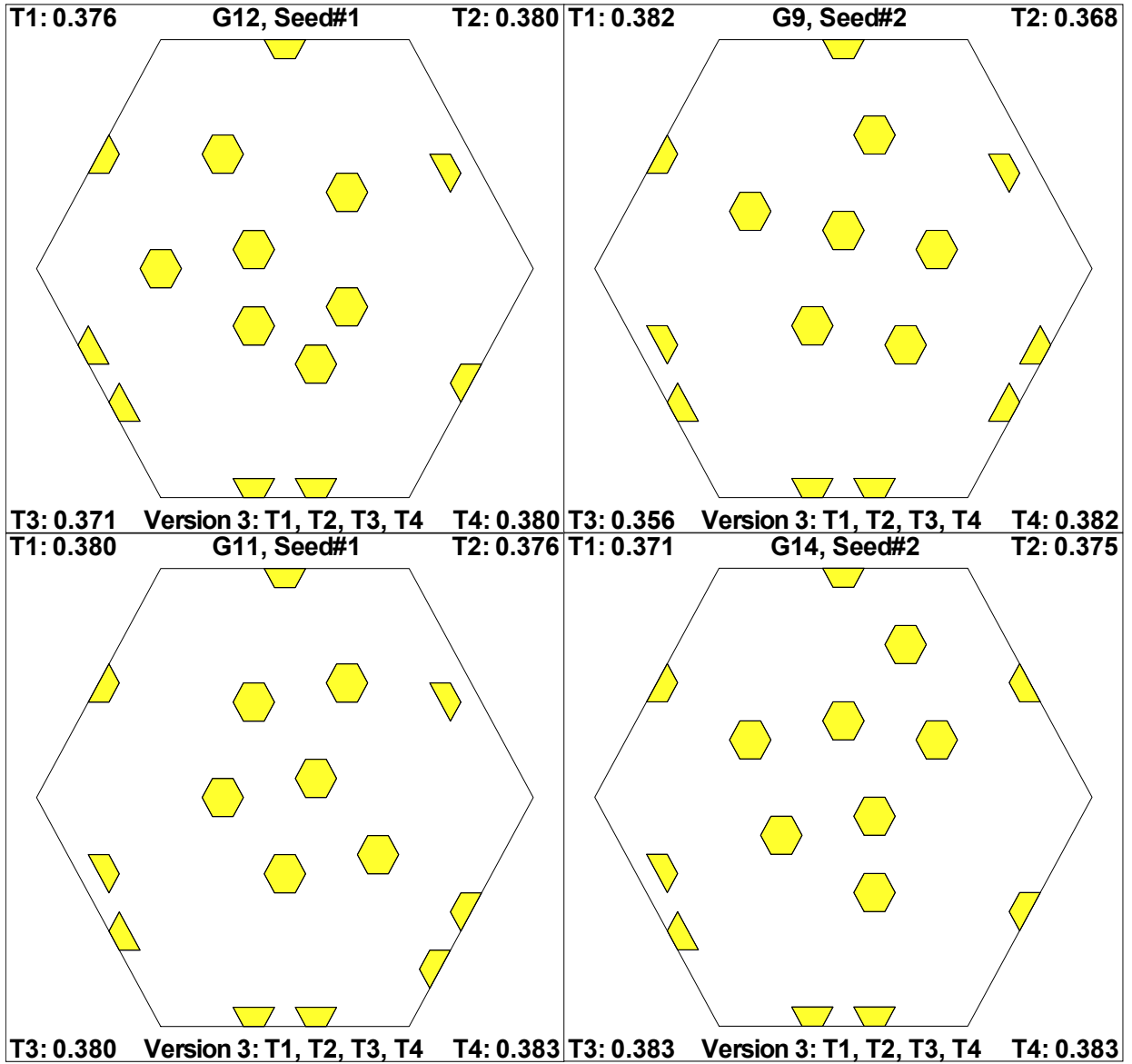


Figure 5.9 RMS error and Optimal location of piezoelectric actuators obtained by GA

Version 3 ( 15 actuators )

Note: The number in each corner in the Figure represents the RMS error corresponding to the specified type of the thermal load.

Table 5.15 Optimal voltages corresponding to optimal location (see Figure 5.9 upper left) for thermal load type T1 (15 actuators)

| Strip Loc. | Voltage V | Strip Loc. | Voltage V | Strip Loc. | Voltage V |
|------------|-----------|------------|-----------|------------|-----------|
| 6          | -451      | 76         | -710      | 137        | -589      |
| 11         | -332      | 91         | -427      | 139        | -825      |
| 25         | -845      | 96         | -604      | 155        | -256      |
| 43         | -815      | 111        | -349      | 166        | -735      |
| 59         | -507      | 132        | -364      | 169        | -672      |

Table 5.16 Optimal voltages corresponding to optimal location (see Figure 5.9 upper left) for thermal load type T2 (15 actuators)

| Strip Loc. | Voltage V | Strip Loc. | Voltage V | Strip Loc. | Voltage V |
|------------|-----------|------------|-----------|------------|-----------|
| 6          | -644      | 76         | -888      | 137        | -85       |
| 11         | -697      | 91         | -563      | 139        | -402      |
| 25         | -1116     | 96         | -536      | 155        | -21       |
| 43         | -1127     | 111        | 6         | 166        | -447      |
| 59         | -862      | 132        | -237      | 169        | -495      |

Table 5.17 Optimal voltages corresponding to optimal location (see Figure 5.9 upper left) for thermal load type T3 (15 actuators)

| Strip Loc. | Voltage V | Strip Loc. | Voltage V | Strip Loc. | Voltage V |
|------------|-----------|------------|-----------|------------|-----------|
| 6          | -1049     | 76         | -229      | 137        | -153      |
| 11         | -1117     | 91         | -362      | 139        | 74        |
| 25         | -1413     | 96         | -540      | 155        | -339      |
| 43         | -107      | 111        | 268       | 166        | -169      |
| 59         | -323      | 132        | 415       | 169        | 356       |

Table 5.18 Optimal voltages corresponding to optimal location (see Figure 5.9 upper left) for thermal load type T4 (15 actuators)

| Strip Loc. | Voltage V | Strip Loc. | Voltage V | Strip Loc. | Voltage V |
|------------|-----------|------------|-----------|------------|-----------|
| 6          | -1116     | 76         | -1396     | 137        | -386      |
| 11         | -1050     | 91         | -881      | 139        | -376      |
| 25         | -1151     | 96         | -1099     | 155        | -265      |
| 43         | 208       | 111        | -311      | 166        | -255      |
| 59         | -255      | 132        | -154      | 169        | -3        |

**Case 4: N=60 actuators**

Micro-GA Version 3: Initial population size 10, population size 5, scale=0.5, random=0,

crossover rate =0.5, mutation rate=0.01, restart control parameter different level=0.0

No\_of\_best\_mutation\_bits=2.

Table 5.19 RMS errors corresponding to optimal placement (60 actuators)

| Generations of inner loop | RMS for initial evaluation |         | RMS for 5000 evaluations |                | RMS for 10000 evaluations |                | RMS for 15000 evaluations |                |
|---------------------------|----------------------------|---------|--------------------------|----------------|---------------------------|----------------|---------------------------|----------------|
|                           | Seed #1                    | Seed #2 | Seed #1                  | Seed #2        | Seed #1                   | Seed #2        | Seed #1                   | Seed #2        |
| 8                         | 0.33310                    | 0.34697 | 0.14527                  | 0.14164        | 0.13996                   | 0.13690        | 0.13850                   | 0.13513        |
| 9                         |                            |         | 0.14180                  | 0.14356        | 0.13861                   | 0.14016        | 0.13565                   | 0.13602        |
| 10                        |                            |         | 0.14266                  | 0.14198        | 0.13815                   | 0.13931        | 0.13558                   | 0.13880        |
| 11                        |                            |         | 0.14130                  | 0.13831        | 0.13858                   | 0.13606        | 0.13564                   | 0.13465        |
| 12                        |                            |         | 0.14425                  | 0.13835        | 0.13986                   | 0.13792        | 0.13769                   | 0.13649        |
| 13                        |                            |         | 0.14059                  | 0.15004        | 0.13802                   | 0.13998        | 0.13697                   | 0.13560        |
| 14                        |                            |         | 0.14780                  | <b>0.13319</b> | 0.13848                   | <b>0.13319</b> | 0.13797                   | 0.13291        |
| 15                        |                            |         | 0.14183                  | 0.14884        | 0.13707                   | 0.14535        | 0.13540                   | 0.14303        |
| 16                        |                            |         | 0.14568                  | 0.14158        | 0.14355                   | 0.14049        | 0.14311                   | 0.14020        |
| 17                        |                            |         | <b>0.14036</b>           | 0.14150        | <b>0.13439</b>            | 0.13463        | <b>0.13358</b>            | <b>0.13164</b> |
| 18                        |                            |         | 0.14834                  | 0.13944        | 0.14438                   | 0.13696        | 0.14244                   | 0.13581        |
| 19                        |                            |         | 0.14763                  | 0.13736        | 0.14030                   | 0.13681        | 0.13810                   | 0.13681        |
| 20                        |                            |         | 0.14293                  | 0.14318        | 0.13889                   | 0.13739        | 0.13441                   | 0.13559        |

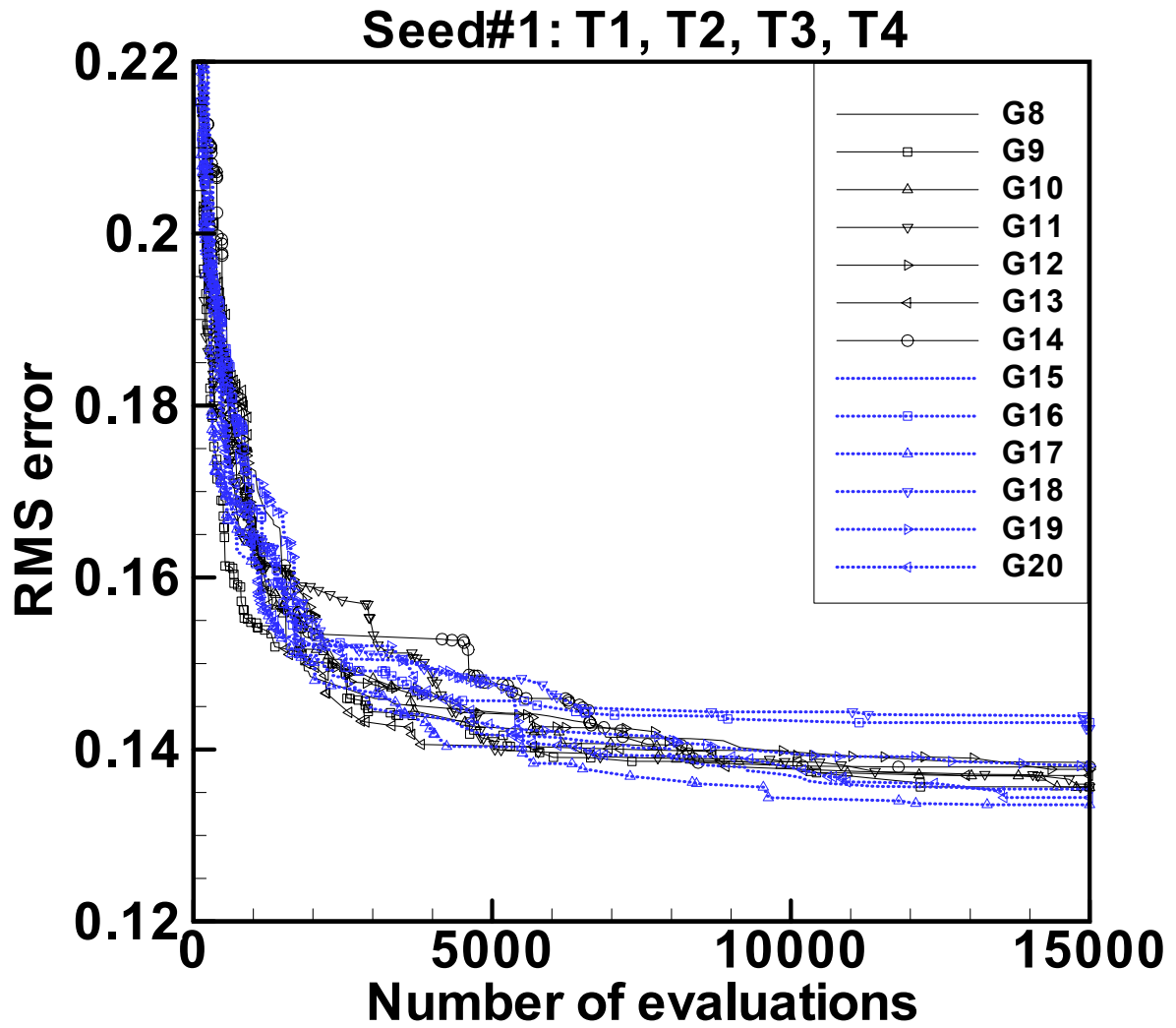


Figure 5.10 a) Performance of the GAs: Maximum of the four minimum RMS errors vs. the number of evaluations ( 60 actuators, seed#1 ).

Note: It is the optimization problem in which one set of actuators is chosen for all four thermal distortions.



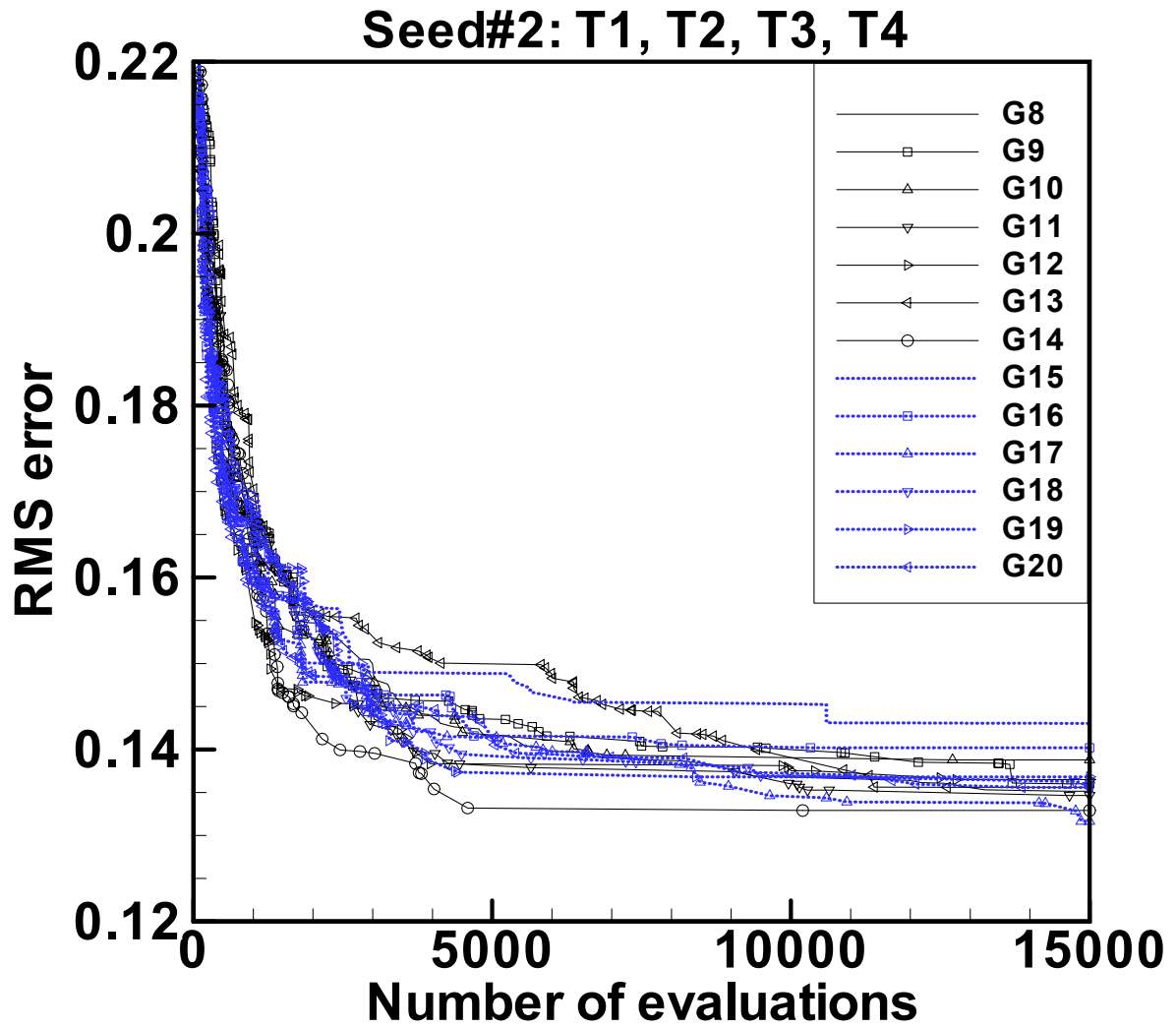


Figure 5.10 b) Performance of the GAs: Maximum of the four minimum RMS errors vs. the number of evaluations ( 60 actuators, seed#2 ).

Note: It is the optimization problem in which one set of actuators is chosen for all four thermal distortions.

For this case (nstrip=60), following observations are made:

- 1) The best number of generations in the inner loop for Seed #1 is consistently 17 for all the three numbers of evaluations used for termination.
- 2) The best number of generations in the inner loop for seed #2 is 14 for the termination condition of 5000 and 10000 evaluations, and 17 for the termination condition of 15000 evaluations. For Seed#2 and the termination condition of 15000 evaluations, the optimal number 17 for the case of 60 actuators is different from those in the case of 30 and 121 actuators (19 for the case of 30 actuators and 20 for the case of 121 actuators).
- 3) Which seed is better for a specific run is dependant on the number of evaluations. For example, the better seed is Seed #1 for 5000 and 10000 evaluations but Seed #2 for 15000 evaluations for the specific run of generations of inner loop equal to 17.
- 4) All the best results for the three termination conditions of 5000, 10000 and 15000 evaluations are obtained by Seed #2. This is quite different from the case of 30 actuators.

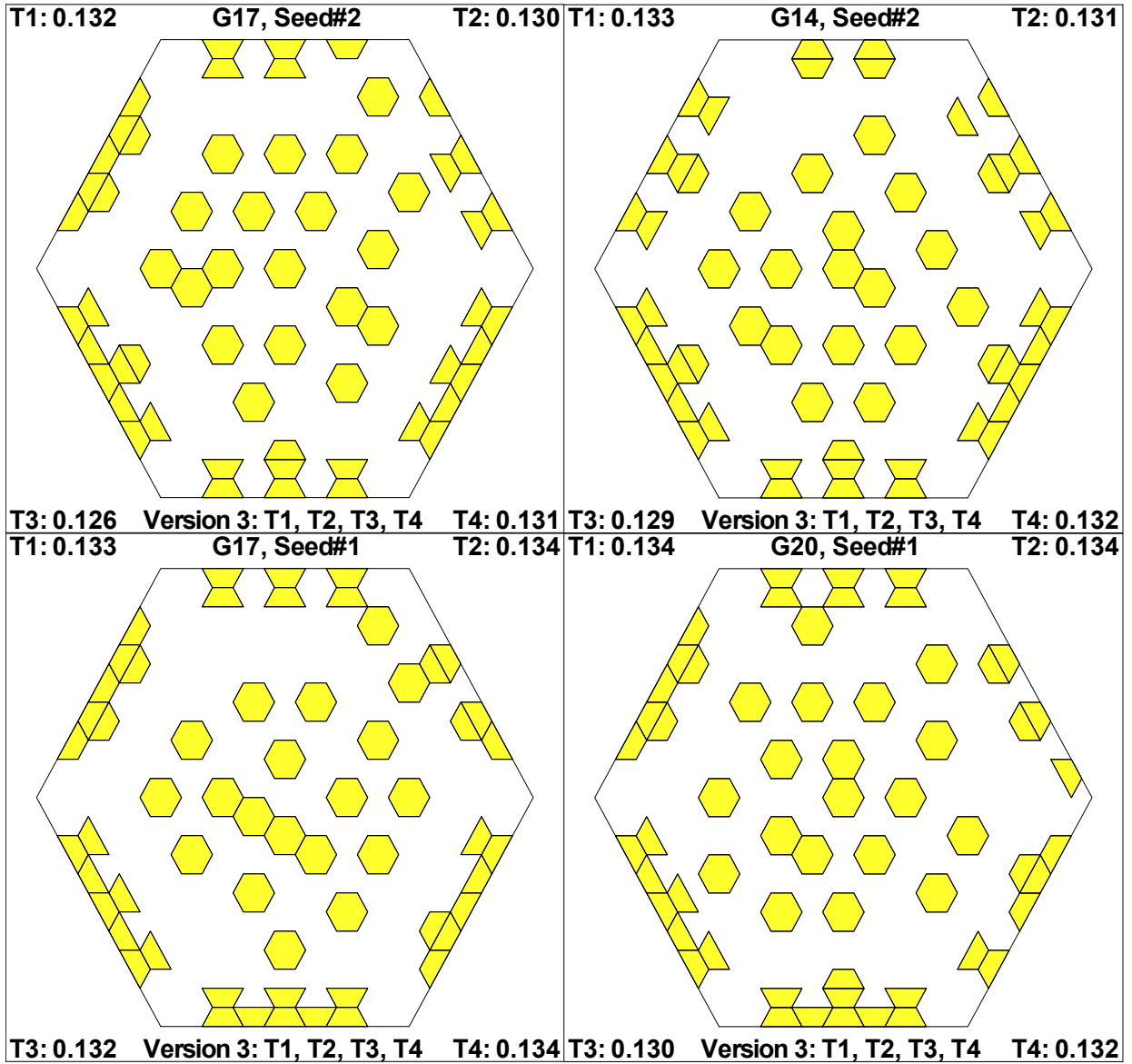


Figure 5.11 RMS error and Optimal location of piezoelectric actuators obtained by GA

Version 3 ( 60 actuators )

Note: The number in each corner in the Figure represents the RMS error corresponding to the specified type of the thermal load.

Table 5.20 Optimal voltages corresponding to optimal location (see Figure 5.11 upper left)  
for thermal load type T1 (60 actuators)

| Strip Loc. | Voltage V | Strip Loc. | Voltage V | Strip Loc. | Voltage V |
|------------|-----------|------------|-----------|------------|-----------|
| 3          | -430      | 54         | -238      | 99         | 331       |
| 4          | 340       | 59         | -674      | 111        | -122      |
| 8          | -760      | 60         | 301       | 119        | -142      |
| 9          | 661       | 64         | -446      | 121        | -204      |
| 10         | -322      | 65         | 339       | 127        | -304      |
| 13         | -426      | 71         | -134      | 129        | -282      |
| 14         | 326       | 74         | -679      | 132        | -153      |
| 20         | -400      | 75         | 469       | 135        | -106      |
| 21         | 366       | 76         | -298      | 140        | -269      |
| 23         | -282      | 79         | -613      | 146        | -382      |
| 25         | -467      | 80         | 405       | 148        | -479      |
| 26         | 273       | 81         | -175      | 151        | -191      |
| 28         | -297      | 88         | -426      | 159        | -347      |
| 30         | -321      | 89         | 334       | 164        | -182      |
| 31         | 207       | 91         | -271      | 166        | -319      |
| 37         | -483      | 93         | -678      | 170        | -167      |
| 38         | 238       | 94         | 883       | 175        | -153      |
| 42         | -868      | 95         | -499      | 177        | -343      |
| 43         | 499       | 96         | -265      | 181        | 137       |
| 47         | -320      | 98         | -398      | 187        | -144      |

Table 5.21 Optimal voltages corresponding to optimal location (see Figure 5.11 upper left)  
for thermal load type T2 (60 actuators)

| Strip Loc. | Voltage V | Strip Loc. | Voltage V | Strip Loc. | Voltage V |
|------------|-----------|------------|-----------|------------|-----------|
| 3          | -798      | 54         | -383      | 99         | 475       |
| 4          | 470       | 59         | -919      | 111        | -8        |
| 8          | -1302     | 60         | 347       | 119        | -30       |
| 9          | 949       | 64         | -617      | 121        | -84       |
| 10         | -390      | 65         | 354       | 127        | -62       |
| 13         | -774      | 71         | -235      | 129        | -112      |
| 14         | 435       | 74         | -809      | 132        | -101      |
| 20         | -547      | 75         | 576       | 135        | -5        |
| 21         | 405       | 76         | -395      | 140        | -139      |
| 23         | -342      | 79         | -815      | 146        | -144      |
| 25         | -694      | 80         | 605       | 148        | -223      |
| 26         | 406       | 81         | -230      | 151        | -156      |
| 28         | -360      | 88         | -608      | 159        | -224      |
| 30         | -479      | 89         | 484       | 164        | -71       |
| 31         | 256       | 91         | -330      | 166        | -152      |
| 37         | -615      | 93         | -875      | 170        | -157      |
| 38         | 249       | 94         | 855       | 175        | -114      |
| 42         | -1083     | 95         | -251      | 177        | -249      |
| 43         | 551       | 96         | -320      | 181        | 120       |
| 47         | -447      | 98         | -588      | 187        | -148      |

Table 5.22 Optimal voltages corresponding to optimal location (see Figure 5.11 upper left)  
for thermal load type T3 (60 actuators)

| Strip Loc. | Voltage V | Strip Loc. | Voltage V | Strip Loc. | Voltage V |
|------------|-----------|------------|-----------|------------|-----------|
| 3          | -958      | 54         | -286      | 99         | 301       |
| 4          | 440       | 59         | -947      | 111        | 109       |
| 8          | -1607     | 60         | 651       | 119        | -30       |
| 9          | 1245      | 64         | -666      | 121        | 114       |
| 10         | -697      | 65         | 582       | 127        | -80       |
| 13         | -906      | 71         | -34       | 129        | 7         |
| 14         | 306       | 74         | -873      | 132        | 149       |
| 20         | -588      | 75         | 788       | 135        | -129      |
| 21         | 293       | 76         | -181      | 140        | 50        |
| 23         | -391      | 79         | -820      | 146        | -175      |
| 25         | -798      | 80         | 742       | 148        | -40       |
| 26         | 427       | 81         | -10       | 151        | 105       |
| 28         | -396      | 88         | -535      | 159        | 41        |
| 30         | -644      | 89         | 560       | 164        | -213      |
| 31         | 443       | 91         | -282      | 166        | -78       |
| 37         | -371      | 93         | -692      | 170        | 117       |
| 38         | 342       | 94         | 728       | 175        | -114      |
| 42         | -671      | 95         | -210      | 177        | -18       |
| 43         | 450       | 96         | -271      | 181        | 217       |
| 47         | -199      | 98         | -391      | 187        | 59        |

Table 5.23 Optimal voltages corresponding to optimal location (see Figure 5.11 upper left)  
for thermal load type T4 (60 actuators)

| Strip Loc. | Voltage V | Strip Loc. | Voltage V | Strip Loc. | Voltage V |
|------------|-----------|------------|-----------|------------|-----------|
| 3          | -901      | 54         | -219      | 99         | 334       |
| 4          | 386       | 59         | -734      | 111        | -119      |
| 8          | -1608     | 60         | 466       | 119        | -94       |
| 9          | 1222      | 64         | -447      | 121        | -133      |
| 10         | -643      | 65         | 345       | 127        | -229      |
| 13         | -957      | 71         | -397      | 129        | -151      |
| 14         | 383       | 74         | -944      | 132        | -72       |
| 20         | -534      | 75         | 634       | 135        | -123      |
| 21         | 340       | 76         | -565      | 140        | -122      |
| 23         | -354      | 79         | -819      | 146        | -229      |
| 25         | -739      | 80         | 513       | 148        | -230      |
| 26         | 443       | 81         | -397      | 151        | -42       |
| 28         | -363      | 88         | -735      | 159        | -121      |
| 30         | -615      | 89         | 378       | 164        | -165      |
| 31         | 469       | 91         | -400      | 166        | -152      |
| 37         | -248      | 93         | -1158     | 170        | 18        |
| 38         | 340       | 94         | 1297      | 175        | -72       |
| 42         | -444      | 95         | -709      | 177        | -87       |
| 43         | 383       | 96         | -398      | 181        | 200       |
| 47         | -55       | 98         | -663      | 187        | 36        |

**Case 4: N=90 actuators**

Micro-GA Version 3: Initial population size 10, population size 5, scale=0.5, random=0,

crossover rate =0.5, mutation rate=0.01, restart control parameter different level=0.0

No\_of\_best\_mutation\_bits=2.

Table 5.24 RMS errors corresponding to optimal placement (90 actuators)

| Generations of inner loop | RMS for initial evaluations |         | RMS for 5000 evaluations |                | RMS for 10000 evaluations |                | RMS for 15000 evaluations |                |
|---------------------------|-----------------------------|---------|--------------------------|----------------|---------------------------|----------------|---------------------------|----------------|
|                           | Seed #1                     | Seed #2 | Seed #1                  | Seed #2        | Seed #1                   | Seed #2        | Seed #1                   | Seed #2        |
| 8                         | 0.23206                     | 0.24537 | 0.10069                  | 0.09227        | 0.09348                   | 0.08907        | 0.09058                   | 0.08658        |
| 9                         |                             |         | 0.09104                  | 0.09300        | 0.08775                   | 0.08818        | 0.08625                   | 0.08724        |
| 10                        |                             |         | 0.09118                  | 0.09243        | <b>0.08657</b>            | 0.08772        | <b>0.08564</b>            | 0.08632        |
| 11                        |                             |         | 0.09263                  | 0.08981        | 0.08831                   | 0.08839        | 0.08733                   | 0.08705        |
| 12                        |                             |         | 0.09141                  | 0.08856        | 0.09018                   | 0.08713        | 0.08970                   | 0.08654        |
| 13                        |                             |         | 0.09096                  | 0.09069        | 0.08737                   | 0.08661        | 0.08731                   | 0.08658        |
| 14                        |                             |         | 0.09143                  | 0.09052        | 0.08766                   | 0.08896        | 0.08667                   | 0.08748        |
| 15                        |                             |         | 0.09060                  | 0.08969        | 0.08766                   | 0.08793        | 0.08714                   | 0.08687        |
| 16                        |                             |         | 0.09003                  | <b>0.08824</b> | 0.08701                   | 0.08652        | 0.08570                   | 0.08612        |
| 17                        |                             |         | 0.08990                  | 0.09110        | 0.08689                   | 0.08858        | 0.08644                   | 0.08701        |
| 18                        |                             |         | <b>0.08924</b>           | 0.09280        | 0.08763                   | <b>0.08403</b> | 0.08666                   | <b>0.08390</b> |
| 19                        |                             |         | 0.08950                  | 0.09213        | 0.08679                   | 0.08757        | 0.08581                   | 0.08702        |
| 20                        |                             |         | 0.08941                  | 0.09083        | 0.08674                   | 0.08666        | 0.08659                   | 0.08539        |



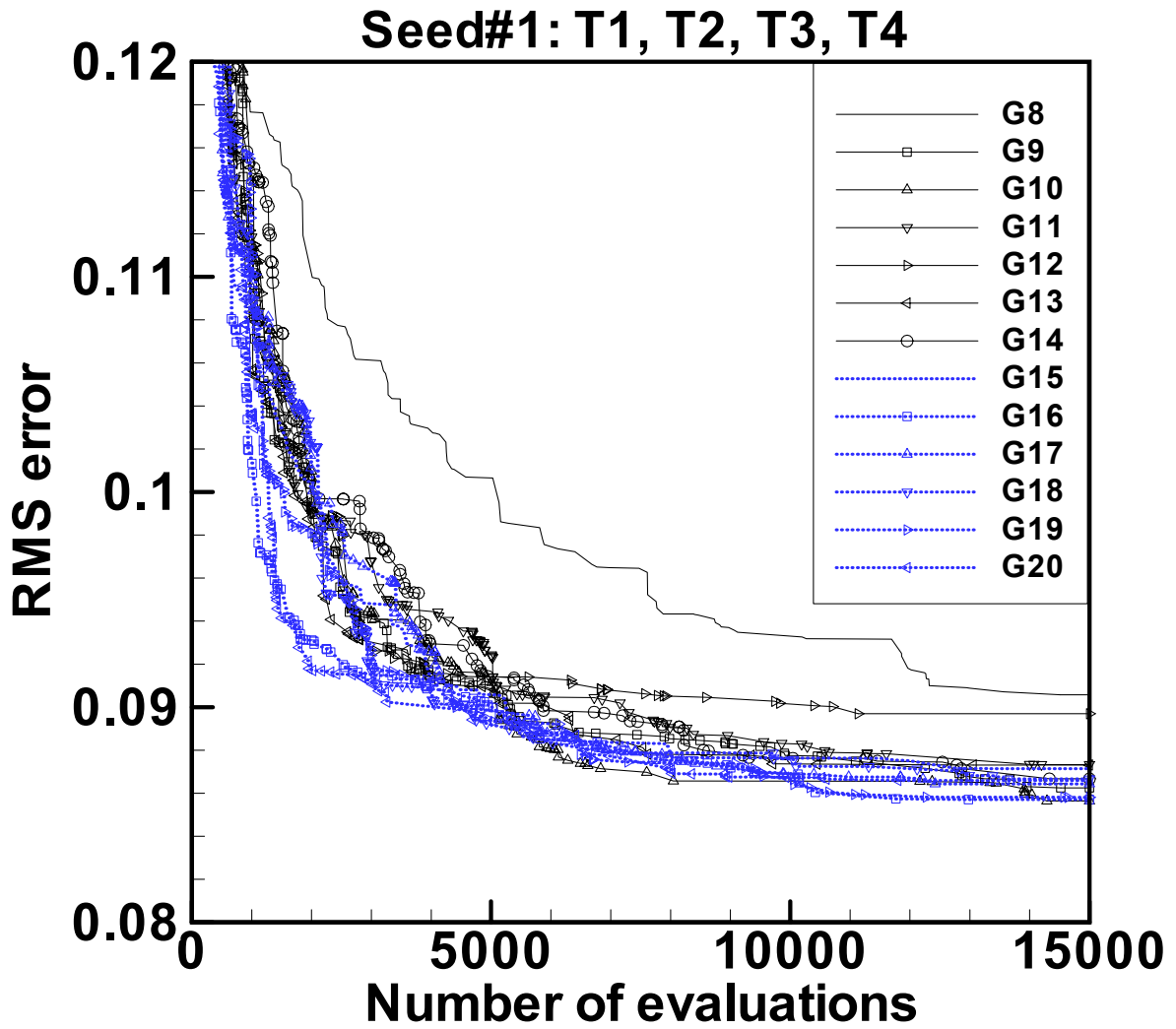


Figure 5.12 a) Performance of the GAs: Maximum of the four minimum RMS errors vs. the number of evaluations ( 90 actuators, seed#1 ).

Note: It is the optimization problem in which one set of actuators is chosen for all four thermal distortions.

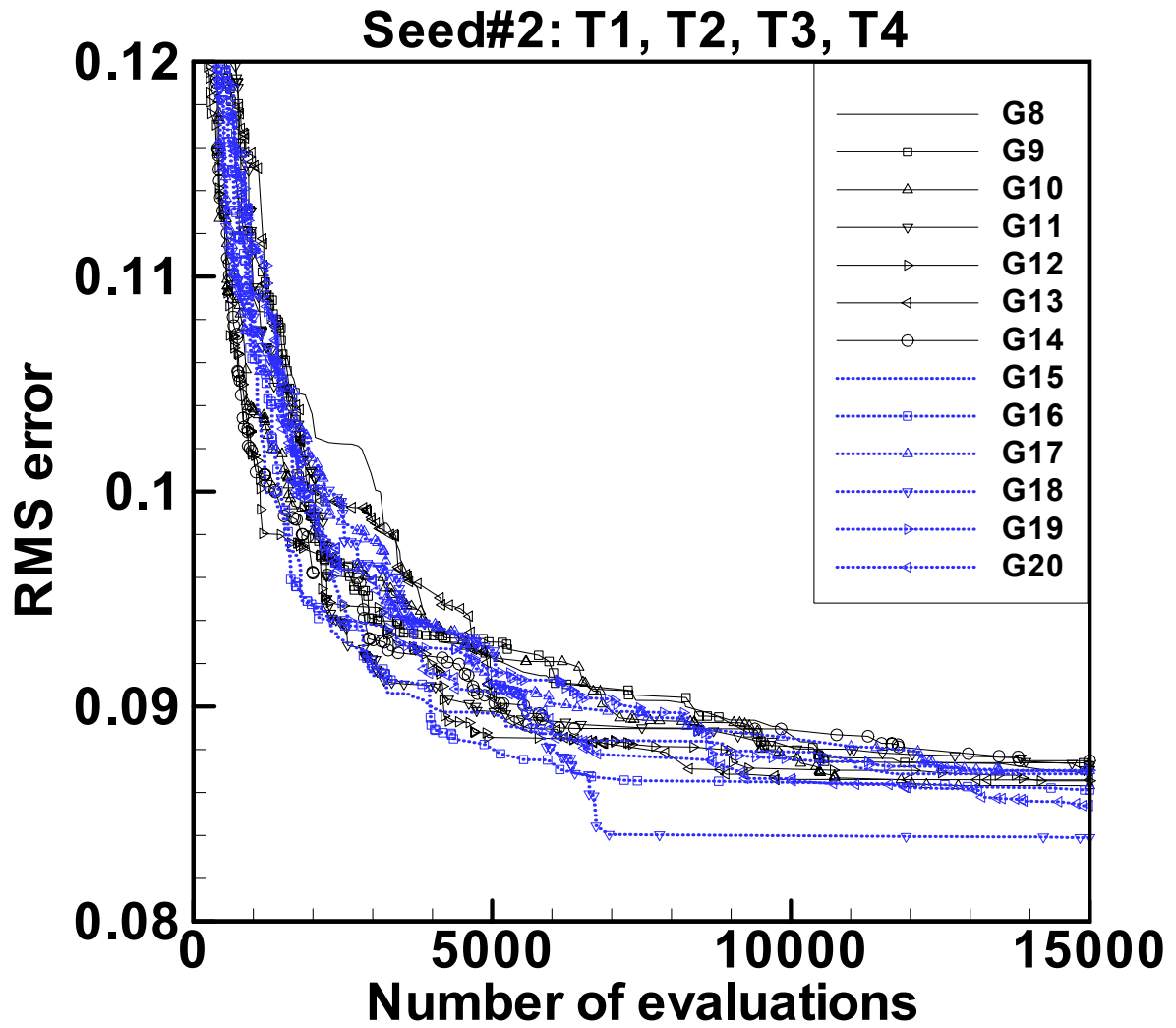


Figure 5.12 b) Performance of the GAs: Maximum of the four minimum RMS errors vs. the number of evaluations ( 90 actuators, seed#2 ).

Note: It is the optimization problem in which one set of actuators is chosen for all four thermal distortions.

For this case (nstrip=90), following observations are made:

- 1) When the number of generations in the inner loop is 18, Seed #2 in case of 10000 and 15000 evaluations shows much more superior performance than Seed#1.
- 2) The best number of generations in the inner loop is dependent on not only the number of evaluations used for termination, but also which seed generator was used. For example, in case of Seed #1, the best number of generations in the inner loop is 18, 10 and 10 corresponding to the 5000, 10000, and 15000 evaluations as the termination condition, respectively; In case of Seed #2, the best number of generations in the inner loop is 16, 18 and 18 corresponding to the 5000, 10000, and 15000 evaluations as the termination condition, respectively.
- 3) For the number of generations in the inner loop, the optimal number 18 in case of seed #2 corresponding to the 10000 and 15000 evaluations is also different from those in the case of 15, 30, 60 and 121 actuators.
- 4) The best solution for the case of 90 actuators is very close to that for the case of 121 actuators in terms of RMS errors.

Overall, the RMS value of the error for the minimum distortion is around 0.08 for 90 actuators compared to 0.07 for 121 actuators, 0.23 for 30 actuators; 0.38 for 15 actuators, 0.14 for 60 actuators; and the RMS value of the error reduces with the number of actuators used. The best number of actuators appears to be 90.

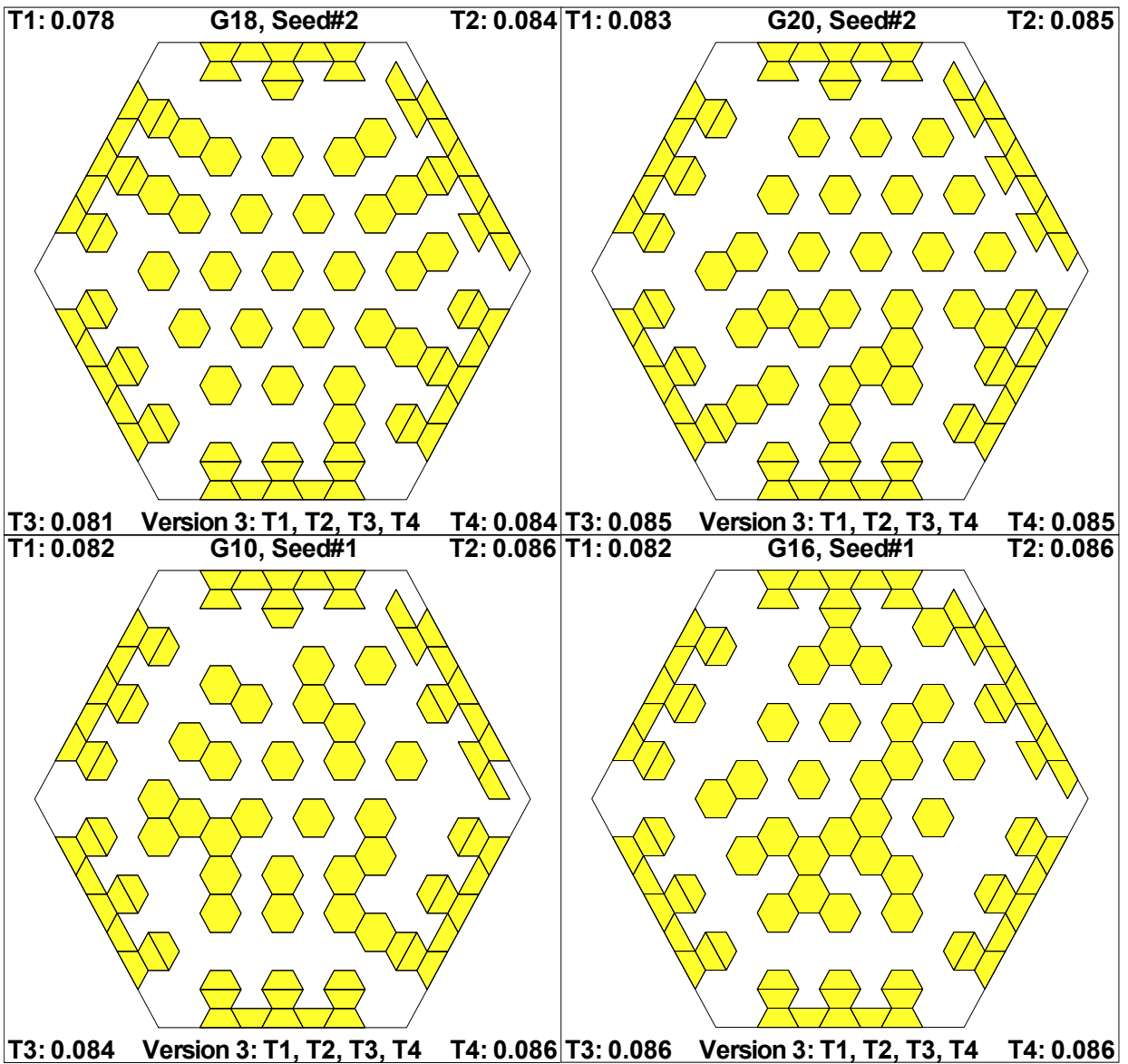


Figure 5.13 RMS error and Optimal location of piezoelectric actuators obtained by GA

Version 3 ( 90 actuators )

Note: The number in each corner in the Figure represents the RMS error corresponding to the specified type of the thermal load.

Table 5.25 Optimal voltages corresponding to optimal location (see Figure 5.13 upper left)  
for thermal load type T1 (90 actuators)

| Strip Loc. | Voltage V | Strip Loc. | Voltage V | Strip Loc. | Voltage V |
|------------|-----------|------------|-----------|------------|-----------|
| 3          | -370      | 47         | -453      | 96         | -259      |
| 4          | 451       | 48         | 333       | 98         | -465      |
| 5          | -83       | 51         | 63        | 99         | 521       |
| 6          | -221      | 54         | -338      | 100        | -122      |
| 8          | -532      | 55         | 312       | 111        | -148      |
| 9          | 616       | 57         | -203      | 113        | 25        |
| 10         | -234      | 59         | -546      | 118        | -198      |
| 11         | -222      | 60         | 644       | 121        | -209      |
| 13         | -376      | 61         | -260      | 123        | 34        |
| 14         | 509       | 62         | -217      | 126        | -134      |
| 15         | -175      | 64         | -338      | 129        | -313      |
| 20         | -467      | 65         | 344       | 132        | -156      |
| 21         | 534       | 71         | -477      | 137        | -312      |
| 22         | -137      | 72         | 588       | 140        | -306      |
| 23         | -254      | 73         | -223      | 145        | -188      |
| 25         | -662      | 74         | -257      | 148        | -363      |
| 26         | 755       | 76         | -663      | 151        | -186      |
| 27         | -354      | 77         | 758       | 156        | -307      |
| 28         | -249      | 78         | -354      | 159        | -310      |
| 30         | -470      | 79         | -258      | 163        | 39        |
| 31         | 530       | 81         | -477      | 164        | -154      |
| 32         | -168      | 82         | 532       | 167        | -312      |
| 35         | 45        | 83         | -149      | 170        | -138      |
| 37         | -464      | 88         | -472      | 175        | -208      |
| 38         | 355       | 89         | 525       | 178        | -209      |
| 40         | -229      | 90         | -143      | 180        | -15       |
| 42         | -693      | 91         | -260      | 183        | 28        |
| 43         | 788       | 93         | -651      | 185        | -148      |
| 44         | -382      | 94         | 714       | 187        | 23        |
| 45         | -216      | 95         | -290      | 191        | -15       |

Table 5.26 Optimal voltages corresponding to optimal location (see Figure 5.13 upper left)  
for thermal load type T2 (90 actuators)

| Strip Loc. | Voltage V | Strip Loc. | Voltage V | Strip Loc. | Voltage V |
|------------|-----------|------------|-----------|------------|-----------|
| 3          | -702      | 47         | -561      | 96         | -306      |
| 4          | 642       | 48         | 393       | 98         | -623      |
| 5          | -130      | 51         | 13        | 99         | 586       |
| 6          | -335      | 54         | -467      | 100        | -99       |
| 8          | -954      | 55         | 335       | 111        | -17       |
| 9          | 900       | 57         | -278      | 113        | 58        |
| 10         | -273      | 59         | -760      | 118        | -30       |
| 11         | -337      | 60         | 833       | 121        | -106      |
| 13         | -701      | 61         | -362      | 123        | 40        |
| 14         | 741       | 62         | -279      | 126        | -2        |
| 15         | -304      | 64         | -485      | 129        | -119      |
| 20         | -635      | 65         | 372       | 132        | -107      |
| 21         | 636       | 71         | -618      | 137        | -110      |
| 22         | -180      | 72         | 682       | 140        | -163      |
| 23         | -310      | 73         | -282      | 145        | -50       |
| 25         | -900      | 74         | -296      | 148        | -169      |
| 26         | 947       | 76         | -843      | 151        | -141      |
| 27         | -436      | 77         | 899       | 156        | -134      |
| 28         | -315      | 78         | -394      | 159        | -205      |
| 30         | -650      | 79         | -295      | 163        | 66        |
| 31         | 649       | 81         | -590      | 164        | -78       |
| 32         | -225      | 82         | 582       | 167        | -188      |
| 35         | 11        | 83         | -110      | 170        | -121      |
| 37         | -558      | 88         | -622      | 175        | -131      |
| 38         | 395       | 89         | 585       | 178        | -171      |
| 40         | -303      | 90         | -92       | 180        | -40       |
| 42         | -860      | 91         | -309      | 183        | 51        |
| 43         | 943       | 93         | -865      | 185        | -108      |
| 44         | -468      | 94         | 810       | 187        | 27        |
| 45         | -299      | 95         | -204      | 191        | -26       |

Table 5.27 Optimal voltages corresponding to optimal location (see Figure 5.13 upper left)  
for thermal load type T3 (90 actuators)

| Strip Loc. | Voltage V | Strip Loc. | Voltage V | Strip Loc. | Voltage V |
|------------|-----------|------------|-----------|------------|-----------|
| 3          | -879      | 47         | -388      | 96         | -253      |
| 4          | 811       | 48         | 336       | 98         | -465      |
| 5          | -312      | 51         | 104       | 99         | 500       |
| 6          | -411      | 54         | -484      | 100        | -121      |
| 8          | -1173     | 55         | 491       | 111        | 73        |
| 9          | 1145      | 57         | -207      | 113        | 94        |
| 10         | -528      | 59         | -673      | 118        | -20       |
| 11         | -411      | 60         | 573       | 121        | 51        |
| 13         | -878      | 61         | 38        | 123        | 85        |
| 14         | 854       | 62         | -230      | 126        | -81       |
| 15         | -432      | 64         | -510      | 129        | 8         |
| 20         | -740      | 65         | 528       | 132        | 84        |
| 21         | 725       | 71         | -409      | 137        | -100      |
| 22         | -321      | 72         | 527       | 140        | 63        |
| 23         | -352      | 73         | -116      | 145        | -151      |
| 25         | -1023     | 74         | -199      | 148        | -21       |
| 26         | 1047      | 76         | -556      | 151        | 120       |
| 27         | -498      | 77         | 647       | 156        | -128      |
| 28         | -342      | 78         | -189      | 159        | 36        |
| 30         | -737      | 79         | -194      | 163        | 29        |
| 31         | 697       | 81         | -339      | 164        | -154      |
| 32         | -209      | 82         | 377       | 167        | -44       |
| 35         | 100       | 83         | 94        | 170        | 78        |
| 37         | -365      | 88         | -492      | 175        | -122      |
| 38         | 329       | 89         | 489       | 178        | 6         |
| 40         | -122      | 90         | 13        | 180        | 56        |
| 42         | -571      | 91         | -256      | 183        | 43        |
| 43         | 639       | 93         | -684      | 185        | -28       |
| 44         | -211      | 94         | 675       | 187        | 71        |
| 45         | -123      | 95         | -157      | 191        | 33        |

Table 5.28 Optimal voltages corresponding to optimal location (see Figure 5.13 upper left)  
for thermal load type T4 (90 actuators)

| Strip Loc. | Voltage V | Strip Loc. | Voltage V | Strip Loc. | Voltage V |
|------------|-----------|------------|-----------|------------|-----------|
| 3          | -841      | 47         | -244      | 96         | -388      |
| 4          | 778       | 48         | 250       | 98         | 797       |
| 5          | -293      | 51         | 141       | 99         | 747       |
| 6          | -406      | 54         | -387      | 100        | -280      |
| 8          | -1177     | 55         | 417       | 111        | -112      |
| 9          | 1132      | 57         | -170      | 113        | 47        |
| 10         | -488      | 59         | -546      | 118        | -150      |
| 11         | -414      | 60         | 554       | 121        | -145      |
| 13         | -908      | 61         | -91       | 123        | 52        |
| 14         | 882       | 62         | -197      | 126        | -118      |
| 15         | -428      | 64         | -335      | 129        | -181      |
| 20         | -648      | 65         | 350       | 132        | -85       |
| 21         | 648       | 71         | -849      | 137        | -196      |
| 22         | -234      | 72         | 849       | 140        | -143      |
| 23         | -315      | 73         | -378      | 145        | -150      |
| 25         | -926      | 74         | -383      | 148        | -172      |
| 26         | 967       | 76         | -1095     | 151        | -36       |
| 27         | -442      | 77         | 1114      | 156        | -170      |
| 28         | -310      | 78         | -530      | 159        | -108      |
| 30         | -672      | 79         | -374      | 163        | 49        |
| 31         | 641       | 81         | -770      | 164        | -128      |
| 32         | -163      | 82         | 728       | 167        | -120      |
| 35         | 127       | 83         | -267      | 170        | -4        |
| 37         | -265      | 88         | -825      | 175        | -117      |
| 38         | 281       | 89         | 761       | 178        | -49       |
| 40         | -49       | 90         | -288      | 180        | 55        |
| 42         | -390      | 91         | -392      | 183        | 57        |
| 43         | 474       | 93         | -1112     | 185        | -41       |
| 44         | -133      | 94         | 1073      | 187        | 57        |
| 45         | -44       | 95         | -455      | 191        | 41        |

In summary, the best result for each case of actuators is shown in Table 5.29.



Table 5.29 RMS error from all cases of actuators (best results only)

| Number of actuators | Generations of inner loop | Seed No. | RMS error for various thermal loads |         |         |         |
|---------------------|---------------------------|----------|-------------------------------------|---------|---------|---------|
|                     |                           |          | T1                                  | T2      | T3      | T4      |
| 15                  | 12                        | 1        | 0.37619                             | 0.37962 | 0.37087 | 0.38018 |
| 30                  | 20                        | 1        | 0.22012                             | 0.22819 | 0.22276 | 0.22882 |
| 60                  | 17                        | 2        | 0.13164                             | 0.13028 | 0.12643 | 0.13118 |
| 90                  | 18                        | 2        | 0.07753                             | 0.08390 | 0.08055 | 0.08382 |
| 121                 | 13                        | 1        | 0.06621                             | 0.07732 | 0.07257 | 0.07788 |

### Comments about the power

The power of the system can be computed by the following formulation,

$$P = \sum_{i=1}^n \frac{U^2}{R}$$

where  $n$  is the number of the piezoelectric actuators,  $U$  is the electric voltage applied across the piezoelectric actuators and  $R$  is the resistant of the piezoelectric actuators. The resistance of the piezoelectric actuators is about 30 M $\Omega$ , which was measured on a sheet of PZT under static conditions at room temperature by Mr. Eric J. Ruggiero (PhD Candidate) and Mr. Eddie Simmers (Master student) at Center for Intelligent Material Systems and Structures, Virginia Tech. So the maximum value of the power for all of the cases is less than 4 W.

### 5.8 Conclusions

Through extensive numerical experiments we found that the most distinct natures of genetic algorithms are random and robust. Here we are not considering theoretical genetic algorithms with unlimited or unrealistic big number of evaluations. Right now we are considering practical genetic algorithms with the limited number of evaluations. By random, we mean that we can not precisely predict the performance of genetic algorithms on future evaluations based on their performance on previous evaluations. By robust, we mean that

although genetic algorithms have their random nature the range of their findings are usually small from their different runs after a certain number of evaluations and they are still capable of finding a very good solution by simply adjusting the parameter setting or using another random seed generator. Because of their nonlinear convergence, the genetic algorithms can be used to get an appropriate solution with a few hundreds of evaluations. The genetic algorithms are also easy to use to generate an alternative solution. To get high quality solutions in the design of complex adaptive structures using finite element analysis and genetic algorithm optimization, the multiple runs including different random seed generators are necessary. The time of the investigation can be significantly reduced using a very coarse grain parallel computing, simply running multiple jobs at the same time. Depending on the load of computer and the number of jobs we can run simultaneously, the time of the investigation can be reduced by a factor of  $n$ . For example, if we can simultaneously submit 4 jobs, we maybe reduce the time of investigation by a factor of 4 at best. From Table 5.29, although the RMS error reduces with the number of actuators, the reduction of RMS error may not be worth the effort of increasing the number of actuators. From the results of the optimal voltages we can see that some voltages are extremely high. This makes us further consider the optimal problems with voltage constraints. Overall, the methodology of using finite element analysis and genetic algorithm optimization is a very good approach and GA version 3 is efficient, reliable and robust optimization tool for the challenging problem – optimal placements of a large number of actuators in the design of next generation adaptive structures.

## References

1. Crawley, E., "Intelligent Structures for Aerospace: A Technology Overview and Assessment," *AIAA Journal*, Vol. 32, No. 8, 1994, pp.1689-1699.
2. Sunar, M. and Rao, S. S., "Recent Advances in Sensing and Control of Flexible Structures via Piezoelectric Materials Technology," *Applied Mechanics Reviews*, Vol. 52, No. 1, 1999, pp. 1-16.
3. Chopra, I., "Review of State of Art of Smart Structures and Integrated Systems," Presented at the *AIAA/ASME/ASCE/AHS/AHC 42<sup>nd</sup> Structures, Structural Dynamics and Materials Conference*, Seattle, WA, April 16-19, 2001; also *AIAA Journal*, Vol. 40, No. 11, 2002, pp. 2145-2187.
4. Garg, D. P., Zikry, M. A., and Anderson G. L., "Current and potential future research activities in adaptive structures: an ARO perspective," *Smart Materials and Structures*, Vol. 10, 2001, pp. 610-623.
5. McGowan, A.-M. R., Washburn, A. E., Horta, L. G., Bryant, R. G., Cox, D. E., Siochi, E. J., Padula, S. L., Holloway, N. M., "Recent Results from NASA's Morphing Project," Industrial and Commercial Applications of Smart Structures Technologies, Proceedings of SPIE, Vol. 4698, 2002, pp. 97-111.
6. Frecker, M. I., "Recent Advances in Optimization of Smart Structures and Actuators," *Journal of Intelligent Material Systems and Structures*, Vol. 14, No. 1, 2003, pp. 207–216.
7. Sanders, B., Crowe, R. and Garcia, E., "Defense Advanced Research Projects Agency – Smart Materials and Structures Demonstration Program Overview," *Journal of Intelligent Material Systems and Structures*, Vol. 15, No. 4, 2004, pp. 227–233.

8. MacMartin, D. G., "Control Challenges for Extremely Large Telescopes," *Industrial and Commercial Applications of Smart Structures Technologies*, Proceedings of SPIE, Vol. 5054, 2003, pp. 275-286.
9. Sheng, L. and Kapania, R. K., "Genetic Algorithms for the Optimization of Piezoelectric Actuator Locations," Presented as Paper AIAA-2000-1581, Proceedings of *AIAA/ASME/ASCE/AHS/AHC 41<sup>st</sup> Structures, Structural Dynamics and Materials Conference*, Atlanta, GA, April 3-6, 2000; also *AIAA Journal*, Vol. 39, No. 9, 2001, pp. 1818-1822.
10. Kapania, R. K. and Sheng, L., "Towards More Effective Genetic Algorithms for the Optimization of Piezoelectric Actuator Locations," Presented as Paper AIAA-2001-1627, Proceedings of *AIAA/ASME/ASCE/AHS/AHC 42<sup>nd</sup> Structures, Structural Dynamics and Materials Conference*, Seattle, WA, April 16-19, 2001; also *AIAA Journal*, Vol. 40, No. 6, 2002, pp. 1246-1250.
11. David. L. Carroll's FORTRAN Genetic Algorithm Driver.  
<http://www.aic.nrl.navy.mil:80/galist/src/#fortran>
12. Kapania, R. K. and Mohan, P., "Static, Free Vibration and Thermal Analysis of Composite Plates and Shells Using a Flat Triangular Shell Element," *Computational Mechanics: An International Journal*, Vol. 17, No. 5, 1996, pp. 343-357.
13. Kapania, R. K., Mohan, P., and Jakubowski, A., "Control of Thermal Deformations of Spherical Mirror Segment," Paper AIAA-96-4145, *Journal of Spacecraft and Rockets*, Vol. 35, No. 2, 1998, pp. 156-162.
14. Pearson, E., and Stepp, L., "Response of Large Optical Mirrors to Thermal Distributions," *Proceedings of SPIE—The International Society for Optical Engineering*,

- Vol. 748, 1987, pp. 215-228.
15. Furuya, H. and Haftka, R. T., "Combining Genetic and Deterministic Algorithms for Locating Actuators on Space Structures," *Journal of Spacecraft and Rockets*, Vol. 33, No. 3, 1996, pp. 422-427.
  16. Hajela, P., "Nongradient Methods in Multidisciplinary Design Optimization—Status and Potential," *JOURNAL OF AIRCRAFT*, Vol. 36, No. 1, 1999, pp. 255-265.
  17. Padula, S. L. and Kincaid, R. K. "Optimization Strategies for Sensor and Actuator Placement," NASA, TM-1999-209126, April, 1999.
  18. Krishnakumar, K., "Micro-Genetic Algorithms for Stationary and Non-Stationary Function Optimization," Proceedings of SPIE, Intelligent Control and Adaptive Systems, Vol. 1196, 1989, pp.289-296.
  19. Grefenstette, J. J. "Optimization of Control Parameters for Genetic Algorithms," IEEE Transactions on Systems, Man, and Cybernetics, Vol. SMC-16, No. 1, pp. 122-128.
  20. Goldberg, D. E., *Genetic Algorithms in Search, Optimization, and Machine Learning*, Addison-Wesley, 1989.
  21. Mitchell, M., *An Introduction to Genetic Algorithms*, MIT Press, 1996.
  22. Michalewicz, Z., *Genetic Algorithms + Data Structures = Evolution Programs*, 3rd ed., Springer, 1996
  23. Holland, J. H., "Genetic algorithms," *Scientific American*, July, 1992, pp. 66-72.
  24. Dasgupta, D. and Michalewicz, Z., "Evolutionary Algorithms—An Overview," in *Evolutionary Algorithms in Engineering Applications*, Dasgupta, D. and Michalewicz, Z. (eds.), Springer, 1997.
  25. De Jong, K., "Evolutionary Computation: Recent Developments and Open Issues," in

*Evolutionary Algorithms in Engineering and Computer Science*, Miettinen, K.,  
Neittaanmaki, P., and etc. (eds.) John Wiley & Sons, Ltd, 1999.

26. Fogel, D., B., “Some Recent Important Foundational Results in Evolutionary  
Computation,” in *Evolutionary Algorithms in Engineering and Computer Science*,  
Miettinen, K., Neittaanmaki, P., and etc. (eds.) John Wiley & Sons, Ltd, 1999.
27. Gen, M., and Cheng, R., *Genetic Algorithms & Engineering Optimization, Chapter 1*,  
John Wiley & Sons, Inc., 2000.

## **Chapter 6. Summary and Conclusions**

### **6.1 Major contributions**

The dissertation first reviewed some basic concepts related to finite element method, genetic algorithms optimization and smart structures and proposed a solution methodology for addressing one of major concerns in the design of next generation large-scale adaptive structures--optimal placement of a large number of actuators by a combination of general finite element analysis techniques and genetic algorithms optimization techniques.

With regard to the finite element analysis, the dissertation first reviewed some fundamental issues of general reliable finite element technology such as convergence, patch test, locking problem and singularity of finite element results, and then reviewed the state-of-the-art plate and shell finite elements. Also, the dissertation presented the three most frequently used approaches to derive the finite element formulation, including Galerkin weighted residual method, principle of virtual work and general variational principles. The dissertation chose the second approach, that is, the principle of virtual work, to derive the finite element formulation. There are two major methodologies to develop the finite element for plates and shells, using flat shell element that is composed of membrane element and bending element or using curved shell element. The dissertation facilitates the first approach by systematically presenting the relevant key techniques. The Allman triangular element was chosen as the membrane element, but derived from linear strain triangular element by using the Cook's transformation. We clearly demonstrated the transformed element was indeed the Allman triangular element (See Section 2.5). The discrete Kirchhoff triangular (DKT) element was chosen as the bending element. Because the high efficiency and accuracy of DKT element but lack of document of its derivation, we derived DKT elements in detail (See Section 2.6).

Many flat shell elements neglect the effects of anisotropic membrane-bending coupling. In the dissertation, the coupling effect is included in the element formulation. The nonlinear finite element formulation, including the linear formulation, was derived for the analysis of smart structures under thermal and electric loads (See Section 2.7).

With regards to optimization techniques, the dissertation chose the most general global optimization technique – Genetic Algorithms as an optimizer. The series of genetic algorithms were developed, which include the high efficient GA Version 3 with hill-climbing technique (See Chapter 3 to 5, and Appendix A).

The global optimum solution is the solution that outperforms all others within the design space. Searching for the global optimum is largely an academic problem. The engineering designer, faced with all of the complexities including qualitative criteria and uncertainty is searching generally for a solution that best satisfies immediate needs whilst outperforming previous designs. The rapid convergence of genetic algorithms demonstrated they are well suited for these situations

With regards to smart structures, the dissertation first reviewed the smart materials and state-of-the-art smart structural technology, and then studied one of the most critical and challenging problem for developing next generation of large scale smart structures -- optimization of a relatively large number of piezoelectric actuator locations. With regards to solution methodology of large complex design problem of smart structures, the dissertation developed the methodology of combining two major tools—finite elements and genetic algorithms. This is the first dissertation to have successfully solved the large-scale optimization problem of optimal placement of a large number of piezoelectric actuators on the adaptive structures by using the method of combined FEA and GAs, and the efficient



optimizer -- genetic algorithms were developed (See Chapter 3 to 5, and Appendix A, and the best designs for 30, 121, 15, 60 and 90 actuators are shown upper left in Figure 5.4, Figure 5.6, Figure 5.8, Figure 5.10, and Figure 5.12, respectively).

## 6.2 Perspective and Future directions

Based on our experience of developing the efficient finite elements and genetic algorithms for the design of large scale smart structures, the following future directions are suggested.

1. In addition to the thermal loads, the real system is usually subjected to vibration environments and may, compared to thickness, undergo large deformations. Therefore, the current linear static finite element analysis should be extended to include both dynamic analysis and nonlinear analysis, including large deformation and nonlinear piezoelectric constitutive relations.
2. Neither the membrane element nor the bending element used in dissertation is perfect. Each of them still has some problems. For example, the membrane element has the rotation degree problem i.e. there is no clear definition of  $\omega$ , not a real rotation,  $u_i$  is not quadratic, thus inferior to the LST, and the element has an unusual zero-energy mode. The bending element doesn't account for shear deformation and is not appropriate to analyze the thick plate because the shear deformation is important for thick plates, especially thick laminated plates. Developing more efficient, reliable triangular flat/curved shell element to solve the co-plane singularity and shear locking still needs some effort. Perhaps the best way to do this is through the use of combination of updated membrane and bending elements. Higher order shear deformation theory can also be included. Also, since no experimental data was available for us, it will be a good practice to check our best results using commercial

software such as MSC/PATRAN/NASTRAN, ABAQUS.

3. Among the optimal solutions obtained here, voltages on certain piezoelectric actuators are very high. It would be important to consider the optimization problem under voltage constraints. This would however require large computational resources.
4. The future advanced mirror systems should maintain highest accuracy of surface during their operation. The systems must make a rapid response to the changing in the environment. Therefore, more complex optimization problem should include real-time control subsystem, which consists of sensors, actuators and micro-controllers.
5. Our research shows that when genetic algorithms are used to solve large complex optimization problems, it is usually a good advice to perform multiple runs from different parameter settings and different seed generators in order to get high quality solutions. It is also shown that the time of total investigation can be significantly reduced by simultaneously running the multiple jobs. From these points it seems that developing parallel GAs is not necessary. However, because the parallel GAs with timely communication best imitate the evolution of nature, they have a greater potential to get better results and are thus worth developing.

## **Appendix A. Optimization of Piezoelectric Actuator Locations by Finite Element Method and Genetic Algorithms**

In this appendix, the performance of the initial combination of FEM and GAs on the first type of optimization problem (GA version I) is documented. The feasibility of using GAs to optimize a large scale of location problem is demonstrated.

### **A.1 Abstract**

Placement of sensors/actuators in an optimal fashion has drawn significant attention recently due to its importance in many applications such as sensing and control of smart structures. One example is to control the surface accuracy of the mirrors to be used in the next generation of astronomical telescopes. A promising method is to use a given number of piezoelectric actuators bonded onto the rear surface of the primary mirror to correct its distortions without imposing a significant weight penalty. The problem is how to find the optimal locations of piezoelectric actuators to maximize their effectiveness. In general, this is a difficult and computationally intensive combinatorial optimization problem. Kapania and Mohan<sup>(1)</sup> used Dlorenzo algorithm---a heuristic integer programming approach, to study two cases: (i) using 30 strips, and (ii) using 121 strips under 4 different temperature distributions. A drawback of Dlorenzo algorithm is its inability to find optimal distribution for more than one type of disturbances. Also the solution obtained by such an approach may be a local minimum. The present work is focused on the general case using a modified genetic algorithm<sup>(2)</sup>---a robust global stochastic search technique based on the mechanism of natural selection and natural genetics, as an optimizer to find the optimal placements for each temperature distribution. A recently developed laminated triangular shell element<sup>(3)</sup> is used to

---

This appendix contains parts of the materials presented at ASME Mechanics and Materials Conference, Virginia Tech., June 27-30, 1999.

model the mirror. The research shows that the modified genetic algorithm gets slightly better results than those given by DeLorenzo's algorithm. The effect of changing the number of actuators is being investigated so as to get the minimum number of actuators needed to meet the required surface accuracy.

### **A.2 DeLorenzo's algorithm**

The DeLorenzo's algorithm, a heuristic integer programming approach, starts with an initial configuration of 193 strips, as shown in Fig.1. The steps in this algorithm are as follows:

- 1) Remove each of the strips from the initial configuration of  $m$  strips ( $m=193$ ) one at a time, and determine the RMS error due to  $m$  configurations of  $m-1$  strips.
- 2) Rank the strips in ascending order of the RMS error.
- 3) Remove the strip that results in the smallest RMS error, to obtain a new configuration of  $m-1$  strips.
- 4) Repeat steps 1-3 until the desired number  $n$  (30 or 121) of strips is reached.

The computational cost of DeLorenzo's algorithm is larger than  $(193+n+1)*((193-n)/2)$  evaluations of the configuration of desired number. For example, for  $n=30$  strips, the total number of evaluations = 18256; and for  $n=121$  strips, Total number of evaluations = 11340. The disadvantage of DeLorenzo's algorithm is that the obtained shape control could be local minimum.

### **A.3 Genetic Algorithms**

The Genetic Algorithms, GA Version 1 was developed by modifying Carroll's FORTRAN Genetic Algorithm Driver<sup>(2)</sup>, such as applying the constraint to bit strings (chromosome), changing selection scheme, and modifying some important parameters.

Coding: directly mapping, 193 bits

Selection: elite selection, tournament selection

Crossover: uniform crossover

### A.4 Case Studies

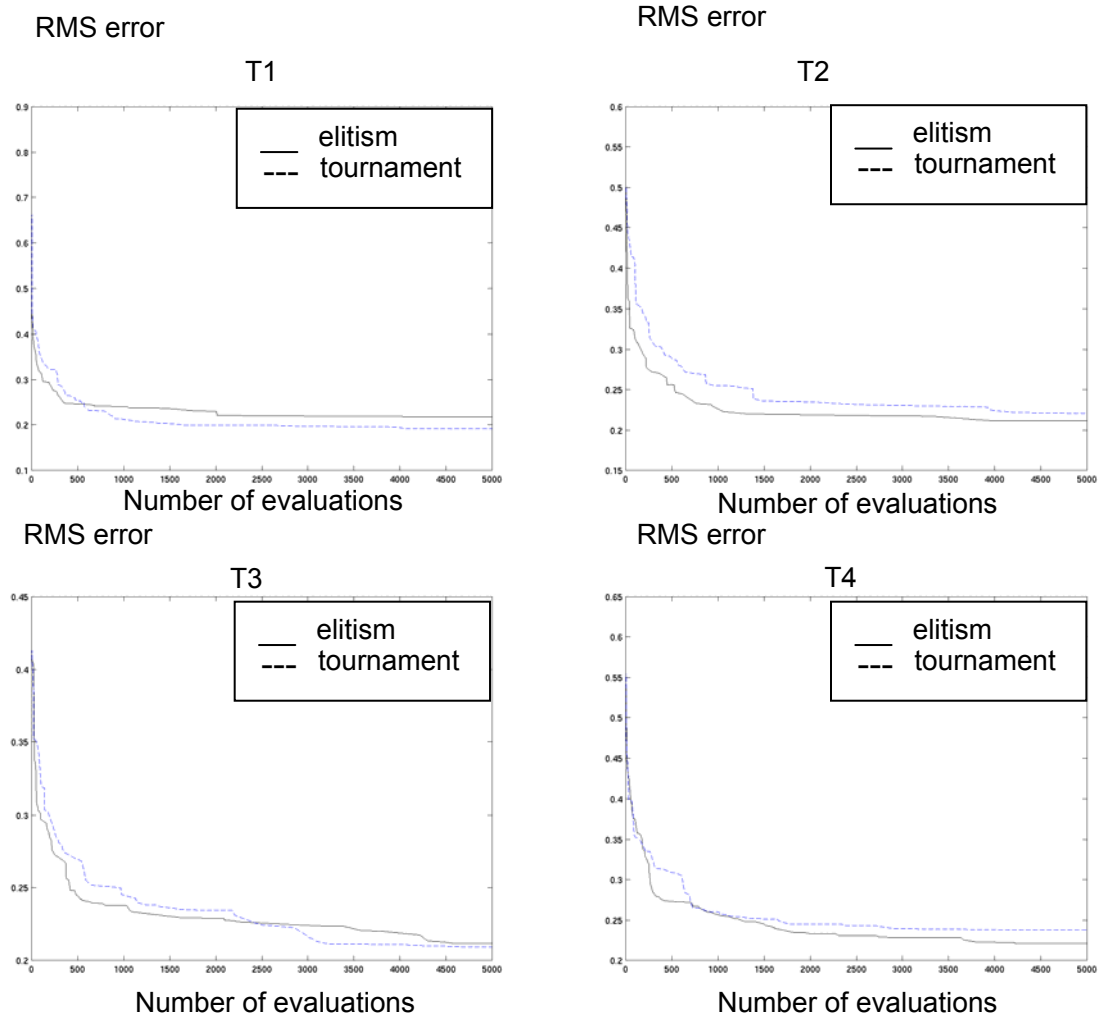


Figure A.1 Performance of the GAs versus the number of evaluations on thermal load T1, T2, T3, and T4, respectively

n=30

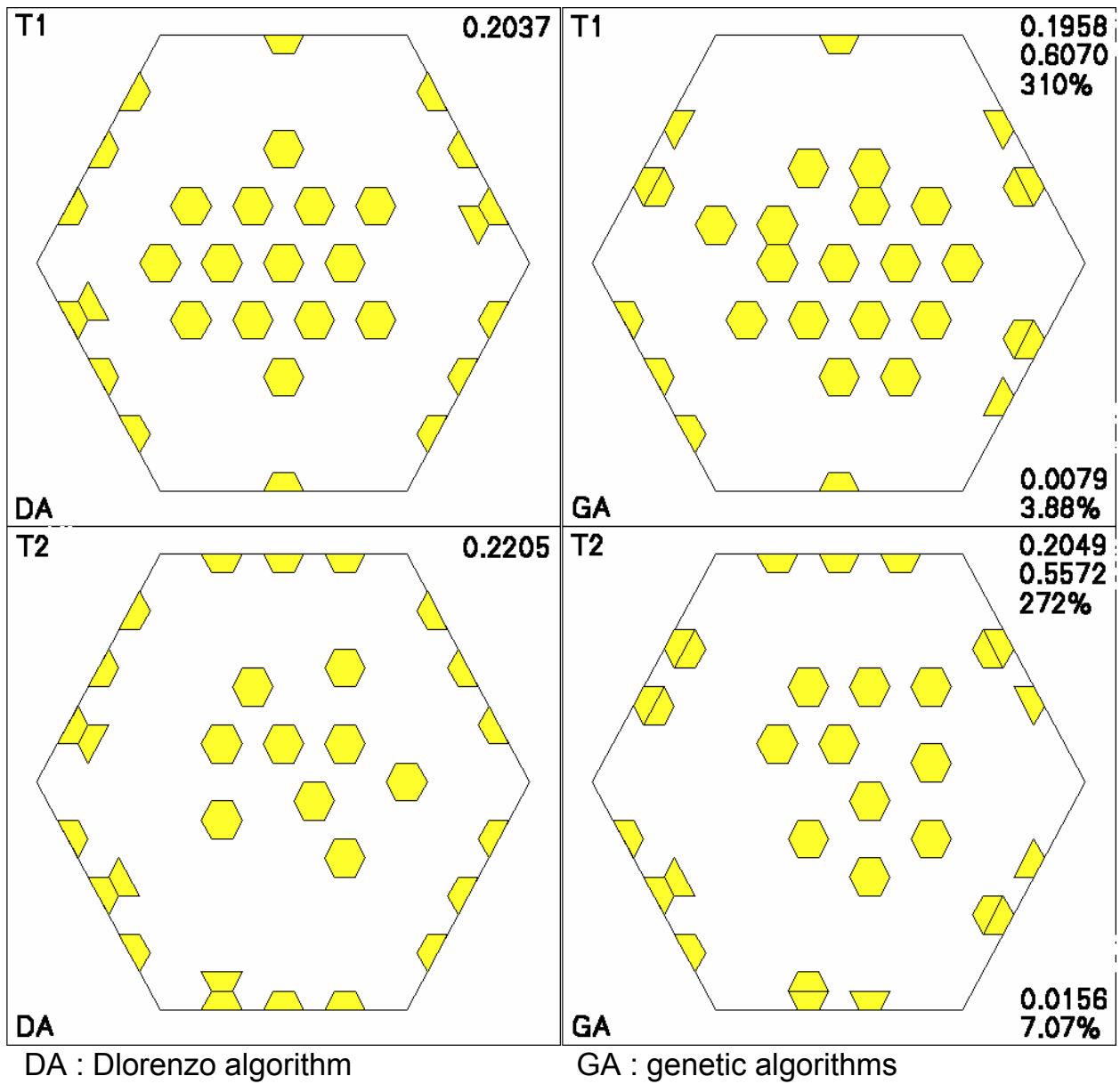


Figure A.2 a) Optimal locations for the thermal load T1 and T2 obtained by DeLorenzo algorithm and Genetic Algorithms ( 30 actuators )

n=30

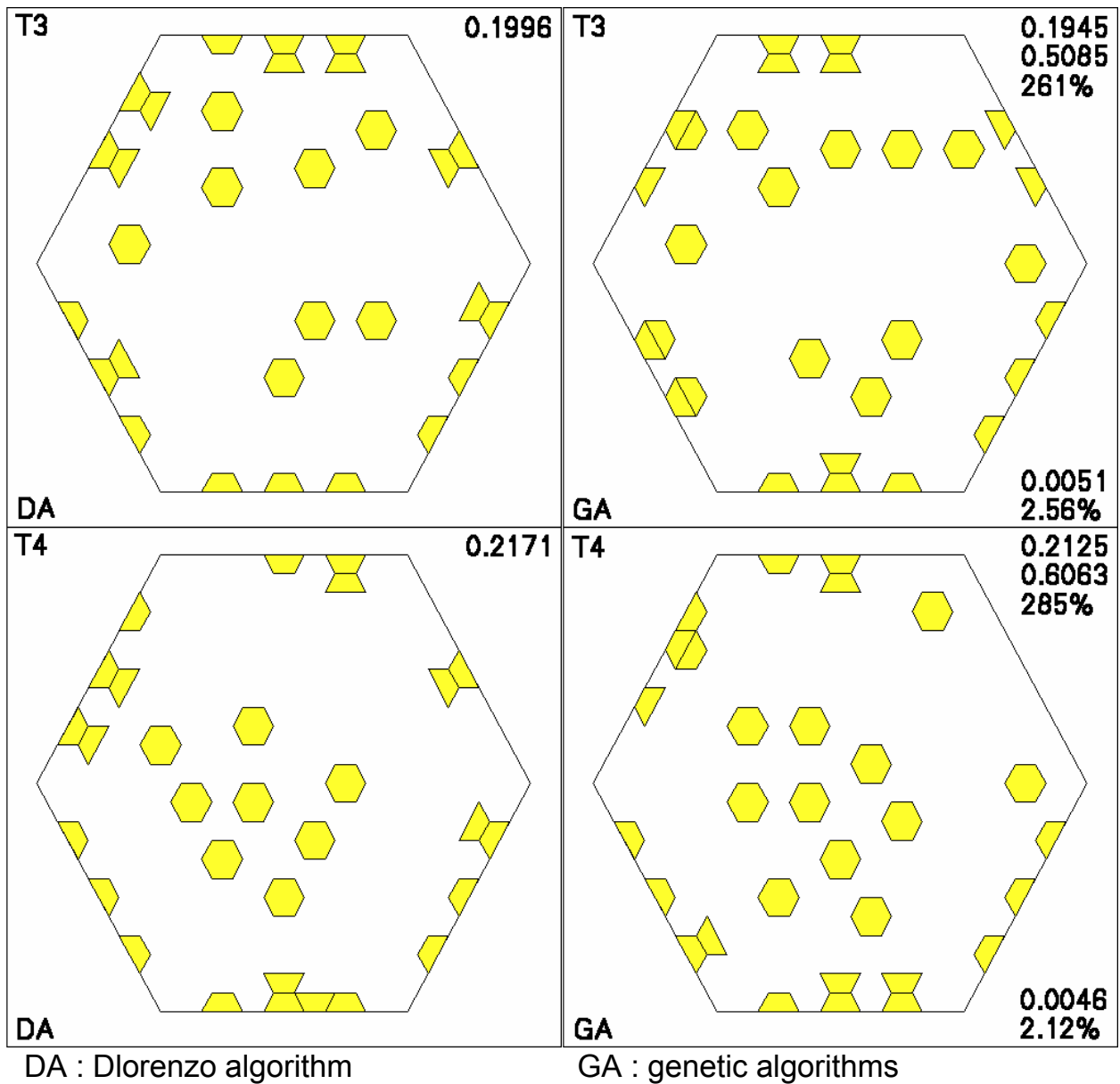
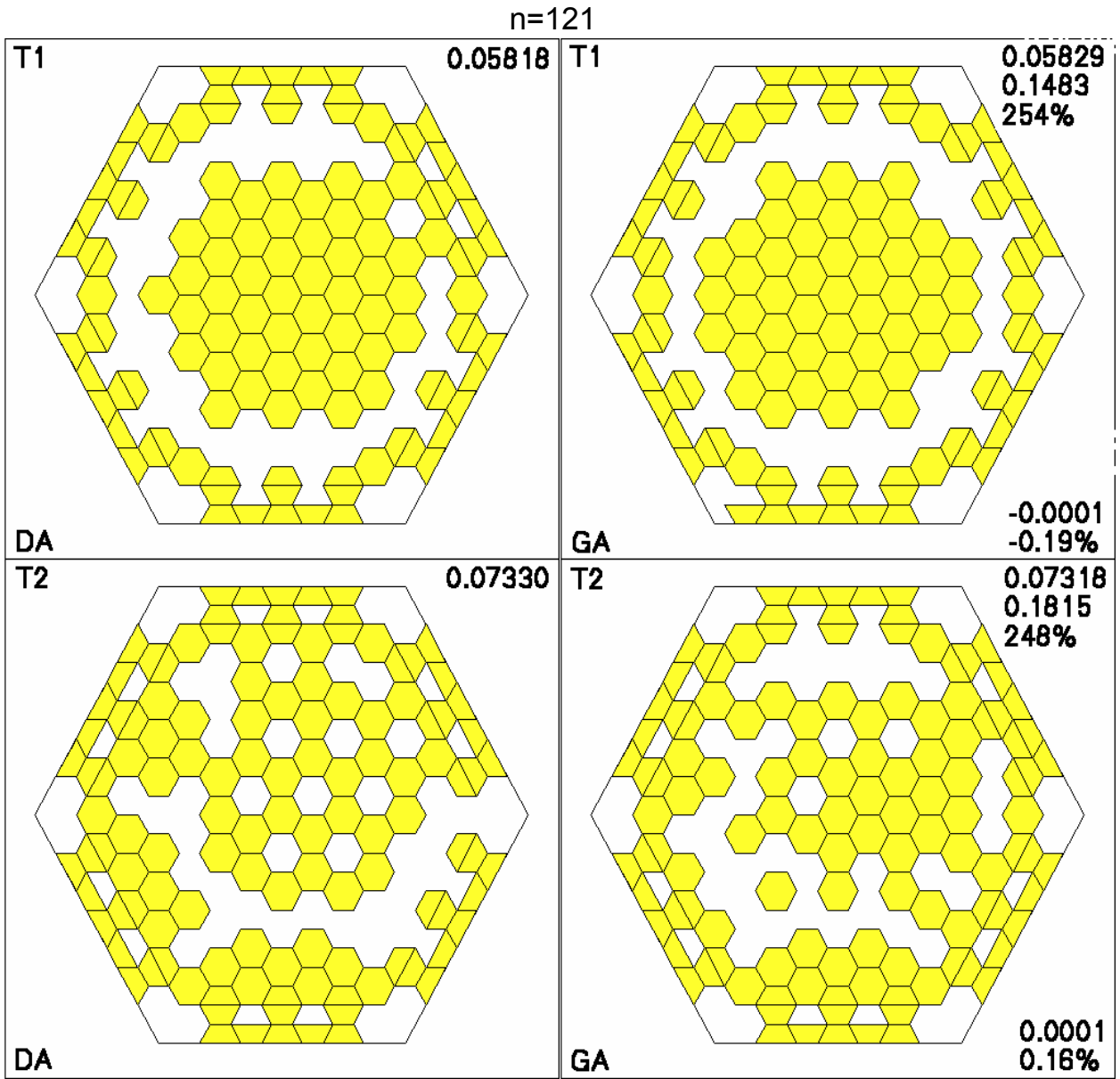


Figure A.2 b) Optimal locations for the thermal load T3 and T4 obtained by DeLorenzo algorithm and Genetic Algorithms ( 30 actuators )



DA : Dlorenzo algorithm

GA : genetic algorithms

Figure A.3 a) Optimal locations for the thermal load T1 and T2 obtained by DeLorenzo algorithm and Genetic Algorithms ( 121 actuators )



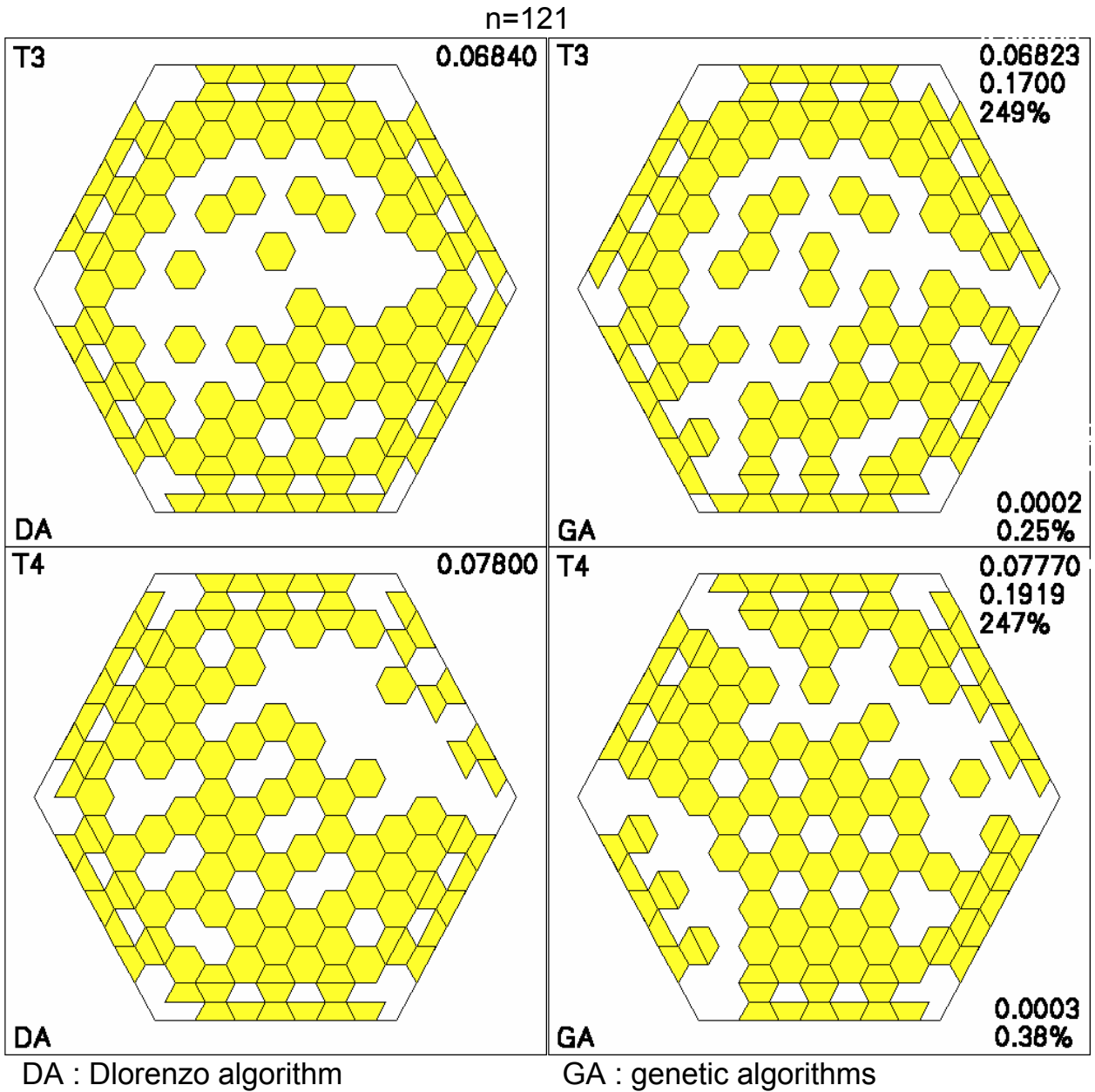
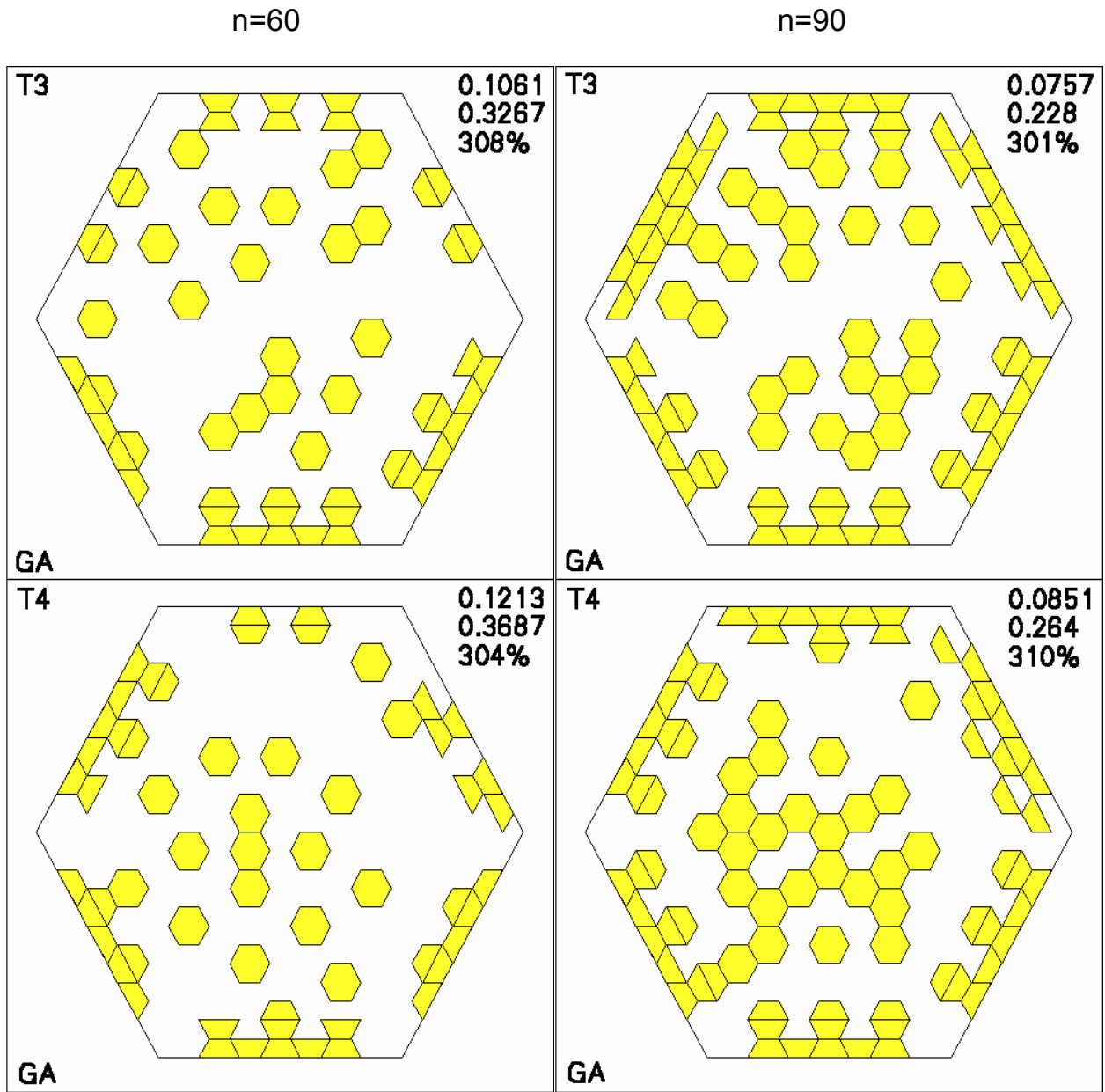


Figure A.3 b) Optimal locations for the thermal load T3 and T4 obtained by DeLorenzo algorithm and Genetic Algorithms ( 121 actuators )



GA : genetic algorithms

Figure A.4 Optimal locations for the thermal load T3 and T4 obtained by Genetic Algorithms ( 60 actuators and 90 actuators )

### A.5 Major Conclusions

- 1) GA Version 1 got slightly better results than DeLorenzo's algorithm.

- 2) The cost of the GA Version 1 is less than DeLorenzo's algorithm for the case of 30 actuators, and more than DeLorenzo's algorithm for the case of 121 actuators.
- 3) The feasibility of using GAs to solve the large scale optimization problem of actuator locations was demonstrated.
- 4) The need to further develop the effective GAs for the optimization of actuator locations was proposed.

## Appendix B. Integration by Parts

### Integration by parts

In one dimension

$$\int_a^b u dv = - \int_a^b v du + uv \Big|_a^b$$

In two dimension

$$\iint_A u \frac{\partial v}{\partial x} dx dy = - \iint_A v \frac{\partial u}{\partial x} dx dy + \oint_l u v n_x dl$$

$$\iint_A u \frac{\partial v}{\partial y} dx dy = - \iint_A v \frac{\partial u}{\partial y} dx dy + \oint_l u v n_y dl$$

In three dimension

$$\iiint_V u \frac{\partial v}{\partial x} dx dy dz = - \iiint_V v \frac{\partial u}{\partial x} dx dy dz + \iint_S u v n_x dS$$

$$\iiint_V u \frac{\partial v}{\partial y} dx dy dz = - \iiint_V v \frac{\partial u}{\partial y} dx dy dz + \iint_S u v n_y dS$$

$$\iiint_V u \frac{\partial v}{\partial z} dx dy dz = - \iiint_V v \frac{\partial u}{\partial z} dx dy dz + \iint_S u v n_z dS$$

## Appendix C. Vector Cross Product, Area of the Triangle, Differential

### Area and Volume Element

#### Vector Cross Product

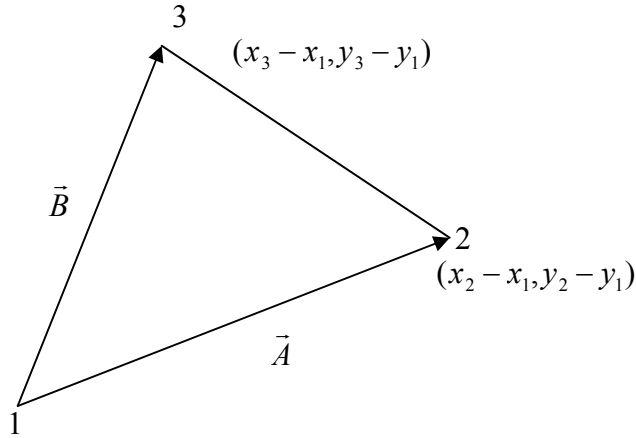


Figure C.1 Vector  $\vec{A}$  and  $\vec{B}$  in the plane of the triangle

$$|\vec{A} \times \vec{B}| = |\vec{A}| |\vec{B}| \sin \alpha = 2\Delta$$

$$\vec{A} \times \vec{B} = \begin{vmatrix} \vec{i} & \vec{j} & \vec{k} \\ x_2 - x_1 & y_2 - y_1 & 0 \\ x_3 - x_1 & y_3 - y_1 & 0 \end{vmatrix}$$

#### Area of the triangle

$$\Delta = \frac{1}{2} \begin{vmatrix} 1 & x_1 & y_1 \\ 1 & x_2 & y_2 \\ 1 & x_3 & y_3 \end{vmatrix}$$

#### Differential area and volume element

$$\vec{A} = \frac{\partial x}{\partial \xi} d\xi \vec{i} + \frac{\partial y}{\partial \xi} d\xi \vec{j}, \quad \vec{B} = \frac{\partial x}{\partial \eta} d\eta \vec{i} + \frac{\partial y}{\partial \eta} d\eta \vec{j}$$

As the length of the vector resulting from a cross product of  $\vec{A} \times \vec{B}$  is equal to the area of the elementary parallelogram, we can write

$$dxdy = \begin{vmatrix} \frac{\partial x}{\partial \xi} & \frac{\partial y}{\partial \xi} \\ \frac{\partial x}{\partial \eta} & \frac{\partial y}{\partial \eta} \end{vmatrix} d\xi d\eta = |J| d\xi d\eta$$

Similarly, a differential volume

$$dxdydz = (\vec{A} \times \vec{B}) \cdot \vec{C} = \begin{vmatrix} \frac{\partial x}{\partial \xi} & \frac{\partial y}{\partial \xi} & \frac{\partial z}{\partial \xi} \\ \frac{\partial x}{\partial \eta} & \frac{\partial y}{\partial \eta} & \frac{\partial z}{\partial \eta} \\ \frac{\partial x}{\partial \zeta} & \frac{\partial y}{\partial \zeta} & \frac{\partial z}{\partial \zeta} \end{vmatrix} d\xi d\eta d\zeta = |J| d\xi d\eta d\zeta$$

## Appendix D. Geometrical Verification of the Relations between the Cartesian Coordinates and Area Coordinates of the Triangle

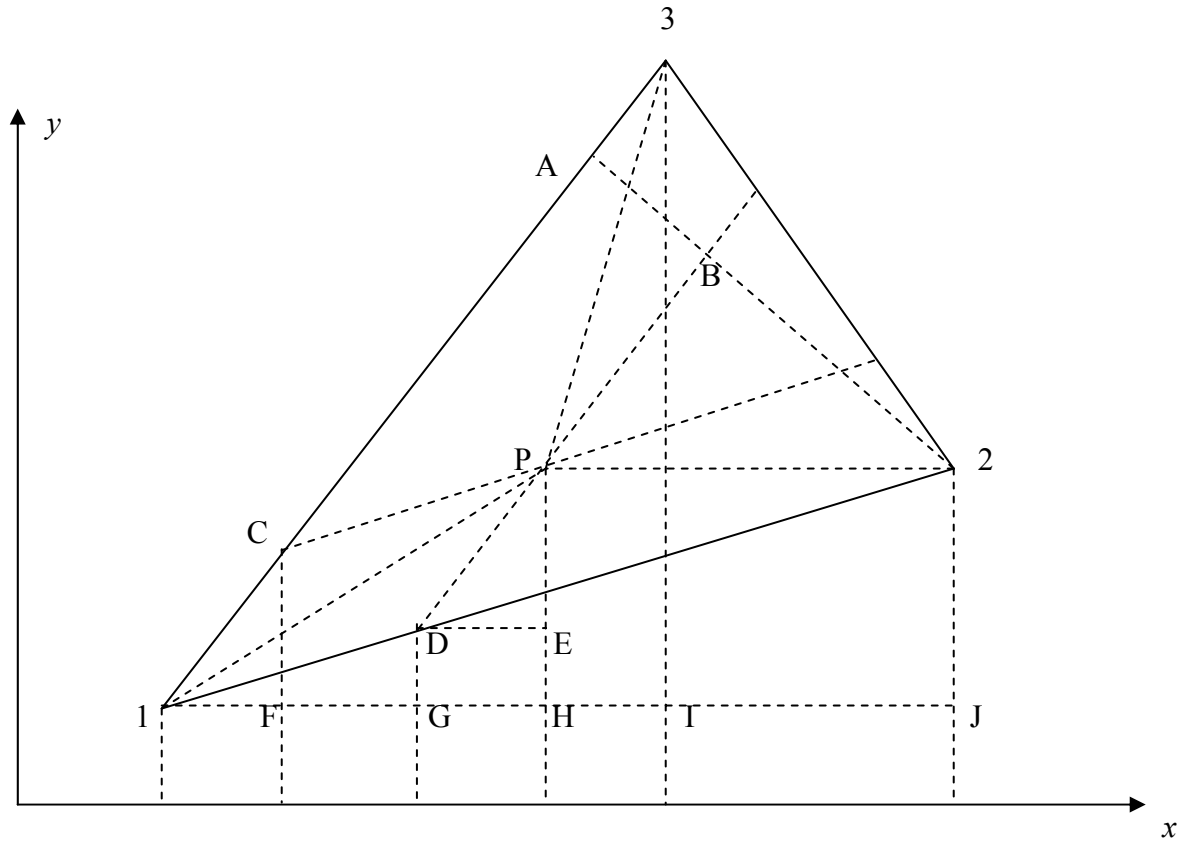


Figure D.1 Cartesian Coordinates and Area Coordinates of the triangle

$$\xi_2 = \frac{S_{\Delta P31}}{S_{\Delta 123}} = \frac{l_{AB}}{l_{A2}} = \frac{l_{1D}}{l_{12}} = \frac{l_{1G}}{l_{1J}}$$

$$\xi_3 = \frac{S_{\Delta P12}}{S_{\Delta 123}} = \frac{l_{1C}}{l_{13}} = \frac{l_{1F}}{l_{1I}}$$

$$x = x_1 + l_{1G} + l_{GH} = x_1 + l_{1G} + l_{DE} = x_1 + l_{1G} + l_{1F} = x_1 + \xi_2(x_2 - x_1) + \xi_3(x_3 - x_1) = \xi_1 x_1 + \xi_2 x_2 + \xi_3 x_3$$

similarly,

$$y = \xi_1 y_1 + \xi_2 y_2 + \xi_3 y_3$$

## Appendix E. Exact Integration of a Polynomial Term in terms of Area

### Coordinates over the Triangular Region

The integral of a polynomial term in terms of area coordinates over the triangular region can be expressed in the following form,

$$\iint_{\Delta} \xi_1^a \xi_2^b \xi_3^c dx dy = \frac{a!b!c!}{(a+b+c+2)!} 2A$$

where  $A$  represents the area of the triangular region. The integral along a side of the triangle is given by

$$\int_l \xi_i^a \xi_j^b dl = \frac{a!b!}{(a+b+1)!} l$$

where  $a$ ,  $b$ , and  $c$  are nonnegative integers.



## Appendix F. Shape Functions and Their Derivatives of Linear Strain Triangular Element (Quadratic Triangular Element)

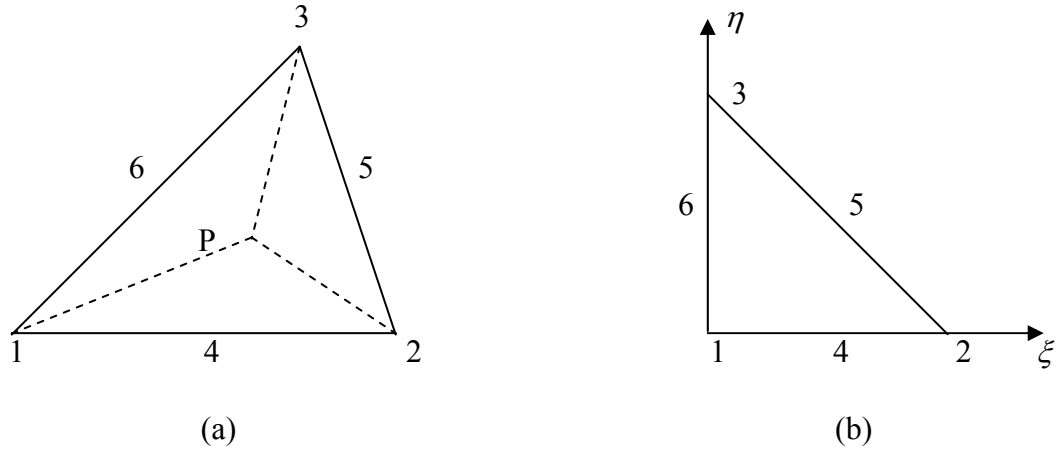


Figure F.1 Linear strain triangular element (Quadratic triangular element) in (a) area coordinate system and (b) natural coordinate system

$$\xi_1 = 1 - \xi - \eta, \quad \xi_2 = \xi, \quad \xi_3 = \eta$$

$$N_1 = \xi_1(2\xi_1 - 1) = 2(1 - \xi - \eta)(0.5 - \xi - \eta)$$

$$N_2 = \xi_2(2\xi_2 - 1) = \xi(2\xi - 1)$$

$$N_3 = \xi_3(2\xi_3 - 1) = \eta(2\eta - 1)$$

$$N_4 = 4\xi_1\xi_2 = 4\xi(1 - \xi - \eta)$$

$$N_5 = 4\xi_2\xi_3 = 4\xi\eta$$

$$N_6 = 4\xi_1\xi_3 = 4\eta(1 - \xi - \eta)$$

$$\{N_{,\xi}\} = \frac{\partial\{N\}}{\partial\xi} = \begin{pmatrix} \frac{\partial N_1}{\partial\xi} \\ \frac{\partial N_2}{\partial\xi} \\ \frac{\partial N_3}{\partial\xi} \\ \frac{\partial N_4}{\partial\xi} \\ \frac{\partial N_5}{\partial\xi} \\ \frac{\partial N_6}{\partial\xi} \end{pmatrix} = \begin{pmatrix} 4\xi + 4\eta - 3 \\ 4\xi - 1 \\ 0 \\ 4 - 8\xi - 4\eta \\ 4\eta \\ -4\eta \end{pmatrix}$$

$$\{N_{,\eta}\} = \frac{\partial\{N\}}{\partial\eta} = \begin{pmatrix} \frac{\partial N_1}{\partial\eta} \\ \frac{\partial N_2}{\partial\eta} \\ \frac{\partial N_3}{\partial\eta} \\ \frac{\partial N_4}{\partial\eta} \\ \frac{\partial N_5}{\partial\eta} \\ \frac{\partial N_6}{\partial\eta} \end{pmatrix} = \begin{pmatrix} 4\xi + 4\eta - 3 \\ 0 \\ 4\eta - 1 \\ -4\xi \\ 4\xi \\ 4 - 4\xi - 8\eta \end{pmatrix}$$

## Appendix G. Derivation of the True Rotation in the Theory of Elasticity in the Allman Triangular Element

The displacement field of the Allman triangular element is

$$\begin{aligned}
 u &= u_1 \xi_1 + u_2 \xi_2 + u_3 \xi_3 + \frac{1}{2} l_{12} \cos \gamma_{12} (\omega_2 - \omega_1) \xi_1 \xi_2 \\
 &\quad + \frac{1}{2} l_{23} \cos \gamma_{23} (\omega_3 - \omega_2) \xi_2 \xi_3 + \frac{1}{2} l_{31} \cos \gamma_{31} (\omega_1 - \omega_3) \xi_3 \xi_1 \\
 v &= v_1 \xi_1 + v_2 \xi_2 + v_3 \xi_3 + \frac{1}{2} l_{12} \sin \gamma_{12} (\omega_2 - \omega_1) \xi_1 \xi_2 \\
 &\quad + \frac{1}{2} l_{23} \sin \gamma_{23} (\omega_3 - \omega_2) \xi_2 \xi_3 + \frac{1}{2} l_{31} \sin \gamma_{31} (\omega_1 - \omega_3) \xi_3 \xi_1
 \end{aligned} \tag{G.1}$$

where  $\sin \gamma_{12} = \frac{x_1 - x_2}{l_{12}}$ ,  $\cos \gamma_{12} = -\frac{y_1 - y_2}{l_{12}}$ , etc.

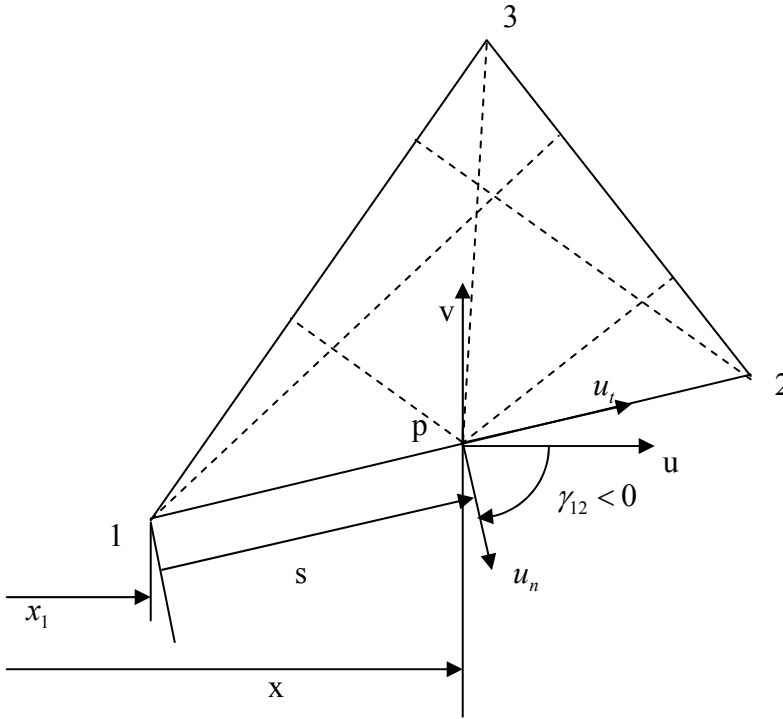


Figure G.1  $\gamma$  definition along the sides of the triangle

Along the element side 12, for example

$$x = x_1 - s \sin \gamma_{12}$$

$$y = y_1 + s \cos \gamma_{12}$$

Therefore, the partial derivative along an element side is

$$\frac{\partial}{\partial s} = \frac{\partial}{\partial x} \frac{\partial x}{\partial s} + \frac{\partial}{\partial y} \frac{\partial y}{\partial s} = -\sin \gamma \frac{\partial}{\partial x} + \cos \gamma \frac{\partial}{\partial y} \quad (\text{G.2})$$

In the field of the Allman triangle, eqn. (G.1), the true rotation  $\Omega$  in the theory of elasticity is

$$\begin{aligned} \Omega &= \frac{1}{2} \left( \frac{\partial v}{\partial x} - \frac{\partial u}{\partial y} \right) \\ &= \frac{1}{2} \left[ \left( \frac{\partial v}{\partial \xi_1} \frac{\partial \xi_1}{\partial x} + \frac{\partial v}{\partial \xi_2} \frac{\partial \xi_2}{\partial x} + \frac{\partial v}{\partial \xi_3} \frac{\partial \xi_3}{\partial x} \right) - \left( \frac{\partial u}{\partial \xi_1} \frac{\partial \xi_1}{\partial y} + \frac{\partial u}{\partial \xi_2} \frac{\partial \xi_2}{\partial y} + \frac{\partial u}{\partial \xi_3} \frac{\partial \xi_3}{\partial y} \right) \right] \\ &= \frac{1}{2} \left[ \left( v_1 + \frac{1}{2} l_{12} \sin \gamma_{12} (\omega_2 - \omega_1) \xi_2 + \frac{1}{2} l_{31} \sin \gamma_{31} (\omega_1 - \omega_3) \xi_3 \right) \frac{b_1}{2A} \right. \\ &\quad + \left( v_2 + \frac{1}{2} l_{12} \sin \gamma_{12} (\omega_2 - \omega_1) \xi_1 + \frac{1}{2} l_{23} \sin \gamma_{23} (\omega_3 - \omega_2) \xi_3 \right) \frac{b_2}{2A} \\ &\quad + \left( v_3 + \frac{1}{2} l_{23} \sin \gamma_{23} (\omega_3 - \omega_2) \xi_2 + \frac{1}{2} l_{31} \sin \gamma_{31} (\omega_1 - \omega_3) \xi_1 \right) \frac{b_3}{2A} \\ &\quad - \left( u_1 + \frac{1}{2} l_{12} \cos \gamma_{12} (\omega_2 - \omega_1) \xi_2 + \frac{1}{2} l_{31} \cos \gamma_{31} (\omega_1 - \omega_3) \xi_3 \right) \frac{c_1}{2A} \\ &\quad - \left( u_2 + \frac{1}{2} l_{12} \cos \gamma_{12} (\omega_2 - \omega_1) \xi_1 + \frac{1}{2} l_{23} \cos \gamma_{23} (\omega_3 - \omega_2) \xi_3 \right) \frac{c_2}{2A} \\ &\quad \left. - \left( u_3 + \frac{1}{2} l_{23} \cos \gamma_{23} (\omega_3 - \omega_2) \xi_2 + \frac{1}{2} l_{31} \cos \gamma_{31} (\omega_1 - \omega_3) \xi_1 \right) \frac{c_3}{2A} \right] \\ &= \frac{1}{4A} \left[ (x_2 - x_3) u_1 + (x_3 - x_1) u_2 + (x_1 - x_2) u_3 + (y_2 - y_3) v_1 + (y_3 - y_1) v_2 + (y_1 - y_2) v_3 \right] + R \end{aligned}$$

where

$$\begin{aligned}
R &= \frac{1}{4} [(l_{12} \sin \gamma_{12} (\omega_2 - \omega_1) \xi_2 + l_{31} \sin \gamma_{31} (\omega_1 - \omega_3) \xi_3) \frac{\partial \xi_1}{\partial x} \\
&\quad + (l_{12} \sin \gamma_{12} (\omega_2 - \omega_1) \xi_1 + l_{23} \sin \gamma_{23} (\omega_3 - \omega_2) \xi_3) \frac{\partial \xi_2}{\partial x} \\
&\quad + (l_{23} \sin \gamma_{23} (\omega_3 - \omega_2) \xi_2 + l_{31} \sin \gamma_{31} (\omega_1 - \omega_3) \xi_1) \frac{\partial \xi_3}{\partial x} \\
&\quad - (l_{12} \cos \gamma_{12} (\omega_2 - \omega_1) \xi_2 + l_{31} \cos \gamma_{31} (\omega_1 - \omega_3) \xi_3) \frac{\partial \xi_1}{\partial y} \\
&\quad - (l_{12} \cos \gamma_{12} (\omega_2 - \omega_1) \xi_1 + l_{23} \cos \gamma_{23} (\omega_3 - \omega_2) \xi_3) \frac{\partial \xi_2}{\partial y} \\
&\quad - (l_{23} \cos \gamma_{23} (\omega_3 - \omega_2) \xi_2 + l_{31} \cos \gamma_{31} (\omega_1 - \omega_3) \xi_1) \frac{\partial \xi_3}{\partial y}] \\
&= \frac{1}{4} [l_{12} (\omega_2 - \omega_1) \xi_2 (\sin \gamma_{12} \frac{\partial \xi_1}{\partial x} - \cos \gamma_{12} \frac{\partial \xi_1}{\partial y}) + l_{12} (\omega_2 - \omega_1) \xi_1 (\sin \gamma_{12} \frac{\partial \xi_2}{\partial x} - \cos \gamma_{12} \frac{\partial \xi_2}{\partial y}) \\
&\quad + l_{31} (\omega_1 - \omega_3) \xi_3 (\sin \gamma_{31} \frac{\partial \xi_1}{\partial x} - \cos \gamma_{31} \frac{\partial \xi_1}{\partial y}) + l_{31} (\omega_1 - \omega_3) \xi_1 (\sin \gamma_{31} \frac{\partial \xi_3}{\partial x} - \cos \gamma_{31} \frac{\partial \xi_3}{\partial y}) \\
&\quad + l_{23} (\omega_3 - \omega_2) \xi_3 (\sin \gamma_{23} \frac{\partial \xi_2}{\partial x} - \cos \gamma_{23} \frac{\partial \xi_2}{\partial y}) + l_{23} (\omega_3 - \omega_2) \xi_2 (\sin \gamma_{23} \frac{\partial \xi_3}{\partial x} - \cos \gamma_{23} \frac{\partial \xi_3}{\partial y})]
\end{aligned}$$

We note that  $\frac{\partial \xi_i}{\partial x}$  and  $\frac{\partial \xi_i}{\partial y}$  are constant in the entire field and on the boundaries we have,

refer to eqn. (G.2),

Along the side 12,

$$\xi_1 = \frac{S_{\Delta P 23}}{S_{\Delta 123}} = 1 - \frac{s}{l_{12}}, \quad \xi_2 = \frac{S_{\Delta P 31}}{S_{\Delta 123}} = \frac{s}{l_{12}}, \quad \xi_3 = 0$$

$$(\sin \gamma_{12} \frac{\partial \xi_1}{\partial x} - \cos \gamma_{12} \frac{\partial \xi_1}{\partial y}) = -\frac{\partial \xi_1}{\partial s} \Big|_{side12} = \frac{1}{l_{12}}, \quad (\sin \gamma_{12} \frac{\partial \xi_2}{\partial x} - \cos \gamma_{12} \frac{\partial \xi_2}{\partial y}) = -\frac{\partial \xi_2}{\partial s} \Big|_{side12} = -\frac{1}{l_{12}}$$

Along the side 31,

$$(\sin \gamma_{31} \frac{\partial \xi_1}{\partial x} - \cos \gamma_{31} \frac{\partial \xi_1}{\partial y}) = -\frac{\partial \xi_1}{\partial s} \Big|_{side31} = -\frac{1}{l_{31}}, \quad (\sin \gamma_{31} \frac{\partial \xi_3}{\partial x} - \cos \gamma_{31} \frac{\partial \xi_3}{\partial y}) = -\frac{\partial \xi_3}{\partial s} \Big|_{side31} = \frac{1}{l_{31}}$$

Along the side 23,

$$(\sin \gamma_{23} \frac{\partial \xi_2}{\partial x} - \cos \gamma_{23} \frac{\partial \xi_2}{\partial y}) = -\frac{\partial \xi_2}{\partial s} \Big|_{side23} = \frac{1}{l_{23}}, \quad (\sin \gamma_{23} \frac{\partial \xi_3}{\partial x} - \cos \gamma_{23} \frac{\partial \xi_3}{\partial y}) = -\frac{\partial \xi_3}{\partial s} \Big|_{side23} = -\frac{1}{l_{23}}$$

So we have,

$$\begin{aligned} R &= \frac{1}{4} [(\omega_2 - \omega_1)\xi_2 - (\omega_2 - \omega_1)\xi_1 - (\omega_1 - \omega_3)\xi_3 + (\omega_1 - \omega_3)\xi_1 + (\omega_3 - \omega_2)\xi_3 - (\omega_3 - \omega_2)\xi_2] \\ &= \frac{1}{4} (2\omega_1\xi_1 - \omega_1\xi_2 - \omega_1\xi_3 + 2\omega_2\xi_2 - \omega_2\xi_1 - \omega_2\xi_3 + 2\omega_3\xi_3 - \omega_3\xi_1 - \omega_3\xi_2) \\ &= \frac{1}{4} (3\omega_1\xi_1 - \omega_1 + 3\omega_2\xi_2 - \omega_2 + 3\omega_3\xi_3 - \omega_3) \\ &= \frac{1}{4} \sum_{i=1}^3 (3\xi_i - 1)\omega_i \end{aligned}$$

So the true rotation in the Allman triangular element is

$$\Omega = \Omega_0 + \frac{1}{4} \sum_{i=1}^3 (3\xi_i - 1)\omega_i \tag{G.3}$$

where  $\Omega_0$ , the rotation at the centroid  $\xi_1 = \xi_2 = \xi_3 = \frac{1}{3}$ , is

$$\Omega_0 = \frac{1}{4A} [(x_2 - x_3)u_1 + (x_3 - x_1)u_2 + (x_1 - x_2)u_3 + (y_2 - y_3)v_1 + (y_3 - y_1)v_2 + (y_1 - y_2)v_3]$$

## Appendix H. Slope at the Mid-Span of Cubic Beam Element

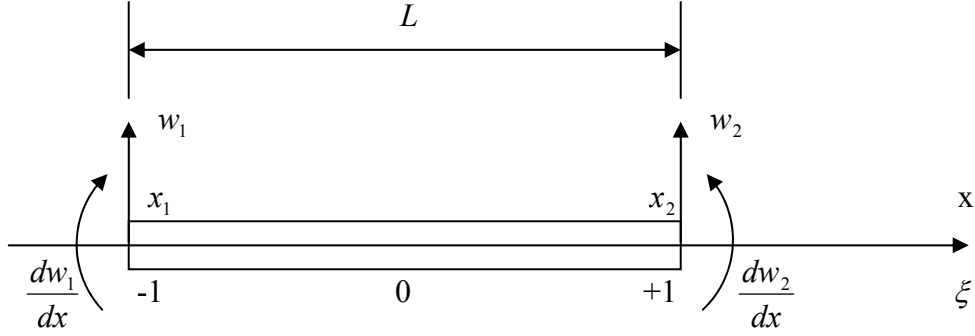


Figure H.1 Cubic beam element

$$\xi = \frac{2x - x_2 - x_1}{x_2 - x_1} = \frac{2x - x_2 - x_1}{L}$$

$$w = w_1 \varphi_1 + \frac{dw_1}{dx} \varphi_2 + w_2 \varphi_3 + \frac{dw_2}{dx} \varphi_4$$

$$\varphi_1 = \frac{1}{4}(2 - 3\xi + \xi^3), \quad \varphi_2 = \frac{L}{8}(1 - \xi - \xi^2 + \xi^3)$$

$$\varphi_3 = \frac{1}{4}(2 + 3\xi - \xi^3), \quad \varphi_4 = \frac{L}{8}(-1 - \xi + \xi^2 + \xi^3)$$

$$\left. \frac{dw}{dx} \right|_{\xi=0} = \left( w_1 \frac{d\varphi_1}{d\xi} + \frac{dw_1}{dx} \frac{d\varphi_2}{d\xi} + w_2 \frac{d\varphi_3}{d\xi} + \frac{dw_2}{dx} \frac{d\varphi_4}{d\xi} \right) \frac{d\xi}{dx} \Big|_{\xi=0} = -\frac{3}{2L} w_1 - \frac{1}{4} \frac{dw_1}{dx} + \frac{3}{2L} w_2 - \frac{1}{4} \frac{dw_2}{dx}$$

# Appendix I. Shape Functions and Their Derivatives of Discrete Kirchhoff

## Triangular (DKT) Element

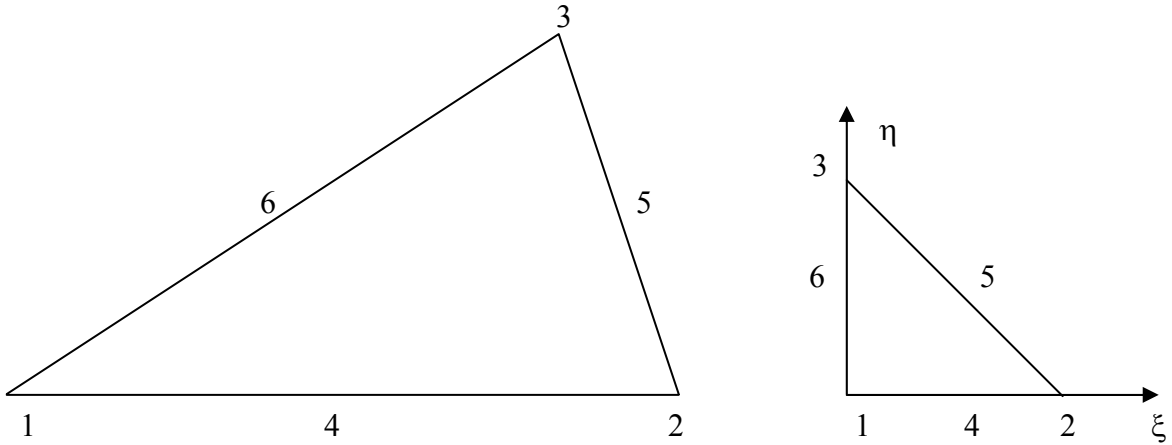


Figure I.1 Node locations of quadratic triangular element

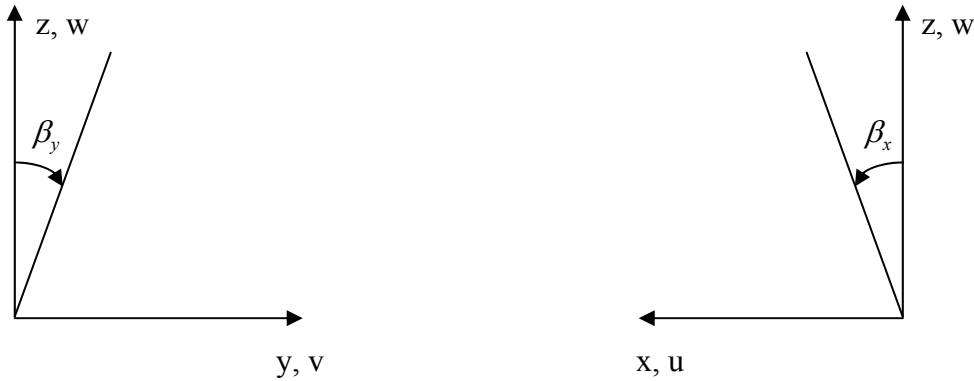


Figure I.2 Positive directions of  $\beta_x$  and  $\beta_y$  in 2D view

$$H_{x_1} = 1.5(a_4 N_4 - a_6 N_6)$$

$$H_{x_2} = b_4 N_4 + b_6 N_6$$

$$H_{x_3} = N_1 - c_4 N_4 - c_6 N_6$$

$$H_{x_4} = 1.5(a_5 N_5 - a_4 N_4)$$

$$H_{x_5} = b_4 N_4 + b_5 N_5$$



$$H_{x_6} = N_2 - c_4 N_4 - c_5 N_5$$

$$H_{x_7} = 1.5(a_6 N_6 - a_5 N_5)$$

$$H_{x_8} = b_5 N_5 + b_6 N_6$$

$$H_{x_9} = N_3 - c_5 N_5 - c_6 N_6$$

$$H_{y_1} = 1.5(d_4 N_4 - d_6 N_6)$$

$$H_{y_2} = -N_1 + e_4 N_4 + e_6 N_6$$

$$H_{y_3} = -b_4 N_4 - b_6 N_6 = -H_{x_2}$$

$$H_{y_4} = 1.5(d_5 N_5 - d_4 N_4)$$

$$H_{y_5} = -N_2 + e_4 N_4 + e_5 N_5$$

$$H_{y_6} = -b_4 N_4 - b_5 N_5 = -H_{x_5}$$

$$H_{y_7} = 1.5(d_6 N_6 - d_5 N_5)$$

$$H_{y_8} = -N_3 + e_5 N_5 + e_6 N_6$$

$$H_{y_9} = -b_5 N_5 - b_6 N_6 = -H_{x_8}$$

$$\beta_x = H_{x_1} w_1 + H_{x_2} \theta_{x_1} + H_{x_3} \theta_{y_1} + H_{x_4} w_2 + H_{x_5} \theta_{x_2} + H_{x_6} \theta_{y_2} + H_{x_7} w_3 + H_{x_8} \theta_{x_3} + H_{x_9} \theta_{y_3}$$

$$\beta_y = H_{y_1} w_1 + H_{y_2} \theta_{x_1} + H_{y_3} \theta_{y_1} + H_{y_4} w_2 + H_{y_5} \theta_{x_2} + H_{y_6} \theta_{y_2} + H_{y_7} w_3 + H_{y_8} \theta_{x_3} + H_{y_9} \theta_{y_3}$$

$$a_4 = -x_{12} / l_{12}^2, \quad a_5 = -x_{23} / l_{23}^2, \quad a_6 = -x_{31} / l_{31}^2$$

$$b_4 = \frac{3}{4} \frac{x_{12} y_{12}}{l_{12}^2}, \quad b_5 = \frac{3}{4} \frac{x_{23} y_{23}}{l_{23}^2}, \quad b_6 = \frac{3}{4} \frac{x_{31} y_{31}}{l_{31}^2}$$

$$c_4 = (\frac{1}{4} x_{12}^2 - \frac{1}{2} y_{12}^2) / l_{12}^2, \quad c_5 = (\frac{1}{4} x_{23}^2 - \frac{1}{2} y_{23}^2) / l_{23}^2, \quad c_6 = (\frac{1}{4} x_{31}^2 - \frac{1}{2} y_{31}^2) / l_{31}^2$$

$$d_4 = -y_{12} / l_{12}^2, \quad d_5 = -y_{23} / l_{23}^2, \quad d_6 = -y_{31} / l_{31}^2$$

$$e_4 = (\frac{1}{4} y_{12}^2 - \frac{1}{2} x_{12}^2) / l_{12}^2, \quad e_5 = (\frac{1}{4} y_{23}^2 - \frac{1}{2} x_{23}^2) / l_{23}^2, \quad e_6 = (\frac{1}{4} y_{31}^2 - \frac{1}{2} x_{31}^2) / l_{31}^2$$

$$x_{ij} = x_i - x_j, \quad y_{ij} = y_i - y_j, \quad l_{ij}^2 = x_{ij}^2 + y_{ij}^2$$

or

$$a_k = -x_{ij} / l_{ij}^2$$

$$b_k = \frac{3}{4} \frac{x_{ij} y_{ij}}{l_{ij}^2}$$

$$c_k = \left( \frac{1}{4} x_{ij}^2 - \frac{1}{2} y_{ij}^2 \right) / l_{ij}^2$$

$$d_k = -y_{ij} / l_{ij}^2$$

$$e_k = \left( \frac{1}{4} y_{ij}^2 - \frac{1}{2} x_{ij}^2 \right) / l_{ij}^2$$

where  $k = 4, 5, 6$  for the sides  $ij = 12, 23, 31$ , respectively.

$$H_x^T = [H_{x_1}, H_{x_2}, H_{x_3}, H_{x_4}, H_{x_5}, H_{x_6}, H_{x_7}, H_{x_8}, H_{x_9}]$$

$$H_{x_\xi} = \left\{ \begin{array}{c} p_4(1-2\xi) + (p_6 - p_4)\eta \\ q_4(1-2\xi) - (q_6 + q_4)\eta \\ -4 + 6(\xi + \eta) + r_4(1-2\xi) - \eta(r_6 + r_4) \\ -p_4(1-2\xi) + \eta(p_5 + p_4) \\ q_4(1-2\xi) - \eta(q_4 - q_5) \\ -2 + 6\xi + r_4(1-2\xi) + \eta(r_5 - r_4) \\ -\eta(p_6 + p_5) \\ \eta(q_5 - q_6) \\ -\eta(r_6 - r_5) \end{array} \right\}$$

$$H_{x,\eta} = \left\{ \begin{array}{c} -p_6(1-2\eta) - \xi(p_4 - p_6) \\ q_6(1-2\eta) - \xi(q_6 + q_4) \\ -4 + 6(\xi + \eta) + r_6(1-2\eta) - \xi(r_6 + r_4) \\ \xi(p_5 + p_4) \\ \xi(q_5 - q_4) \\ -\xi(r_4 - r_5) \\ p_6(1-2\eta) - \xi(p_5 + p_6) \\ q_6(1-2\eta) + \xi(q_5 - q_6) \\ -2 + 6\eta + r_6(1-2\eta) + \xi(r_5 - r_6) \end{array} \right\}$$

$$H_y^T = [H_{y_1}, H_{y_2}, H_{y_3}, H_{y_4}, H_{y_5}, H_{y_6}, H_{y_7}, H_{y_8}, H_{y_9}]$$

$$H_{y,\xi} = \left\{ \begin{array}{c} t_4(1-2\xi) + (t_6 - t_4)\eta \\ 1 + r_4(1-2\xi) - (r_6 + r_4)\eta \\ -q_4(1-2\xi) + \eta(q_6 + q_4) \\ -t_4(1-2\xi) + \eta(t_5 + t_4) \\ -1 + r_4(1-2\xi) + \eta(r_5 - r_4) \\ -q_4(1-2\xi) - \eta(q_5 - q_4) \\ -\eta(t_5 + t_6) \\ \eta(r_5 - r_6) \\ -\eta(q_5 - q_6) \end{array} \right\}$$

$$H_{y,\eta} = \left\{ \begin{array}{c} -t_6(1-2\eta) - \xi(t_4 - t_6) \\ 1 + r_6(1-2\eta) - \xi(r_6 + r_4) \\ -q_6(1-2\eta) + \xi(q_6 + q_4) \\ \xi(t_5 + t_4) \\ \xi(r_5 - r_4) \\ -\xi(q_5 - q_4) \\ t_6(1-2\eta) - \xi(t_5 + t_6) \\ -1 + r_6(1-2\eta) + \xi(r_5 - r_6) \\ -q_6(1-2\eta) - \xi(q_5 - q_6) \end{array} \right\}$$

where

$$p_4 = -6x_{12}/l_{12}^2 = 6a_4, \quad p_5 = -6x_{23}/l_{23}^2 = 6a_5, \quad p_6 = -6x_{31}/l_{31}^2 = 6a_6$$

$$t_4 = -6y_{12}/l_{12}^2 = 6d_4, \quad t_5 = -6y_{23}/l_{23}^2 = 6d_5, \quad t_6 = -6y_{31}/l_{31}^2 = 6d_6$$

$$q_4 = \frac{3x_{12}y_{12}}{l_{12}^2} = 4b_4, \quad q_5 = \frac{3x_{23}y_{23}}{l_{23}^2} = 4b_5, \quad q_6 = \frac{3x_{31}y_{31}}{l_{31}^2} = 4b_6$$

$$r_4 = 3y_{12}^2 / l_{12}^2, \quad r_5 = 3y_{23}^2 / l_{23}^2, \quad r_6 = 3y_{31}^2 / l_{31}^2$$

$$x_{ij} = x_i - x_j, \quad y_{ij} = y_i - y_j, \quad l_{ij}^2 = x_{ij}^2 + y_{ij}^2$$

or

$$p_k = -6x_{ij} / l_{ij}^2 = 6a_k$$

$$t_k = -6y_{ij} / l_{ij}^2 = 6d_k$$

$$q_k = \frac{3x_{ij}y_{ij}}{l_{ij}^2} = 4b_k$$

$$r_k = 3y_{ij}^2 / l_{ij}^2$$

where  $k = 4, 5, 6$  for the sides  $ij = 12, 23, 31$ , respectively.

## References

1. Zienkiewicz, O. C. and Taylor, R. L., *The Finite Element Method*, 5<sup>th</sup> ed., Vol. 1, 2, & 3, Butterworth-Heinemann, 2000.
2. Bathe, K. J., *Finite Element Procedures*, Prentice-Hall, Inc., 1996.
3. Cook, R. D., Malkus, D. S., Plesha, M. E., and Witt, R. J., *Concepts and Applications of Finite Element Analysis*, 4<sup>th</sup> ed., John Wiley & Sons, Inc., 2002.
4. Yang, T. Y., *Finite Element Structural Analysis*, Prentice-Hall, Inc., 1986.
5. Hughes, T. J. R., *The Finite Element Method: Linear Static and Dynamic Finite Element Analysis*, Prentice-Hall, Inc., 1987.
6. Jones, R. M., *Mechanics of Composite Materials*, 2<sup>nd</sup> ed., Philadelphia, PA, Taylor & Francis, 1999.
7. Reddy, J. N., *Mechanics of Laminated Composite Plates and Shells: Theory and Analysis*, 2<sup>nd</sup> ed., CRC Press, Boca Raton, FL, 2004.
8. Reddy, J. N., *An Introduction to Nonlinear Finite Element Analysis*, Oxford University Press, New York, 2004.
9. Huebner, K., H., Dewhurst, D. L., Smith, D. E., and Byrom, T. G., *The Finite Element Method for Engineers*, 4<sup>th</sup> ed., John Wiley & Sons, Inc., 2001.
10. Kwon, Y. W. and Bang, H., *The Finite Element Method Using MATLAB*, 2<sup>nd</sup> ed. CRC Press, Boca Raton, Florida, 2000.
11. Rao, S. S., *The Finite Element Method in Engineering*, 3<sup>rd</sup>, Pergamon Press, 1999.
12. MacNeal, R. H., *Finite Elements: Their Design and Performance*, Marcel Dekker, New York, 1994.
13. Hartmann, F., Katz, C., *Structural Analysis with Finite Elements*, Springer-Verlag,

- 2004.
14. Kardestuncer, H. and Norrie, D. H. (eds.) *Finite Element Handbook*, McGraw-Hill, New York, 1987.
  15. Shames, I. H. and Dym, C. L., *Energy and finite element methods in structural mechanics*, Hemisphere Publishing Corporation, 1985.
  16. Washizu, K., *Variational Methods in Elasticity and Plasticity*, 3<sup>rd</sup> ed., Pergamon Press, 1982.
  17. Reddy, J. N., *Energy Principles and Variational Methods in Applied Mechanics*, 2<sup>nd</sup> ed., John Wiley, New York, 2002.
  18. Wunderlich, W. and Pilkey, W. D., *Mechanics of Structures: Variational and Computational Methods*, 2<sup>nd</sup> ed., CRC Press, 2003.
  19. Zhang, X., (editor in chief) *Advanced Theory of Elasticity*, BUAA Press, 1994. (in Chinese)
  20. Zhang, Z., (editor in chief) *Mechanics of Composite Structures*, BUAA Press, 1993. (in Chinese)
  21. Chia, C. Y., *Nonlinear Analysis of Plates*, McGraw-Hill, 1980.
  22. Gallagher, R. H., *Finite Element Analysis: Fundamentals*, Prentice-Hall, Inc., 1975.
  23. Timoshenko, S. P. and Woinowsky-Krieger, S., *Theory of plates and Shells*, 2<sup>nd</sup> ed., McGraw-Hill, New York, 1959.
  24. Zienkiewicz, O. C., "The birth of the finite element method and of computational mechanics," *International Journal for Numerical Methods in Engineering*, Vol. 60, 2004, pp. 3-10.
  25. Oden, J. T., Belytschko, T., Ivo Babuska, I. and, Hughes, T. J. R., "Research directions

- in computational mechanics,” *Computer Methods in Applied Mechanics and Engineering*, Vol. 192, 2003, 913-922.
26. Gallagher, R. H., “Problems and Progress in Thin Shell Finite Element Analysis,” In *Finite Elements for Thin Shells and Curved Members*, Edited by D. G. Ashwell and R. H. Gallagher, pp. 1-14. John Wiley & Sons, New York, 1976.
  27. Yang, H. T. Y., Saigal, S., and Liaw, D. G., “Advance of Thin Shell Finite Elements and Some Applications – Version I,” *Computers & Structures*, Vol. 35, No. 4, 1990, pp. 481–504.
  28. Noor, A. K., Burton, W. S., and Bert, C. W., “Computational Models for Sandwich Panels and Shells,” *ASME Applied Mechanics Reviews*, Vol. 49, No. 3, 1996, pp. 155-199.
  29. Bucalem, M. L. and Bathe, K. J., “Finite Element Analysis of Shell Structures,” *Archives of Computational Methods in Engineering*, Vol. 4, No. 1, 1997, pp. 3-61.
  30. Yang, H. T. Y., Saigal, S., Masud, A., Kapania, R. K., “A Survey of Recent Shell Finite Elements,” *International Journal for Numerical Methods in Engineering*, Vol. 47, 2000, pp. 101-127.
  31. Zienkiewicz, O. C. and Taylor, R. L., “The finite element patch test revisited: test for convergence, validation and error estimates,” *Computer Methods in Applied Mechanics and Engineering*, Vol. 149, 1997, pp. 223-254.
  32. Courant, R., “Variational Methods for the Solution of Problems of Equilibrium and Vibrations,” *Bulletin of the American Mathematical Society*, Vol. 49, 1943, pp. 1-23.  
(Reprinted with an appreciation by C. A. Felippa in *International Journal for Numerical Methods in Engineering*, Vol. 37, No. 13, 1994, pp. 2159-2187.)

33. Argyris, J. H. and Kelsey, S. "Energy Theorems and Structural Analysis," *Aircraft Engineering*, Vols. 26 and 27, Oct. 1954 to May, 1955, Part I is by J. H. Argyris, and Part II is by J. H. Argyris and S. Kelsey.
34. Turner, M. J., Clough, R. W., Martin, H. C. and Topp, L. J., "Stiffness and deflection analysis of complex structures. *Journal of the Aeronautical Sciences*, Vol. 23, 1956, pp. 805-823.
35. Clough, R. W., "The Finite Element Method in Plane Stress Analysis," Proceedings, *Second ASCE Conference on Electronic Computation, Pittsburgh, PA, 1960*, pp. 345-378.
36. Bazeley, G. P., Cheung, Y. K., Irons, B. M. and Zienkiewicz, O. C., "Triangular elements in bending -- conforming and non-conforming Solutions," In J. S. Przemienicki, R. M. Bader, W. F. Bozich, J. R. Johnson and W. J. Mykytow (eds), Proceedings, *First Conference Matrix Methods in Structural Mechanics*, Volume AFFDL-TR-66-80, Air Force Flight Dynamics Laboratory, Wright Patterson Air Force Base, OH, Oct., 1966, pp. 547-576.
37. Bogner, F. K., Fox, R. L., and Schmit, L. A., "The generation of interelement-compatible stiffness and mass matrices by the use of interpolation formulae," In J. S. Przemienicki, R. M. Bader, W. F. Bozich, J. R. Johnson and W. J. Mykytow (eds), Proceedings, *First Conference Matrix Methods in Structural Mechanics*, Volume AFFDL-TR-66-80, Air Force Flight Dynamics Laboratory, Wright Patterson Air Force Base, OH, Oct., 1966, pp. 397-443.
38. Wempner, G. A., Oden, J. T. and Cross, D. A., "Finite Element Analysis of Thin Shells," *ASCE Journal of Engineering Mechanics Division*, Vol. 94, No. EM6, 1968,



pp. 1273-1294.

39. Stricklin, J. A., Haisler, W., Tisdale, P. and Gunderson, R., "A rapidly converging triangle plate element," *AIAA Journal*, Vol. 7, No. 1, 1969, pp. 180-181.
40. Dhatt, G. S., "Numerical Analysis of Thin Shells by Curved Triangular Elements Based on Discrete Kirchhoff Hypothesis," In Proceedings of *the Conference on Application of Finite Element Method in Civil Engineering*, Vandervilt University, Nashville, TN, 1969, pp. 255-278.
41. Ahmad, S., Irons, B. M. and Zienkiewicz, O. C., "Analysis of thick and thin shell structures by curved elements," *International Journal for Numerical Methods in Engineering*, Vol. 2, 1970, pp. 419-451.
42. Zienkiewicz, O. C., Too, J. and Taylor, R. L., "Reduced integration technique in general analysis of plates and shells," *International Journal for Numerical Methods in Engineering*, Vol. 3, 1971, pp. 275-90.
43. Hughes, T. J. R. and Taylor, R. L. and Kanoknukulchai, W., "A simple and efficient element for plate bending," *International Journal for Numerical Methods in Engineering*, Vol. 11, 1977, pp. 1529-1543.
44. Averill, R. C. and Reddy, J. N., "Behavior of plate elements based on the first-order shear deformation theory," *Engineering Computation*, Vol. 7, No. 1, 1990, pp. 57-74.
45. Irons, B. M. and Draper, J. K., "Inadequacy of nodal connections in a stiffness solution for plate bending," *AIAA Journal*, Vol. 3, No. 5, 1965, p. 961.
46. Pian T. H. H., "Derivation of element stiffness matrices by assumed stress distributions," *AIAA Journal*, Vol. 2, 1964, pp. 1333-1336.
47. Pian, T. H. H. and Tong, P. "Basis of Finite Element Methods for Solid Continua,"

- International Journal for Numerical Methods in Engineering*, Vol. 1, 1969, pp. 3-28.
48. Pian, T. H. H., "Reflections and Remarks on Hybrid and Mixed Finite Element Methods," In: *Hybrid and Mixed Finite Element Methods*, edited by S. N. Atluri, R. H. Gallagher and O. C. Zienkiewicz, John Wiley & Sons Ltd., 1983, pp. 565-570.
  49. Pian, T. H. H., "State-of-the-art development of hybrid/mixed finite element method," *Finite Elements in Analysis and Design*, Vol. 21, Nos. 1&2, 1995, pp. 5-20.
  50. Wunderlich, W., "Mixed Models for Plates and Shells: Principles – Elements – Examples," In: *Hybrid and Mixed Finite Element Methods*, edited by S. N. Atluri, R. H. Gallagher and O. C. Zienkiewicz, John Wiley & Sons Ltd., 1983, pp. 215-241.
  51. B. Fraeijns de Veubeke, "Displacement and Equilibrium models in finite element method," In *Stress Analysis*, edited by O. C. Zienkiewicz and G. S. Holister GS, published by John Wiley & Sons, New York, 1965, pp. 145-197. (reprinted with remarks by O. C. Zienkiewicz in *International Journal for Numerical Methods in Engineering*, Vol. 52, 2001, pp. 287-342.).
  52. Robinson, J., "Element evaluation – a set of assessment points and standard tests," In: *Finite Element Methods in the Commercial Environment*, Vol. 1, edited by J. Robinson, Robinson and Associates, 1978, pp. 217-247.
  53. Hughes, T. J. R. and Tezduyar, T. E., "Finite elements based upon Mindlin plate theory with particular reference to the four-node bilinear isoparametric element element," *Journal of Applied Mechanics*, Vol. 48, 1981, pp. 587-596.
  54. MacNeal, R. H., "Derivation of element stiffness matrices by assumed strain distributions," *Nuclear Engineering and Design*, Vol. 70, 1982, pp. 3-12.
  55. MacNeal, R. H. and Harder, R. L., "A Proposed Standard Set of Problems to Test Finite

- Element Accuracy,” *Finite Elements in Analysis and Design*, Vol. 1, No. 1, 1985, pp. 3-20.
56. MacNeal, R. H., “Toward a defect-free four-noded membrane element,” *Finite Elements in Analysis and Design*, Vol. 5, No. 1, 1989, pp. 31-37.
57. MacNeal, R. H., “The Evolution of Lower Order Plate and Shell Elements in MSC/NASTRAN,” *Finite Elements in Analysis and Design*, Vol. 5, No. 3, 1989, pp. 197-222.
58. MacNeal, R. H., “Perspective on finite elements for shell analysis,” *Finite Elements in Analysis and Design*, Vol. 30, No. 3, 1998, pp. 175-186.
59. MacNeal, R. H., Wilson, C. T., Harder, R. L. and Hoff, C. C., “The treatment of shell normals in finite element analysis,” *Finite Elements in Analysis and Design*, Vol. 30, No. 3, 1998, pp. 235-242.
60. Sze, K. Y., Liu, X. H. and Lo, S. H., “Popular benchmark problems for geometric nonlinear analysis of shells,” *Finite Elements in Analysis and Design*, Vol. 40, 2004, pp. 1551-1569.
61. Stolarski, H. and Belytschko, T., “Shear and membrane locking in curved  $C^0$  elements,” *Computer Methods in Applied Mechanics and Engineering*, Vol. 41, 1983, pp. 279-296.
62. *The Standard NAFEMS Benchmarks* (Revision), National Agency for Finite Elements Methods and Standards, Glasgow, UK, 1989.
63. Park, K. C. and G.M. Stanley, G. M., “A Curved  $C^0$  Shell Element Based on Assumed Natural-Coordinate Strains,” *ASME Journal of Applied Mechanics*, Vol. 53, No. 2, 1986, pp. 278-290.

64. Stanley, G. M., Park, K. C. and Hughes, T. J. R., "Continuum-based resultant shell elements," In: *Finite Element Methods for Plate and Shell Structures: Vol. 1, Element Technology*, edited by T. J. R. Hughes and E. Hinton, Pineridge Press Limited, 1986, pp. 1-45.
65. Huang, H. C. and Hinton, E., "A New Nine Node Degenerated Shell Element with Enhanced Membrane and Shear Interpolation," *International Journal for Numerical Methods in Engineering*, Vol. 22, 1986, pp. 73-92.
66. Hinton, E. and Huang, H. C., "A Family of Quadrilateral Mindlin Plate Elements with Substitute Shear Strain Fields," *Computers & Structures*, Vol. 23, 1986, pp. 409-431.
67. Huang, H. C. and Hinton, E., "Elastic-Plastic and Geometrically non-linear analysis of plates and shells using a New, Nine-Noded Element," In P. G. Bergan, K. J. Bathe and W. Wunderlich. (eds), *Finite Elements for Nonlinear Problems*, Springer-Verlag, Berlin, 1986, pp. 283-97.
68. Simo, J. C., Fox, D. D., and Rifai, M. S. "On a stress resultant geometrically exact shell model. Part II, the linear theory; computational aspects." *Computer Methods in Applied Mechanics and Engineering*, Vol. 73, 1989, pp. 53-92.
69. Knight Jr, N. F., "The Raasch Challenge for Shell Elements," *AIAA Journal*, Vol. 35, 1997, pp. 375-381.
70. Dvorkin E. N, Bathe K. J., "A continuum mechanics based four-node shell element for general nonlinear analysis," *Engineering Computations*, Vol. 1, 1984, pp. 77-88.
71. Bathe, K. J. and Dvorkin, E. N., "A four-node plate bending element based on Mindlin/Reissner plate theory and a mixed interpolation," *International Journal for Numerical Methods in Engineering*, Vol. 21, 1985, pp. 367-383.

72. Bathe K. J, Dvorkin E. N., "A formulation of general shell elements—the use of mixed interpolation of tensorial components," *International Journal for Numerical Methods in Engineering*, Vol. 22, 1986, pp. 697-722.
73. Bucalem M. L, Bathe K. J., "Higher-order MITC general shell elements," *International Journal for Numerical Methods in Engineering*, Vol. 36, 1993, pp. 3729-54.
74. Chapelle, D. and Bathe, K. J., "Fundamental considerations for the finite element analysis of shell structures," *Computers & Structures*, Vol. 66, 1998, pp. 19-36.
75. Bathe, K. J., Iosilevich, A. and Chapelle, D., "An evaluation of the MITC shell elements," *Computers and Structures*, Vol. 75, 2000, pp. 1-30.
76. Bathe, K. J., Lee, P. S. and Hiller, J. F., "Towards improving the MITC9 shell element," *Computers & Structures*, Vol. 81, 2003, 477–489.
77. Hiller, J. F. and Bathe, K. J., "Measuring convergence of mixed finite element discretizations: an application to shell structures," *Computers & Structures*, Vol. 81, 2003, pp. 639–654.
78. Lee, P. S. and Bathe, K. J., "Development of MITC isotropic triangular shell finite elements," *Computers & Structures*, Vol. 82, 2004, pp. 945–962.
79. Argyris JH, Papadrakakis M, Apostolopoulou C, Koutsourelakis S., "The TRIC shell element: theoretical and numerical investigation," *Computer Methods in Applied Mechanics and Engineering*, Vol. 182, 2000, pp. 217-45.
80. Hammer, P. C., Marlowe, O. J., and Stroud, A. H., "Numerical Integration over Simplexes and Cones," *Mathematical Tables and Other Aids to Computation*, Vol. X, No. 54, 1956, pp. 130-137.
81. Cowper, G. R., "Gaussian Quadrature Formulas for Triangles," *International Journal*

- for Numerical Methods in Engineering*, Vol. 7, 1973, pp. 405-408.
82. Dunavant, D. A., "High Degree Efficient Symmetrical Gaussian Quadrature Rules for the Triangle," *International Journal for Numerical Methods in Engineering*, Vol. 21, No. 7, 1985.
  83. Malkus, D. S. and Hughes, T. J. R. "Mixed Finite Element Methods – Reduced and Selective Integration Techniques: A Unification of Concepts," *Computer Methods in Applied Mechanics and Engineering*, Vol. 15, 1978, pp. 63-81. (reprinted in the Special Edition of the 20<sup>th</sup> Anniversary in the journal, Vol. 81, Aug., 1990. This special edition contains the 5 most cited articles published in the journal since its inception in 1970. The selection of the most-cited papers is based on data from the ISI® file of SCI® articles 1945-1988 which have been cited 50 or more times.)
  84. Zienkiewicz, O. C. and Nakazawa, S. "On Variational Formulations and its Modification for Numerical Solution," *Computers & Structures*, Vol. 19, 1984, pp. 303-313.
  85. Allman, D. J., "A Compatible Triangular Element Including Vertex Rotations For Plane Elasticity Analysis," *Computers & Structures*, Vol. 19, 1984, pp. 1-8.
  86. Allman, D. J., "A Quadrilateral Finite Element Including Vertex Rotations for Plane Elasticity Analysis," *International Journal for Numerical Methods in Engineering*, Vol. 26, No. 3, 1988, pp. 717-730.
  87. Allman, D. J., "Evaluation of the Constant Strain Triangle with Drilling Rotations", *International Journal for Numerical Methods in Engineering*, Vol. 26, 1988, pp. 2645-2655.
  88. Allman, D. J., "Variational Validation of a Membrane Finite Element with Drilling

- Rotations,” *Communications in applied numerical methods*. Vol. 9, 1993, pp. 345-351
89. Allman, D. J., “A Basic Flat Facet Finite Element for the Analysis of General Shells,” *International journal for numerical methods in engineering*. Vol. 37, no. 1, 1994, pp. 19-35.
90. Cook, R. D., “On The Allman Triangle and Related Quadrilateral Element,” *Computers & Structures*, Vol. 22, 1986, pp. 1065-1067.
91. Cook, R. D., “Further Development of a Three-Node Triangular Shell Element,” *International Journal for Numerical Methods in Engineering*, Vol. 36, No. 8, 1993, 1413-1425.
92. Bergan, P. G. and Fellipa, C. A., “A Triangular Membrane Element with Rotational Degrees of Freedom,” *Computer Methods in Applied Mechanics and Engineering*, Vol. 50, No. 1, 1985, pp. 25-69.
93. Fellipa, C. A. and Alexander, S., “Membrane Triangles With Corner Drilling Freedoms III. Implementation and Performance Evaluation,” *Finite Elements in Analysis and Design*, Vol. 12, 1992, pp. 203-239.
94. Fellipa, C. A., “A Study of Optimal Membrane Triangles with Drilling Freedoms,” *Computer Methods in Applied Mechanics and Engineering*, Vol. 192, 2003, pp. 2125-2168.
95. Long, Y. and Xu, Y., “Generalized Conforming Triangular Membrane Element with Vertex Rigid Rotational Freedoms,” *Finite Elements in Analysis and Design*, Vol. 17, No. 4, 1994, pp. 259-271.
96. Hughes, T. J. R., Masud, A., and Harari, I., “Dynamic Analysis and Drilling Degrees of Freedom,” *International journal for numerical methods in engineering*. Vol. 38, no. 19,

- 1995, pp. 3193-3210
97. Hughes, T. J. R., Masud, A., and Harari, I., "Numerical assessment of some membrane elements with drilling degrees of freedom," *Computers & structures*. Vol., 55, no. 2, 1995, pp. 297-314.
  98. Batoz, J. L., Bathe, K. J. and Ho, L. W., "A Study of Three Noded Triangular Plate Bending Elements," *International Journal for Numerical Methods in Engineering*, Vol. 15, No. 12, 1980, 1771-1812.
  99. Batoz, J. L., "An explicit formulation for an efficient triangular plate bending element," *International Journal for Numerical Methods in Engineering*, Vol. 18, No. 7, 1982, 1077-1089.
  100. Batoz, J. L. and Lardeur, P., "A discrete shear triangular nine d.o.f. element for the analysis of thick to very thin plates," *International Journal for Numerical Methods in Engineering*, Vol. 28, 1989, pp. 533-560.
  101. Fafard, M., Dhatt, G., and Batoz, J. L., "A new discrete Kirchhoff plate/shell element with updated procedures," *Computers & Structures*, Vol. 31, 1989, pp. 591-606.
  102. Batoz, J. L., Zheng, C. L., Hammadi, F., "Formulation and evaluation of new triangular, quadrilateral, pentagonal and hexagonal discrete Kirchhoff plate/shell elements," *International journal for numerical methods in engineering*. Vol. 52, Part 5/6, 2001, pp. 615--630
  103. Jayachandrabose, C. and Kirkhope, J., and Babu, C. R., "An Alternative Explicit Formulation for the DKT Plate Bending Element," *International Journal for Numerical Methods in Engineering*, Vol. 21, No. 7, 1985, pp. 1289-1293.
  104. Jayachandrabose, C. and Kirkhope, J., "Construction of New Efficient Three-Node



- Triangular Thin-Plate Bending Elements,” *Computers & structures*. Vol., 23, no. 5, 1986, pp. 587-603.
105. C. Wanji and Y. K. Cheung, “Refined Triangular Discrete Kirchhoff Plate Element for Thin Plate Bending, Vibration and Buckling Analysis,” *International journal for numerical methods in engineering*. Vol. 41, No. 8, 1998, pp. 1507-1525.
106. Specht, B., “Modified Shape Functions for the Three Node Plate Bending Element Passing the Patch Test,” *International Journal for Numerical Methods in Engineering*, Vol. 26, 1988, pp. 705-715.
107. Zienkiewicz, O. C., Taylor, R. L., Papadopoulos, P. and Onate, E., “Plate Bending Elements With Discrete Constraints: New Triangular Elements,” *Computers and Structures*, Vol. 35, 1990, pp. 505-522.
108. Zienkiewicz, O. C. and Lefebvre, D., “A robust triangular plate bending element of the Reissner-Mindlin type,” *International journal for numerical methods in engineering*. Vol. 26, 1988, pp. 1169-1184.
109. Ibrahimbegovic, A., Taylor, R. L., Wilson, E. L., “A Robust Quadrilateral Membrane Finite Element with Drilling Degrees of Freedom,” *International journal for numerical methods in engineering*. Vol. 30, 1990, pp. 445-
110. Papadopoulos, P. and Taylor, R. L., “A triangular element based on Reissner-Mindlin plate theory,” ,” *International journal for numerical methods in engineering*. Vol. 30, 1990, pp. 1029-49.
111. Onate, E., Zienkiewicz, O. C., Suarez, B. and Taylor, R. L., “A general methodology for deriving shear constrained Reissner-Mindlin plate elements,” ,” *International journal for numerical methods in engineering*. Vol. 33, 1992, pp. 345-367.

112. Auricchio, F. and Taylor, R. L., "A Triangular Thick Plate Finite Element with an Exact Thin Limit," *Finite Elements in Analysis and Design*, Vol. 19, Nos. 1&2, 1995, pp. 57-68.
113. R. Piltner, R. and Taylor, R. L., "Triangular finite elements with rotational degrees of freedom and enhanced strain modes," *Computers & structures*. Vol., 75, 2000, pp. 361-368.
114. Ertas, A., Krafcik, J. T., and Ekwaro-Osire, S., "Performance of an Anisotropic Allman/DKT 3-Node Thin Triangular Flat Shell Element," *Composites Engineering*, Vol. 2, 1992, pp.269-280.
115. Bathe, K. J., Ramm, E. and Wilson, E. L., "Finite Element Formulations for Large Deformation Dynamic Analysis," *International Journal for Numerical Methods in Engineering*, Vol. 9, 1975, pp. 353-386.
116. Meek, J. L. and Ristic, S., "Large Displacement Analysis of Thin Plates and Shells Using a Flat Facet Finite Element Formulation," *Computer Methods in Applied Mechanics and Engineering*, Vol. 145, Nos.3-4, 1997, pp. 285-299.
117. Xu, Z., "A simple and efficient triangular finite element for plate bending," *Acta Mechanica, Sinica*, Vol. 2, 1986, 185-192.
118. Xu, Z., "A thick-thin triangular plate element," *International Journal for Numerical Methods in Engineering*, Vol. 33, 1992, pp. 963-973.
119. Simo, J. C., and Rifai, S, "A class of mixed assumed strain methods and the method of incompatible modes," *International Journal for Numerical Methods in Engineering*, Vol. 29, 1990, pp. 1595-1638
120. Hausser, C. and Ramm, E., "Efficient three-node shear deformable plate/shell elements

- an almost hopeless undertaking,” In *Advances in finite element Technology*, edited by B. H. V. Topping, Civil-Comp Press, Edinburgh, 1996, pp. 203-215.
121. Bischoff, M. and Ramm, E., “Shear Deformable Shell Elements for Large Strains and Rotations,” *International Journal for Numerical Methods in Engineering*, Vol. 40, 1997, pp. 4427-4449.
122. Bletzinger, K. U., Bischoff, M. and Ramm, E., “A unified approach for shear-locking-free triangular and rectangular shell finite elements,” *Computers & structures*. Vol., 75, 2000, pp. 321-334.
123. Ramm, E. and Wall, W. A., “Shell structures—a sensitive interrelation between physics and numerics,” *International Journal for Numerical Methods in Engineering*, Vol. 60, 2004, pp. 381-427.
124. Fogel, L. J., Owens, A. J., and Walsh, M. J., *Artificial Intelligence through Simulated Evolution*, Wiley, New York, 1966.
125. Rechenburg, I., *Cybernetic Solution Path of an Experimental Problem*, Royal Aircraft Establishment Library Translation No 1122, 1965.
126. Holland, J. H., *Adaptation in Natural and Artificial Systems*, MIT Press, 1992.
127. Goldberg, D. E., *Genetic Algorithms in Search, Optimization, and Machine Learning*, Addison-Wesley, 1989.
128. Davis, L., ed. *Handbook of Genetic Algorithms*, Van Nostrand Reinhold, New York, 1991.
129. Mitchell, M., *An Introduction to Genetic Algorithms*, MIT Press, 1996.
130. Michalewicz, Z., *Genetic Algorithms + Data Structures = Evolution Programs*, 3rd ed., Springer, 1996.

131. Cantu-Paz, E., *Efficient and Accurate Parallel Genetic Algorithms*, Kluwer Academic Publishers, Massachusetts, 2000.
132. Fogel, D. B., *Evolutionary Computation: Toward a New Philosophy of Machine Intelligence*, 2<sup>nd</sup> ed., IEEE Press, 2000.
133. Goldberg, D. E., *The Design of Innovation: Lessons from and for Competent Genetic Algorithms*, Kluwer Academic Publishers, 2002.
134. Kirkpatrick, S., Gellatt, Jr, C. D., and Vecchi, M. P., "Optimization by Simulated Annealing," *Science*, Vol. 220, No. 4598, 1983, 671-680.
135. Glover, F. and Laguna, M., *Tabu Search*, Kluwer Academic Publishers, Boston, 1997.
136. Koza, J. R., Bennett III, F. H., Andre, D., and Keane, M. A., *Genetic Programming III: Darwinian Invention and Problem Solving*, Morgan Kaufmann Publishers, 1999.
137. Holland, J. H., "Genetic algorithms," *Scientific American*, July, 1992, pp. 66-72.
138. Forrest, S., "Genetic Algorithms: Principles of Natural Selection Applied to Computation," *Science*, Vol. 261, 1993, pp. 872-878.
139. Forrest, S. and Mitchell, M., "What Makes a Problem Hard for a Genetic Algorithm? Some Anomalous Results and Their Explanation," *Machine Learning*, Vol. 13, 1993, pp. 285-319.
140. Goldberg, D. E., "Genetic and Evolutionary Algorithms Come of Age," *Communications of the ACM*, Vol. 37, No. 3, 1994, pp. 113-119.
141. De Jong, K. A., "Genetic Algorithms: A 25 Year Perspective," *IEEE Computational Intelligence: Imitating Life, 1994*, pp. 125-134.
142. Whitley, D., "A Genetic Algorithm Tutorial," *Statistics and Computing*, Vol. 4, 1994, pp. 65-85.

143. Dasgupta, D. and Michalewicz, Z., “*Evolutionary Algorithms—An Overview*,” in *Evolutionary Algorithms in Engineering Applications*, Dasgupta, D. and Michalewicz, Z. (eds.), Springer, 1997.
144. Wolpert, D. H. and Macready, W. G., “No Free Lunch Theorems for Optimization,” *IEEE Transactions on Evolutionary Computation*, Vol. 1, No. 1, 1997, pp. 67-82.
145. De Jong, K., “Evolutionary Computation: Recent Developments and Open Issues,” in *Evolutionary Algorithms in Engineering and Computer Science*, Miettinen, K., Neittaanmaki, P., and etc. (eds.) John Wiley & Sons, Ltd, 1999.
146. Fogel, D., B., “Some Recent Important Foundational Results in Evolutionary Computation,” in *Evolutionary Algorithms in Engineering and Computer Science*, Miettinen, K., Neittaanmaki, P., and etc. (eds.) John Wiley & Sons, Ltd, 1999.
147. Gen, M., and Cheng, R., *Genetic Algorithms & Engineering Optimization, Chapter 1*, John Wiley & Sons, Inc., 2000.
148. Grefenstette, J. J. “Optimization of Control Parameters for Genetic Algorithms,” *IEEE Transactions on Systems, Man, and Cybernetics*, Vol. SMC-16, No. 1, 1986, pp. 122-128.
149. Krishnakumar, K., “Micro-Genetic Algorithms for Stationary and Non-Stationary Function Optimization,” Proceedings of *SPIE, Intelligent Control and Adaptive Systems*, Vol. 1196, 1989, pp.289-296.
150. David. L. Carroll’s FORTRAN Genetic Algorithm Driver.  
<http://www.aic.nrl.navy.mil:80/galist/src/#fortran>
151. Carroll, D. L., “Genetic Algorithms and Optimizing Chemical Oxygen-Iodine Lasers,” In *Developments in Theoretical and Applied Mechanics*, Vol. XVIII, eds. H. Wilson, R.

- Batra, C. Bert, A. Davis, R. Schapery, D. Stewart, and F. Swinson, School of Engineering, The University of Alabama, 1996, pp. 411-424.
152. Carroll, D. L., "Chemical Laser Modeling with Genetic Algorithms," *AIAA Journal*, Vol. 34, No. 2, 1996, pp. 338-346.
153. Daly, P. and Ngo. D., "Multidisciplinary Structural Optimization Utilizing Genetic Algorithm Capabilities," AIAA-98-4776, pp. 553-558.
154. Abu-Lebdeh, G. and Benekohal, F., "Convergence Variability and Population Sizing in Micro-Genetic Algorithms," *Computer-Aided Civil and Infrastructure Engineering*, Vol. 14, 1999, pp. 321-334.
155. The Genetic Algorithms Archive: <http://www.aic.nrl.navy.mil/galist>
156. Chipperfield, A., Fonseca, C., Fleming, P., and Pohlheim, H., Genetic Algorithm Toolbox for MATLAB: <http://www.shef.ac.uk/uni/projects/gaipp/gatbx.html>
157. Punch, W. F., Averill, R. C., Goodman, E. D., Lin, S. C., Ding, Y., and Yip, Y. C., "Optimal Design of Laminated Composite Structures Using Coarse-grain Parallel Genetic Algorithms," *Computing Systems in Engineering*, Vol. 5, No. 4-6, 1994, pp. 415-423.
158. Henderson, J. L., "Laminated Plate Design Using Genetic Algorithms and Parallel Processing," *Computing Systems in Engineering*, Vol. 5, No. 4-6, 1994, pp. 441-453.
159. Soremekun, G., Gurdal, Z., Haftka, R. T., and Watson, L. T., "Composite laminate design optimization by genetic algorithm with generalized elitist selection," *Computers & structures*. Vol., 79, No. 2, 2001, pp. 131-143.
160. Rogers, J. L., "A Parallel Approach to Optimum Actuator Selection with a Genetic Algorithm," AIAA-2000-4484. pp. 1-10.

161. Plassman, G. E. and Sobieszczanski-Sobieski, J., "Experience with a Genetic Algorithm Implemented on a Multiprocessor Computer," AIAA-2000-4844, pp. 1-16.
162. Jones, B. R., Crossley, W. A., and Lyrintzis, A. S., "Aerodynamic and Aeroacoustic Optimization of Rotorcraft Airfoils via a Parallel Genetic Algorithm," *Journal of Aircraft*, Vol. 37, No. 6, 2000, pp. 1088-1096.
163. Abdullah, M. M., Richardson, A., and Hanif, J., "Placement of Sensors/Actuators on Civil Structures using Genetic Algorithms," *Earthquake Engineering and Structural Dynamics*, Vol. 30, 2001, pp. 1167-1184.
164. Jaramillo, J. H., Bhadury, J., and Batta, R., "On the Use of Genetic Algorithms to Solve Location Problems," *Computers & Operations Research*, Vol. 29, 2002, pp. 761-779.
165. Alba, E. and Troya, J., "Improving Flexibility and Efficiency by Adding Parallelism to Genetic Algorithms," *Statistics and Computing*, Vol. 12, 2002, pp. 91-114.
166. Lee, J. and Hajela, P., "Parallel Genetic Algorithm Implementation in Multidisciplinary Rotor Blade Design," *Journal of Aircraft*, Vol. 33., No. 5, 1996, pp. 962-969.
167. Hajela, P., "Nongradient Methods in Multidisciplinary Design Optimization—Status and Potential," *Journal of Aircraft*, Vol. 36, No. 1, 1999, pp. 255-265.
168. Masters, B. P. and Crawley, E. F., "Evolutionary Design of Controlled Structures," *Journal of Aircraft*, Vol. 36, No. 1, 1999, pp. 209-217.
169. Wada, B. K., Fanson, J. L., and Crawley, E. F., "Adaptive Structures," *Journal of Intelligent Material Systems and Structures*, Vol. 1, No. 2, 1990, pp. 157-174.
170. Anderson, G. L., Crowson, A. and Chandra, J., "Introduction to Smart Structures," In, *Intelligent Structural Systems*, edited by H. S. Tzou and G. L. Anderson, Kluwer Academic Publishers, 1992, pp. 1-8.

171. Crawley, E., "Intelligent Structures for Aerospace: A Technology Overview and Assessment," *AIAA Journal*, Vol. 32, No. 8, 1994, pp. 1689–1699.
172. Chee, C.Y. K., Tong, L., and Steven, G. P., "A review on the Modeling of Piezoelectric Sensors and Actuators Incorporated in Intelligent Structures," *Journal of Intelligent Material Systems and Structures*, Vol. 9, No. 1, 1998, pp. 3–19.
173. Sunar, M., and Rao, S. S., "Recent Advances in Sensing and Control of Flexible Structures via Piezoelectric Materials Technology," *Applied Mechanics Reviews*, Vol. 52, No. 1, 1999, pp. 1–16.
174. Saravanan, D. A. and Heyliger, P. R., "Mechanics and computational models for laminated piezoelectric beams, plates, and shells," *Applied Mechanics Reviews*, Vol. 52, No. 10, 1999, pp. 305–319.
175. Reddy, J. N., "On laminated composite plates with integrated sensors and actuators," *Engineering Structures*, Vol. 21, 1999, 568-593.
176. Wang, J. and Yang, J., "Higher-order theories of piezoelectric plates and applications," *Applied Mechanics Reviews*, Vol. 53, No. 4, 2000, pp. 87–99.
177. Benjeddou, A., "Advances in Piezoelectric Finite Element Modeling of Adaptive Structural Elements: A Survey," *Computers and Structures*, Vol. 76, No. 4, 2000, pp. 347–363.
178. Gopinathan, S. V., Varadan, V. V., and Varadan, V. K., "A Review and Critique of Theories for Piezoelectric Laminates," *Smart Materials and Structures*, Vol. 9, No. 1, 2000, pp. 24–48.
179. Chopra, I., "Status of Application of Smart Structures Technology to Rotorcraft Systems," *Journal of the American Helicopter Society*, Vol. 45, No. 4, 2000, pp. 228–



252.

180. Sater, J. M., Crowe, C. R., Antcliff, R. and Das, A., “Smart Air and Space Structures,” *Structures Technology for Future Aerospace Systems*, Progress in Astronautics and Aeronautics, Ed. A. K. Noor, Vol. 188, AIAA, Reston, VA, 2000, pp. 269-349.
181. Das, A. and Wada, B, *Selected Papers on Smart Structures for Spacecraft*, SPIE Milestone Series, Vol. MS 167, 2001.
182. Garg, D. P., Zikry, M. A., and Anderson, G. L., “Current and Potential Future Research Activities in Adaptive Structures: An ARO Perspective,” *Smart Materials and Structures*, Vol. 10, No. 4, 2001, pp. 610–623.
183. Rao, V. S. and Sana, S., “An Overview of Control Design Methods for Smart Structural System,” *Proceedings of SPIE*, Vol. 4326, 2001, pp.1-13.
184. Chopra, I., “Review of State of Art of Smart Structures and Integrated Systems,” *AIAA Journal*, Vol. 40, No. 11, 2002, pp. 2145–2187.
185. Schweiger, J., “Aircraft Control, Applications of Smart Structures,” In: *Encyclopedia of Smart Materials*, Edited by M. Schwartz, John Wiley & Sons, Inc., Vol. 1, 2002, pp. 42-59.
186. McGowan, A.-M. R., Washburn, A. E., Horta, L. G., Bryant, R. G., Cox, D. E., Siochi, E. J., Padula, S. L., Holloway, N. M., “Recent Results from NASA’s Morphing Project,” *Industrial and Commercial Applications of Smart Structures Technologies*, Proceedings of SPIE, Vol. 4698, 2002, pp. 97-111.
187. Frecker, M. I., “Recent Advances in Optimization of Smart Structures and Actuators,” *Journal of Intelligent Material Systems and Structures*, Vol. 14, No. 1, 2003, pp. 207–216.

188. MacMartin, D. G., "Control Challenges for Extremely Large Telescopes," *Industrial and Commercial Applications of Smart Structures Technologies*, Proceedings of SPIE, Vol. 5054, 2003, pp. 275-286.
189. Sanders, B., Crowe, R. and Garcia, E., "Defense Advanced Research Projects Agency – Smart Materials and Structures Demonstration Program Overview," *Journal of Intelligent Material Systems and Structures*, Vol. 15, No. 4, 2004, pp. 227–233.
190. Cady, W. G., *Piezoelectricity*, Dover, New York, 1964.
191. Inst. of Electrical and Electronics Engineers *Standard on Piezoelectricity*, Std, 176, ANSI/IEEE, 1987.
192. Joshi, S. P., "Nonlinear Constitutive relations for Piezoceramic Materials," In Knowles, G. J., ed., *Proceedings of the ADPA/AIAA/ASME/SPIE Conference on Active Materials and Adaptive Structures*, Alexandria, VA, 1991, pp. 217-222.
193. Tiersten, H. F., "Electroelastic equations for electroded thin plates subject to large driving voltages," *Journal of Applied Physics*, Vol. 74, 1993, pp. 3389-93.
194. Sirohi, J., and Chopra, I., "Fundamental Behavior of Piezoceramic Sheet Actuators," *Journal of Intelligent Material Systems and Structures*, Vol. 11, No. 1, 2000, pp. 47–61.
195. Sirohi, J., and Chopra, I., "Fundamental Understanding of Piezoelectric Strain Sensors," *Journal of Intelligent Material Systems and Structures*, Vol. 11, No. 4, 2000, pp. 246–257.
196. Jordan, T. L. and Ounaies, Z., "Characterization of Piezoelectric Ceramic Materials," In: *Encyclopedia of Smart Materials*, Edited by M. Schwartz, John Wiley & Sons, Inc., Vol.1, 2002, pp. 162-173.
197. Harrison, J. S. and Ounaies, Z., "Polymers, Piezoelectric," In: *Encyclopedia of Smart*

- Materials*, Edited by M. Schwartz, John Wiley & Sons, Inc., Vol. 2, 2002, pp. 860-873.
198. Schulz, M. J., Sundaresan, M. J., McMichael, J., Clayton, D., Sadler, R., and Nagel, B., "Piezoelectric Materials at Elevated Temperature," *Journal of Intelligent Material Systems and Structures*, Vol. 14, 2003, pp. 693–705.
199. Park, S.-E. and ShROUT, T. R., "Ultra-high strain and piezoelectric behavior in relaxor ferroelectric single crystals," *Journal of Applied Physics*, Vol. 82, No. 4, 1997, pp. 1804-1811.
200. Giurgiutiu, V and Lyshevski, S. E., *MicroMechatronics: modeling, analysis, and design with Matlab*, CRC Press, 2004.
201. Tauchert, T. R., "Piezothermoelastic Behavior of A Laminated Plate," *Journal of Thermal Stresses*, Vol.15, 1992, pp. 25-37.
202. Bailey, A., and Hubbard, J. E., "Distributed Piezoelectric-Polymer Active Vibration Control of a Cantilevered Beam," *Journal of Guidance, Control, and Dynamics*, Vol. 8, No. 5, 1985, pp. 605–611.
203. Hagood, N. W., Chung, W. H., and Flotow, A. V., "Modeling of Piezoelectric Actuator Dynamics for Active Structural Control," *Journal of Intelligent Material Systems and Structures*, Vol. 1, No. 3, 1990, pp. 327–354.
204. Lee, C. K., "Theory of Laminated Piezoelectric Plates for the Design of Distributed Sensors/Actuators: Part I: Governing Equations and Reciprocal Relationships," *Journal of Acoustical Society of America*, Vol. 87, No. 3, 1990, pp. 1144–1158.
205. Lee, C. K., "Piezoelectric Laminates: Theory and Experiment for Distributed Sensors and Actuators," *Intelligent Structural Systems*, edited by H. S. Tzou and G. L. Anderson, Kluwer Academic, Norwell, MA, 1992, pp. 75–168.

206. Hanagud, S., Obal, M.W., and Calise, A. J., "Optimal Vibration Control by the Use of Piezoelectric Sensors and Actuators," *Journal of Guidance, Control, and Dynamics*, Vol. 15, No. 5, 1992, pp. 1199–1206.
207. Dosch, J. J., Inman, D. J., and Garcia, E., "A Self-Sensing Piezoelectric Actuator for Collocated Control," *Journal of Intelligent Material Systems and Structures*, Vol. 3, No. 1, 1992, pp. 166–185.
208. Wang, B. T., Burdisso, R. A., and Fuller, C. R., "Optimal Placement of Piezoelectric Actuators for Active Structural Acoustic Control," *Journal of Intelligent Material Systems and Structures*, Vol. 5, No. 1, 1994, pp. 67–77.
209. Anderson, E. H., and Hagood, N.W., "Simultaneous Piezoelectric Sensing/Actuation: Analysis and Application to Controlled Structures," *Journal of Sound and Vibration*, Vol. 174, No. 5, 1994, pp. 617–639.
210. Varadan, V. V., Kim, J., and Varadan, V. K., "Optimal Placement of Piezoelectric Actuators for Active Noise Control," *AIAA Journal*, Vol. 35, No. 3, 1997, pp. 526-533.
211. Crawley, E., and de Luis, J., "Use of Piezoceramic Actuators as Elements of Intelligent Structures," *AIAA Journal*, Vol. 25, No. 10, 1987, pp. 1373–1385.
212. Crawley, E., and Anderson, E., "Detailed Models of Piezoceramic Actuation of Beams," *Journal of Intelligent Material Systems and Structures*, Vol. 1, No. 1, 1990, pp. 4–25.
213. Crawley, E. F., and Lazarus, K. B., "Induced Strain Actuation of Isotropic and Anisotropic Plates," *AIAA Journal*, Vol. 23, No. 6, 1991, pp. 944–951.
214. Ha, S. K., Keilers, C., and Chang, F. K., "Finite Element Analysis of Composite Structures Containing Distributed Piezoceramic Sensors and Actuators," *AIAA Journal*,

- Vol. 30, No. 3, 1992, pp. 772–780.
215. Jonnalagadda, K. D., Blandford, G. E. and Tauchert, T. R., “Piezothermoelastic Composite Plate Analysis Using First-order Shear Deformation Theory,” *Computers and Structures*, Vol. 51, 1994, pp. 79-89.
216. Detwiler, D. T., Shen, M. -H. H., and Venkayya, V. B., “Finite Element Analysis of Laminated Composite Structures Containing Distributed Piezoelectric Actuators and Sensors,” *Finite Elements in Analysis and Design*, Vol. 20, No. 2, 1995, pp. 87-100.
217. Kim, J., Varadan, V. V., and Varadan, V. K., “Finite Element Modelling of Structures Including Piezoelectric Active Devices,” *International Journal for Numerical Methods in Engineering*, Vol. 40, 1997, pp. 817-832.
218. Saravanos, D.A., Heyliger, P.R., and Hopkins, D.A., “Layerwise Mechanics and Finite Element for the Dynamic Analysis of Piezoelectric Composite Plates,” *International Journal of Solids Structure*, Vol. 34, No. 3, 1997, pp. 359-378.
219. Hong, C. H., and Chopra, I., “Modeling and Validation of Induced Strain Actuation of Composite Coupled Plates,” *AIAA Journal*, Vol. 37, No. 3, 1999, pp. 372–377.
220. Chattopadhyay, A., Li, J., and Gu, H., “Coupled Thermo-Piezoelectric-Mechanical Model for Smart Composite Laminate,” *AIAA Journal*, Vol. 37, No. 12, 1999, pp. 1633–1638.
221. Zhou, X., Chattopadhyay, A., and Gu, H., “Dynamic Response of Smart Composites Using a Coupled Thermo-Piezoelectric-Mechanical Model,” *AIAA Journal*, Vol. 38, No. 10, 2000, pp. 1939–1948.
222. Vel, S. S., and Batra, R. C., “Three-Dimensional Analytical Solution for Hybrid Multilayered Piezoelectric Plates,” *Journal of Applied Mechanics*, Vol. 67, No. 3, 2000,

pp. 558–567.

223. Batra, R. C., and Vidoli, S., “Higher-Order Piezoelectric Plate Theory Derived from a Three-Dimensional Variational Principle,” *AIAA Journal*, Vol. 40, No. 1, 2002, pp. 91–104.
224. Kim, H. S., Chattopadhyay, A., and Nam, C., “Implementation of A Coupled Thermo-piezoelectric-mechanical Model in The LQG Controller Design for Smart Composite Shells,” *Journal of Intelligent Material Systems and Structures*, Vol. 13, 2002, pp. 513–524.
225. Freed, B. D. and Babuska, V., “Finite Element Modeling of Composite Piezoelectric Structures with MSC/NASTRAN,” SPIE Vol. 3041, pp. 676-688.
226. Reaves, M. C. and Horta, L. G., “Test Cases for Modeling and Validation of Structures with Piezoelectric Actuators,” AIAA-2001-1466, pp. 1-11.
227. Batra, R. C., Liang, X. Q., and Yang, J. S., “Shape Control of Vibrating Simply Supported Rectangular Plates,” *AIAA Journal*, Vol. 34, No. 1, 1996, pp. 116–122.
228. Lazarus, K. B., Crawley, E. F., and Lin, C. Y., “Multivariable High-Authority Control of Plate-Like Active Structures,” *Journal of guidance, control, and dynamics*, Vol. 19, no. 6, 1996, pp. 1357-1363.
229. Lin, C. Y., Crawley, E. F., Heeg, J., “Open- and Closed-loop Results of a Strain-Actuated Active Aeroelastic Wing,” *Journal of Aircraft*, Vol. 33, No. 5, 1996, pp. 987-994.
230. Nam, C., Kim, Y., and Weisshaar, T. A., “Optimal Sizing and Placement of Piezo-actuators for Active Flutter Suppression,” *Smart Materials and Structures*, Vol. 5, 1996, pp. 216-224.

231. Maillard, J. P. and Fuller, C. R., "Active Control of Sound Radiation from Cylinders with Piezoelectric Actuators and Structural Acoustic Sensing," *Journal of Sound and Vibration*, Vol. 222, No. 3, 1999, pp. 363-388.
232. Park, C. H. and Baz, A., "Vibration Control of Bending Modes of Plates Using Active Constrained Layer Damping," *Journal of Sound and Vibration*, Vol. 227, No. 4, 1999, pp. 711-734.
233. Schulz, M. J., Pai, P. F., and Inman, D. J., "Health Monitoring and Active Control of Composite Structures Using Piezoceramic Patches," *Composites: Part B*, Vol. 30, 1999, pp. 713-725.
234. Park, H. M. and Agarwal, R., "Fuzzy Logic Control of Plate Vibrations," AIAA-2000-1424, pp. 1-10.
235. Shen, Y. and Homaifar, A., "Vibration Control of Flexible Structures with PZT Sensors and Actuators," *Journal of Vibration and Control*, Vol. 7, 2001, pp. 417-451.
236. Bevan, J. S. and Mei, C., "Piezoelectric Actuator Placement for Structural Acoustic and Vibration Control of Flat and Curved Panels," *Smart Structures and Materials: Smart Structures and Integrated System*, Proceedings of SPIE, Vol. 4327, 2001, pp. 698-708.
237. Voracek, D., Reaves, M., Horta, L. G., and Potter, S., "Ground and Flight Test Structural Excitation using Piezoelectric Actuators," AIAA-2002-1349, pp. 1-13.
238. Ardelean, E. V., McEver, M. A., Cole, D. G., and Clark, R. L., "Flutter Suppression using V-Stack Piezoelectric Actuator," AIAA-2003-1796.
239. Sheta, E. F., Moses, R. W., Huttshell, L. J., and Harrand, V. J., "Active Control of F/A-18 Vertical Tail Buffeting using Piezoelectric Actuators," AIAA-2003-1887, pp. 1-11.
240. Murayama, H., Kageyama, K., Naruse, H., Shimada, A., and Uzawa, K., "Application

- of Fiber-Optic Distributed Sensors to Health Monitoring for Full-Scale Composite Structures,” *Journal of Intelligent Material Systems and Structures*, Vol. 14, 2003, pp. 3-13.
241. Jha, R. and He, C., “Design and Experimental Validation of an Adaptive Neurocontroller for Vibration Suppression,” *Journal of Intelligent Material Systems and Structures*, Vol. 14, 2003, pp. 497–506.
242. Ghoshal, A., Chattopadhyay, A., Schulz, M. J., Thornburgh, R., and Waldron, K., “Experimental Investigation of Damage Detection in Composite Material Structures Using a Laser Vibrometer and Piezoelectric Actuators,” *Journal of Intelligent Material Systems and Structures*, Vol. 14, 2003, pp. 521–537.
243. Jha, A. K. and Inman, D. J., “Optimal Sizes and Placements of Piezoelectric Actuators and Sensors for an Inflated Torus,” *Journal of Intelligent Material Systems and Structures*, Vol. 14, 2003, pp. 563–576.
244. Varelis, D. and Saravanos, D. A., “Mechanics and Finite Element for Nonlinear Response of Active Laminated Piezoelectric Plates,” *AIAA Journal*, Vol. 42, No. 6, 2004, pp. 1227–35.
245. Andoh, F., Washington, G., Yoon, H. S. and Utkin, V., “Efficient Shape Control of Distributed Reflectors with Discrete Piezoelectric Actuators,” *Journal of Intelligent Material Systems and Structures*, Vol. 15, No. 1, 2004, pp. 3–15.
246. Haftka, R. T. and Adelman, H. M., “Selection of Actuator Locations for Static Shape Control of Large Space Structures by Heuristic Integer Programming,” *Computers and Structures*, Vol. 20, 1985, pp. 572-582.
247. Pearson, E., and Stepp, L., “ Response of Large Optical Mirrors to Thermal



- Distributions,” *Proceedings of SPIE—The International Society for Optical Engineering*, Vol. 748, 1987, pp. 215-228.
248. Tabata, M., Itoh, N., Miyawaki, K., Satori, A., Iye, M., Yamashita, Y., Noguchi, T., and Tanaka, W., “Shape Control Experiments with a Functional Model for Large Optical Reflectors,” In Wada, B. K., Fanson, J. L., and Miura, K., ed., *First Joint U.S./Japan Conference on Adaptive Structures*, Maui, Hawaii, 1990, pp. 615-630.
249. Kuo, C. P., Bruno, R., “Optimal Actuator Placement on an Active Reflector Using a Modified Simulated Annealing Technique,” In Wada, B. K., Fanson, J. L., and Miura, K., ed., *First Joint U.S./Japan Conference on Adaptive Structures*, Maui, Hawaii, 1990, pp. 1056-1067.
250. Kuo, C. P., “Optical Tests of an Intelligently Deformable Mirror for Space Telescope Technology,” *Proceedings of the SPIE*, Vol. 2040 1993, pp. 631-646.
251. Padula, S. L. and Palumbo, D. L., “Optimal Sensor/Actuator Locations for Active Structural Acoustic Control,” Paper AIAA-98-1865, 1998.
252. Padula, S. L. and Kincaid, R. K. “Optimization Strategies for Sensor and Actuator Placement,” NASA, TM-1999-209126, April, 1999.
253. Chen, G. S., Bruno, R. J., and Salama, M., “Optimal Placement of Active/Passive Members in Truss Structures Using Simulated Annealing,” *AIAA Journal*, Vol. 29, No. 8, 1991, pp1327-1334.
254. Rao, S. S., Pan, T. S., and Venkayya, V. B., “Optimal Placement of Actuators in Actively Controlled Structures Using Genetic Algorithms,” *AIAA Journal*, Vol. 29, No. 6, 1991, pp. 942-943.
255. Sunar, M. and Rao, S. S., “Thermopiezoelectric Control Design and Actuator

- Placement,” *AIAA Journal*, Vol. 35, No. 3, 1997, pp. 534-539.
256. Furuya, H. and Haftka, R. T., “Combining Genetic and Deterministic Algorithms for Locating Actuators on Space Structures,” *Journal of Spacecraft and Rockets*, Vol. 33, No. 3, 1996, pp. 422-427.
257. Lee, I. and Han, J. H., “Optimal Placement of Piezoelectric Sensors and Actuators for Vibration Control of a Composite Plate Using Genetic Algorithms,” *Smart Materials and Structures*, Vol. 8, 1999, Vol. 257-267.
258. Sadri, A. M., Wright, J. R., and Wynne, R. J., “Modeling and Optimal Placement of Piezoelectric Actuators in Isotropic Plates Using Genetic Algorithms,” *Smart Materials and Structures*, Vol. 8, 1999, Vol. 490-498.
259. Hu, Z., Jakiela, M., Pitt, D., and Burnham, J., “Reducing Aerodynamic Vibration with Piezoelectric Actuators – A Genetic Algorithm Optimization,” *Industrial and Commercial Applications of Smart Structures Technologies*, Proceedings of SPIE, Vol. 5388, 2004, pp. 276-287.
260. Kapania, R. K., and Mohan, P., “Static, Free Vibration and Thermal Analysis of Composite Plates and Shells Using a Flat Triangular Shell Element,” *Computational Mechanics*, Vol. 17, 1996, pp. 343-357.
261. Kapania, R. K., Mohan, P., and Jakubowski, A., “Control of Thermal Deformations of Spherical Mirror Segment,” Paper AIAA-96-4145, *Journal of Spacecraft and Rockets*, Vol. 35, No. 2, 1998, pp. 156-162.
262. Mohan, P. and Kapania, R. K., “Updated Lagrangian Formulation of a Flat Triangular Element for Thin Laminated Shells,” *AIAA Journal*, Vol. 36, No. 2, 1998, pp.273-281.
263. Sheng, L. and Zhang, Z., “A General Higher-Order Finite Element Analysis of

- Composite Laminate and Sandwich Panels, Considering the Transverse Shear Stress and Normal Strain,” Proceedings of 9<sup>th</sup> National Conference on Composite Materials (NCCM-9), Vol. 1, 1996, pp. 338-343. (in Chinese)
264. Sheng, L., *Higher-Order Finite Element Analysis of Composite Laminate and Sandwich Panels*, M.S. Thesis, Beijing University of Aeronautics and Astronautics, 1995. (in Chinese)
265. Kapania, R. K. and Sheng, L., “Optimization of Piezoelectric Actuator Locations by Genetic Algorithms,” presented at *ASME Mechanics and Materials Conference*, Virginia Tech., June 27-30, 1999.
266. Sheng, L. and Kapania, R. K., “Genetic Algorithms for the Optimization of Piezoelectric Actuator Locations,” Presented as Paper AIAA-2000-1581, Proceedings of *AIAA/ASME/ASCE/AHS/AHC 41<sup>st</sup> Structures, Structural Dynamics and Materials Conference*, Atlanta, GA, April 3-6, 2000.
267. Sheng, L. and Kapania, R. K., “Genetic Algorithms for the Optimization of Piezoelectric Actuator Locations,” *AIAA Journal*, Vol. 39, No. 9, 2001, pp. 1818-1822.
268. Kapania, R. K. and Sheng, L., “Towards More Effective Genetic Algorithms for the Optimization of Piezoelectric Actuator Locations,” Presented as Paper AIAA-2001-1627, Proceedings of *AIAA/ASME/ASCE/AHS/AHC 42<sup>nd</sup> Structures, Structural Dynamics and Materials Conference*, Seattle, WA, April 16-19, 2001.
269. Bland, S. M., Sheng, L. and Kapania, R. K., “Design of Complex Adaptive Structures Using the Genetic Algorithm,” In *Complex Adaptive Structures*, edited by W. B. Spillman, Jr., Proceedings of SPIE, Vol. 4512, 2001, pp. 212-223.
270. Kapania, R. K. and Sheng, L., “Towards More Effective Genetic Algorithms for the

Optimization of Piezoelectric Actuator Locations,” *AIAA Journal*, Vol. 40, No. 6, 2002, pp. 1246-1250.

271. Sheng, L. and Kapania, R. K., “Extensive Experiments on Genetic Algorithms for the Optimization of Piezoelectric Actuator Locations through Parallel Computation,” submitted to *AIAA/ASME/ASCE/AHS/AHC 46<sup>th</sup> Structures, Structural Dynamics and Materials Conference & 1<sup>st</sup> AIAA Multidisciplinary Design Optimization Specialist Conference*, Austin, Texas, April 18-21, 2005. (already accepted, Paper Number: AIAA-2005-1899)

## **Vita**

Lizeng Sheng was born on June 26, 1965 in Ji County, Tianjin, China. He graduated from First High School in Ji County in 1982. He then enrolled at Beijing University of Aeronautics and Astronautics and received his bachelor's and master's degrees in Solid Mechanics in 1986 and 1995, respectively. During 1986 to 1997, he worked as an aerospace engineer in Second Academy of China Aerospace Industry Corporation, Beijing, China. He started his PhD study in Aerospace Engineering at Virginia Tech. in August, 1997. For the last years he has been worked as a teaching assistant for various undergraduate and graduate courses and a research assistant for developing the finite elements and genetic algorithms for the optimization of piezoelectric actuator locations on the smart structures.